GEOCHEMICAL FINGERPRINTING OF CARBONATE WALL ROCK ALTERATION AT MAJOR BASE METAL SULPHIDE DEPOSITS IN THE OTAVI MOUNTAIN LAND, NAMIBIA

BY

DESHENTHREE CHETTY

Dissertation submitted in fulfilment of the requirements for the degree of Master of Science (Geology) at the University of Cape Town, Cape Town, South Africa.

Department of Geological Sciences
April 1998

ABSTRACT

The Otavi Mountain Land is a base metal ore province in which base metal sulphide deposits are hosted by platform carbonates in a foreland fold-and-thrust belt on the northern edge of the Pan- African Damara Belt. Deposits have been classified as the Berg Aukas- and Tsumeb-types, based on differences in ore association, stratigraphic position and geochemistry of ores and gangue carbonates. Mineralisation at each of these deposits is accompanied by carbonate alteration in the form of dolomite and calcite veins, carbonate recrystallisation, calcitisation and carbonate silicification.

Optical cathodoluminescence imaging, electron probe micro analysis, X-ray fluorescence spectrometry, X-ray diffraction, high performance ion chromatography, proton probe micro analysis, stable isotope techniques, and fluid inclusion microthermometry were employed (i) to differentiate between carbonate generations associated with the alteration and mineralisation, particularly for the more economic Tsumeb-type deposits, represented by Tsumeb and Kombat, as well as in comparing between Berg Aukas- and Tsumeb-type deposits; (ii) to set constraints on the fluids effecting such alteration and associated mineralisation; (iii) to determine the relationship of the Khusib Springs deposit, for which little geochemical data exists, to deposits of the Tsumeb-type, and (iv) to identify those parameters which are diagnostic of Tsumeb-type mineralisation.

Carbonate generations within each deposit can be grouped into barren and mineralised carbonates. The mineralised carbonates show slight differences which can be explained by changes in physicochemical conditions such as Eh, pH, temperature, stratigraphic controls and fluid rock interaction. These indicate that the ore-bearing fluids precipitated sulphides under reducing, acidic, high temperature conditions. These were followed by oxidising, alkaline, lower temperature conditions during which ore remobilisation took place. Stark differences, especially in trace element concentrations, compared to host rocks for Tsumeb-type deposits indicate that fluids which precipitated the alteration phases and associated mineralisation, were derived from a source outside the Otavi Mountain Land, in contrast to

fluids responsible for Berg Aukas-type mineralisation. Fluid salinities, on the other hand, appear to be very similar for both Berg Aukas- and Tsumeb-type mineralisation, in contrast to previous findings. The salinities for both fluid types were likely derived from evaporitic formation waters. Former evaporite deposits probably also provided the sulphur source for the mineralisation. Similarities in trace element content, formation temperatures, ore associations, and structural relations point to a strong Tsumeb-type affinity for the Khusib Springs deposit. Furthermore, stable isotope ratios for carbonate alteration phases at Khusib Springs are distinct from those for carbonate alteration at Berg Aukas. Enrichments in Mn, Sr, Y and REE in carbonate alteration phases relative to the host rock compositions, and higher temperatures of formation, are diagnostic of economic Tsumeb-type mineralisation. Integration of all geochemical aspects, in conjunction with structural and stratigraphic controls, may help in identifying and further exploiting economic mineralisation in the Otavi Mountain Land.

TABLE OF CONTENTS

ABSTRACT i

LIST OF FIGURES vii

LIST OF TABLES xi

CHAPTER ONE: INTRODUCTION 1

1.1 Introduction 1
1.2 Aims of study and methods of approach 3
1.3 Previous work 4

CHAPTER TWO: GEOLOGICAL SETTING OF THE OTAVI MOUNTAIN LAND 6

2.1 Introduction 6
2.2 Tectono-stratigraphic setting of the Otavi Mountain Land 6
Tectonic history 9
2.3 Geology of the Otavi Mountain Land 13
2.3.1 Stratigraphy 13
2.3.2 Structure 19
2.3.3 Metamorphism 20

CHAPTER THREE: GEOLOGY OF MAJOR ORE DEPOSITS IN THE OTAVI MOUNTAIN LAND 21

3.1 Introduction 21
3.2 Tsumeb-type deposits 21
3.2.1 Tsumeb 21
3.2.1.1 Stratigraphy 21
3.2.1.2 Rock types 24
3.2.1.3 Structure 25
3.2.1.4 Alteration 26
3.2.1.5 Mineralisation 26
3.2.2 Kombat 27
3.2.2.1 Stratigraphy 27
3.2.2.2 Rock types 27
3.2.2.3 Structure and deformation 30
3.2.2.4 Alteration 31
3.2.2.5 Mineralisation 33

3.2.3 Khusib Springs..... 33
3.2.3.1 Stratigraphy..... 34
3.2.3.2 Rock types..... 34
3.2.3.3 Structure..... 35
3.2.3.4 Alteration..... 38
3.2.3.5 Mineralisation..... 39
3.3 Berg Aukas-type deposits..... 40
Berg Aukas..... 40

CHAPTER FOUR: ALTERATION..... **42**

4.1 Introduction..... 42
4.2 Petrography and mineralogy..... 43
4.2.1 Tsumeb..... 43
4.2.2 Khusib Springs..... 44
4.2.3 Kombat..... 46
4.2.4 Berg Aukas..... 47
4.3 Carbonate mineral chemistry..... 51
4.4 Paragenesis..... 55
4.4.1 Tsumeb..... 55
4.4.2 Khusib Springs..... 56
4.4.3 Kombat..... 58

CHAPTER FIVE: ELEMENTAL DISTRIBUTION..... **59**

5.1 Introduction..... 59
5.2 Trace element distribution..... 59
5.2.1 Analytical methods..... 59
5.2.2 Results..... 60
5.2.2.1 Tsumeb..... 60
5.2.2.2 Khusib Springs..... 64
5.2.2.3 Kombat..... 64
5.2.2.4 Berg Aukas..... 66
5.3 Rare earth element distribution..... 67
5.3.1 Analytical methods..... 67
5.3.2 Results..... 68
5.3.2.1 Tsumeb..... 68
5.3.2.2 Khusib Springs..... 69
5.3.2.3 Kombat..... 70
5.3.2.4 Berg Aukas..... 70

6. STABLE (C, O) ISOTOPE DISTRIBUTION 72

6.1 Introduction 72
6.1.1 Terminology 72
6.1.2 Oxygen and carbon isotopes in hydrothermal ore deposits 73
6.1.3 Aims 75
6.2 Analytical methods 75
6.3 Results 75
6.3.1 Tsumeb 75
6.3.2 Khûsib Springs 77
6.3.3 Kombat 77
6.3.4 Berg Aukas 79
6.4 Comparison between deposits 79

CHAPTER SEVEN: FLUID INCLUSION STUDIES **81**

7.1 Introduction 81
7.2 Aims 81
7.3 Microthermometry 81
7.3.1 Petrography 81
7.3.1.1 Tsumeb 82
7.3.1.2 Khusib Springs 84
7.3.1.3 Kombat 85
7.3.2 Results 86
7.3.2.1 Tsumeb 86
7.3.2.2 Khusib Springs 88
7.3.2.3 Kombat 91
7.4 Fluid chemistry 91
7.4.1 Feasibility of bulk chemical analysis 91
7.4.2 Methods 92
7.4.2.1 Crush-leach analysis, using High Performance Ion Chromatography (HPIC) 93
7.4.2.2 Proton-induced X-ray emission (PIXE) analysis of fluid inclusions 93
7.4.2.3 Comparison of PIXE and HPIC as tools for the detection of Na, Br and Cl in carbonate-hosted fluid inclusions 93
7.4.3 Results of crush-leach experiments 96
7.5 Discussion 98
7.5.1 Comparison of fluid composition determined by bulk chemistry and microthermometry 98
7.5.2 Na-Br-Cl systematics: overview and application to the present study 102
7.5.2.1 Seawater composition 104
7.5.2.2 Na-Br-Cl systematics of Otavi Mountain Land leachates 105
(a) Mass balance considerations 106
(b) Salinity relations 109

CHAPTER EIGHT: DISCUSSION **111**

8.1 Berg Aukas-type mineralisation 111
8.2 Tsumeb-type mineralisation 113

CHAPTER NINE: CONCLUSIONS **129**

Implications for exploration 130

ACKNOWLEDGEMENTS **132**

REFERENCES **134**

APPENDICES

A1 Sample descriptions and localities A-1
A2 Analytical techniques and data tables A-6
A2.1 Optical cathodoluminescence imagery A-6
A2.2 Electron probe microanalysis A-6
A2.3 X-ray fluorescence spectrometry A-11
A2.4 REE analysis A-13
A2.5 Stable (C, O) isotope analysis A-16
A2.6 Microthermometry A-21
A2.7 Crush-leach method of bulk fluid inclusion analysis A-27

LIST OF FIGURES

Figure 1.1 Sketch map of Namibia, showing the locality of the Otavi Mountain Land, and important deposits under consideration in this study. 1 = Tsumeb; 2 = Khusib Springs; 3 = Kombat; 4 = Berg Aukas.

Figure 2.1 Post-orogenic positions of Pan-African rift sequences in the southern part of Africa and the eastern part of South America (after Frimmel *et al.*, 1996; Frimmel and Frank, 1998). *WC* = West Congo Belt; *L* = Lufilian Arc; *Z* = Zambezi Belt; *S* = Saldania Belt; *R* = Ribeira Belt.

Figure 2.2 Map of the Damara and Kaoko belts, showing tectonostratigraphic zones (after Miller, 1983). Rectangle shows position of the OML.

Figure 2.3 Positions of pre-orogenic rift structures during early depositional evolution of the Damara and Kaoko belts. Rift margins have been inferred from facies analysis rather than fault exposure (Frimmel *et al.*, 1997, after Porada, 1989). Rifts: 1 = Kaoko Rift, 2 = Sesfontein Rift, 3 = Northern Rift, 4 = Central Rift (half graben), 5 = Southern Rift (half graben), 6 = Khomas Rift (hypothetical). Black areas are basement exposures. The Kaoko and Sesfontein rifts represent opening of the Adamastor Ocean to the west, whereas the Northern and combined Central, Southern and Khomas rifts represent opening of the Khomas Sea between the Kalahari and Angola plates.

Figure 2.4 Geological map of the Otavi Mountain Land, showing major occurrences of Tsumeb- and Berg Aukas type mineralisation. (after Frimmel *et al.*, 1997).

Figure 3.1 Map of the surface geology around the Tsumeb Mine (from Lombaard *et al.*, 1986).

Figure 3.2 Section of the Tsumeb pipe, looking approximately west (after Hughes, 1987; Theron, 1994). Zones of carbonate alteration, mineralisation and rock types are as shown. The stromatolite beds present in the lower part of zone T6 are called Tutten 1, 2 and 3.

Figure 3.3 (**a**) Surface geology of the Kombat group of deposits, with horizontal projections of the ore bodies, and cross sections of the (**b**) Asis West; (**c**) Kombat Central and (**d**) E900 ore bodies (from Innes and Chaplin, 1986).

Figure 3.4 Schematic section of a Kombat-type ore lens, showing distribution of alteration and ore at the contact between phyllite of the Kombat Formation, and dolostone of the Hüttenberg Formation (from Deane, 1995).

Figure 3.5 (**a**) Surface plan of the Khusib Springs mining area, showing the horizontal projection of the ore body (after King, 1995; Verran, 1996). Cross section C-D is given in Appedix A1.

Figure 3.5 (**b**) Cross section A-B from Figure 3.5 (a), showing the position of the massive and disseminated ore in the dolomite (T3) succession at Khusib Springs (after King, 1995; Verran, 1996).

Figure 3.6 Simplified N-S section through the Berg Aukas deposit, looking east, and showing the position of the Northern Ore Horizon, Central Ore Body and Hanging Wall Ore Body, along with carbonate rock types present (from Chadwick, 1993).

Figure 4.1 (**a**) Transmitted light (PPL) photomicrograph of sparry dolomite (SD) and dolomicrite host (H) at Tsumeb; (**b**) CL image encompassing the area in (a) in the middle left portion of the image; (**c**) transmitted light (PPL) photomicrograph of coarsely recrystallised dolomite at Tsumeb; (**d**) CL image encompassing area in (c) towards the middle portion of the image.

Figure 4.2 (**a**) Transmitted light (PPL) photomicrograph of dolomicrite host (H) with Fe-bearing dolomite (FD) crystals showing Fe-oxide rich edges and surrounded by sparry dolomite (SD) at Khusib Springs; (**b**) CL image of the same area. Calcitic zones (C) not evident in PPL, are delineated by their different CL colour to the dolomites.

Figure 4.3 CL image of pink sparry calcite associated with Fe-Mn oxide ore at Kombat. Zoning

towards a more red CL colour near the contact with the ore is evident.

Figure 4.4 (**a**) Transmitted light (PPL) photomicrograph of rhythmite of the Dolomite II (DII) generation of Frimmel *et al.* (1997), and sparry dolomite of the Dolomite IV (DIV) generation at Berg Aukas; (**b**) CL image showing the rhythmite banding on a larger scale. The transmitted light photograph is from the upper right portion of the CL image.

Figure 4.5 Variations in the $MgCO_3/CaCO_3$ ratio of different dolomite generations at Tsumeb, Khusib Springs and Kombat.

Figure 4.6 Compositional plots of different carbonate alteration types at Tsumeb, Khusib Springs and Kombat.

Figure 5.1 Trace element distribution in different carbonate generations at Tsumeb, normalised to the least altered host Dolomite I (sample 2965/300).

Figure 5.2 Trace element distribution in different carbonate generations at Khusib Springs, normalised to the least altered host Dolomite I (sample KH91/181.85).

Figure 5.3 Trace element distribution in different carbonate generations at Kombat, normalised to the least altered host Dolomite I (sample DCK1).

Figure 5.4 Trace element distributions in different carbonate generations at Berg Aukas, normalised to the host Dolomite I (sample Q1-4(I)).

Figure 5.5 Chondrite-normalised REE abundances in carbonate generations as observed at (**a**) Tsumeb, (**b**) Khusib Springs, (**c**) Kombat and (**d**) Berg Aukas. Dol = Dolomite; Cal = Calcite; Qtz = Quartz; gyp = gypsum association. Chondrite composition after Sun and McDonough (1989).

Figure 6.1 $\delta^{13}C$ vs $\delta^{18}O$ plots for carbonate generations from the four major deposits in the OML. Cal-s= calcite with native sulphur; for other mineral abbreviations, see Figure 5.5.

Figure 6.2 Plot of fields of hydrothermal carbonates with which base metal sulphide mineralisation is associated at the major deposits of interest in the OML.

Figure 7.1 **(a)** Fluid inclusion types; **(b)** occurrence in dolomite and quartz at Tsumeb; **(c)** occurrence in dolomite at Khusib Springs.

Figure 7.2 Histograms of salinity and T_h for aqueous inclusions in **(a)** quartz associated with Calcite II, Tsumeb, **(b)** Dolomite III and associated quartz, Tsumeb and **(c)** Dolomite II and associated quartz, Khusib Springs.

Figure 7.3 T_h vs Salinity plots for aqueous inclusions hosted in **(a)** quartz (samples 3153/18 and 3153/36) associated with Calcite II, Tsumeb, **(b)** Dolomite III (sample 2965/106) and associated quartz (samples 2944/248, 2944/225, DCT4, DCT5), Tsumeb and **(c)** Dolomite II (sample DV30 D) and associated quartz (samples DV30 Q and KH62/75.3 Q).

Figure 7.4 Diagram comparing magnitudes of errors (1σ) in the determination of Cl/Br ratios using HPIC as opposed to PIXE as analytical methods for the determination of Br and Cl concentrations in fluid inclusions.

Figure 7.5 Compositional plots of fluid inclusion leachates from different minerals.

Figure 7.6 Bivariate plot of fluid composition in terms of anion and cation ratios. The charge imbalance is expressed as CO_3^{2-}, which, in turn, comprises a number of related species such as HCO_3^-, H_2CO_3 and COO^-. All data plot above the 1:1 curve, indicating a predominance of Cl^- over Na^+ in the fluids. T_e tends to be higher as the slope of the regression lines for each generation approach unity.

Figure 7.7 Na-Br-Cl systematics of fluid inclusion leachates from various minerals and carbonate generations at the deposits under consideration. Although no microthermometry data were obtainable for certain generations, leachate compositions of these were nevertheless included in the plot (after, Kesler *et al.*, 1995; mean seawater composition from Horita *et al.*, 1991). Bars on the right indicate errors in the ratios due to instrument conditions.

Figure 8.1 fO_2 vs pH diagram for equal activities of Eu^{2+} and Eu^{3+} at 25°C and 250°C. The SO_4^{2-}/ HS^- equilibrium is also shown for the same temperatures (after Sverjensky, 1984; Pourbaix, 1966). The effects of increasing temperature and complex formation on the Eu redox equilibrium are indicated by arrows.

Figure 8.2 Diagram showing the effect of temperature, fO_2 and pH on the Eu redox boundary at constant pressure (after Bau, 1991). Higher temperatures, coupled with a pH increase, result in increased fO_2 for the reduction of Eu^{3+} to Eu^{2+}.

Figure 8.3 Variation in $\delta^{13}C$ values of relatively unaltered carbonates as a function of their stratigraphic position in the OML. Diamonds and squares = data from Frimmel *et al.* (1997); triangles = data from Kaufman *et al.* (1991); after Frimmel *et al.* (1997).

Figure 8.4 Plot of isochores for the dominant fluid populations characterising the Calcite II, Dolomite III (Tsumeb) and Dolomite II (Khusib Springs) generations.

LIST OF TABLES

Table 2.1 Stratigraphic correlation of the Damara Supergroup in the northern, central and southern parts of the Damara Belt (from Hoffmann, 1989). The Swakop Terrane corresponds to the Central Zone of Miller (1983); Khomas Terrane = Okahandja Lineament Zone and Southern Zone, Hakos Terrane = Southern Margin Zone; Zaris Basin and Witvlei Ridge = Southern Foreland and Platform. The Chuos Formation in the Otavi Mountain Land has been renamed the Ghaub Formation (Hoffmann and Prave, 1996); Naauwpoort Formation volcanics inthe lower Nosib Group correspond to the Askevold Formation volcanics of SACS (1980).

Table 2.2 Lithostratigraphic column of the Damara Supergroup as exposed in the Otavi Mountain Land (after SACS, 1980; Hoffmann, 1989; Hoffmann and Prave, 1996).

Table 4.1 Compositional ranges (wt%) of different carbonate generations at Tsumeb, Khusib Springs and Kombat.

Table 5.1 Trace element compositions of carbonate generations from Tsumeb, Khusib Springs, Kombat and Berg Aukas.

Table 8.1 $\delta^{18}O$ isotope-temperature relations and the calculation of δ Ö of fluids associated with mineralisation.

Table A 2.2.1 Standards, lower limits of detection (LLD) and counting statistics for analysed samples.

Table A2.2.2 Carbonate mineral compositions (wt% carbonate) for various generations from Tsumeb, Khusib Springs and Kombat.

Table A2.3.1 Lower limits of detection (LLD) and counting statistics for trace element analysis by XRF.

Table A2.4.1 Reproducibility of the rare-earth element determination by HPIC (after le Roex and Watkins, 1990).

Table A2.4.2 Accuracy and precision of REE data for synthetic standard Std-S against Std-A, after on-line concentration (n=5) (after Ridley, 1992).

Table A2.5.1 Stable (C, O) isotope data (‰) for various carbonate generations from Tsumeb, Khusib Springs, Kombat and Berg Aukas.

Table A2.6.1 Fluid inclusion data.

Table A2.7.1 Reproducibility determinations of Na^+ and K^+ on standards AK1, AK3 and AK4.

Table A2.7.2 Repeat analyses for Cl^- and Br^- in Std AN3.

Table A2.7.3 Anion and cation concentrations, and pertinent molar ratios from fluid inclusion leachates.

CHAPTER ONE: INTRODUCTION

1.1 INTRODUCTION

The Otavi Mountain Land (OML) is a base metal ore province situated in northern Namibia, ~ 400 km north of Windhoek. This ore province covers an area of ~10 000 km^2, encompassing the towns of Tsumeb, Grootfontein and Otavi (Fig. 1.1). Over 600 occurrences of Cu-Pb-Zn mineralisation are known from here, a number of these with associated Ag and V. The mineralisation is hosted by late Proterozoic platform carbonates of the Otavi Group in a foreland fold-and-thrust belt on the northern margin of the Damara Belt.

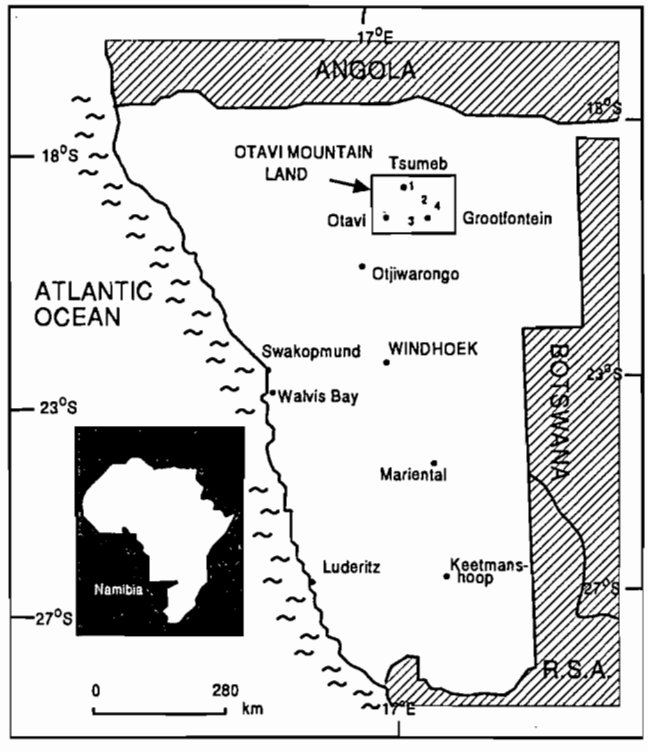

Figure 1.1 Sketch map of Namibia, showing the locality of the Otavi Mountain Land, and important deposits under consideration in this study. 1 = Tsumeb; 2 = Khusib Springs; 3 = Kombat; 4 = Berg Aukas.

The largest deposits of note in the OML are Tsumeb, Kombat, Berg Aukas, Abenab, and the Khusib Springs deposit, at which mining operations recently (1995) began. The only other currently mined ore bodies are those of Kombat. The Berg Aukas and Abenab deposits are no longer considered economically viable. Mining of these deposits had ceased by the 1970's. Operations at Tsumeb came to an end in 1996, owing to diminished reserves.

On a broad scale, the various base metal sulphide deposits of the OML have many characteristics in common, and a number of views have been put forward concerning their genesis (Lombaard *et al.*, 1986; Innes and Chaplin, 1986; Misiewicz, 1988). The mineralisation is hosted by carbonates, and is epigenetic in nature, with karsting having played a prominent role in developing porosity for ore mineral deposition from circulating hydrothermal fluids. However, salient differences between the various deposits have led workers to differentiate between two types of base metal sulphide deposits in the OML: the Tsumeb- and Berg Aukas-types, after the type localities (Hughes, 1987; Misiewicz, 1988; Pirajno, 1992; Pirajno and Joubert, 1993; Frimmel *et al.*, 1997).

Berg Aukas-type deposits host Pb-Zn-V mineralisation comparable to the Mississippi Valley Type (MVT), whereas Tsumeb-type deposits are highly cupriferous, with variable amounts of Pb, Zn and Ag. It is the cupriferous nature of the Tsumeb-type which makes it the favoured base metal mineralisation for exploitation at present. Berg Aukas-type deposits are stratabound and confined to lower stratigraphic levels within the Otavi Group (Abenab Subgroup), whereas Tsumeb-type deposits are cross-cutting, and usually confined to the upper part of the Otavi Group (Tsumeb Subgroup). In addition, differences with respect to ore mineralogy, geochemistry, and geological features, have led workers to conclude that Berg Aukas- and Tsumeb-types of mineralisation were spatially and temporally distinct (Pirajno and Joubert, 1993; Frimmel *et al.*, 1997).

The deposits classified as Tsumeb-type are Tsumeb, the type locality, and ore bodies at Kombat, whereas Berg Aukas and Abenab constitute the Berg Aukas-type. The Khusib Springs deposit has provisionally been classified under the Tsumeb-type, primarily on the basis of its cupriferous nature and the perceived timing of the mineralisation.

1.2 AIMS OF STUDY AND METHODS OF APPROACH

The gangue phases in ore deposits are just as significant as the ores in that they provide valuable information on the conditions of the mineralising fluid during ore precipitation. To this end, geochemical characterisation of the carbonate alteration around base metal sulphide deposits in the OML not only allows comparisons to be made, but can also be used in setting constraints on ore genesis. The prime aspect with which this study is concerned is therefore the geochemistry of carbonate wall rock alteration within and around selected base metal sulphide deposits in the OML. As Tsumeb-type deposits are considered economically favourable, geochemical aspects of carbonate alteration were investigated for Tsumeb, Kombat and Khusib Springs. In certain instances, data were also collected on carbonate alteration products from the Berg Aukas deposit for comparative purposes.

The aims of the project were:

- to compare different generations of carbonate alteration within and between each of the deposits under consideration, in terms of their geochemical characteristics;
- from the gathered information and literature, to set constraints on the fluids responsible for effecting the alteration, and hence the associated mineralisation; in addition, fluids responsible for Tsumeb- as opposed to Berg Aukas-type mineralisation could be compared;
- to determine the relationship of the Khusib Springs deposit to Tsumeb-type mineralisation;
- to determine which geochemical parameters, if any, are diagnostic of the presence of economic mineralisation of the Tsumeb-type. Such parameters could then be implemented in geochemical exploration for such deposits.

The methods employed in the investigation of various geochemical parameter were:

- optical cathodoluminescence (CL) imaging, of carbonate generations, as a means of differentiating between them;
- electron probe microanalysis (EPMA) for carbonate mineral chemistry;
- X-ray fluorescence spectrometry (XRF) and gradient high performance ion

chromatography (HPIC) for determining trace element, including rare earth element (REE) distribution in the various carbonate generations;

- use of an existing C and O isotope line, as well as the Bremen technique, for determining C and O isotope ratios in various carbonate generations; qualitative X-ray diffraction (XRD) was employed during sample preparation for stable isotope analysis;
- fluid inclusion microthermometry, for obtaining homogenisation temperatures and salinities of fluid inclusions in appropriate gangue phases;
- the crush leach technique, using HPIC as a means of determining ionic compositions of fluid inclusion leachates; proton probe micro analysis for Br and Cl in fluid inclusions was also investigated, and compared with the crush-leach technique.

1.3 PREVIOUS WORK

Although a number of geochemical studies have been carried out on the various deposits in the OML, the bulk of these involved isotope and trace element analysis of the ores (e.g. Allsopp *et al.*, 1981; Emslie and Beukes, 1981; Lombaard *et al.*, 1986; Innes and Chaplin, 1986; Hughes, 1987). Very few studies have concentrated on the geochemistry of carbonate wall rock alteration around the deposits. Where this has been the case, C, O and Sr isotope studies were carried out on alteration phases (e.g. Allsopp and Ferguson, 1970; Hughes, 1987; Theron and Beukes, 1993; 1995; Frimmel *et al.*, 1997). The findings of the various workers are discussed in Chapters 6 and 8.

Aspects such as trace element studies have only been dealt with to a small extent in unpublished reports for Goldfields Namibia Limited (GFNL) by Theron and Beukes (1992; 1993). These involved microscopic scale analysis for Mn, Fe, Sr, and the base metals in diagenetic and hydrothermal alteration products around the North Break Zone at Tsumeb. Mn and Sr were found to be enriched in the hydrothermal phases relative to host dolomite compositions, accompanied by a depletion in Fe concentration. No trends were observed with respect to the base metals. Rare earth element (REE) distribution in carbonate alteration products around base metal deposits in the OML, has not been investigated by previous workers, in spite of its wide applicability in the

study of MVT and other carbonate-hosted Pb-Zn deposits (Graf, 1984; Lottermoser, 1992; McLennan, 1989; Möller *et al.*, 1979).

Fluid inclusion studies in the OML were conducted by Ypma (1978; 1984), the results of which were presented in unpublished reports for the Tsumeb Corporation Limited (TCL) and Department of Economic Geology, University of Adelaide. These included studies on the Tsumeb, Berg Aukas and Kombat deposits. Haynes (1984) studied a limited number of fluid inclusions in quartz gangue from Tsumeb, and used the results in discussing ore paragenesis. Misiewicz (1988) conducted limited microthermometry on sphalerite and dolomite from the Berg Aukas deposit. Later studies were carried out by King (1990) on mineralised quartz veins from the Olifantsfontein grant in the Khusib Springs/Berg Aukas vicinity. Although the results of these workers point to generally high salinity fluids (~23 wt% $NaCl_{eq}$) for Berg Aukas-type mineralisation, and lower salinity fluids (~2-12 wt% $NaCl_{eq}$) for Tsumeb-type mineralisation, discrepancies remained with respect to the relationships between the fluids studied and the main phases of mineralisation.

Geochemical research on the recently discovered (1993) Khusib Springs deposit has been only very limited to date. Some preliminary stable isotope (C, O) and fluid inclusion data for carbonate alteration phases were presented in an unpublished Honours thesis by Verran (1996). With the exception of an extended abstract (Chetty *et al.*, 1997), no work on this deposit has been published to date.

CHAPTER TWO: GEOLOGICAL SETTING OF THE OTAVI MOUNTAIN LAND

2.1 INTRODUCTION

Before discussing the major base metal sulphide ore deposits in the OML, it is pertinent to consider their geological setting in terms of the OML and its tectono-stratigraphic relationship with the Damara Belt. This chapter deals with the OML in the larger context of the Damaran orogeny, followed by regional stratigraphy, structure and metamorphism in the OML base metal province.

2.2 TECTONO-STRATIGRAPHIC SETTING OF THE OTAVI MOUNTAIN LAND

As already mentioned, the OML is a base metal ore province in which deposits are hosted by platform carbonates in a foreland fold-and-thrust belt on the northern margin of the Damara Belt. The Damara Belt is a 400 km wide, NE-trending intracontinental belt, and is one of three Neoproterozoic (Pan African) belts in Namibia, the other two being the Kaoko and Gariep belts (Fig. 2.1). The three belts are closely linked in terms of their tectonic evolution, and can be correlated with a series of Pan African rift sequences and associated passive margin deposits, evolved into orogenic belts which surround and transect the present African and South American continents (Miller, 1983; Porada, 1989; Fig. 2.1). The coastal Kaoko and Gariep belts are only partially preserved, owing to the opening of the modern Atlantic Ocean during the Cretaceous (Stanistreet *et al.*, 1991). However, the South American equivalent may be found in the Dom Feliciano Belt flanking the Rio de la Plata Plate in South America (Fernandes *et al.*, 1992). On the African continent, the Kaoko and Damara Belts flank the Angola Plate to the north, whereas the Damara and Gariep belts flank the Kalahari Plate to the south (Fig. 2.1).

The Damara Belt has been divided into a number of zones based on stratigraphy, structure,

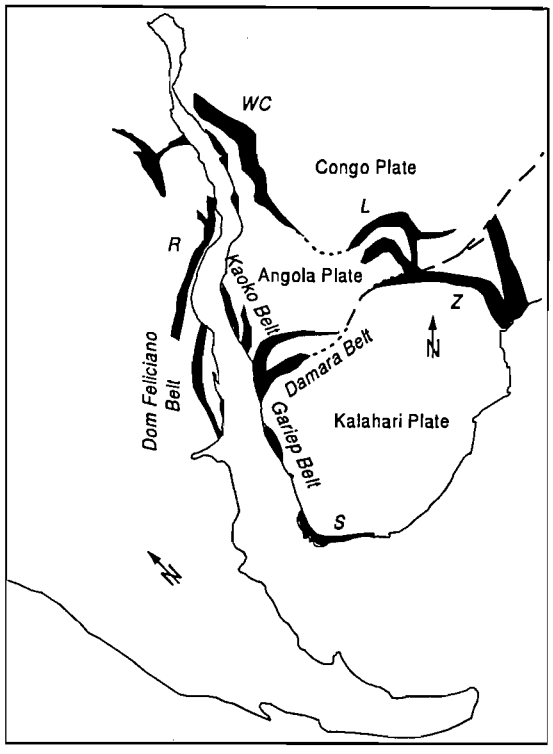

Figure 2.1 Post-orogenic positions of Pan-African rift sequences in the southern part of Africa and the eastern part of South America (after Frimmel *et al.*, 1996; Frimmel and Frank, 1998). *WC* = West Congo Belt; *L* = Lufilian Arc; *Z* = Zambezi Belt; *S* = Saldania Belt; *R* = Ribeira Belt.

metamorphic grade and aeromagnetic characteristics (Miller, 1983). From north to south these are (Fig. 2.2): the Northern Platform (NP), Northern Zone (NZ), Central Zone (CZ), Okahandja Lineament Zone (OLZ), Southern Zone (SZ) and Southern Marginal Zone (SMZ). Further south, a Southern Foreland (SF) grades into an undeformed Southern Platform. In this area, Hoffmann (1989) distinguished between the Witvlei Ridge to the north, and the Zaris Basin to the south. These zones are bounded by faults, major lineaments, or approximate stratigraphic boundaries (Miller, 1983; Fig. 2.2). Hoffmann (1989) referred to the Central Zone as the Swakop Terrane, and the Southern Marginal Zone as the Hakos Terrane. The Okahandja Lineament Zone and the Southern Zone together represent the Khomas Terrane (also known as the Khomas Trough, Miller, 1983).

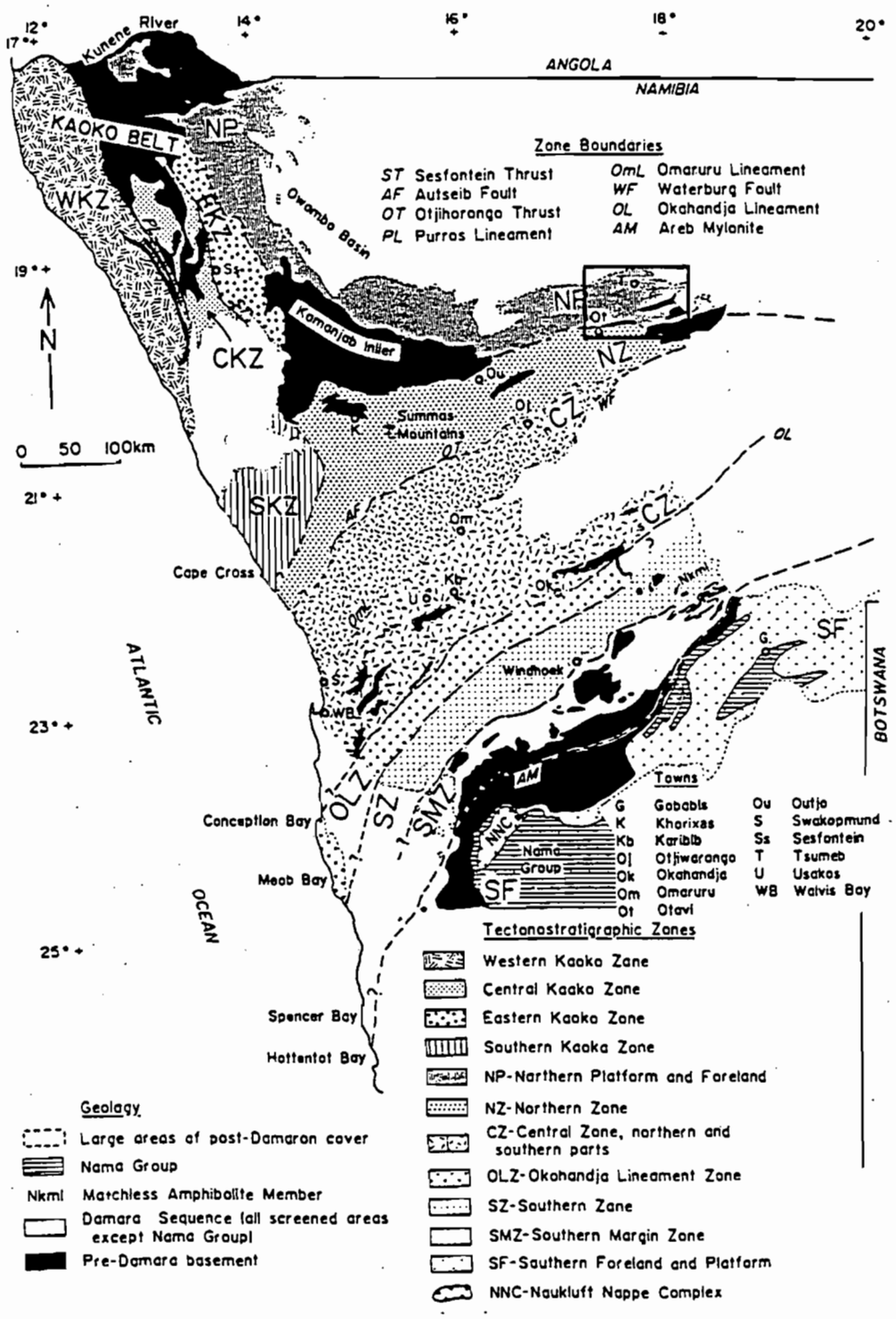

Figure 2.2 Map of the Damara and Kaoko belts, showing tectonostratigraphic zones (after Miller, 1983). Rectangle shows position of the OML.

The OML is located at the eastern end of the Northern Platform, which, in turn, is flanked by the Kaoko Belt to the west, and the Northern Zone of the Damara Belt to the south. Carbonate sedimentation occurred to the north of Pre-Damara basement palaeohighs separating the Northern Platform and Northern Zone. The Kamanjab Inlier (Fig. 2.2) is an example of such a palaeohigh exposed to the west. In the OML the palaeohighs are exposed as the Grootfontein basement complex. The sedimentary succession which was deposited and deformed during periods of extension and compression in the Damara Belt, is referred to as the Damara Supergroup. This succession, as it occurs in the Northern Platform, central and southern parts of the Damara Belt, is shown in the stratigraphic column in Table 2.1 (Hoffmann, 1989). In the OML, carbonate sedimentation is reflected by the Otavi Group, which hosts the base metal sulphide mineralisation.

Tectonic history of the Otavi Mountain Land

Rifting of the supercontinent which had amalgamated during the Kibaran orogeny (~1.0 Ga) resulted in the separation of the Angola, Kalahari and South American (Rio de la Plata) plates. During this phase, a series of NE trending rift grabens developed between the Angola Plate to the north and the Kalahari Plate to the south. These grabens have been identified as the Northern, Central, Khomas and Southern Rifts (Fig. 2.3) which developed into an oceanic basin, the Khomas Sea (Miller, 1983; Porada, 1989). The rifting phase was accompanied by bimodal volcanism and coarse clastic sedimentation (Nosib Group). Minimum age constraints (single zircon U-Pb) from rift-related igneous rocks are placed at 756±2 Ma for terrigenous sedimentation in the lower Nosib Group (Hoffman *et al.*, 1996). Felsic volcanics in the upper part of the Nosib Group in the Summas Mountains area yielded a U-Pb age of 746±2 Ma (Hoffman *et al.*, 1996). Thus igneous activity associated with the rifting phase is believed to have lasted for at least 10 Ma. To the west, rifting between the African (Angola, Kalahari) and South American plates (Rio de la Plata) resulted in the opening of the so-called Adamastor Ocean (Hartnady *et al.*, 1985; Stanistreet *et al.*, 1991). In the Gariep Belt, rifting is thought to have occurred between ~781 and 741 Ma (Frimmel *et al.*, 1996; Frimmel and Frank, 1998).

Table 2.1 Stratigraphic correlation of the Damara Supergroup in the northern, central and southern parts of the Damara Belt (from Hoffmann, 1989). The Swakop Terrane corresponds to the Central Zone of Miller (1983); Khomas Terrane = Okahandja Lineament Zone and Southern Zone, Hakos Terrane = Southern Margin Zone; Zaris Basin and Witvlei Ridge = Southern Foreland and Platform. The Chuos Formation in the Otavi Mountain Land has been renamed the Ghaub Formation (Hoffmann and Prave, 1996); Naauwpoort Formation volcanics in the lower Nosib Group correspond to the Askevold Formation volcanics of SACS (1980).

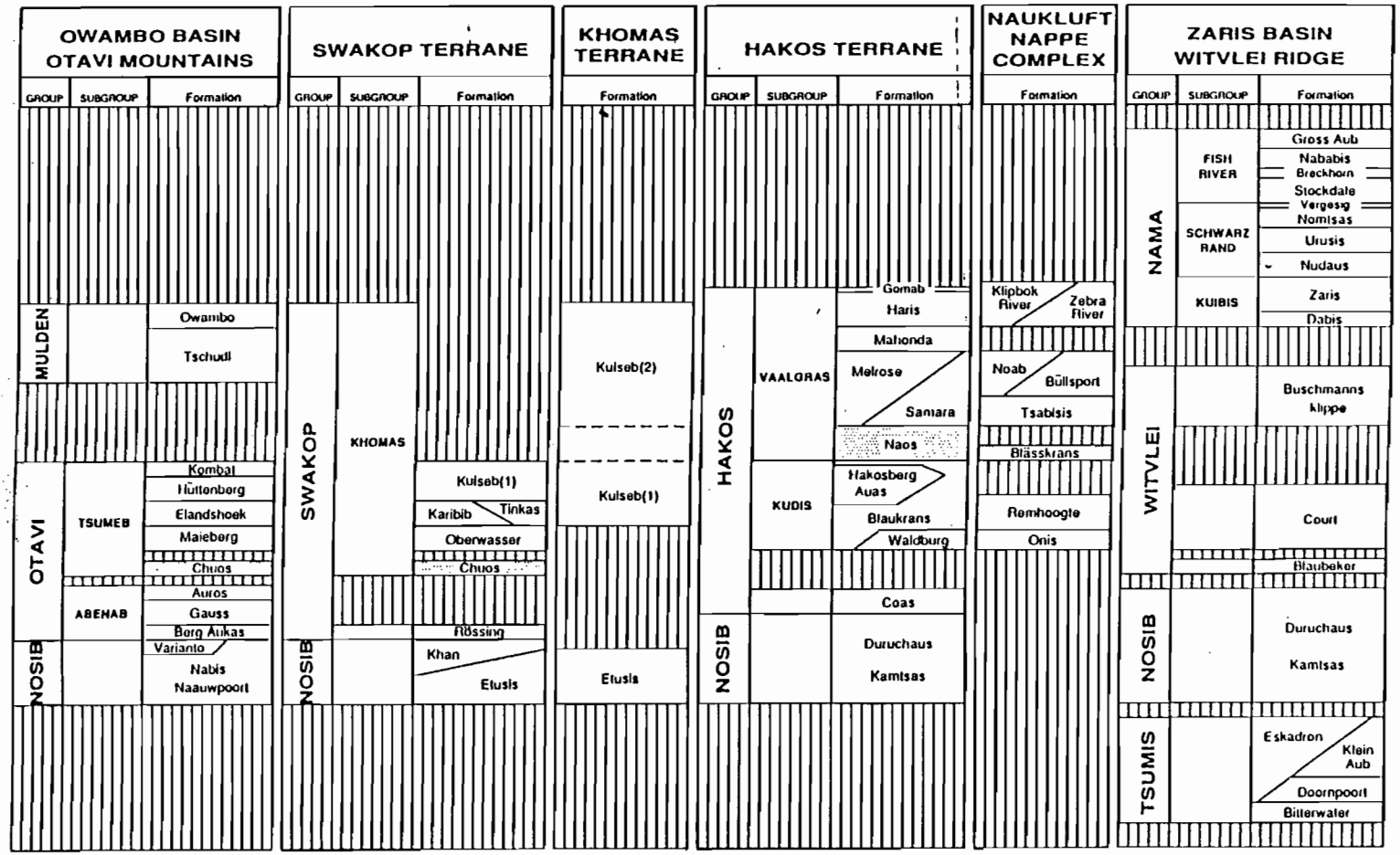

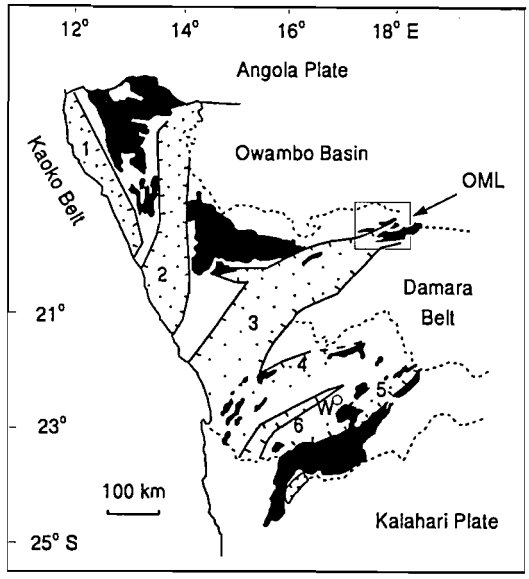

Figure 2.3 Positions of pre-orogenic rift structures during early depositional evolution of the Damara and Kaoko belts. Rift margins have been inferred from facies analysis rather than fault exposure (Frimmel *et al.*, 1997; after Porada, 1989). Rifts: 1 = Kaoko Rift, 2 = Sesfontein Rift, 3 = Northern Rift, 4 = Central Rift (half graben), 5 = Southern Rift (half graben), 6 = Khomas Rift (hypothetical). Black areas are basement exposures. The Kaoko and Sesfontein rifts represent opening of the Adamastor Ocean to the west, whereas the Northern and combined Central, Southern and Khomas rifts represent opening of the Khomas Sea between the Kalahari and Angola plates.

Development of the Khomas Sea led to carbonate shelf sedimentation and subsequent massive turbidite deposition, reflected by sedimentary rocks of the Swakop Group in the central part of the belt. On the northern margin of the Northern Rift, the Nosib Group is not well developed. In addition, owing to the platform environment, massive carbonate sedimentation dominated over clastic sedimentation, such that the turbiditic sequences of the Swakop Group are not developed in the OML, but the Otavi Group carbonates make up the succession instead. Within the carbonate sequence, two diamictite horizons are found. The Varianto Formation, which occurs at the top of the Nosib Group in the OML, and thought to be glaciogenic in origin, is constrained by a minimum age of 747±2 Ma, derived from felsic volcanics in the upper Naauwpoort Formation, directly north of the Summas Mountains (Hoffman *et al.*, 1996). Two glacial episodes

have been recognised worldwide as having taken place during the Neoproterozoic: the Sturtian and the Varangian (Young, 1995; Meert and van de Voo, 1994). The age derived for the Varianto Formation in the OML correlates with that proposed for the Sturtian glacial episode (~750 Ma, Young, 1995; Hoffman *et al.*, 1996).

The second diamictite horizon in the Otavi Group is referred to as the Ghaub Formation[1] (Hoffmann and Prave, 1996). Unless this formation represents a glacial episode not recorded during the Neoproterozoic, it can be correlated with the younger Varangian episode, constrained between 625 and 580 Ma (Meert and van de Voo, 1994). Thus a maximum age constraint for deposition of the Tsumeb Subgroup (Table 2.1) lies within this age range.

Tectonic inversion resulted in closure of the Adamastor Ocean and Khomas Sea. Frimmel and Frank (1998), using Ar-Ar mineral cooling ages for the Gariep Belt and published age data for the Damara Belt, suggested initial closure of the northern Adamastor Ocean, represented by the Kaoko Belt, followed by closure of the Khomas Sea, with subduction of Khomas sea floor sediments and part of the Kalahari Plate to the northwest. This sequence of closure is supported by stratigraphic and sedimentological analysis of Prave (1996). Miller (1983) indirectly dated closure of the Khomas Sea at 650 Ma, based on early syn-tectonic granitoids in the Central Zone. Syn- to post-tectonic granitoids in the Damara Belt (Miller, 1983) were used to constrain timing of collision of the Angola and Kalahari plates between 590 and 550 Ma (Frimmel and Frank, 1998). Finally, closure of the southern Adamastor Ocean and continental collision culminated in the Gariep Belt at 545 Ma.

Closure of the different oceanic basins and subsequent continent-continent collision was accompanied by deformation, uplift and denudation of high-lying areas. In the OML, the Mulden Group was deposited as a syn-tectonic molasse. In addition, mineralisation at Kombat and Tsumeb is thought to have been contemporaneous with deformation related to continental collision in the Damara Belt (Lombaard *et al.*, 1986; Innes and Chaplin, 1986).

---

[1] Previously referred to as the Chuos Formation in the OML (South African Committee for Stratigraphy, SACS, 1980; Hoffmann, 1989, Table 2.1) but renamed the Ghaub Formation, because the Varianto Formation in the OML is now correlated with the regional Chuos Formation (Hoffmann and Prave, 1996; section 2.3.1).

2.3 GEOLOGY OF THE OTAVI MOUNTAIN LAND

The Otavi Mountain Land has been extensively mapped, and its geology well documented by numerous workers, chief amongst them Söhnge (1957), whose detailed mapping formed the basis for subsequent geological work in the OML. Other notable contributions include those of Grobler (1961), Hedberg (1979) and work by Misiewicz (1988). Numerous reports by TCL and GFNL geologists have also contributed to a better understanding of the geology and mineralisation in the OML. Figure 2.4 is a geological map of the OML, showing also major occurrences of Berg Aukas- and Tsumeb-type mineralisation.

2.3.1 Stratigraphy

The Damara Supergroup, as defined in the OML, is shown in the stratigraphic column of Table 2.2, along with a description of the rock types and average thicknesses of the various formations and lithozones. Here, three groups comprise the Damara Supergroup: the lower volcaniclastic succession of the Nosib Group, the carbonate-dominated Otavi Group, and the clastic-dominated Mulden Group. The Otavi Group disconformably overlies the Nosib Group, and in places, unconformably overlies granites and gabbros of the lower Proterozoic Grootfontein basement complex. The Mulden Group, in turn, unconformably overlies the Otavi Group.

The Nosib Group comprises the clastic Nabis and Varianto formations, and the volcanic Askevold Formation (Fig. 2.4, Table 2.2). The Nabis Formation represents clastic graben infill during the rifting phase of the Damara orogeny. The Varianto Formation contains a diamictite/mixtite horizon thought to be of glacial origin (Botha, 1960; Simpson, 1957, in Martin, 1965).

The Otavi Group is well defined in the OML, being the dominant succession in the Northern Platform (Fig. 2.2). The Otavi Group is divided into the lower Abenab Subgroup, and the upper Tsumeb Subgroup, both of which are separated by a disconformity (Table 2.2).

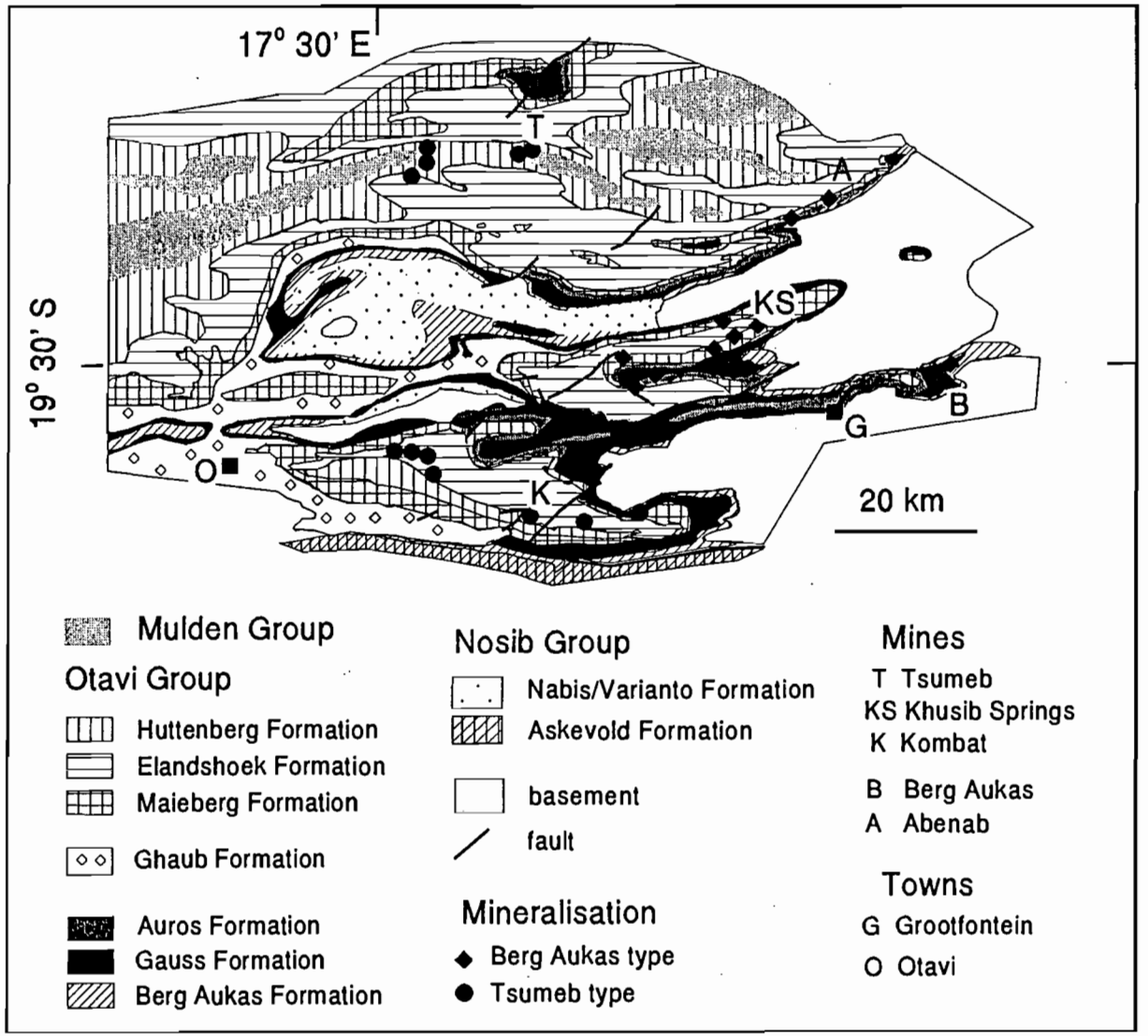

Figure 2.4 Geological map of the Otavi Mountain Land, showing major occurrences of Tsumeb- and Berg Aukas-type mineralisation (after Frimmel *et al.*, 1997).

Table 2.2 Lithostratigraphic column of the Damara Supergroup as exposed in the Otavi Mountain Land (after SACS, 1980; Hoffmann, 1989; Hoffmann and Prave, 1996).

GROUP	SUBGROUP	FORMATION	INFORMAL LITHOZONE	ROCK TYPES	THICKNESS (m)
MULDEN		Owambo		Red vuggy shale, feldspathic sandstone and siltstone, marl, grey to black shale, limestone and dolostone	>700
		Tschudi		Feldspathic sandstone, subgreywacke; argillite and conglomerate interbeds in basal portion	
		DISCONFORMITY			
OTAVI	TSUMEB	Kombat and Hüttenberg	T8	Dolomite, bedded light to medium grey; oolitic chert and stromatolite layers near top; phyllite in Kombat Formation	240
			T7	Dolomite, bedded dark grey; limestone, shale and chert interbeds	300
			T6	Dolomite, bedded light grey; abundant chert; stromatolite interbeds in lower part	300
		Elandshoek	T5	Dolomite, bedded and massive light grey	1200
			T4	Dolomite, massive light grey	
		Maieberg	T3	Dolomite, thinly bedded light and dark grey	180
			T2	Limestone, bedded light and dark grey	700
		Ghaub [+]	T1	Diamictite, quartzite, shale, minor dolomite and limestone	200
		DISCONFORMITY			
	ABENAB	Auros		Dolomite, bedded and massive light to medium grey; limestone, marl, shale, oolite and stromatolite interbeds	350
		Gauss		Dolomite, massive light to dark grey; local oolite and stromatolite interbeds	750
		Berg Aukas		Dolomite, laminated and massive light and dark grey; black limestone, shale	550
		DISCONFORMITY			
NOSIB		Varianto		Quartzite, conglomerate, arkosic mixtite, dolomite, ferruginous shale	?
		Askevold*		Phyllitic agglomerate, tuff; epidosite	750
		Nabis		Feldspathic quartzite, arkose, conglomerate	?
		UNCONFORMITY			
GROOTFONTEIN BASEMENT COMPLEX				Granite, gneiss, mafic schist	

* Naaupoort Formation in Table 2.1

[+] Chuos Formation in Table 2.1

The Abenab Subgroup comprises the Berg Aukas, Gauss and Auros formations. The Berg Aukas Formation is thought to be a transitional sequence between the Nosib Group and the carbonates of the Otavi Group (Miller, 1983). The Gauss Formation comprises sediments accumulated in a platform margin and tidal flat setting (Frimmel *et al.*, 1997). However, the presence of unstratified light grey dolostones of this formation indicate deposition in fairly stable, moderately deep waters, according to Misiewicz (1988). The Auros Formation is thought to have been deposited during shallowing of a sea, as evidenced by stromatolitic reefs.

The Tsumeb Subgroup is a 3000 m thick succession dominated by carbonates, but also including mixtites of the Ghaub Formation (previously Chuos Formation, see below) at its base. From the base to the top, the Tsumeb Subgroup comprises the Ghaub, Maieberg, Elandshoek and Hüttenberg Formations. These formations have been further informally subdivided into eight zones (T1-T8) based on facies and lithological properties (Söhnge, 1957).

The Ghaub Formation (T1) has been described as a tillite, fluvioglacial and debris flow deposit by different workers (Söhnge, 1957, Martin *et al.*, 1985, Henry *et al.*, 1986). Schermerhorn (1975) and Miller (1983) described this unit as a deep water mass flow deposit, whereas Martin (1965) and Kröner and Rankama (1972) attributed it to a glacial/glacial marine origin. Hoffmann, (1990) suggested deposition under continental to shallow glacio-marine conditions. This formation is an important stratigraphic marker in the carbonate succession. However, more recently, Hoffmann and Prave (1996) have suggested a major revision of the lithostratigraphic division based on the correlation of the two diamictites in the OML with those in the Kaokoveld. According to the old nomenclature, the Chuos Formation in the OML and eastern Kaokoveld was thought to be the same horizon, however, the Chuos Formation in the Eastern Kaokoveld has been found to correlate with the Varianto Formation in the OML. A second, thinner diamictite horizon in the Kaokoveld has been correlated with the more extensive Chuos Formation of the OML in the old nomenclature. Hoffmann and Prave (1996) have therefore renamed the Chuos Formation the Ghaub Formation in the OML. Thus, the Varianto Formation in the OML can be correlated with the Chuos Formation in the Kaokoveld, and the Ghaub Formation is found in both the eastern Kaokoveld and OML. It is not clear what the relationship is between the Ghaub Formation in the OML and the Chuos Formation in the Swakop Terrane,

for example. In this dissertation, the Chuos Formation is referred to as the Ghaub Formation, following the proposal of Hoffmann and Prave (1996).

The Maieberg Formation (T2 and T3) is approximately 1800 m thick and widely developed throughout the OML. Laminated carbonates of the T2 lithozone indicate deposition on a platform slope under deepening water conditions. Rhythmites and turbidites grading into slumps and intraformational breccias in this formation in the Kaokoveld led Prave (1996) to conclude that these facies represent sediment gravity-flow deposition under deep basin conditions. The T2 zone comprises limestones, whereas the T3 zone is dolomitised. Extensive karst topography has resulted from subaerial exposure of the limestone sequences. This is further evidenced by the presence of carbonate lithoclasts (Prave, 1996). Hoffmann and Prave (1996) included a basal member, the Keilberg Member to the Maiberg Formation, being a "cap dolostone" to the underlying Ghaub Formation.

The Elandshoek Formation (T4 and T5) overlies the Maieberg Formation conformably. This Formation is also extensively developed and best exposed in the Tsumeb Syncline (Misiewicz, 1988). Although zone T4 comprises predominantly massive dolomite, it also hosts an extensive stratabound zone of brecciation, interpreted as a syndepositional feature caused by creep and slide on a palaeoslope, caused by fault reactivation (Misiewicz, 1988). The regionally extensive brecciation is considered an important regional aquifer, which could have provided conduits for the movement of brines. Some of these breccias are hosts to base metal sulphide mineralisation.

The Hüttenberg Formation conformably overlies the Elandshoek Formation, and comprises zones T6, T7 and T8. It is disconformably overlain by clastic sequences of the Mulden Group. Within the T6 lithozone is a locally developed 10 m thick zone of alteration and brecciation, conformable with the bedding. This is the North Break Zone, which is interpreted as a palaeo-aquifer (Lombaard *et al.*, 1986). Alteration here is manganiferous, ferruginous and calcitic, and base metal contents are anomalous (Misiewicz, 1988). Lithozones T7 and T8 are lagoonal sequences. These mark the change from deeper water environments (Elandshoek and Maieberg Formations), to shallow lagoonal shelves on which algal reefs flourished prior to the pre-Mulden uplift and subaerial exposure. A prominent marker horizon, called the Augen Marker, contains

calcite nodules, interpreted as pseudomorphs after anhydrite (Lombaard *et al.*, 1986). This indicates the development of evaporites in the shallowing environment.

The Mulden Group is a syn-tectonic molasse-type sedimentary sequence (Martin, 1965), and marks the change from marine conditions during Otavi times to a continental regime (Hedberg, 1979). The Mulden Group unconformably overlies the Hüttenberg Formation of the Tsumeb Subgroup in the Otavi Group. Debate exists as to the formations constituting the Mulden Group. According to the South African Committee for Stratigraphy (SACS, 1980), the Mulden Group comprises a lower Tschudi Formation, grading up into shales of the Kombat Formation. Hoffmann (1989) on the other hand, divided the Mulden Group into the lower Tschudi Formation, and an upper Owambo Formation. The Kombat Formation was assigned to the Otavi Group on lithostratigraphic grounds. This division is supported by evidence from stratigraphic investigations by Deane (1995). Frimmel *et al.* (1997), following the same subdivision, attribute the presence of the phyllites of Kombat Formation south of Kombat to rapid drowning of the Northern Rift along a growth fault. To the north, shallow marine carbonates of the upper Tsumeb Subgroup dominated instead. Alternatively, these phyllites may represent prodelta deposits, being a distal equivalent to the Tschudi Formation sandstones (Miller, 1983).

The Tschudi Formation overlies a basal, ill-defined unit of 30-40 m thick subgreywacke and sand-supported chert pebble conglomerate. This basal unit is thought to have been deposited as playa mud flat or shallow lacustrine sediments. The Tschudi Formation was deposited in a deltaic setting. Sedimentation took place on an erosional karst surface, as established by TCL exploration geologists (Misiewicz, 1988). Arenites of the Tschudi Formation were deposited by fluvial processes, with the sediment source being inliers and footwall rocks, as a result of uplift and denudation to the south (and west) of the OML (Hedberg, 1979). The Owambo Formation, as defined by Hoffmann (1989), marks the return to marine conditions after the continental clastic Tschudi sedimentation.

2.3.2 Structure

The structures characterising the Northern Platform and OML have resulted from rifting and orogenic processes during separation and subsequent collision of the Angola and Kalahari plates. The intensity of the deformation brought about by collision decreases northwards in both the Northern Platform and OML.

Structures related to the rifting phase during which the Nosib Group was deposited include basement growth faults which were reactivated during the later stages of rifting, in the development of the Northern Rift. Thus secondary rift grabens formed at the eastern edge of the Northern Rift characterise the basement topography (Misiewicz, 1988).

Structures relating to orogenesis are characterised by EW-trending folds (F_1 of Misiewicz, 1988), related to the D_2 deformational event in the Damara Belt (Miller, 1983; Fig. 2.4). Folds developed perpendicular to these were caused by mild E-W compression, and are ascribed to the D_3 deformational phase of Miller (1983; F_2 of Misiewicz, 1988). Thus overprinting by the second folding event (D_3) caused fold interference, and the formation of a series of doubly plunging synclines, found throughout the Northern Platform (Misiewicz, 1988). The D_1 event has not been recognised in the OML, but only in the Kaoko Belt. D_2 was the most intense phase of deformation and resulted in tight and often overturned recumbent folding, as seen, for example, in the Otavi Valley to the south, where overthrusting to the north is exhibited (Innes and Chaplin, 1986; Deane, 1993). D_3 was less intense, but responsible for widespread jointing and fracturing.

Oblique transverse faults are also present in the OML (Misiewicz, 1988). The major oblique faults trend NE (Fig. 2.4) and are correlated with major lineaments in the Central Zone of the Damara Belt (Fig. 2.2). These faults are regarded as basement features which were reactivated during carbonate sedimentation and the D_2 deformation event.

2.3.3 Metamorphism

The OML has been affected by very low to low grade metamorphism, the peak of which was reached during the regional D_2 deformational phase. The metamorphic grade decreases towards the north. Lower greenschist facies pressure-temperature conditions prevailed in the Kombat area, with the biotite-in isograd in pelitic rocks occurring just south of the OML (Miller, 1983). In addition, the calcite-quartz-dolomite assemblage is stable throughout the OML, except at mineralisation sites. Further to the north in the Owambo Basin, zeolite facies to prehnite-pumpellyite facies mineral assemblages have been recognised in the Mulden Group metasedimentary rocks (Clauer and Kröner, 1979). Peak temperatures reached in the OML have been estimated at 300-400°C. No good constraints on the peak pressure during metamorphism are available. Assuming an average continental geotherm, the low grade metamorphic conditions for the OML could correspond to a peak metamorphic pressure of 2-3 kb (Frimmel *et al.*, 1997).

CHAPTER THREE: GEOLOGY OF MAJOR ORE DEPOSITS IN THE OTAVI MOUNTAIN LAND

3.1 INTRODUCTION

As mentioned previously, the OML is a base metal province in which more than 600 occurrences of base metal sulphide mineralisation have been recognised. This chapter addresses four major ore deposits in the OML, *viz.* Tsumeb, Kombat, Khusib Springs and Berg Aukas. Of these, only Kombat and Khusib Springs are currently mined. Tsumeb is the type locality for Tsumeb-type mineralisation, whereas Berg Aukas typifies the Berg Aukas-type of mineralisation. These latter two deposits are therefore important in describing base metal mineralisation in the OML.

3.2 TSUMEB-TYPE DEPOSITS

3.2.1 Tsumeb

3.2.1.1 Stratigraphy

The Tsumeb ore body is hosted by dolomitic rocks of the upper Elandshoek and Hüttenberg Formations in the Tsumeb Subgroup. The ore body, which forms a pipe-like structure, extends from lithozone T8 in the Hüttenberg Formation, down to lithozone T4 in the Elandshoek Formation (Table 2.2; Figs. 3.1, 3.2). In total, the Tsumeb pipe cuts across a minimum of 1000 m of the upper part of the Tsumeb Subgroup, and is known to extend to depths as great as 1716 m (Lombaard *et al.*, 1986).

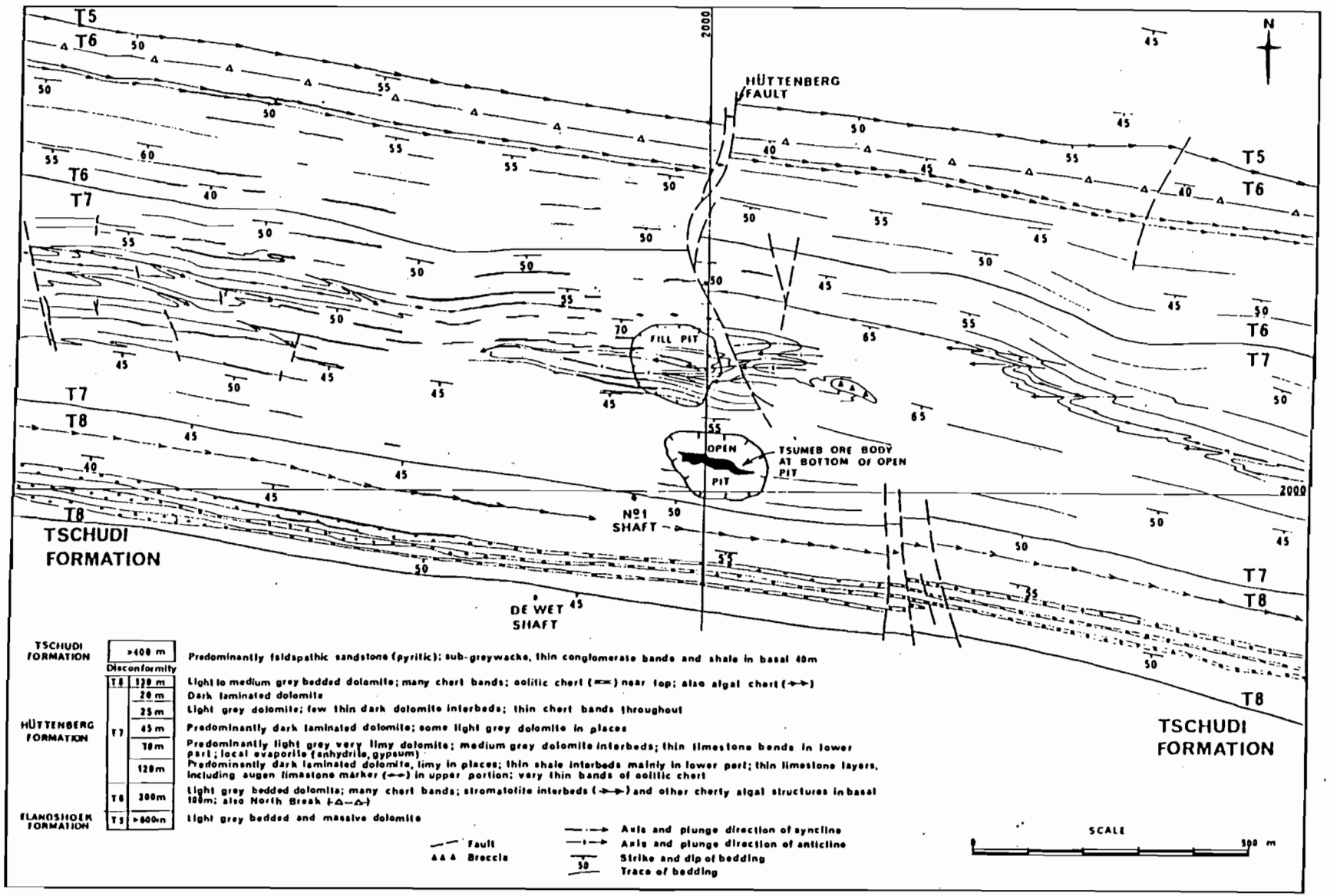

Figure 3.1 Map of the surface geology around the Tsumeb Mine (from Lombaard *et al.*, 1986).

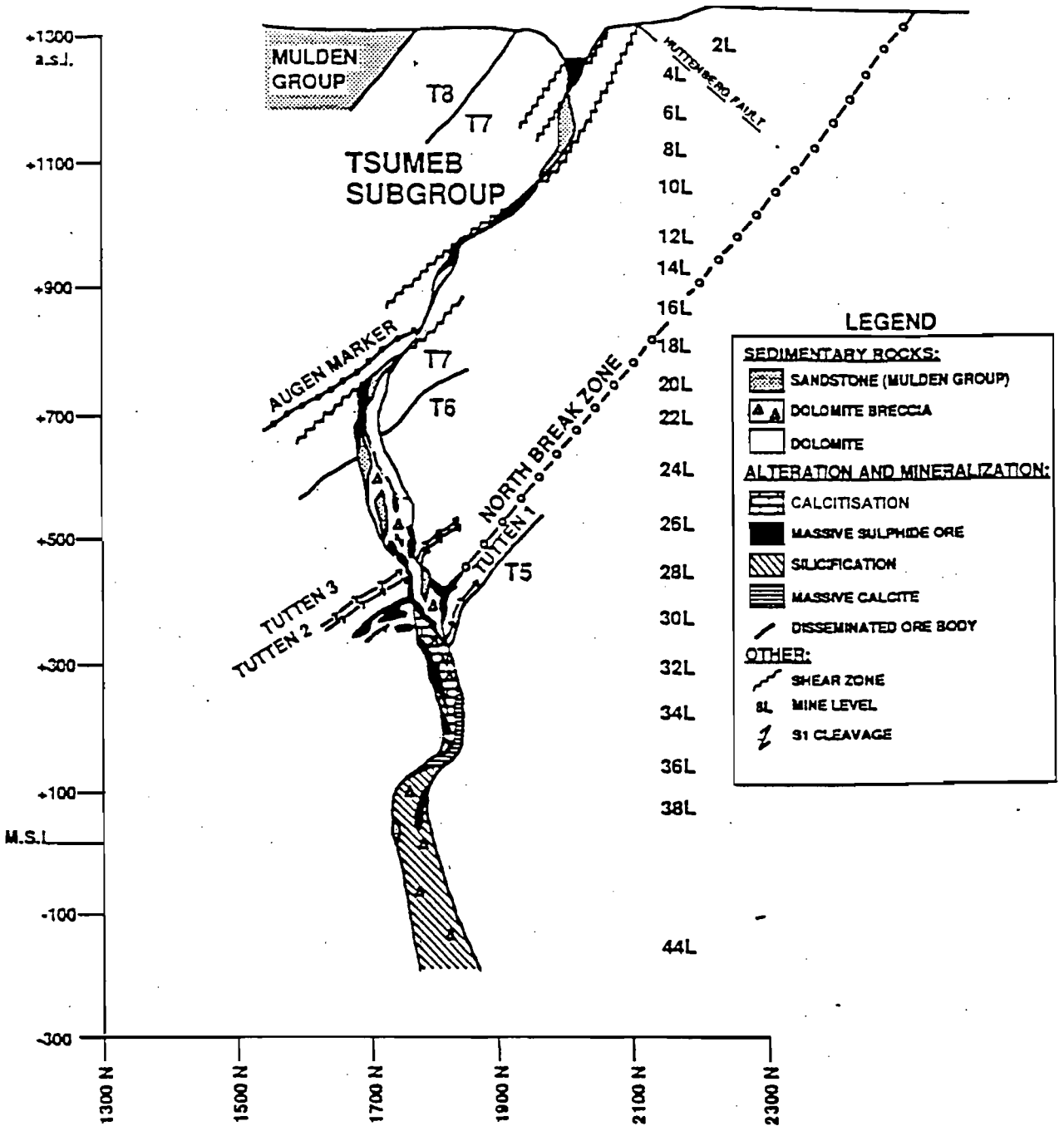

Figure 3.2 Section of the Tsumeb pipe, looking approximately west (after Hughes, 1987; Theron, 1994). Zones of carbonate alteration, mineralisation and rock types are as shown. The stromatolite beds present in the lower part of zone T6 are called Tutten 1, 2 and 3.

3.2.1.2 Rock types

The rock types constituting the various lithozones of the upper Tsumeb Subgroup were described in Table 2.2. Near the base of zone T6 is the North Break Zone, a zone of high porosity, in which brecciation and alteration are extensive. Stromatolite beds are developed in the vicinity (Fig. 3.2). On the surface, the North Break Zone occurs as a discontinuous horizon of siliceous, ferruginous, calcitic, and manganiferous dolomite, from 3 km W to 1 km E of the mine area (Lombaard *et al.*, 1986; Fig. 3.1). Above the North Break Zone, surface exposures indicate that solution collapse breccia has formed in many places, in some, extending into the T8 unit. The breccia fragments occur in a dark dolomite matrix, texturally similar to the country rock.

The pipe structure itself is defined by the mineralisation, dolomite brecciation, the occurrence of feldspathic sandstone, alteration of the host rock, and arcuate fracturing (Pirajno, 1992; Fig. 3.2). The feldspathic sandstone is light to medium grey in colour, and an important host to the mineralisation in the pipe. This rock type was previously referred to as pseudo-aplite, owing to its stratigraphically discordant, yet sedimentary character, however, subsequent reevaluation showed that it can be correlated with arenaceous equivalents in the Tschudi Formation of the overlying Mulden Group (Lombaard *et al.*, 1986; Hughes, 1987).

Breccia types in the Tsumeb pipe comprise dark dolomite breccia, and lighter coloured dolomite breccia which has undergone alteration. The dark dolomite breccia occurs from 21 Level to 30 Level, and in insignificant proportions down to 41 Level (Lombaard *et al.*, 1986). At each particular level, clasts in the dark dolomite breccia appear to be derived from an overlying zone and comprise chert and dolomite. The matrix is dark in colour, and is thought to comprise either black dolomite and argillite, or quartz, dolomite and possibly graphite (Lombaard *et al.*, 1986). The lighter coloured dolomite breccia has been calcitised and silicified.

Dolomite breccias within the pipe structure have been attributed to more than one origin. Lombaard *et al.* (1986) and Pirajno (1992) attribute the breccia formation to solution-collapse, distinguishing between two main types. The first (dark dolomite breccia) is thought to have formed by dissolution of folded, cleaved and fractured dolomite by circulating meteoric water

above and below the North Break Zone. Above the North Break Zone, dissolution continued upward until a channel formed. This channel broke through the floor on which Tschudi Formation sedimentation was occurring, resulting in an influx of unconsolidated arenaceous material from above, to form what is now the feldspathic sandstone. The second breccia type (dolomite breccia) is thought to have formed by the subsequent solution activity caused, in turn, by ascending hydrothermal fluids along fracture cleavages. The hydrothermal activity resulted in rock alteration, arcuate collapse fractures in the breccia and adjoining bedded dolomite. However, more recent work on the North Break Zone by Theron (1994) suggests that it did not act as a palaeoaquifer through which meteoric fluids may have descended to cause dolomite brecciation. Brecciation is instead attributed to hydraulic fracturing by ascending hydrothermal fluids, followed by fluidisation and related solution collapse. Breaching of the overlying unconformity with the Tschudi Formation clastics occurred during the fluidisation stage, causing the feldspathic sandstone to reach great depths within the Tsumeb pipe.

In addition to the dark dolomite and dolomite breccia, Lombaard *et al.* (1986) described *in situ* brecciation, defined by net vein systems of calcite-quartz-dolomite at the deposit periphery, and tectonic brecciation recognised within the dolomite breccia. The origin of these breccias is also in accordance with the model proposed by Theron (1994).

3.2.1.3 Structure

The Tsumeb ore body occurs on the northern limb of the Tsumeb Syncline, a doubly plunging, slightly asymmetric fold (Fig. 2.4). Parasitic folds occur to the east and west of the mine. These have opposing plunges towards the ore body, and are best developed within thinly bedded limestones in the T7 unit (Fig. 3.1). Vertical to subvertical axial planar cleavage is also present. The T7 unit also contains bedding-parallel shearing caused by flexural slip folding, as well as bedding thrusts. The plunge of the pipe is almost perpendicular to bedding in the lower levels and subparallel to the bedding in the upper levels. This is again caused by flexural slip folding as a result of the competency contrast between the more competent dolomites, and the incompetent limestones. Bedding slip therefore occurred in the upper levels (limestone units), giving rise to a lensoid plan shape of the pipe, while the lower dolomite units are undeformed, giving an

elliptical plan shape for the pipe (Pirajno, 1992). The ore body fold zone is another feature attributed to flexural slip folding (Grant, 1995). This zone is closely associated with the ore body, and comprises an anticline to the south and a syncline to the north, with an axial planar cleavage that strikes parallel to the long axis of the ore body. Arcuate fractures associated with the ore body fold zone are ore-bearing. The ore body fold zone persists to greater depths (44 Level) than the parasitic folds developed in the T7 zone (Lombaard *et al.*, 1986).

3.2.1.4 Alteration

Two main alteration types exist at Tsumeb. Calcitisation occurs within the pipe, extending upwards to about 570 m below the present surface, and is most intense at a depth of 1120 m. At depths greater than this, silicification is the main alteration type. This is discussed further in Chapter 4.

3.2.1.5 Mineralisation

Both hypogene and supergene ores are found in the Tsumeb deposit. The hypogene ores are epigenetic, hydrothermal-replacement and fracture-filling in character.

Massive ore is concentrated mainly along the periphery of the deposit. In addition, ores occur in places as mantos in adjacent bedded dolomite. Lower down in the deposit, the mineralisation becomes disseminated and stringer ores are more important. Secondary ores are of economic significance down to a depth of 300 m, and again from 750-1160 m. The pipe is vertically zoned in terms of ore mineralogy, total and relative metal abundance and alteration (Lombaard *et al.*, 1986).

The primary ore minerals are galena, tennantite, sphalerite, chalcocite, bornite, pyrite and enargite. Smaller amounts of sulphide and sulphosalts of Ge, Ga, V, Sn and W also occur; these are irregular in distribution (Lombaard *et al.*, 1986).

Ore textures indicate that deposition occurred as a series of overlapping phases, such that some

minerals were deposited over long durations, whereas others were deposited in a series of separate phases. A complex paragenesis is therefore inferred. However, Lombaard *et al.* (1986) described the sequence as: pyrite, followed by Cu-Fe-Ge-(Zn) sulphosalts and sulphides, then sphalerite, tennantite, bornite, and lastly, galena. Chalcocite is also important, both as a hypogene replacement ore, and as supergene ore. In addition, a host of supergene minerals occur in the upper (surface to 11 Level) and lower (24-35 Level) oxidation zones. Increased metal:sulphur ratios are exhibited from early to late formed ores in the paragenesis.

3.2.2 Kombat

The Kombat ore bodies are Asis East (Ost), E900, Kombat East, Kombat Central, Kombat West, and Asis West. All of these deposits occur along the northern limb of the Otavi Valley Syncline (Figs. 2.4, 3.3).

3.2.2.1 Stratigraphy

The Kombat ore bodies occur in the Hüttenberg Formation of the Tsumeb Subgroup. They are developed in the T7 and T8 zones at and along the contact with shales and phyllites of the overlying Kombat Formation (Innes and Chaplin, 1986; Pirajno, 1992; Deane, 1995; Fig. 3.3).

3.2.2.2 Rock types

The dominant rock types in the Otavi Valley Syncline are phyllites of the Kombat Formation, feldspathic sandstone (Mulden Group), with which the ore is intimately associated, and dolostone host rock of the Hüttenberg Formation.

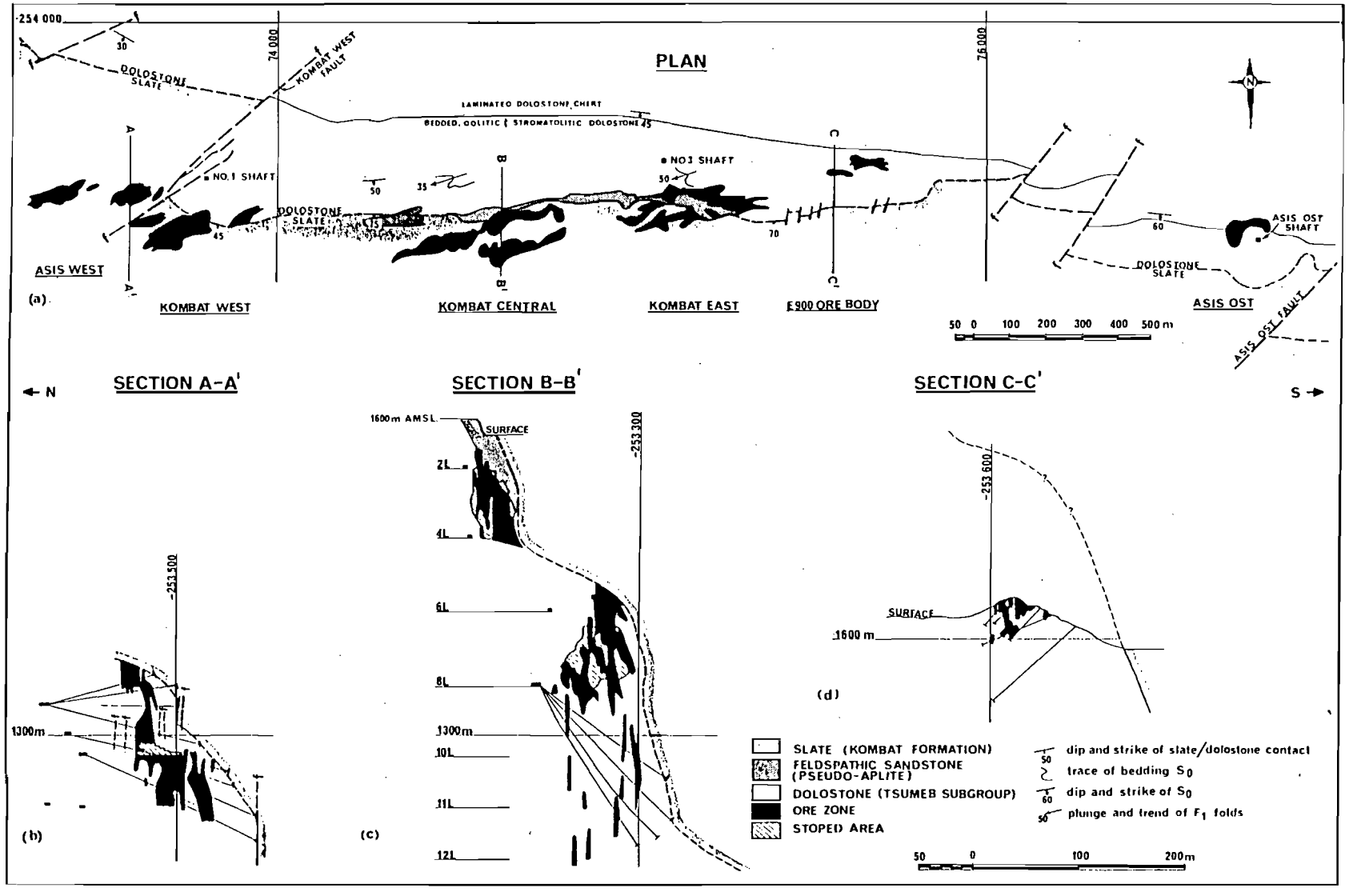

Figure 3.3 (a) Surface geology of the Kombat group of deposits, with horizontal projections of the ore bodies, and cross sections of the (b) Asis West; (c) Kombat Central and (d) E900 ore bodies (from Innes and Chaplin, 1986).

Deane (1993) described three different phyllite types, based on pyrite content and textural features: (i) a dark grey, pyrite-rich phyllite thought to have originally been deposited under anoxic conditions. This phyllite shows a strong foliation, with pyrite inverting to pyrrhotite along S_1 foliation planes (Innes and Chaplin, 1986); (ii) finely-laminated, dark grey phyllite. This type has a lower pyrite content, with the pyrite occurring as small euhedral flecks along foliation planes; (iii) banded, pyrite-poor phyllite. This phyllite forms the thickest unit in the phyllite sequence, and exhibits alternating creamy-grey and medium grey colour bands with kink folds and occasional soft-sediment deformation structures.

Feldspathic sandstone occurs as isolated lenses, pods and stringers over a 15 km strike distance along the disconformable contact between the Kombat and Hüttenberg Formations on the northern flank of the syncline (Innes and Chaplin, 1986). Deane (1993, 1995) called these sandstones the Otavi sandstones, and, based on exposures at the Kombat mine, divided these into two types: massive, well-sorted, poorly-mineralised, green, chlorite-rich sandstone, and dark grey, well-mineralised, calcite-rich sandstone. The feldspathic sandstone bodies described by Innes and Chaplin (1986) also exhibit depositional features such as conglomerate interbands, cross-bedding laminae, clay galls and load casts.

The dolostone of the Hüttenberg Formation is host to the ore and directly underlies the Kombat Formation on the north flank of the Otavi Valley Syncline, with a maximum thickness of 700 m. The upper part of the Hüttenberg Formation comprises light to dark grey micritic dolostone with minor limy dolostone and dolomitic limestone. The lower part of the formation which hosts the ore lenses of Asis Ost comprises massively bedded, micritic, light to medium grey dolostones with bedded diagenetic cherts (Innes and Chaplin, 1986).

In addition to the above rock types, a number of breccias have been described from the Otavi Valley. Deane (1993) grouped these into sedimentary, chemical, hydrothermal and tectonic breccias. Sedimentary breccias comprise mass sediment flow and slump breccias, debris flow breccias, talus breccias, "transitional breccias", and storm breccias. Chemical breccias are subdivided into solution collapse, and replacement breccias, in which dolomite is replaced by calcite; both are associated with ore mineralisation. Tectonic breccias include karst breccias,

which formed by structurally controlled karsting in the Otavi Valley. Those associated with the ore bodies are found in karst structures filled with feldspathic sandstone. Fault breccias, mylonites and cataclasites are also classified under this group. Hydraulic breccias occur as two types: ore-forming breccias and crackle breccias. The ore-forming breccia comprises a matrix of sulphide ore and fragments of host dolomite. Crackle brecciation involves silica vein networks in the more massive carbonates of the Upper Tsumeb Subgroup. These breccias are devoid of mineralisation.

3.2.2.3 Structure and deformation

The ore bodies at Kombat are generally associated with faults and fractures along the contact between the T7 and T8 zones of the Hüttenberg Formation, and phyllites of the Kombat Formation (Innes and Chaplin, 1986). On a more regional scale, three folding phases have been recognised in the Otavi Valley. The first, F_1, is an isoclinal phase with an east-trending axial planar cleavage (S_1) present in slates and phyllites of the Kombat Formation, and is correlated with the regional D_1 deformation (Deane, 1995), not so well expressed in the rest of the OML.

A second folding phase, F_2, is correlated with the regional D_2 deformation, and resulted in the development of the E-W trending, isoclinal Otavi Valley Syncline. Deane (1995) divided this episode into D_{2a}, which produced north-verging recumbent folds on the southern limb of the syncline, and D_{2b}, which caused rupturing of the Otavi Valley Syncline along its synclinal axis. F_2 also resulted in the folding of the S_1 cleavage into a nearly coaxial, concentric pattern. Sulphides, originally present on the S_1 surface, have been mobilised into an S_2 crenulation cleavage, which overprinted S_1. Within the dolostone of the Hüttenberg Formation, disharmonic small-scale F_1 and F_2 folds are found. Some axial plane foliations to these folds host foliated lenses of barite and feldspathic sandstone (Innes and Chaplin, 1986).

The third folding event, F_3 (regional D_3) caused NE trending interference folds. These gave rise to the "canoe" shape of the doubly plunging Otavi Valley Syncline (Deane, 1995). F_3 resulted in minor chevron type folds and kink bands, associated with an axial planar S_3 fracture cleavage. These F_3 structures are thought to be related to northeast-trending dip and strike-slip faults (Innes

and Chaplin, 1986).

Many of the ore loci in the dolostone along the contact with the Kombat Formation show intensely foliated, steep, northeast-trending zones of deformation. These zones represent shear extensions of pinched out fold hinges (Innes and Chaplin, 1986).

The ore lenses show minor displacement caused by a number of northeast-trending faults. The Asis West and Kombat West ore bodies, however, are significantly displaced by the Kombat West fault. High angle, reverse and normal faults striking ENE, occur across the Hüttenberg/Kombat Formation contact. These are of unknown age (Innes and Chaplin, 1986).

The ore loci themselves are defined by breccia bodies in the dolostone and are structurally controlled. These controls include steeply-dipping zones of net vein fractures, joints and fracture cleavages. The ore bodies exhibit an *en échelon* pattern in strike due to the divergence from the phyllite/dolostone contact, of these sub-parallel planar structures. The phyllite/dolostone contact dips 40-80° S. The mineralisation is concentrated below monoclinal flexures (F_1/F_2, Innes and Chaplin, 1986) on the contact. These flexures are locally known as "roll structures" and are characterised by fissures in the footwall dolomite (Pirajno, 1992). However, Deane (1993) considers the term "roll structure" misleading, as it is not a monoclinal flexure, but a term describing the folded and sheared contact between the Otavi Group/Kombat Formation directly above the ore loci. In profile, the individual ore lenses abut against the contact and "hang" like pendants beneath the "roll structure" (Fig. 3.4). The ore lenses have a steep orientation and cross-cut the stratigraphy. With increasing depth, the massive sulphides become disseminated, and form threads and stringers in calcitised zones of net-vein fracturing. The "roll structures" have amplitudes between 75-200 m and wavelengths of 150-250 m. These strike E to ENE and have a shallow, westward plunge.

3.2.2.4 Alteration

The host dolostones have undergone extensive hydrothermal alteration. The ore lenses are surrounded by broad zones of pervasive calcitisation. The alteration increases in intensity with

depth, such that root zones comprise 200-300 m wide zones of fine- to medium-grained, white saccharoidal textured limestone. Sedimentary and tectonic brecciation, and net-vein fracturing is accompanied by calcitisation and manganese alteration in the form of manganoan calcite (Innes and Chaplin, 1986).

Hydrothermal silicification is relatively minor, but may be important in some sandstone lenses. Metasomatised dolostone containing amphiboles and micas are intimately associated with Fe and Mn ore lenses (Innes and Chaplin, 1986). Alteration will be discussed further in Chapter 4.

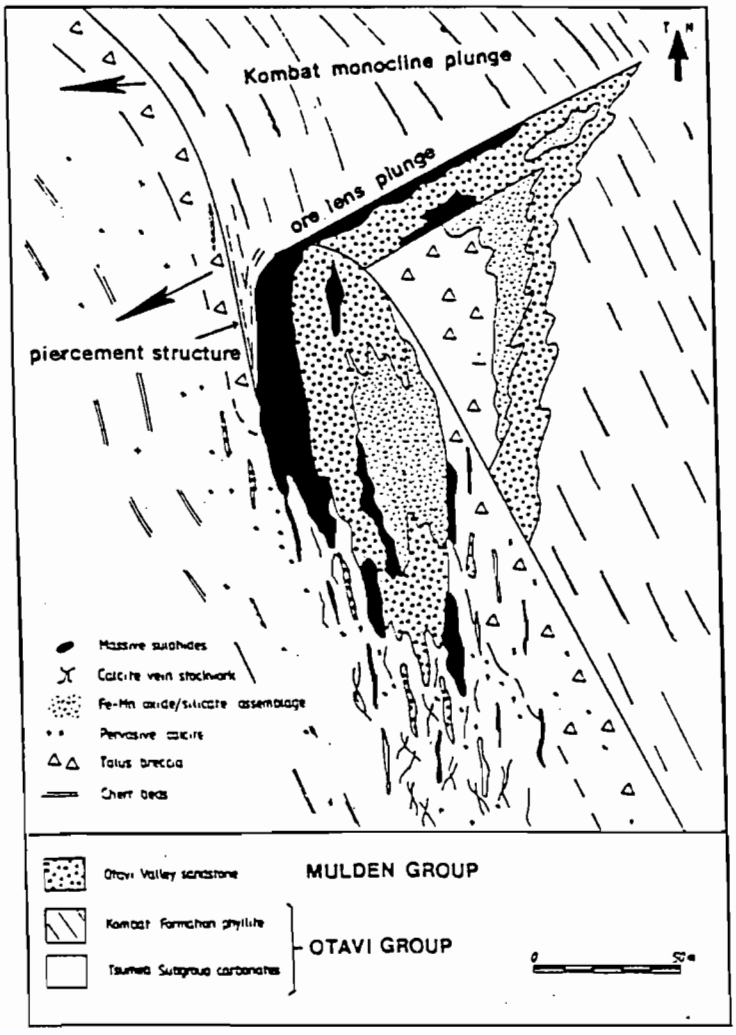

Figure 3.4 Schematic section of a Kombat-type ore lens, showing distribution of alteration and ore at the contact between phyllite of the Kombat Formation, and dolostone of the Hüttenberg Formation (from Deane, 1995).

3.2.2.5 Mineralisation

Mineralisation at Kombat occurs as sulphide bodies with overlying Fe-Mn bodies. Four main ore associations are present: massive and semi-massive sulphides; mineralised net vein fracture systems; an Fe-Mn assemblage and mineralised fracture fillings. Massive and semi-massive sulphides comprise primary bornite, chalcopyrite, galena, tennantite, and supergene chalcocite, digenite and malachite, sometimes with associated covellite, cuprite, native copper and native silver (Innes and Chaplin, 1986). This ore association is spatially related to areas of hydraulic brecciation, in which the ore is concentrated in the breccia matrices. Ore of this association is also well developed in sandstone lenses, and associated with calcitisation (Deane, 1995). Net vein fracture systems are found below the massive sulphide bodies in the "roll structures" (Fig. 3.4). These are filled with calcite which may be barren or host coarse bornite, chalcopyrite and galena. The Fe-Mn bodies comprise oxide, silicate and carbonate facies, as well as metasomatic borate and arsenate assemblages. Magnetite and haematite generally separate the Fe-Mn bodies from the sulphide ores. The Fe-Mn bodies exhibit a complex mineralogy. Minerals present include hausmannite, jacobsite, haematite, magnetite, barite, calcite, tephroite, alleghanyite, pyrochroite, manganosite, galaxite, glaucochtoite, spessartine, andradite and vesuvianite (Innes and Chaplin, 1986). Fracture fillings comprise bornite, chalcopyrite, pyrite, chalcocite and galena, and are closely associated with strong shearing (Deane, 1995; Fig. 3.4).

Economically important supergene minerals (e.g. at the Asis Ost ore body) include chalcocite, cuprite, malachite, cerussite and mottramite. The sulphide ore bodies exhibit zonation, with Cu enrichment in the centre and Pb-, Zn- and Fe-rich zones further away from the centre. Ag is associated with the Cu-bearing phases.

3.2.3 Khusib Springs

The Khusib Springs deposit is located on the northern limb of the Olifantsfontein-Harasib Syncline, ~50 km southeast of Tsumeb. The prospect was acquired by TCL in 1983, but initial exploration activity did not yield economic mineralisation potential. However, interest in the

prospect was renewed in 1991, owing to diminishing reserves at Tsumeb. Roesener (1991) carried out detailed mapping, and diamond drilling commenced in 1992, motivated by Pb isotope studies (Eglington, 1992). Massive Cu sulphide mineralisation was intersected in January 1993, leading to the definition of the high grade, low tonnage Cu-Pb-Zn-Ag Khusib Springs deposit. Production commenced there in 1995. Figure 3.5 shows the horizontal projection of the geology, along with a cross section through the massive sulphide body. Owing to the relatively recent discovery and beginning of mining operations, an account of the geology of the Khusib Springs deposit has not been published, and the description as given below is taken from GFNL company reports, as well as an unpublished Honours thesis by Verran (1996).

3.2.3.1 Stratigraphy

The Khusib Springs deposit is situated in dolomite and limestone beds of the Maieberg Formation, with mineralisation occurring along the contact between T2 limestone and T3 dolomite. Locally, the thickness of the Maieberg Formation is ~1200 m. Of this thickness, T2 limestone comprises 700 m. The overlying T3 dolomite has a thickness of 600 m to the east of the deposit, but thins out westwards (King, 1994).

3.2.3.2 Rock types

Host rocks of the mineralisation are dolomites, limestones and breccias of the Maieberg Formation. The T2 unit locally comprises thinly-laminated mudstone. Lower down, the T2 unit is characterised by massive mudstone varieties, which become progressively interbedded with dolomitic mudstone higher up. The upper contact of the limestone is characterised by the presence of a large, mudstone-supported chaotic breccia (King, 1994).

The overlying T3 dolomite is made up of predominantly medium to dark grey dolomitic mudstone or dolomicrite, which varies from massive to thinly laminated in texture. Stylolites are ubiquitous in the local T3 dolomite. Four breccia types have been recognised locally: dolomite-supported (mudstone-supported); dolospar-supported; crackle and rip-up breccias.

The dolomite (mudstone) supported breccia is a large "chaotic breccia" described by King (1994), and extends into the overlying T3 dolomite. The matrix is dolomitic mudstone, which supports polymictic fragments, including thinly-laminated, dark grey mudstone and massive, light grey grainstone of varying size and shape. These breccias show a brown surface colouration, which King (1994) attributed to weathering of finely-disseminated pyrite present in the fragments and matrix. The chaotic nature of this breccia, along with the dolomitic mudstone matrix (found as dolomitic mud infill in the lower limestone beds) supports a karst or solution collapse origin for this breccia type.

The dolospar-supported breccia occurs in the same area as the chaotic breccia, but is not as widespread. The matrix is composed of a coarsely crystalline, white sparry dolomite. The fragments are angular, polymictic, and of variable size. This breccia has either formed by hydraulic fracturing, or by hydrothermal replacement of the dolomitic mudstone matrix by infiltrating fluids.

Crackle breccia is found within folded limestone-dolomite beds. This breccia type is a tectonic breccia related to open kink and box folds. It has formed in ruptured fold hinge zones, with fluid infiltration into fractures.

Rip-up breccias are sedimentary in origin and occur directly below the T2/T3 contact. This breccia is a thin (±50 cm), laterally continuous unit, parallel to the limestone bedding. It comprises elongate, angular fragments of varying size, which represent reworking of limestone beds during a storm event (Verran, 1996).

3.2.3.3 Structure

In the regional context, the Khusib Springs deposit is situated on the northern limb of the northeast-trending, westerly plunging Olifantsfontein-Harasib Syncline, a D_2 structure (Fig. 2.4). In addition, the bedding in this vicinity tilts towards the south, again related to the D_2 event described for the OML.

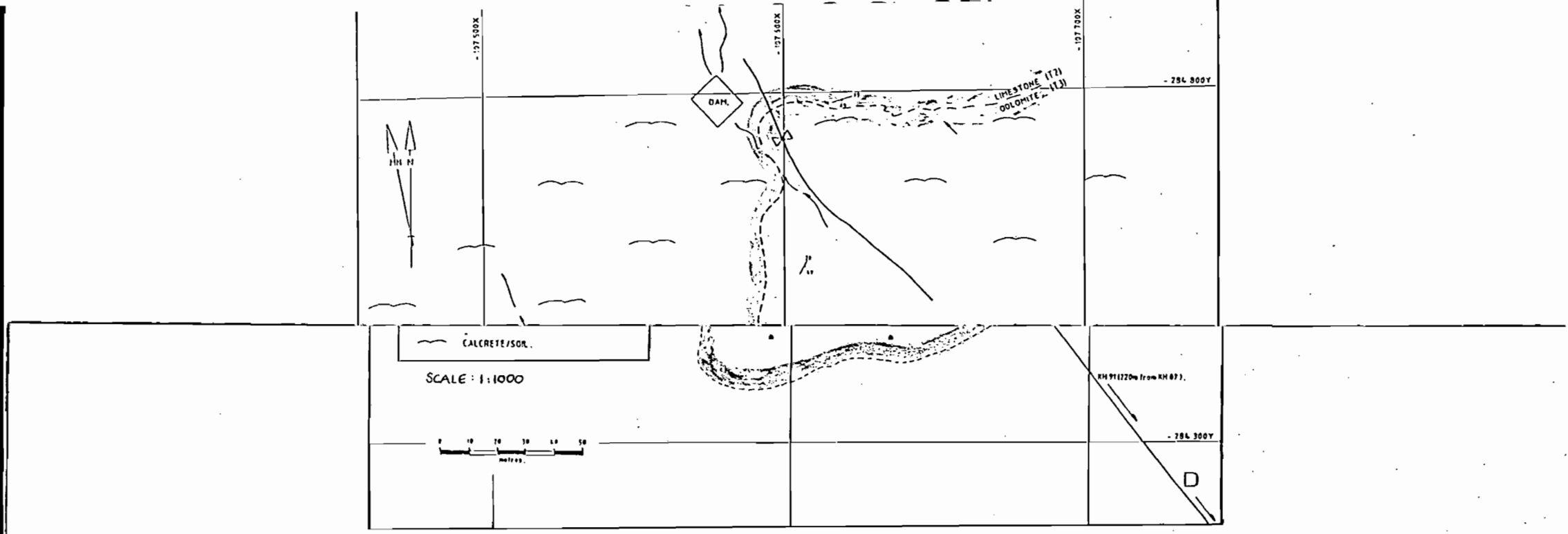

Figure 3.5 (a) Surface plan of the Khusib Springs mining area, showing the horizontal projection of the ore body (after King, 1995; Verran, 1996). Cross section C-D is given in Appendix A1.

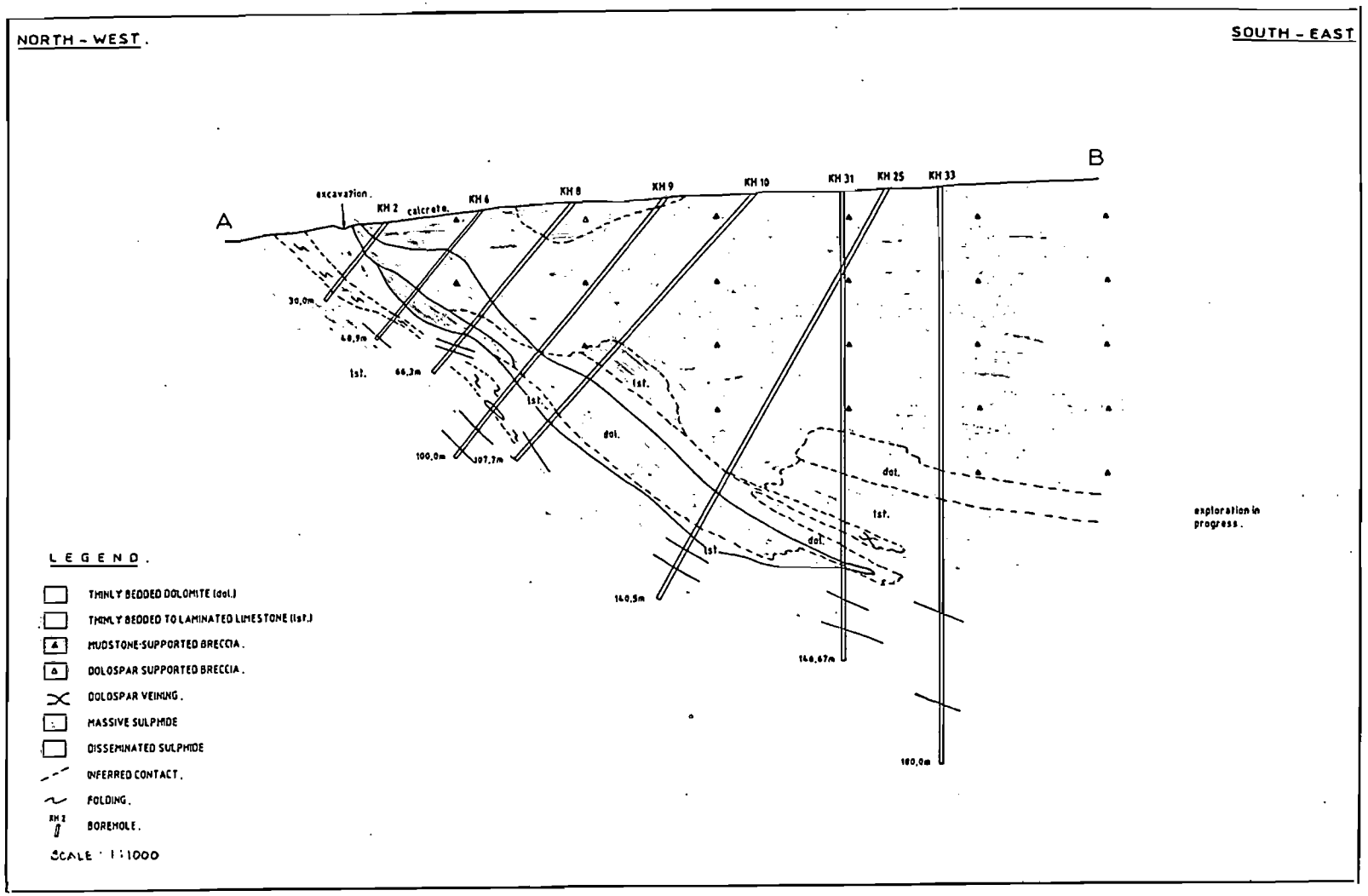

Figure 3.5 (b) Cross section A-B from Figure 3.5 (a), showing the position of the massive and disseminated ore in the dolomite (T3) succession at Khusib Springs (after King, 1995; Verran, 1996).

A prominent dextral N-S fault occurs in the Khusib Springs Prospect, displacing the upper limestone contact of the Maieberg Formation by ~260 m. Two similar dextral faults, of 120 m and 90 m displacements, have been delineated west of the prospect (King, 1994). However, all three faults do not appear to extend into the overlying upper Maieberg and Elandshoek Formations, as the dolomite beds there are not displaced.

Percussion drilling shows the Khusib ore body to be structurally located close to the axis of a monoclinal fold. Similar monoclinal "flexures" have been defined along strike of the T2/T3 contact (Prinsloo, 1995). However, based on detailed mapping and logging of cores, King (1995) postulates that mineralisation is related to a relatively narrow zone of folding within a much larger, symmetrical fold structure.

An 18 m wide zone of kink and box folds occurs within the limestone beds immediately below the base of the interpolated fault (King, 1994). Many fold hinges have ruptured, and in some cases, sheared, owing to intense deformation. The fold axes have an average trend and plunge of 175/34 S (Verran, 1996). The box folds would appear to be small-scale equivalents of larger-scale open antiforms and synforms. The average strike indicates an E-W compression, which can therefore be correlated with the regional D_3 event.

Mineralisation and alteration is restricted to zones of folding and brecciation. Brecciation has provided the necessary porosity for infiltration of the mineralising fluids. The faults present may have been important conduits for the fluids (King, 1994). Mineral lenses of the deposit seem to have been displaced by later reactivation of the fault zones.

3.2.3.4 Alteration

Alteration at Khusib Springs is predominantly dolomitisation. Calcite and silica alteration are also evident, but secondary in nature, as regards the mineralisation event. As with the other deposits, alteration at Khusib Springs will be considered further in Chapter 4.

3.2.3.5 Mineralisation

Diamond drilling has delineated a semi-continuous, stratabound sulphide zone. This extends from surface to the current drilling depth of 300 m, dipping ~40° S. The mineralised zone thins and decreases in grade at a vertical depth of 110 m, after which size and grade increase further down dip. The 100 m depth marks the separation between an upper ore zone, and a lower ore zone, with the former being presently investigated (King, 1994; Verran, 1996).

The upper ore zone contains an upper Cu/Ag-rich lens consisting of massive, patchy and disseminated sulphide mineralisation, and a stratigraphically lower, smaller Zn-rich/Ag-poor sulphide lens. The upper Cu/Ag-rich lens contains two pods of massive sulphide, each ~4 m thick, in a zone of patchy, disseminated Cu mineralisation. This lens occurs at or below the chaotic breccia base, within the underlying laminated dolomite unit, as well as within a stratabound zone of dolomite alteration. The lower Zn-rich/Ag-poor stratabound lens is stratigraphically present ~7 m below the Cu-rich lens and contains large patches of massive red sphalerite and minor galena (King, 1994).

Major sulphide minerals are tennantite, galena and sphalerite. Minor ore minerals include enargite, chalcopyrite, bornite and pyrite. Minor quantities of bournonite may also be present, as suggested by XRD analysis (Morgan, 1994, in King, 1994). No native silver has been identified, but Ag is present in high grades in solid solution phases, such as proustite and possibly pyrargyrite, in the tennantite.

3.3 BERG AUKAS-TYPE DEPOSITS

Berg Aukas

The Berg Aukas deposit forms the type locality for Berg Aukas type mineralisation. It is hosted by the Light Grey Dolostone of the Gauss Formation in the Abenab Subgroup.

The mineralisation occurs in dolomite breccia, and was deposited as open space fillings formed by karsting. The deposit comprises three distinct ore bodies: the Northern Ore Horizon, which is stratabound; a discordant Central Ore Body and a stratabound Hanging Wall Ore Horizon (Misiewicz, 1988; Fig. 3.6). The Northern Ore horizon comprises three stratabound lenses of massive sulphide. The upper part is oxidised to willemite, cerussite and smithsonite. Dolomite breccia, enriched in descloizite, caps the ore. The Central Ore Body is a brecciated, pipe-like, mineralised zone. Here the ore has been extensively oxidised and enriched in vanadiferous muds and breccia. The breccia comprises blocks of barren host dolomite and partially oxidised sulphide mixed with vanadiferous caliche (Pirajno, 1992). The Hanging Wall Ore Horizon is made up of N-S trending lenses of steeply-dipping ore-filled fractures hosted by dolomitic rocks above the Northern Ore Horizon.

The main minerals comprising the massive sulphide are sphalerite and galena. Other sulphides include pyrite, tennantite, enargite, chalcopyrite and renierite. As a result of the extensive oxidation caused by circulating meteoric water during late-stage karsting, the deposit is abundant in secondary, supergene minerals such as willemite, smithsonite, cerussite and descloizite. Traces of Cd and Ge are present in the sphalerite (Emslie and Beukes, 1981).

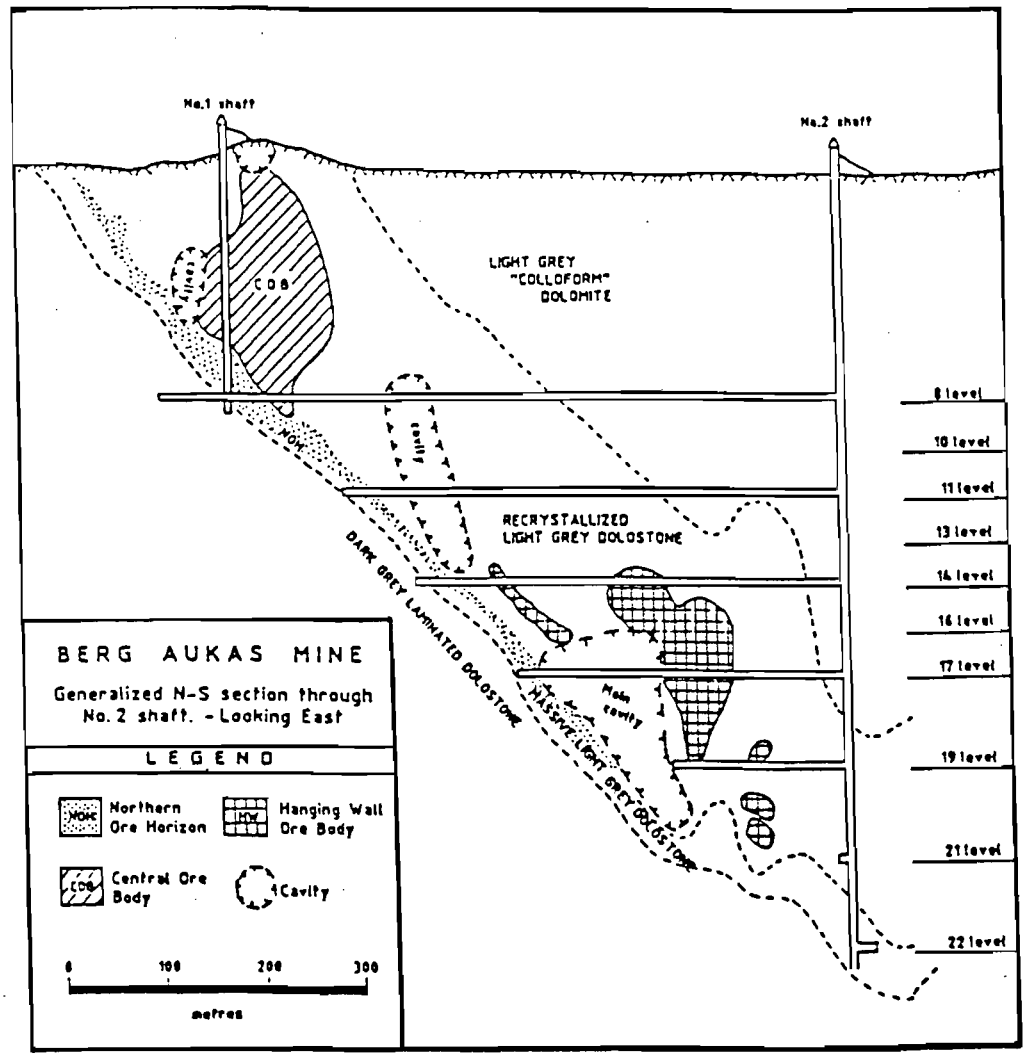

Figure 3.6 Simplified N-S section through the Berg Aukas deposit, looking east, and showing the position of the Northern Ore Horizon, Central Ore Body and Hanging Wall Ore Body, along with carbonate rock types present (from Chadwick, 1993).

CHAPTER FOUR: ALTERATION

4.1 INTRODUCTION

Carbonate alteration throughout much of the OML has been that of dolomitisation. Dolomite is very difficult to precipitate directly from solution, and is therefore seldomly a primary product at Earth surface temperatures (e.g. Chilingar *et al.*, 1979). The presence of extensive dolomite "deposits" in the stratigraphic record, however, has given rise to the debated "dolomite problem" amongst geologists (Zenger, 1972). Numerous theories have been put forward for the formation of such massive dolomite, ranging from synsedimentary to late diagenetic and epigenetic processes. The literature on the subject is thus voluminous (e.g. reviews by Hardie, 1987; Chilingar *et al.*, 1979; Zenger *et al.*, 1980), and treatment thereof is beyond the scope of this dissertation.

Dolomitisation in the Tsumeb Subgroup is selective on a regional and local scale (Deane, 1993). It has been attributed to early diagenetic processes such as mixing of marine and meteoric waters, and to burial diagenesis (Theron, 1994).

Alteration in the context of the mineralising episode(s) is the focus of this chapter, and will be discussed for each deposit. Such alteration at this stage is described as any textural or mineralogical change from that of the "original" dolomite/limestone host, or that carbonate deemed least altered. In defining the alteration around the ore deposits under consideration, it is important to distinguish between different carbonate generations, and to identify, in particular, those generations associated with the ore. In order to achieve this, textural relationships, mineralogy, chemistry and cathodoluminescence (CL) of the various carbonate generations were examined.

4.2 PETROGRAPHY AND MINERALOGY

Carbonate generations were identified in hand specimens and cores on the basis of textural relationships, veining and mineralogy (using dilute, 0.1 M HCl and XRD for distinguishing between dolomite and calcite). Thin section petrography was undertaken to determine textural relationships on a micro-scale, as well as in preparation for EPMA. Cathodoluminescence imaging was carried out principally to distinguish further between carbonate generations already identified in hand specimen and thin section, thus ensuring homogeneity of the carbonate samples used for further geochemical analysis. This was effected using a Technosyn cold cathodoluminescence model 8200 MkII at the Electron Microscope Unit, University of Cape Town. Further details are provided in Appendix A2.1.

4.2.1 Tsumeb

Silicification and calcite alteration are predominant features associated with mineralisation in the Tsumeb pipe structure (Lombaard *et al.*, 1986), but dolomite veining also occurs in places. The following carbonate generations and rock types, mainly from the lower parts of the pipe, were identified in the present study:

- The host rock, a medium grey, very fine-grained (<0.1 mm) dolomicrite (Fig. 4.1a). Thin section petrography revealed the preservation of primary features, such as allochems. Although this rock type is considered to be the least altered in terms of texture, some degree of recrystallisation has occurred. In thin section, this generation is characterised by a dull, murky texture, probably caused by the original lime mud. This texture could also be imparted by the presence of admixed hydrocarbons. Host dolomite occurs either as massive dolomite, or as clasts in breccias. A dull CL was observed for this generation (Fig. 4.1b);
- Coarsely recrystallised dolomite (0.5-2 mm grain size; Fig. 4.1c), found at higher levels in the mine. Discrete domains of white sparry dolomite are delineated by hydrocarbons in this generation. This rock type hosts sulphide mineralisation, albeit in the more hydrocarbon-rich portions. A bright red CL colour is exhibited by this carbonate (Fig.

4.1d);

- Sparry dolomite, occurring in the form of coarsely crystalline (0.5-3 mm; Fig. 4.1a) veins, containing in some parts sulphides and sulphosalts. The sparry dolomite may form discrete veins, occur intergrown with ore phases, or act as the matrix in tectonic breccias ("mosaic" breccia) found at deeper levels of the mine. As with the coarsely recrystallised dolomite, a bright red CL colour was observed (Fig. 4.1b);
- Silicified host dolomicrite, in which silicification is pervasive. In thin section this appears as a completely intergrown mixture of quartz and dolomite. As a more discrete phase, quartz occurs with the sparry dolomite in places, indicating possible crystallisation from the same fluids responsible for pervasive silicification, sparry dolomite precipitation and associated mineralisation. Silicification seems to be associated with oxidised mineralisation, and occurs predominantly in the lower levels of the pipe;
- Calcitised dolomite, showing minor recrystallisation. XRD shows a presence of ~45 vol% calcite;
- Sparry calcite (0.5-3 mm grain size) veins, hosting Cu sulphosalts and sulphides. Associated with the calcite is quartz;
- Late, barren, blocky calcite (2-5 mm grain size), cross-cutting mineralised dolomite.

An additional carbonate type sampled from core of the T7 zone is sparry dolomite replacing sulphate (either as anhydrite or gypsum blebs). Besides the carbonate phases present, feldspathic sandstone also forms a constituent in the pipe and, in many places, an important host to mineralisation. This rock type has been described occurring as plug-like structures in a pinch-and-swell fashion in the pipe (Lombaard *et al.*, 1986).

4.2.2 Khusib Springs

Alteration at Khusib Springs is simpler than at Tsumeb. Based on mineralogical differences, three alteration types are evident at Khusib Springs: dolomite, calcite and silica alteration. On a textural basis, the dolomite alteration can be subdivided into at least four generations:

- The host rock, a very fine-grained (<0.05 mm; Fig. 4.2a), medium to dark grey

dolomicrite, seemingly rich in hydrocarbons in places, which imparts the darker colour to the rock. No apparent textural alteration is evident for this rock type. This dolomite makes up the T3 zone of the Maieberg Formation. As with the Tsumeb host dolomite, a rather dull CL was obtained for this generation (Fig. 4.2b);

- Veins of very light grey to white, coarsely crystalline (1-4 mm), sparry dolomite, forming an anastomosing network (Verran, 1996). These veins host sulphide mineralisation in the form of sphalerite, galena and various Cu-sulphides such as enargite and chalcopyrite, and hence comprise the most important carbonate generation in this respect. The characteristic CL colour is bright red;
- Coarsely recrystallised (2-4 mm) grey dolomite, closely associated with the sparry dolomite. On closer inspection, this generation consists, in places, of discrete domains of sparry dolomite, bounded by darker hydrocarbon material. The degree of recrystallisation varies from almost unaltered to almost completely sparry dolomite. A similar CL colour to that of the sparry dolomite was obtained;
- Veins of sparry dolomite, as described above (Fig. 4.2a), but occurring further away from the ore body, and associated with Fe-bearing dolomite. A zonation in the Fe-bearing dolomite crystals due to chemical (and mineralogical) differences is reflected in the CL colours (Fig. 4.2b).

Vague cross-cutting relationships within the sparry dolomite, along with the presence of azurite and malachite in some parts, suggest that two subtypes of this generation may exist. This possibility has been investigated further using geochemistry, particularly REE signatures (Chapter 5).

Calcite alteration is evidenced by a single generation of calcite veining, in addition to possible host limestone alteration. The vein calcite is coarsely crystalline (2-6 mm) and is yellow in colour. The calcite has precipitated in vugs, fractures and tension gashes, and is devoid of mineralisation. A distinct cross-cutting relationship between the calcite and the sparry dolomite veining shows it to post-date the dolomite veining, and hence the mineralising episode. Limestone of the T2 zone of the Maieberg Formation in the vicinity of the deposit is dark in colour and very fine grained (<0.05 mm). As with the dark dolomicrite host, the dark colour of

this limestone is imparted by the presence of hydrocarbons, and may be a hydrothermal effect.

Silica alteration is recognised as two stages of quartz associations: quartz associated with the white sparry dolomite veining and quartz veins which show cross-cutting relationships with the earlier dolomite veins. The latter is also found associated with the late calcite veins.

4.2.3 Kombat

Calcitisation is the dominant alteration type evident at Kombat, pertaining to the carbonates. Silicification is a minor alteration feature associated with the calcitisation. The following carbonate generations were identified:

- The host rock, a light coloured, fine-grained (0.05-0.5 mm) dolostone. A small amount of calcite (~3 vol%) is present in this host;
- Calcitisation of the host dolomite. This alteration type is pervasive, and its product is either light or dark in colour. The light calcitisation shows a homogenous texture with a light blue-grey colour in drill core samples from the Asis West deposit. This is accompanied by recrystallisation (grain size of 0.1-0.5 mm), replacement of the dolostone host to varying degrees, and sulphide mineralisation. At the E900 ore body, calcitisation occurs as both light and dark types, in a complex interfingering relationship. The dark type also forms the matrix between brecciated fragments of light coloured dolostone, and comprises a high proportion of silica (~50 vol%). In addition, this calcitisation type is host to finely disseminated sulphide mineralisation. The light coloured calcitised dolostone is slightly coarser grained (0.5-1 mm), with XRD revealing a calcite content of ~80 vol%;
- Sparry pink calcite associated with the Fe-Mn ore assemblage at the Asis West ore body. This calcite occurs intergrown with the ore, and displays a bright yellow CL colour, with a degree of zoning evident (Fig. 4.3);
- Milky, coarsely crystalline (2-5 mm), blocky calcite veins, associated with chalcopyrite and bornite in places, at the Asis West deposit.

As with the Tsumeb deposit, feldspathic sandstone is also found at Kombat, and is closely associated with sulphide mineralisation in parts.

4.2.4 Berg Aukas

Alteration at Berg Aukas consists of dolomitisation and a small degree of silicification. Frimmel *et al.* (1997) distinguished between five groups of dolomites based on degree of crystallinity, textures and CL observations:

- The host rock (Dolomite I), a poorly recrystallised, very fine-grained (<0.05 mm) dolomicrite which represents the least altered country rock in the Berg Aukas vicinity. Primary laminations are well preserved in this type;
- Coarsely to very coarsely crystalline dolomitic rhythmite (Dolomite II). The rhythmite is defined by alternating light and dark grey bands of radiating bladed dolomite crystals (Fig. 4.4a). The alternating bands show light and dark red colours in the CL images[2] (Fig. 4.4b). Silicification is most pronounced in this generation;
- "Mosaic" dolomite, ranging from finely (~0.1 mm) to coarsely (0.5-1 mm) recrystallised, granoblastic dolomite (Dolomite III). In places, this replaces the earlier rhythmite. Massive Pb and Zn sulphide mineralisation is intergrown with this generation. Selective silicification of stromatolitic laminations is also found in this alteration type;
- White sparry dolomite, occurring as a coarse-grained void or fracture-filling (Dolomite IV, Fig. 4.4a). Secondary, mobilised sulphides are hosted by this generation. This shows a red intensity under CL.
- Dolomitic karst filling, comprising fine- to medium-grained, crystalline microspar (Dolomite V).

[2] The red colours are not so well developed in Fig. 4.4 owing to development of the film in different emulsions, and at different laboratories to those images from the other deposits. Nevertheless, the pertinent textures are still evident.

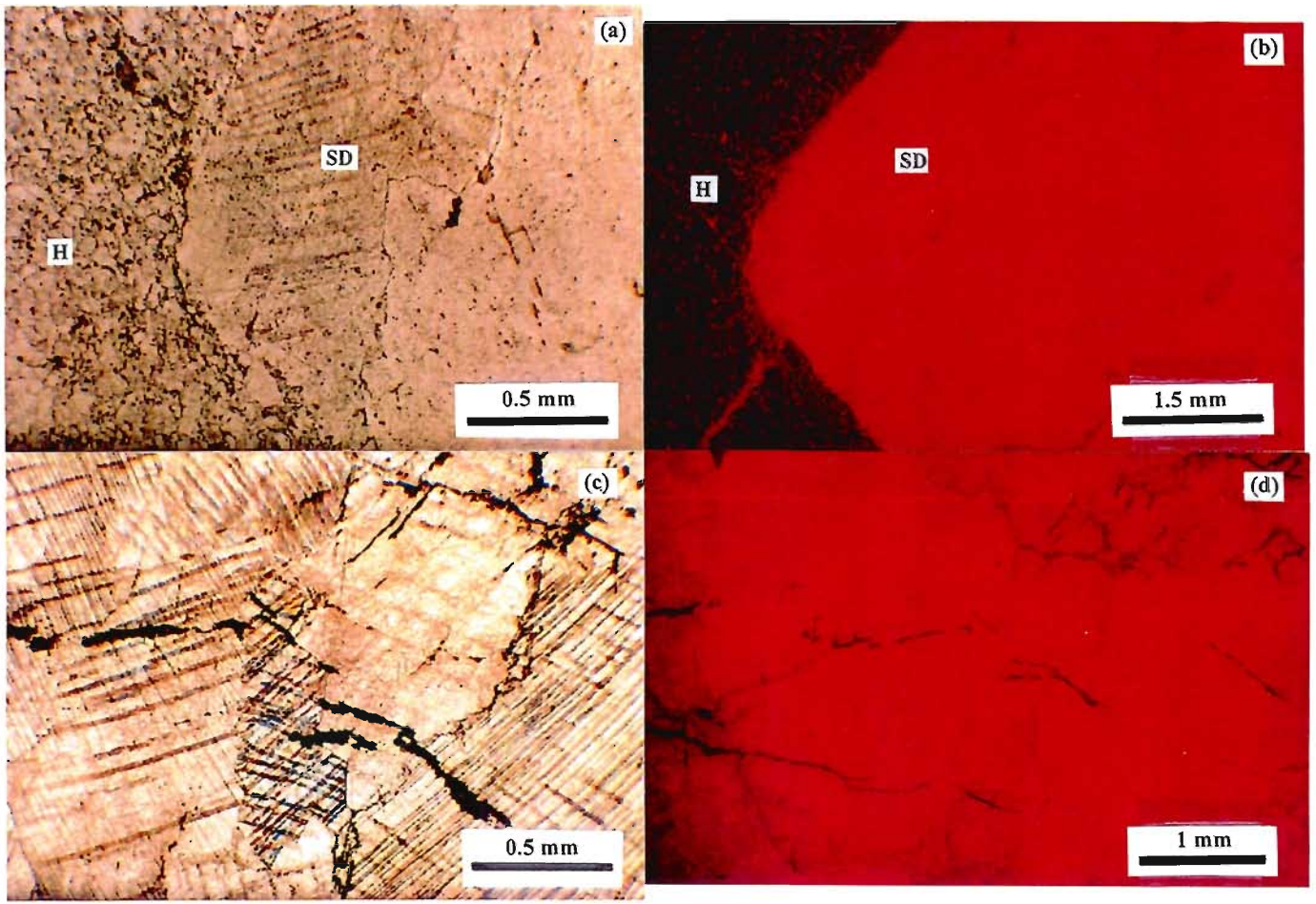

Figure 4.1 (**a**) Transmitted light (PPL) photomicrograph of sparry dolomite (SD) and dolomicrite host (H) at Tsumeb; (**b**) CL image encompassing the area in (a) in the middle left portion of the image; (**c**) transmitted light (PPL) photomicrograph of coarsely recrystallised dolomite at Tsumeb; (**d**) CL image encompassing area in (c) towards the middle portion of the image.

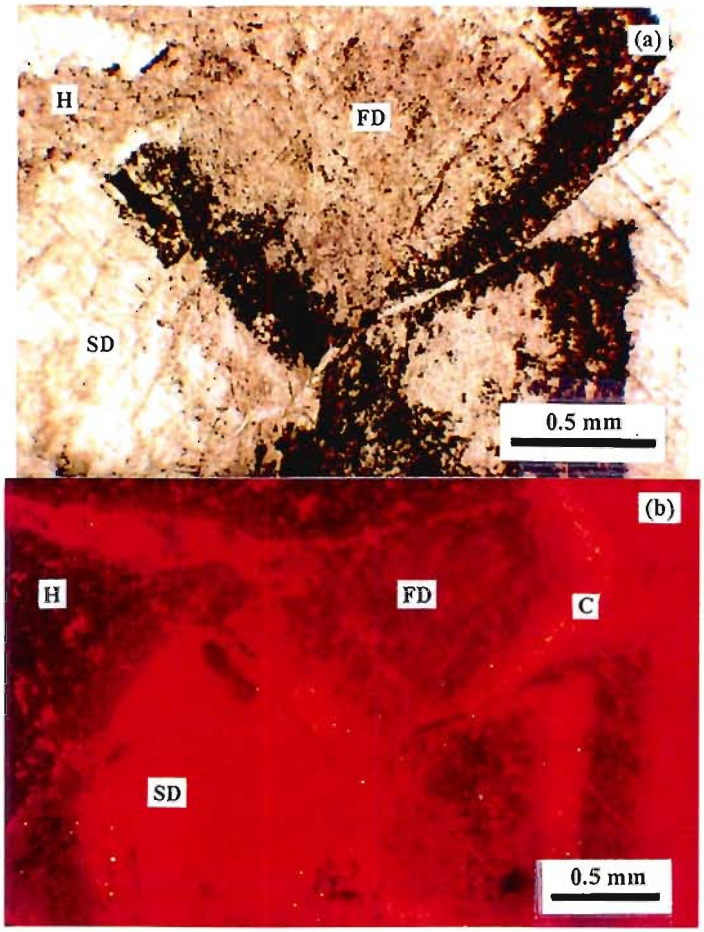

Figure 4.2 (a) Transmitted light (PPL) photomicrograph of dolomicrite host (H) with Fe-bearing dolomite (FD) crystals showing Fe-oxide rich edges and surrounded by sparry dolomite (SD) at Khusib Springs; **(b)** CL image of the same area. Calcitic zones (C) not evident in PPL, are delineated by their different CL colour to the dolomites.

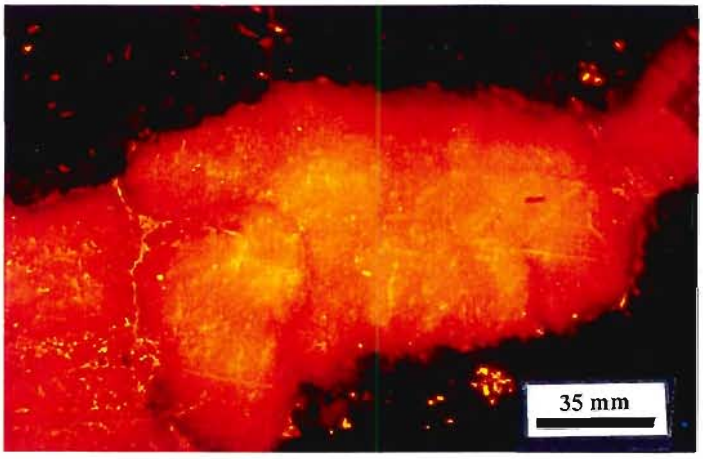

Figure 4.3 CL image of pink sparry calcite associated with Fe-Mn oxide ore at Kombat. Zoning towards a more red CL colour near the contact with the ore is evident.

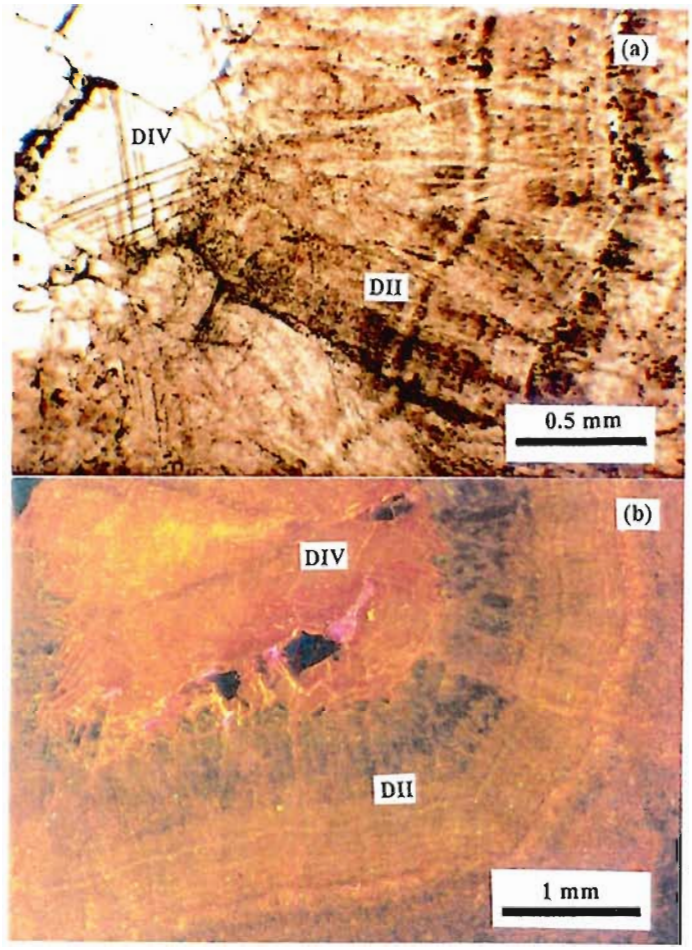

Figure 4.4 (a) Transmitted light (PPL) photomicrograph of rhythmite of the Dolomite II (DII) generation of Frimmel *et al.* (1997), and sparry dolomite of the Dolomite IV (DIV) generation at Berg Aukas; **(b)** CL image showing the rhythmite banding on a larger scale. The transmitted light photomicrograph is from the upper right portion of the CL image.

4.3 CARBONATE MINERAL CHEMISTRY

Carbonates from the various generations were analysed by EPMA to determine possible changes in stoichiometry with different stages of alteration, and to compare similar generations between different deposits. Details of the analytical procedures are given in Appendix A2.2, along with the full set of carbonate analyses. Table 4.1 lists compositional ranges for carbonate generations recognised at Tsumeb, Khusib Springs and Kombat.

With the exception of the Fe-bearing dolomite grains from Khusib Springs, dolomite compositions from all three deposits are close to stoichiometric, ranging in $MgCO_3/CaCO_3$ from 0.76 to 0.88 (Fig. 4.5). Stoichiometry does not provide a means for differentiating between generations as the ranges in ratios of $MgCO_3/CaCO_3$ overlap for different generations within the same deposit, and for similar generations between deposits (Fig. 4.5).

Calcite compositions from Tsumeb and Kombat are variable. Up to 1.26 wt% $MgCO_3$ may be present in calcite at Tsumeb. At Kombat calcite grains in the calcitised dolostone are variable in $MgCO_3$ content, with up to 2.09 wt% $MgCO_3$ present in these grains. This deviation from stoichiometry, coupled with the presence of grains with dolomite compositions, suggests incomplete removal of Mg from the system during calcitisation. Pink sparry calcite and milky white calcite at Kombat are non-stoichiometric, containing significant amounts of $MnCO_3$ and $FeCO_3$ in addition to $MgCO_3$ (Table 4.1, Fig. 4.6). In general, calcites from Kombat and Tsumeb can be described as low-Mg calcites (Veizer, 1983a).

Fe and Mn are either present in very low concentrations or below the detection limit in many of the carbonate phases analysed. However, in spite of this, certain trends are evident within and between different generations of carbonate from the deposits (Fig. 4.6). An increase in $MnCO_3$ is observed from host dolomite to sparry dolomite at Tsumeb and Khusib Springs, with the increase being more pronounced in the Khusib Springs sparry dolomite (Table 4.1; Fig. 4.6). In addition, sparry dolomite at Tsumeb contains detectable Fe. Coarsely recrystallised dolomite from Khusib Springs contains Mn in concentrations similar to the sparry dolomite, with Fe below detection. However, both Fe and Mn are below detection in the coarsely recrystallised dolomite

Table 4.1 Compositional ranges (wt%) of different carbonate generations at Tsumeb, Khusib Springs and Kombat.

Deposit	Tsumeb				Khusib Springs					Kombat			
Alt. Type*	1	2	3	4	1	2	3	4	5	1	2	3	4
No. Analyses	15	26	12	15	5	23	8	5	3	5	19	10	13
$CaCO_3$	53.71-56.21	53.94-56.81	54.45-56.57	98.25-100.15	53.73-54.99	52.95-55.78	55.07-56.35	53.56-55.38	53.24-54.31	54.10-55.49	96.20 - 99.96	89.72-94.65	95.64-99.75
$MgCO_3$	43.72-46.28	43.39-45.62	43.30-45.69	0.83-1.26	44.43-45.67	43.22-46.54	43.34-45.10	42.19-44.40	39.22-40.73	44.25-45.62	0.19-2.09	<LLD-1.97	0.25-2.34
$MnCO_3$	<LLD-0.31	<LLD-0.53	<LLD-0.42	<LLD	<LLD	0.32-1.54	0.78-1.54	0.28-1.26	0.21-0.44	<LLD-0.51	<LLD-1.37	3.58-5.19	0.49-1.44
$FeCO_3$	<LLD-0.50	<LLD-0.41	<LLD	<LLD	<LLD-0.36	<LLD	<LLD	<LLD	3.54-5.08	<LLD	<LLD	0.32-2.83	<LLD-0.92
Total	**98.41-101.66**	**99.15-101.75**	**97.96-101.50**	**99.08-101.18**	**98.51-99.61**	**99.45-101.95**	**100.47-101.72**	**98.32-98.81**	**97.92-99.05**	**98.42-101.43**	**98.68-101.95**	**98.58-101.57**	**98.37-101.56**

* Tsumeb: 1 = host dolomicrite
2 = sparry dolomite
3 = coarsely recrystallised dolomite
4 = sparry calcite

Kombat: 1 = dolomite grains in calcitised dolomite
2 = calcite grains in calcitised dolomite
3 = sparry pink calcite
4 = blocky white calcite

Khusib springs: 1 = host dolomite
2 = sparry dolomite
3 = coarsely recrystallised dolomite
4 = sparry dolomite associated with Fe-bearing dolomite
5 = Fe-bearing dolomite

LLD = lower limit of detection

from Tsumeb. Fe-bearing dolomite grains at Khusib Springs contain significant Fe over Mn contents in their cores. Towards the edges of these grains however, the composition becomes calcitic (Appendix A2.2), with low to undetectable Fe, and Mn concentrations below detection. The sparry dolomite associated with these grains (Fig. 4.2) is slightly depleted in Mn relative to the sparry dolomite described from within the deposit (Table 4.1).

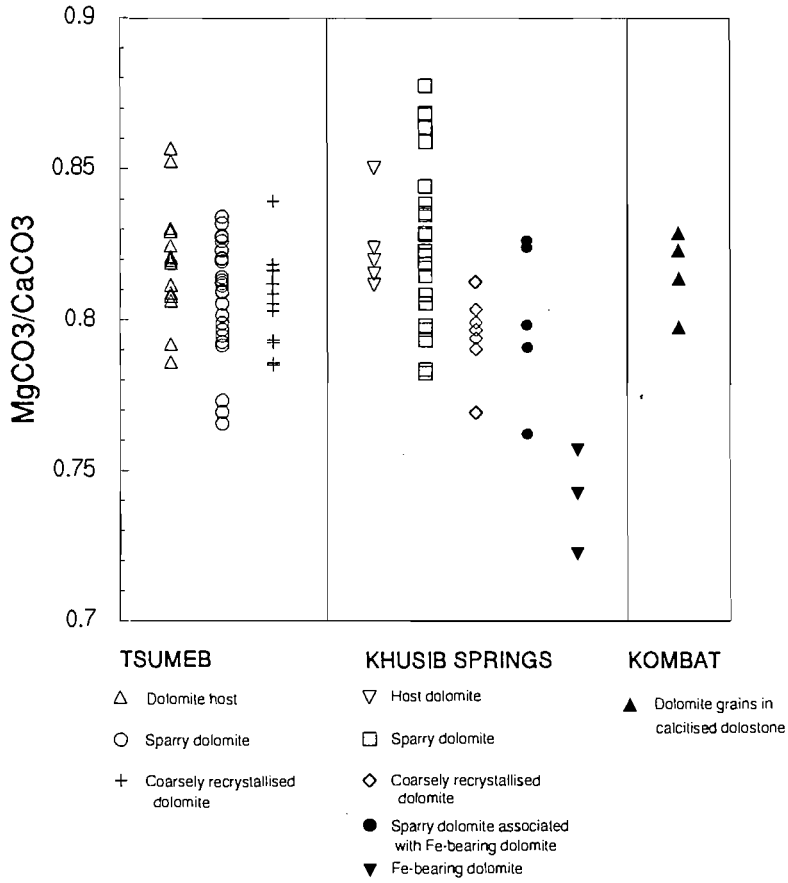

Figure 4.5 Variations in the $MgCO_3/CaCO_3$ ratio of different dolomite generations at Tsumeb, Khusib Springs and Kombat.

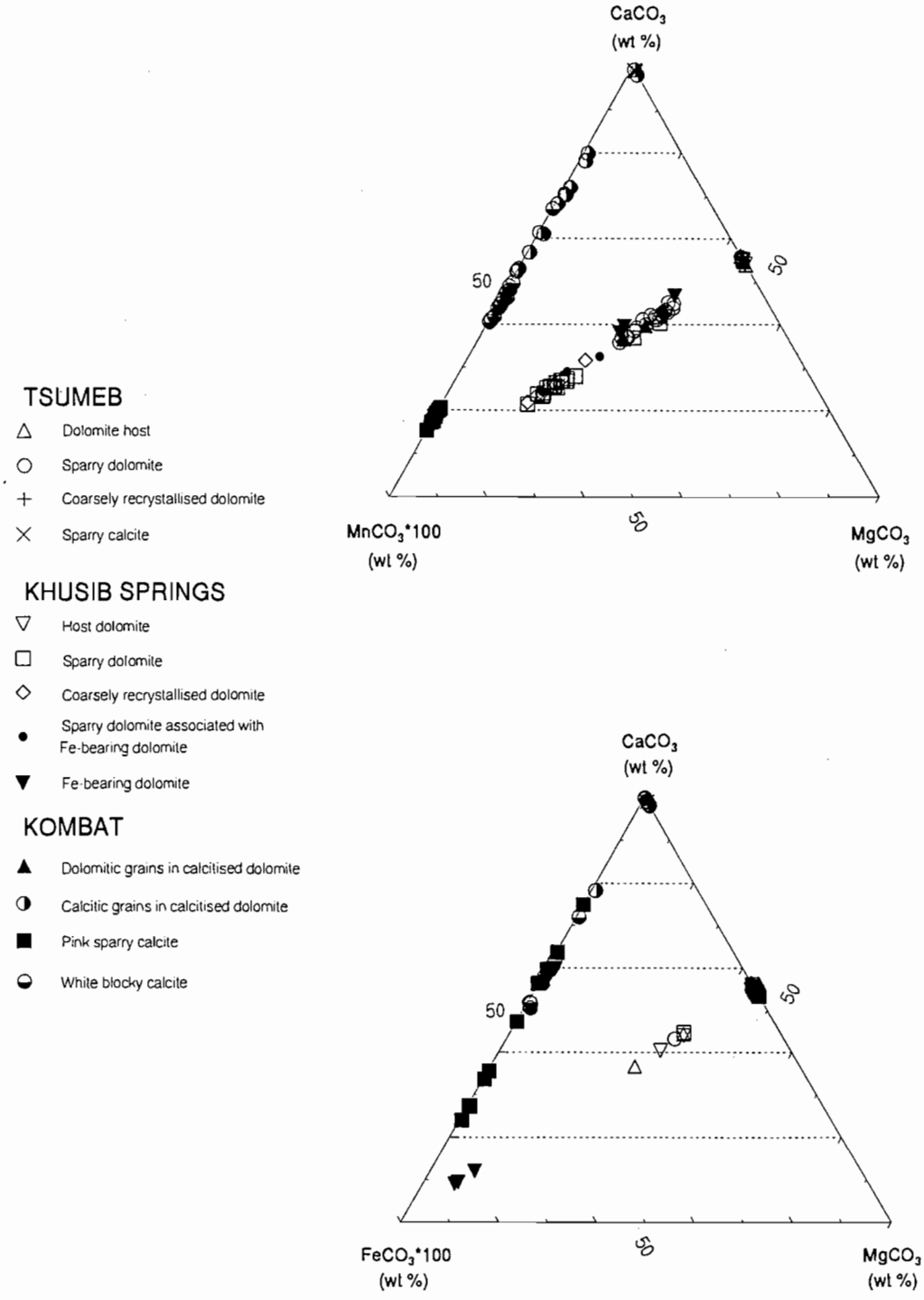

Figure 4.6 Compositional plots of different carbonate alteration types at Tsumeb, Khusib Springs and Kombat.

The differences in Fe and Mn concentrations in these dolomites is reflected in their CL behaviour. The suppression or activation of CL in calcite and dolomite has been attributed to the presence of these two elements. Mn activates CL, whereas Fe suppresses it (Sommers, 1972; Pierson, 1981; Ten Have and Heijnen, 1985; Hemming *et al.*, 1989). The increase in the intensity of red in the sparry dolomites compared to the dolomicrite host can hence be correlated with trends of Mn enrichment relative to Fe with alteration. This is also reflected in the trace element concentrations of Mn in bulk analyses (Chapter 5). Although Mn is below detection in certain samples (e.g. coarsely recrystallised dolomite from Tsumeb), a bright red CL colour is nevertheless observed. This is because only trace amounts of Mn are required to activate CL (~100 ppm) whereas larger concentrations of Fe (>10000 ppm) are required to quench it (Hemming *et al.*, 1989).

Calcites from Kombat are also enriched in Mn relative to Fe. Pink sparry calcite contains significant Mn, along with lesser (but variable) amounts of Fe (Fig. 4.6). The association of this carbonate with the Fe-Mn ore assemblage may account for this enrichment relative to the other calcites.

4.4 PARAGENESIS

4.4.1 Tsumeb

The paragenesis of carbonate alteration and ore mineralisation at Tsumeb is rather complex, but has been described in simplified terms by Lombaard *et al.* (1986) and Theron and Beukes (1993). It was not possible to deal with all the generations of carbonates at this deposit. However, pertinent generations have been dealt with here, where their relationship to the ore mineralisation has been established. For the Tsumeb deposit, it would seem that host dolomicrite was infiltrated by fluids, possibly bearing hydrocarbons, which caused recrystallisation in some parts, giving rise to the coarsely recrystallised dolomite. It is possible that these fluids also precipitated the sparry dolomite veins, along with sulphide and sulphosalt minerals. Lower down in the pipe structure, silicification was the dominant alteration mechanism, in which silica bearing fluids

pervasively infiltrated the host dolomicrite, precipitating also siliceous dolomite veins. Three generations of calcite alteration seem evident at Tsumeb, the first relating to the pervasive calcitisation described by Lombaard *et al.* (1986), initiated prior to mineralisation. The second was possibly coeval with the sparry dolomite crystallisation episode. This generation is associated with ore mineral phases such as tennantite and pyrite. The third calcite generation would have crystallised later in the paragenetic sequence, forming cross-cutting relationships with the mineralised host dolomite; this generation is barren with respect to mineralisation.

Thus the paragenesis of carbonate/silicic alteration as observed from samples obtained for this study can be described as:

Dolomite I : host dolomicrite;

Calcite I: early calcitisation of dolomite host, pre-mineralisation feature;

Dolomite II: coarsely recrystallised dolomite, with either introduced or remobilised hydrocarbons;

Dolomite III: sparry dolomite, occurring as veins or forming the matrix in tectonic breccias. This generation may have been coeval with Dolomite II;

Quartz-dolomite I: silicified dolomite, which is the host dolomite altered by silica-rich fluids. This generation may be coeval with the sparry dolomite of Dolomite III, as the quartz also occurs in the sparry dolomite veins;

Calcite II: sparry calcite veining, with a quartz association, hosting sulphide ore;

Calcite III: late, cross-cutting calcite, devoid of mineralisation.

4.4.2 Khusib Springs

A similar paragenesis to that described for Tsumeb is evident at Khusib Springs. However, the dominant alteration type at this deposit is dolomite alteration.

From the textural, mineralogical and CL evidence, it would seem that the host dolomicrite (dull, almost non-luminescent) was infiltrated by fluids which either introduced or remobilised hydrocarbons, in much the same way as was described for Tsumeb. The host is darker in colour

closer to the deposit, indicating an increase in hydrocarbon content. This may be a hydrothermal effect, and the host is thus divided into a dark host dolomicrite, close to and within the deposit, and a medium grey host dolomite, further away from the deposit. The occurrence of hydrocarbons lining grain boundaries in the coarsely recrystallised dolomite suggests that hot, infiltrating fluids caused recrystallisation of the dark dolomite host, remobilising the hydrocarbons such that these lined the recrystallised dolomite grains. Associated with this event was the precipitation of sparry dolomite veins and sulphide deposition, such as tennantite, enargite and pyrite into the inner part of the ore body, and galena and sphalerite, towards the outer part of the ore body. Vague cross cutting relationships between sparry dolomite veins, along with the presence of malachite and azurite in some of these sparry veins, suggests a second generation of sparry dolomite. Further away from the ore body, sparry dolomite is closely associated with Fe-bearing dolomite. Other alteration types evident at Khusib Springs are calcite and silica alteration. Silica occurs as quartz intergrown with the sparry dolomite hosting the sulphides. Unlike the silica at Tsumeb, which in thin section is difficult to define as an individual mineral in the silicified dolomite, the quartz associated with the sparry dolomite is discrete, although still too fine-grained to be physically separated by hand picking in certain parts of these sparry dolomite veins. Another generation of quartz is associated with paragenetically late calcite veining, as this quartz also individually cross-cuts sparry dolomite veins, and, with the calcite, occupies tension gashes.

The paragenetic sequence at Khusib Springs can thus be described:

Dolomite Ia: host dolomicrite, fine grained and medium grey in colour, belonging to the dolomitised T3 portion of the Maieberg Formation;

Dolomite Ib: host dolomicrite, fine grained and dark grey to black in colour, within and immediately surrounding the deposit;

Limestone I: Host limestone of the T2 zone within the deposit, dark in colour;

Dolomite IIa: sparry dolomite veining, hosting sulphide mineralisation;

Dolomite IIb: coarsely recrystallised dolomite;

Dolomite IIc: sparry dolomite with an Fe-bearing dolomite association in the distal areas to the ore body. This may be a distal equivalent to Dolomite IIa and b, and is hence included as a subgeneration;

Quartz I: associated with the sparry dolomite, Dolomite IIa;

Dolomite III: later sparry dolomite associated with secondary, oxidised mineralisation;

Calcite I: late calcite veining, devoid of mineralisation;

Quartz II: associated with Calcite I and cross-cutting Dolomite IIa.

4.4.3 Kombat

The principal generations described from Kombat include: calcitised dolomite from different ore bodies in the Kombat group of mines, either devoid of mineralisation or hosting predominantly chalcopyrite and bornite, with minor chalcocite and covellite in places; sparry pink calcite, occurring within the Fe-Mn oxide assemblage, and blocky calcite veining, associated with chalcopyrite and minor bornite in places. The paragenesis suggested is :

Dolomite I: host dolomite, with perhaps incipient calcitisation, forming the fragments in breccia;

Calcite I: sparry pink calcite associated with the Fe-Mn assemblage, which is considered to be the earliest in the ore paragenetic sequence at Kombat (Innes and Chaplin, 1986; Frimmel *et al.*, 1997);

Calcite IIa: light coloured, blue-grey calcitisation, pervasive, hosting chalcopyrite and bornite (Drill core AU, Asis West), or chalcopyrite, bornite, chalcocite and covellite (Drill core KSW-1A, Asis West);

Calcite IIb: calcitisation occurring as a buff-coloured, recrystallised type (E900 ore body environs);

Calcite IIc: dark coloured, siliceous calcitisation, forming the matrix in breccias, hosting finely disseminated chalcopyrite and bornite;

Calcite III: blocky, white calcite veining, associated with chalcopyrite and minor bornite in places.

CHAPTER FIVE: ELEMENTAL DISTRIBUTION

5.1 INTRODUCTION

Trace element, including rare earth element (REE), distributions in carbonate rocks have been extensively investigated with respect to diagenetic and mineralisation processes, particularly for MVT occurrences (e.g. Banner *et al.*, 1988; Brand and Veizer, 1980; Buelter and Guillemette, 1988; Bustillo *et al.*, 1992; Graf, 1984; Vahrenkamp and Swart, 1990; Veizer, 1983a). Trace element incorporation into carbonate phases during precipitation, either as primary, diagenetic or hydrothermal products, has also been discussed by a number of workers (e.g. Dromgoole and Walter, 1990; Ichikuni, 1973; Jacobson and Usdowski, 1976; Lorens, 1981; Möller, 1991; Möller and Morteani, 1983; Morse, 1983; Spangenberg, 1995; Veizer, 1983a)..

The aim of this part of the study was to compare the REE and other trace element distributions in the various carbonate generations of the Tsumeb, Kombat and Khusib Springs deposits. Where possible, comparisons were also made with the Berg Aukas deposit. To this end, elemental distributions in the carbonate generations for the Tsumeb, Kombat and Khusib Springs deposits, along with the Berg Aukas deposit, were investigated using XRF for trace elements, and gradient HPIC for REE.

5.2 TRACE ELEMENT DISTRIBUTION

5.2.1 Analytical methods

Trace element analysis was carried out on thirty-three carbonate samples from the localities of Tsumeb, Khusib Springs, Kombat and Berg Aukas. These included whole-rock and mineral separate analyses on dolomites and calcites of various generations. Mineral separates were obtained by hand picking from vein samples.

Trace elements analysed for included Mo, Nb, Zr, Y, Sr, U, Rb, Th, Pb, Zn, Cu, Ni, Ba, Sc, Co, Cr, V and Mn. Details of the analytical procedure are outlined in Appendix A2.3. Certain carbonate samples contained sulphide mineralisation of a finely disseminated nature, and could therefore not be completely separated from the sulphide fraction. As a result, anomalously high concentrations of Cu, Pb and Zn were observed in these samples. In addition, not all samples yielded material sufficient to analyse. Consequently, trace element distributions in certain generations are not represented.

5.2.2 Results

The trace element compositions for the various carbonate generations at Khusib Springs, Tsumeb, Kombat and Berg Aukas are presented in Table 5.1.

5.2.2.1 Tsumeb

Trace element concentrations were normalised with respect to sample 2965/300, a medium grey dolomicrite host, Dolomite I, texturally the least altered dolomite. All other generations (including other host dolomites), with the exception of the dolomite associated with gypsum, are enriched in trace element abundance compared to the least altered dolomite (Fig. 5.1). There appears to be a consistent trend with respect to Y, Sr, Ba and Mn in the various generations, again with the exception of the dolomite associated with gypsum. The four elements are variably enriched relative to concentrations in the least altered host, whereas a general depletion in Rb is evident in the alteration products, probably due to Rb being restricted to the clay fraction of the host dolomicrite. Trace element abundances in the silicified dolomite of the Quartz-Dolomite I generation may be even higher should only the carbonate fraction be considered, as trace elements are not expected to substitute into quartz to any significant extent.

The base metal concentrations are variable in the alteration phases. Anomalously high concentrations are due to the presence of sulphide mineralisation, evidenced by the high S contents (Table 5.1). Mo, Zr, Sc and Cr were below detection in the least altered Dolomite I. This

Table 5.1 Trace element compositions of carbonate generations from Tsumeb, Khusib Springs, Kombat and Berg Aukas.

Sample			KH91/1 181.85#	KH91/1H1 382.9#	DV30#	DV23	DV7	DV10	DV4#	DV27	KH91/1SV 382.9	DV19	DV21	DV24	2965/289#	2965/300#	DCT4H	2965/62	DCT10#	2965/106	DCT4S.V.	DCT5
Deposit*			1	1	1	1	1	1	1	1	1	1	1	1	2	2	2	2	2	2	2	2
Generation			Dol Ia	Dol Ia	Dol Ib	Lst I	Dol IIa	Dol IIa	Dol IIb	Dol IIb	Dol IIc	Dol III	Dol III	Cal I	Dol I	Dol I	Dol I	Cal I	Dol II	Dol III	Dol III	Dol III
Mo (ppm)			1.4		2.9	3.3	1.6	1.2	2.1	4.7		n.d.	n.d.	4.2	n.d.	n.d.	n.d.	n.d.	4.1	n.d.	n.d.	
Zr			3.5		11.7	3.6	n.d.	n.d.	14	9.4		n.d.	3.4	n.d.	1.8	n.d.	5.8	1.2	5	n.d.	n.d.	
Y			1.8		4.2	3.6	6	5.6	6.6	6.5		4.8	6	74	1.5	0.8	1.6	2.5	2.9	7.8	7.1	
Sr			65		143	870	175	175	169	169		166	177	258	60	53	58	150	97	178	156	
Rb			4		23	6.2	n.d.	n.d.	16.5	8.3		1.7	2.6	n.d.	2.3	2.3	7.1	n.d.	1	n.d.	n.d.	
Ba			10.8		47	31.7	6	4.5	57	29		n.d.	n.d.	5.3	9.4	4.3	25	11	14.2	6.2	6.5	
Sc			n.d.		3.6	n.d.	n.d.	n.d.	2.8	3.6		n.d.	n.d.	n.d.	n.d.	n.d.	1.6	n.d.	1.7	n.d.	n.d.	
Cr			3.8		9.1	6	n.d.	n.d.	8.8	5.5		n.d.	n.d.	n.d.	1.6	n.d.	2.7	2	5.6	n.d.	n.d.	
V			4.4		14.6	n.d.	5.8	2.8	15.1	11		n.d.	n.d.	n.d.	1.9	1.8	7	n.d.	10.9	3.9	1.7	
Mn			107		3060	1406	8042	6708	6518	6451		6747	5419	2538	625	327	351	2688	1080	2096	1637	
Pb			9.1		66	11.2	11.7	57	769	31		40	47	79	43	14.4	15.9	11.2	1201	9.3	n.d.	
Zn			27		128	16.7	281	509	691	610		209	264	91	41	23	879	16.8	3864	12.6	51	
Cu			9.2		103	6.8	2.9	7.5	5.9	2401		42	45	9	42	17	64	19.2	12869	7.3	2.7	
U			n.d.		n.d.	n.d.	n.d.	n.d.	n.d.	n.d.		2.3	2.9	n.d.	n.d.	n.d.	n.d.	n.d.	n.d.	n.d.	n.d.	
Nb			n.d.		n.d.	n.d.	n.d.	n.d.	n.d.	n.d.		0.2	0.3	n.d.	n.d.	n.d.	n.d.	n.d.	n.d.	n.d.	n.d.	
Co			n.d.		1.7	n.d.	n.d.	n.d.	1.7	n.d.		n.d.	n.d.	n.d.	n.d.	n.d.	2.2	n.d.	2.5	n.d.	n.d.	
Th			n.d.		n.d.	n.d.	n.d.	n.d.	n.d.	n.d.		3.7	3.2	n.d.	n.d.	n.d.	n.d.	n.d.	n.d.	n.d.	n.d.	
Ni			n.d.		2.2	n.d.	n.d.	n.d.	n.d.	n.d.		0.9	n.d.	n.d.	n.d.	n.d.	2	n.d.	n.d.	n.d.	n.d.	
S															588	449	651	637	2657	477	19.3	
REE	CHONDRITE	NASC																				
La (ppm)	0.237	32	0.88	1.08	2.49		2.41	8.11	8.44	4.25	5.41	0.92	0.53	20.58	1.37			0.93	2.76	0.72	1.09	0.56
Ce	0.612	73	1.47	2.46	6.52		5.93	18.4	21	10.13	12.72	2.6	1.69	52.3	2.13	0.51		1.85	6.08	1.74	3.46	1.45
Pr	0.095	7.9		0.28	0.98		0.75		1.96	1.32	1.95			8.14					0.67	0.22	0.63	0.25
Nd	0.467	33	0.68	1.23	3.96		3.16	6.37	8.33	5.15	6.91	1.86	1.23	31.7	0.92	0.22		1.12	2.78	1.05	2.52	1.14
Sm	0.153	5.7	0.14	0.28	0.74		0.76	1.15	1.57	1.01	1.3	0.45	0.34	6.9	0.21	0.06		0.26	0.61	0.27	0.72	0.36
Eu	0.058	1.24		0.06	0.15		0.19	0.31	0.35	0.18	0.33	0.1	0.07	2.31				0.07	0.15	0.07	0.13	0.07
Gd	0.206	5.2	0.16	0.27	0.65		0.8	1.03	1.4	0.81	1.03	0.48	0.34	7.34	0.2	0.08		0.37	0.6	0.32	0.75	0.37
Tb	0.037	0.85	0.03	0.04	0.09		0.13	0.16	0.22	0.11	0.13	0.09	0.06	1.2				0.07	0.09	0.05	0.17	0.09
Dy	0.254	5.8	0.17	0.28	0.6		0.73	0.92	1.34	0.76	0.81	0.56	0.38	9.3	0.19	0.08		0.42	0.6	0.38	1.09	0.55
Er	0.166	3.4	0.1	0.16	0.27		0.38	0.46	0.78	0.5	0.29	0.31	0.2	4.05	0.09	0.05		0.2	0.36	0.25	0.71	0.37
Yb	0.17	3.1	0.07	0.09	0.15		0.28	0.27	0.61	0.42	0.12	0.26	0.14	2.53				0.09	0.28	0.27	0.58	0.27
Total REE	2.455	171.19	3.7	6.23	16.6		15.52	37.18	46	24.64	31	7.63	4.98	146.35	5.11	1		5.38	14.98	5.34	11.85	5.48
Eu/Eu*(CN)			0	0.65	0.66		0.76	0.86	0.73	0.62	0.72	0.64	0.63	0.99				0.73	0.76	0.71	0.54	0.58
La/Yb (CN)			9.02	8.42	11.91		6.12	21.24	9.97	7.26	22.23	2.54	2.72	5.83				7.06	7.07	1.93	1.35	1.5

Table 5.1 cont.

Sample	DCT1	DCT2	3153/28A	3153/18	S67B	DCK1#	AU13/88	KSW-1A	KSW-1A	KSW-1A	DCK4	DCK3	AU17/83	AU17/83	Q1-4(I)	Q1-4(II)	Q1-4(III)	HB-2	HFO-1	BAD14/12	BAD7/4B	CH-1b
							115.80	1023.3	1037.4	1037.9			247.4	255.5								
Deposit*	2	2	2	2	2	3	3	3	3	3	3	3	3	3	4	4	4	4	4	4	4	4
Generation	Qtz-Dol I	Qtz-Dol I	Cal IIa	Cal IIb	Dol-gyp	Dol I	Cal I	Cal IIa	Cal IIa	Cal IIa	Cal IIb	Cal IIc	Cal III	Cal III	Dol I	Dol II	Dol III	Dol III	Dol III	Dol I	Dol III	Dol IV
Mo (ppm)	0.8	1.4			n.d.	n.d.		n.d.	n.d.	n.d.	n.d.	75	n.d.	n.d.	1	1	1.2	2.1	n.d.			
Zr	2.6	n.d.			n.d.	5.7		1.1	2.4	n.d.	1.4	n.d.	2.4	1.9	n.d.	n.d.	n.d.	1.5	3.9			
Y	2.3	1.3			1.9	2.4		2.1	5.2	1.5	3.7	13.2	96	74	n.d.	n.d.	n.d.	n.d.	5.1			
Sr	93	31			109	63		113	118	123	151	125	697	805	81	64	71	83	138			
Rb	3.1	n.d.			n.d.	6.8		n.d.	n.d.	n.d.	n.d.	22	n.d.	1.3	n.d.	n.d.	n.d.	n.d.	1.5			
Ba	15.3	n.d.			n.d.	39		10.3	12	12.1	7.5	165	11	11.2	2.5	4.5	3	n.d.	n.d.			
Sc	2.4	2.9			n.d.	n.d.		n.d.	n.d.	n.d.	n.d.	2.6	n.d.	n.d.	n.d.	n.d.	3.7	n.d.	n.d.			
Cr	2.8	12.8			n.d.	7.2		2.3	n.d.	n.d.	3.7	27	n.d.	n.d.	1.9	n.d.	2.3	n.d.	n.d.			
V	3.2	3.1			8.7	8.2		n.d.	3.3	n.d.	5.4	354	n.d.	n.d.	n.d.	n.d.	2.1	n.d.	n.d.			
Mn	1716	507			197	1206		2198	1799	3169	6227	2610	4705	4257	292	294	958	565	1497			
Pb	118	6.5			n.d.	n.d.		5	4.9	10.8	6.9	29541	10.8	8.7	n.d.	n.d.	n.d.	64	15.6			
Zn	489	89			3.2	9.2		6.2	52	40	n.d.	330	5.8	5.4	9.2	6.8	6.5	6028	235			
Cu	49	5.7			6.2	4.2		18.3	150	67	6122	15124	4	4.1	3.6	2.5	1.3	3.7	11.1			
U	n.d.	n.d.			n.d.	n.d.		n.d.	n.d.	n.d.	n.d.	102	n.d.	n.d.	n.d.	n.d.	n.d.	n.d.	3.6			
Nb	n.d.	n.d.			n.d.	n.d.		n.d.	n.d.	n.d.	n.d.	n.d.	n.d.	n.d.	n.d.	n.d.	n.d.	n.d.	n.d.			
Co	n.d.	n.d.			n.d.	n.d.		n.d.	n.d.	n.d.	n.d.	26	n.d.	n.d.	n.d.	n.d.	n.d.	n.d.	n.d.			
Th	n.d.	n.d.			n.d.	n.d.		n.d.	n.d.	n.d.	n.d.	5.9	n.d.	n.d.	n.d.	n.d.	n.d.	n.d.	1.2			
Ni	4.6	3			n.d.	n.d.		n.d.	n.d.	n.d.	n.d.	4.9	n.d.	n.d.	n.d.	n.d.	n.d.	1.6	n.d.			
S	107	52			151	58		494	318	332	1889	34617	21	26								
La (ppm)	0.58	1.09	18.68	10.42	3.02	0.72	23.28		3.56	1.73			2.32	2.77								
Ce	1.41	1.94	39.89	35.09	6.05	2.09	65.65		7.46	2.56			6.1	7.02					1.69	1.56	0.73	0.38
Pr	0.17		4.65	5.57	0.7									1.06					0.27	0.17		
Nd	0.79	0.9	17.53	24.15	2.74	1.17	42.22		2.64	1.02			6.12	5.04					1.24	0.62	0.41	0.17
Sm	0.19	0.2	3.47	6.93	0.58	0.29	13.92		0.59	0.19			1.32	1.2					0.3	0.15	0.15	0.05
Eu	0.04	0.03	1.28	1.34	0.18	0.07	3.83		0.14	0.05			2.42	2.13					0.07	0.07	0.06	
Gd	0.23	0.19	3.43	8.28	0.51	0.32	15.18		0.62	0.21			5.63	4.31					0.37	0.2	0.24	0.05
Tb	0.05	0.03	0.51	1.49	0.08	0.05	2.60		0.11	0.03			1.57	1.35					0.06	0.04	0.05	0.01
Dy	0.34	0.23	2.86	9.26	0.51	0.28	13.98		0.7	0.19									0.46	0.23	0.38	0.06
Er	0.23	0.15	1.23	4.2	0.28	0.17	6.11		0.4	0.09			9.5	8.81					0.3	0.16	0.31	0.04
Yb	0.24	0.18	0.87	2.85	0.24	0.1	4.51		0.31				8.28	8.33								
Total REE	4.27	4.94	94.4	109.58	14.89	5.26	191.28		16.53	6.07			43.26	42.02					4.76	3.2	2.33	0.76
Eu/Eu*(CN)	0.58	0.47	1.14	0.54	0.99	0.67	0.81		0.70	0.79			2.72	2.87					0.69	1.26	0.91	
La/Yb (CN)	1.72	4.37	15.40	2.62	9.10	4.97	3.7		8.14				0.20	0.24								

* 1 = Khusib Springs
2 = Tsumeb
3 = Kombat
4 = Berg Aukas
# = sample solutions with 'insoluble residue'
n.d. = not detected
blank = not analysed

Phases: Dol = dolomite, Cal = calcite, Lst = limestone, Qtz = quartz

Chondrite values from Sun end McDonaugh (1989)
NASC = North American shale composite, values from McLennan (1989)

Eu/Eu* (CN) = Eu (CN)/(Sm(CN)*Gd(CN))exp0.5; CN = Chondrite normalised values

is generally true for the other carbonate generations as well (Table 5.1). The remaining trace elements analysed for (except S) were also below detection in most cases.

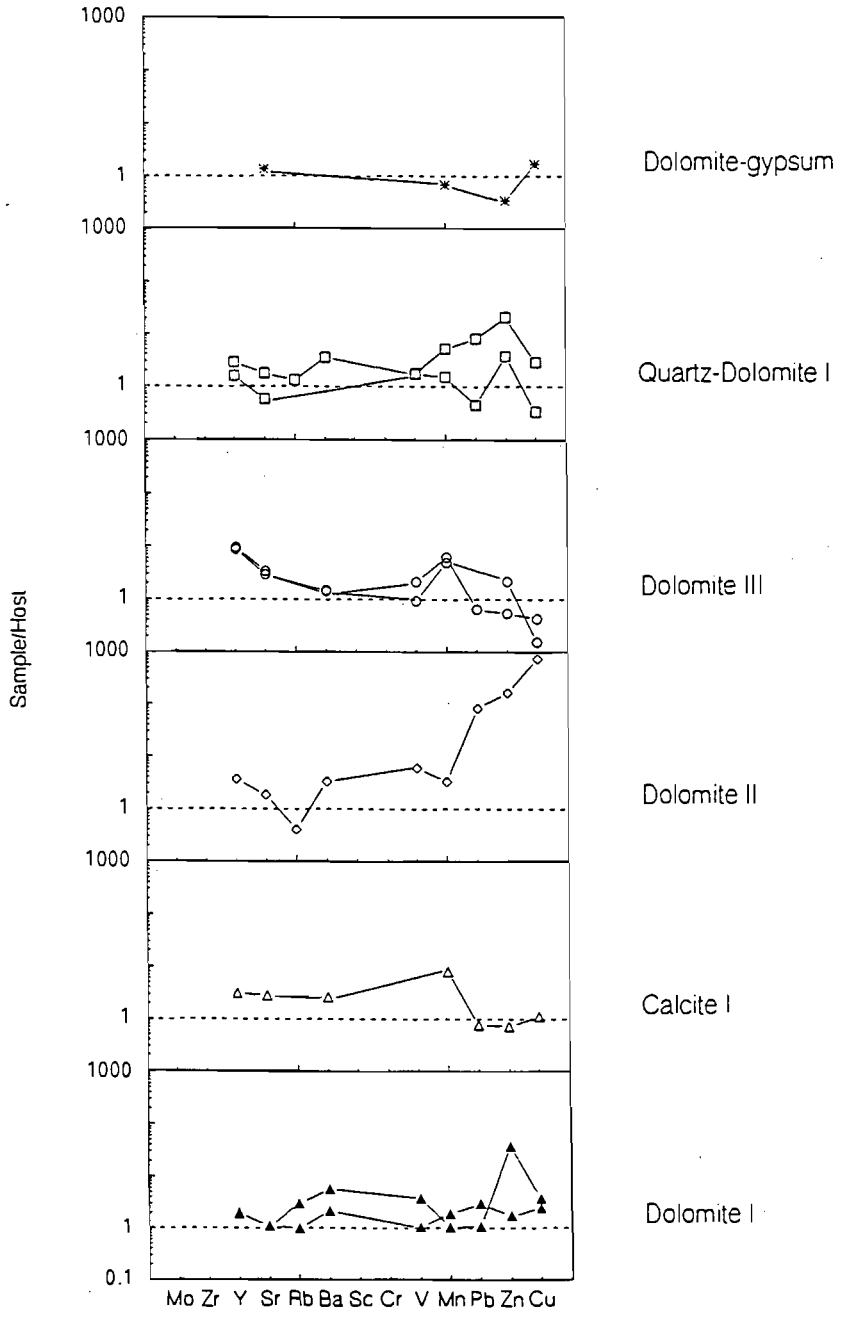

Figure 5.1 Trace element distribution in different carbonate generations at Tsumeb, normalised to the least altered host Dolomite I (sample 2965/300).

5.2.2.2 Khusib Springs

The trace elements of the various generations were normalised relative to the least altered host dolomite (sample KH91/181.85). Normalisation shows all the hydrothermal dolomites to be enriched relative to the host in most trace elements (Fig. 5.2). The only depletions observed are for Rb, Ba, V and Cr in Dolomite IIa, Dolomite III and Calcite I, and Zr in Dolomite IIa and Calcite I. Enrichment in Sr, Y and Mn is a common feature in alteration phases relative to host rock compositions at Tsumeb and Khusib Springs. Ba, however, is enriched in hydrothermal phases relative to the host at Tsumeb, whereas a depletion in its concentration in the hydrothermal phases relative to the host is evident at Khusib Springs (Fig. 5.2).

As was the case at Tsumeb, base metal concentrations are variable in concentration in the various generations at Khusib Springs (Fig. 5.2). For Dolomite IIb this may be due to minor amounts of finely disseminated ore in the rock. In Dolomite IIa, these elements may be present in the carbonate lattice, as no visible ore phases were present during mineral separation. Such variability in Cu, Pb and Zn was also found from PIXE analyses on sparry dolomite from the North Break Zone and Tsumeb ore body (Theron and Beukes, 1993).

5.2.2.3 Kombat

Trace element normalisation was carried out with respect to sample DCK1, the least altered host dolomite in terms of calcitisation. All hydrothermal phases are depleted in Zr, and with the exception of Calcite IIc, in Rb, Ba, Cr and V (Fig. 5.3). As with other hydrothermal phases from Tsumeb and Khusib Springs, there is a general enrichment in Y, Sr and Mn for the hydrothermal calcite generations at Kombat (Fig. 5.3). Anomalous enrichment in the base metals in Calcite IIb and IIc are attributed to contamination by sulphide mineralisation in these samples.

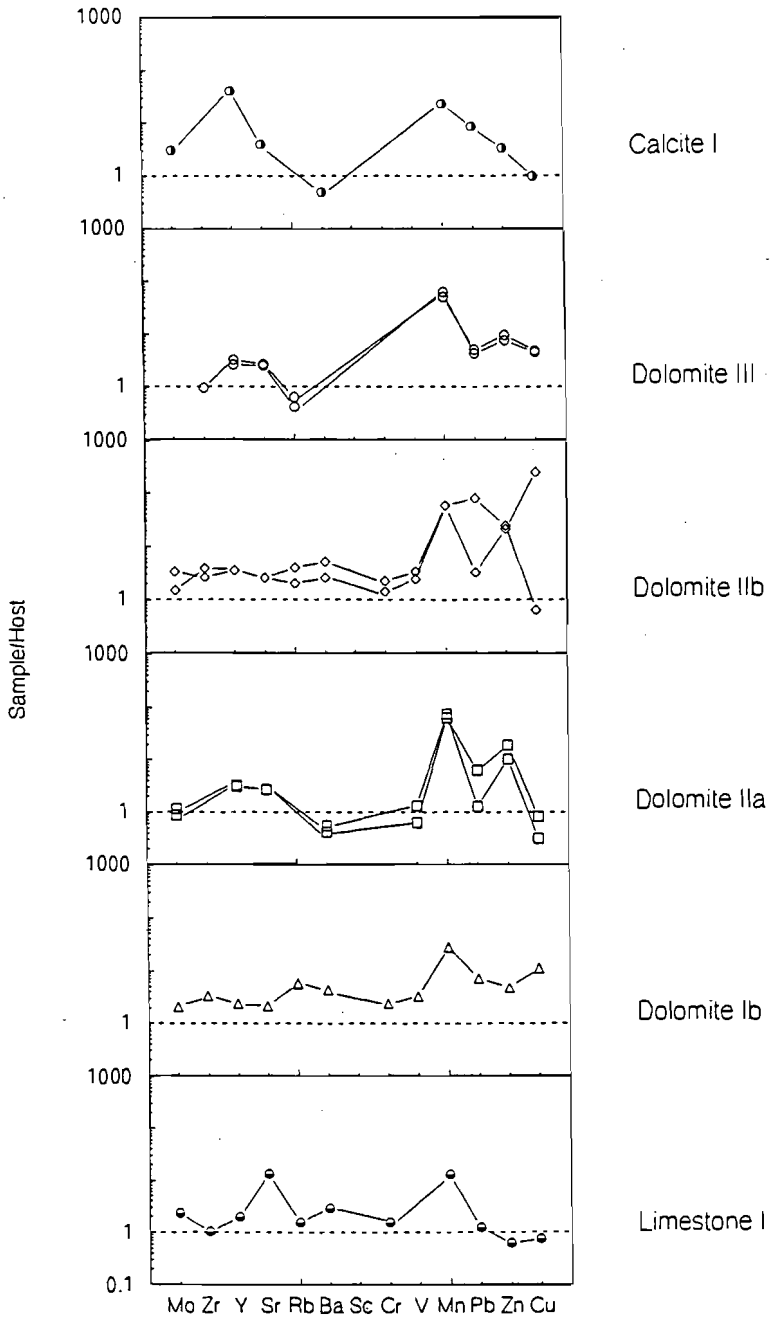

Figure 5.2 Trace element distribution in different carbonate generations at Khusib Springs, normalised to the least altered host Dolomite I (sample KH91/181.85).

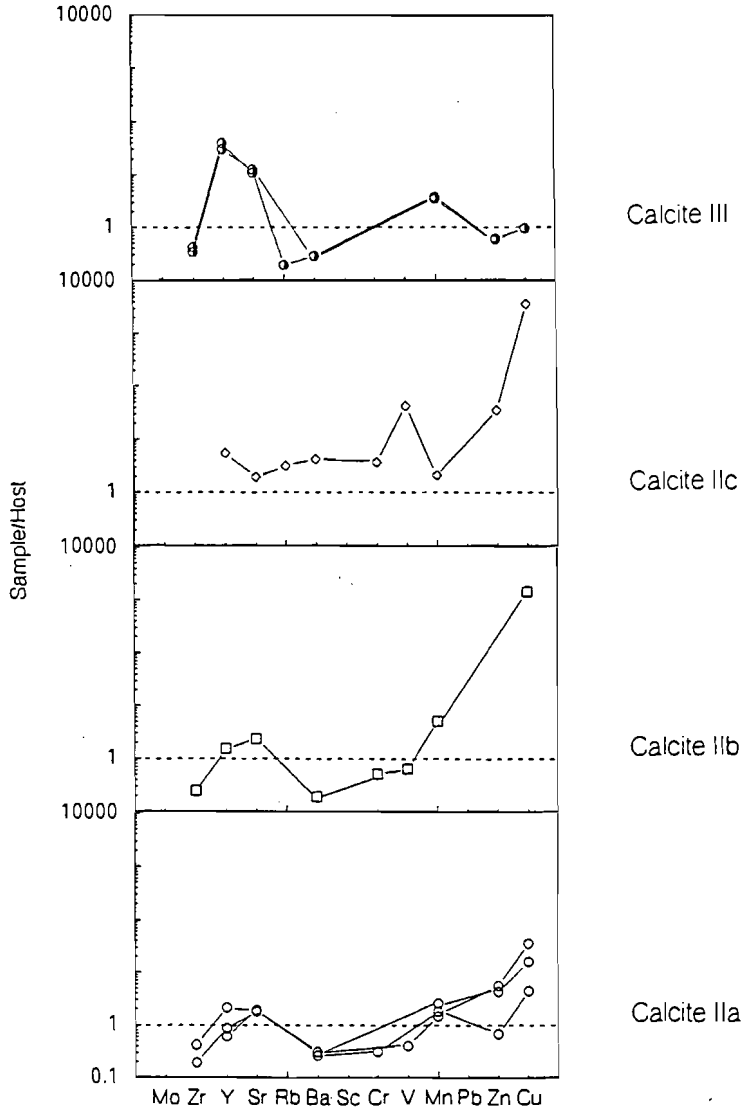

Figure 5.3 Trace element distribution in different carbonate generations at Kombat, normalised to the least altered host Dolomite I (sample DCK1).

5.2.2.4 Berg Aukas

Samples from Berg Aukas were normalised relative to the host Dolomite I, a medium grey dolomicrite. In general, most trace elements analysed for were below detection in the host and alteration phases. Dolomite II exhibits a slight enrichment in Ba, but is depleted in most of the other trace elements relative to the host (Fig. 5.4). Mn, Mo and Sr are similar to host

concentrations. Dolomite III shows a significant increase in Mn concentration over that in Dolomite I and Dolomite II. Other trace elements in this generation are variably enriched and depleted (Fig. 5.4). Anomalous enrichment of Zn in one sample of Dolomite III is attributed to contamination by sphalerite. In general, trace element concentrations in hydrothermal phases at Berg Aukas are markedly depleted compared to those in hydrothermal generations at Tsumeb, Kombat and Khusib Springs.

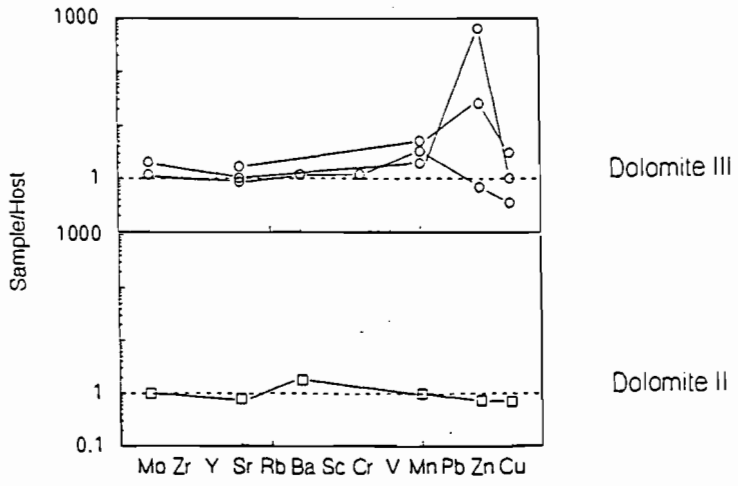

Figure 5.4 Trace element distributions in different carbonate generations at Berg Aukas, normalised to the least altered host Dolomite I (sample Q1-4(I)).

5.3 RARE EARTH ELEMENT DISTRIBUTION

5.3.1 Analytical methods

REE determinations were carried out on 35 carbonate samples of different generations from Tsumeb, Kombat, Khusib Springs and Berg Aukas. Analysis was effected via gradient HPIC, on solutions of samples analysed for trace elements, as well as additional samples, following the method of le Roex and Watkins (1990). Appendix A2.4 summarises the dissolution procedure and instrument conditions during analysis. Dissolution was effected in HF, thereby resulting in

silica and sulphide dissolution where present. Neither quartz (e.g. de Baar *et al.*, 1985) nor sulphides are expected to contain detectable REE concentrations, and the only effect would thus be one of dilution. Consideration of trace element data showed no significant contribution from clastic components related to REE-bearing phases, which would have affected the analyses by dissolution in HF. The data are therefore interpreted as for REE behaviour in carbonates. Where this is not necessarily the case, alternative interpretations must be invoked.

Host rock and certain coarsely recrystallised dolomite samples yielded insoluble residue, likely carbonaceous material. Unless these phases contain extremely high concentrations of REE, they are assumed not to have influenced REE abundances (or patterns) to any significant extent, as they constitute <2 wt% of the initial sample mass.

5.3.2 Results

5.3.2.1 Tsumeb

Pertinent observations from the chondrite-normalised pattern of the carbonate generations (Fig. 5.5a) at Tsumeb are: enrichment in REE of all hydrothermal carbonate generations relative to the host Dolomite I; enrichment in REE of Calcite II compared to the other carbonates and differences in the REE patterns amongst the various carbonate generations.

REE abundances are lowest in the host Dolomite I by up to an order of magnitude compared to the other dolomite generations. An enrichment in light rare earth elements (LREE) relative to heavy rare earth elements (HREE) is evident, with Eu below detection for this generation. A similar enrichment in LREE is observed for Dolomite II, which also shows a negative Eu anomaly[3]. Sulphides present in this generation (~2 wt%) are not considered to have significantly affected the REE pattern, which is very similar to that of Dolomite II at Khusib Springs (Fig. 5.5b).

---

[3]Eu anomaly is calculated as: $(Eu/Eu^*)_{CN} = Eu_{CN}/(Sm_{CN}*Gd_{CN})^{0.5}$; values **<1**= negative anomaly, **>1**= positive anomaly, **=1**= no anomaly. Equation after McLennan (1989).

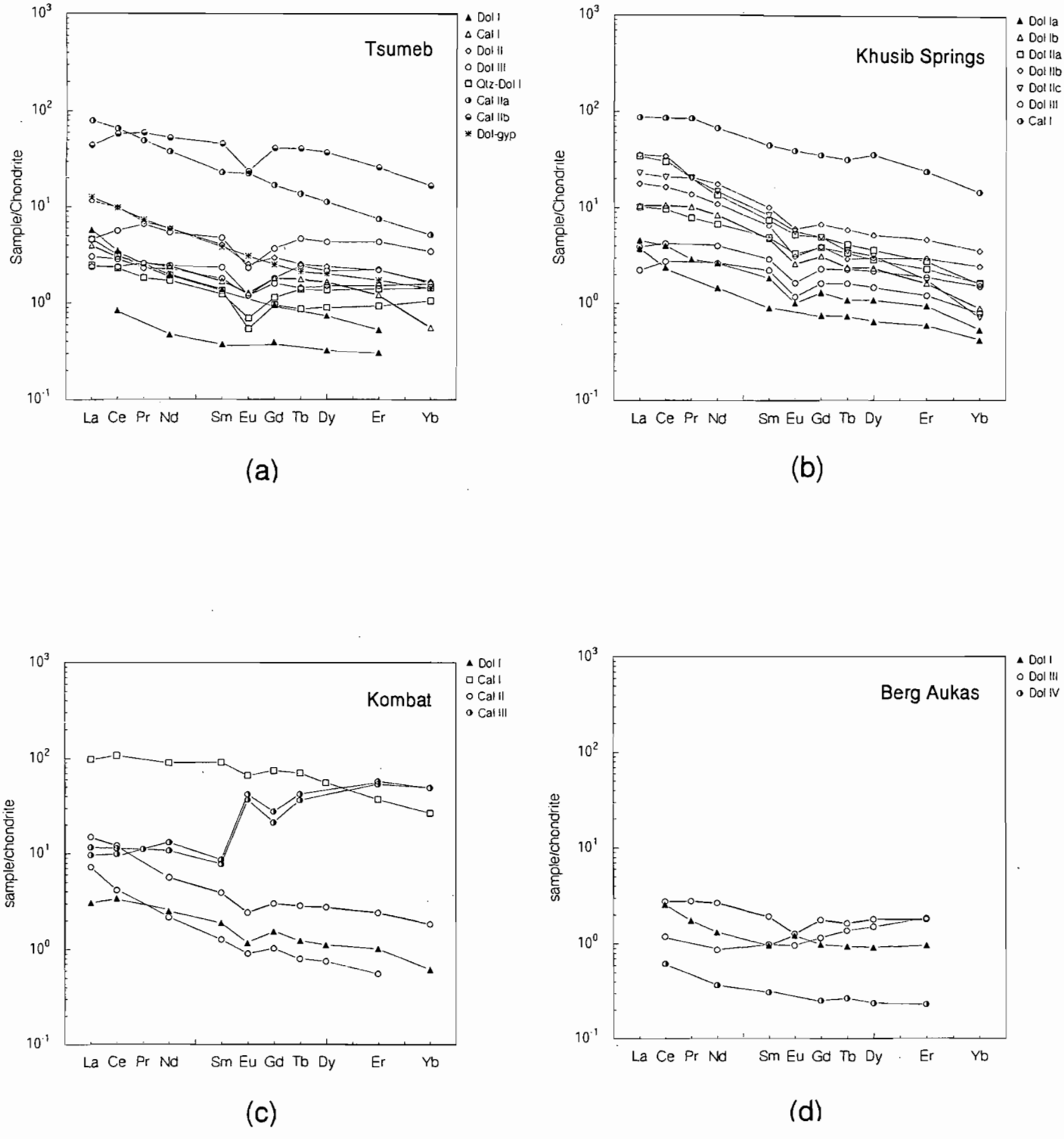

Figure 5.5 Chondrite-normalised REE abundances in carbonate generations as observed at **(a)** Tsumeb, **(b)** Khusib Springs, **(c)** Kombat and **(d)** Berg Aukas. Dol = Dolomite; Cal = Calcite; Qtz = Quartz; gyp = gypsum association. Chondrite composition after Sun and McDonough (1989).

CHAPTER SIX: STABLE (C, O) ISOTOPE DISTRIBUTION

6.1 INTRODUCTION

Stable isotope studies have made major advances in the field of ore deposit geology, particularly with respect to the origin of hydrothermal mineralising fluids and conditions of ore precipitation (e.g. Ohmoto and Rye, 1979; Ohmoto, 1986; Spangenberg *et al.*, 1996). For carbonate rocks, the stable isotopes of importance are those of C and O. These isotopes have also been useful in the study of diagenesis and dolomitisation (e.g. Hudson, 1977; Dickson and Coleman, 1980; Veizer, 1983a, 1983b; Land, 1983), as well as in the study of mineralising fluids which have precipitated carbonate gangue phases, as seen in the MVT deposits (e.g. Fritz, 1969; Hannah and Stein, 1984; Fontboté and Gorzawski, 1990).

6.1.1 Terminology

Oxygen and carbon isotope compositions are expressed in terms of the difference in isotope ratio of $^{18}O/^{16}O$ and $^{13}C/^{12}C$ (respectively) with respect to an internationally defined standard. This difference is expressed in terms of the δ value, with units given as per mil (‰). For carbon isotope compositions, the standard referred to is PDB, a Cretaceous belemnite from the Pedee Formation, South Carolina, United States, and the isotope composition is expressed as:

$$\delta^{13}C = [(^{13}C/^{12}C)_{sample} / (^{13}C/^{12}C)_{PDB} - 1]*1000 \quad (5.1)$$

For oxygen, the standard referred to in this dissertation is V-SMOW, Vienna Standard Mean Ocean Water, and the isotope composition is expressed as:

$$\delta^{18}O = [(^{18}O/^{16}O)_{sample} / (^{18}O/^{16}O)_{VSMOW} - 1]*1000 \quad (5.2)$$

Isotope fractionation is the process whereby isotopes of an element shared in common between

two substances are exchanged between those substances. This is expressed in terms of the fractionation factor α:

$$\alpha_{A\text{-}B} = R_A/R_B \quad (5.3)$$

where A and B are the substances between which isotope exchange occurs and R is the ratio of the heavy to the light isotope in each substance. Expressing the fractionation factor in terms of the measured δ values, this relationship becomes:

$$\alpha_{A\text{-}B} = (1000 + \delta_A) / (1000 + \delta_B) \quad (5.4)$$

Furthermore, this relationship can be expressed in terms of the "per mil fractionation" $10^3 \ln\alpha$, which, for values <10, can be approximated by the Δ value:

$$\Delta_{A\text{-}B} = \delta_A - \delta_B \cong 10^3 \ln \alpha_{A\text{-}B} \quad (5.5)$$

Fractionation factors have been used to express isotope fractionation between a number of substances, for example, oxygen isotope fractionation between a fluid and a carbonate mineral precipitating from that fluid, or carbon isotope fractionation between two different carbon-bearing species in a fluid. In addition, $\alpha_{A\text{-}B}$ is a temperature dependent quantity, so that an unknown δ for either A or B can be determined if the temperature at which fractionation occurred is known (e.g. Northrop and Clayton, 1966, Friedman and O'Neil, 1977).

6.1.2 Oxygen and carbon isotopes in hydrothermal ore deposits

Oxygen isotope characteristics in hydrothermal ore deposits can be used to estimate the isotopic composition of fluids from which the minerals studied precipitated. Thus it is possible to place constraints on the origins of these fluids. Ohmoto (1986) differentiated between reference waters (seawater, meteoric and juvenile water) and recycled, subsurface waters derived from one or more of the reference waters (connate, geothermal, metamorphic, magmatic, and ore-forming

waters). Thus hydrothermal fluids may contain water derived from one or more of these sources.

Oxygen isotopic variations in hydrothermal ore deposits may be caused by temperature changes, fluid mixing, and fluid-rock interaction, amongst other parameters. At a given temperature and salinity, the O isotope composition in the hydrothermal fluid is controlled to a large extent by H_2O (Taylor, 1974; Ohmoto, 1986). Fluid/rock ratios are also of importance in determining $\delta^{18}O$ of the fluid.

Carbon occurs in many oxidation states in nature, and this is reflected in its isotope variation. The most reduced forms (C^{4-}) usually occur in organic compounds, the most oxidised (C^{4+}) in carbonates, either as ions in solution or as precipitated minerals. Carbon of zero valency occurs as graphite or diamond, the former being of importance in the sedimentary carbonate environment. Changes in the redox state of C can occur by a number of mechanisms, both biological and non-biogenic (Ohmoto, 1986). The oxidised species are isotopically enriched in ^{13}C, such that under equilibrium conditions, $\delta^{13}C$ decreases for the species in the order carbonate > graphite > methane. Thus oxidised carbonates, usually of marine origin, may exhibit $\delta^{13}C$ values of 0±4 ‰, whereas CH_4, produced by biogenic reduction of HCO_3^- at the sediment-water interface, has been recorded with $\delta^{13}C$ values of -110 to -55 ‰ (Schoell, 1984).

Carbon isotope variations in hydrothermal systems will therefore be controlled by concentrations of the different carbon species in the fluid, among these, H_2CO_3, aqueous CO_2, HCO_3^-, CO_3^{2-} and CH_4. These concentrations are, in turn, dependent on fO_2, pH and temperature (Ohmoto, 1972; Ohmoto and Rye, 1979; Ohmoto, 1986). In addition, owing to the low concentration of C compared to O in fluids, carbonate mineral precipitation can lead to significant C isotope variation, such that earlier carbonates tend to be $\delta^{13}C$ enriched compared to later phases precipitated from the same fluid under closed system conditions.

6.1.3 Aims

The aim of the stable isotope study was to further characterise the generations at each of the deposits under consideration. In addition, integration with other data and comparison with the literature was done to determine whether each deposit has a distinct C and O isotopic signature in terms of the carbonate generations associated with mineralisation. Possible mechanisms leading to variations in the isotope signatures of these carbonates were also considered (Chapter 8).

6.2 ANALYTICAL METHODS

Stable isotope analyses were carried out using two techniques: the Bremen Line method was used for determining C and O isotope composition of calcite samples with <10 % dolomite contamination. This was carried out at the Department of Archaeology, University of Cape Town. Further details regarding the technique are given in Appendix A2.5. As this method was not found to be suitable for similar analysis on dolomite samples or mixed dolomite/calcite samples with >10% contamination from either mineral, the more conventional method of McCrea (1950) was employed, with modifications as outlined by Al-Aasm *et al.* (1990), in sample preparation before analysis by mass spectrometry.

6.3 RESULTS

6.3.1 Tsumeb

Dolomite I ranges in $\delta^{18}O$ from 22 to 23.6 ‰ (Fig. 6.1). The lower value is exhibited by dolomicrite occurring as fragments in breccia, of which the matrix is sparry dolomite. The higher value is shown by more massive dolostone of the T4 zone. Isotope compositions of Dolomite I plot within the range of common marine carbonates ($\delta^{18}O$ = ~29 to 18.5 ‰ SMOW; $\delta^{13}C$ = 5 to -5 ‰ PDB) as defined by Hudson (1977).

Dolomite II plots in the same region as hydrothermal dolomite at Tsumeb, determined by Hughes (1987; Fig. 6.1). $\delta^{13}C$ and $\delta^{18}O$ values for Dolomite III range from -1.7 to 0.5 ‰ and 20.2 to 21.4‰ respectively. The dolomite fractions of samples of Qtz-Dol I show no variation in $\delta^{13}C$, but range in $\delta^{18}O$ from 21.2 to 22.4 ‰. The narrow range in isotope compositions for these two generations suggests that silicification and Dolomite III precipitation may have been coeval. Both generations also plot within the broad range of values determined for hydrothermal dolomite at Tsumeb (Fig. 6.1), which includes sparry dolomite and calcitised dolostone (Hughes, 1987). However, a discrepancy exists with respect to the $\delta^{13}C$ values of hydrothermal dolomite of Theron and Beukes (1993). This can either be due to different generations being compared, or that different areas were sampled, such that similar generations yield different $\delta^{13}C$ values. Hydrothermal dolomite described by Theron and Beukes (1993) displays very similar characteristics to Dolomite III of this study (e.g. sparry texture, bright red CL, Sr and Mn enrichment relative to host dolomite), suggesting that both generations are comparable. The second explanation is therefore favoured, as hydrothermal dolomite of Theron and Beukes (1993) was sampled higher in the pipe (T7 zone) than in this study (T4/T5 zone).

Calcite I comprises dolomite and calcite fractions which yielded $\delta^{18}O$ values of 21.4 and 21.3 ‰ and $\delta^{13}C$ of -0.2 and 0.5 ‰ respectively. Such values suggest conditions of disequilibrium, even if both components crystallised together at high temperatures. Alternatively, crystallisation of each component could have taken place at different temperatures. Although Calcite I shows slightly higher $\delta^{18}O$ values than the hydrothermal calcite of Hughes (1987), both components of this generation can nevertheless be correlated with his hydrothermal dolomite, which included calcitised dolostone (whole rock composition). Calcite II, as with Dolomite III, plots in the range of isotopic compositions for hydrothermal calcite as determined by Hughes (1987) and Theron and Beukes (1993). Calcite III, on the other hand, is significantly depleted in ^{13}C compared to other calcite (and dolomite) generations (Fig. 6.1).

Dolomite associated with gypsum found in the T7 lithozone yields $\delta^{13}C$ and $\delta^{18}O$ values of 4.8 and 23 ‰ respectively. These values are comparable with other hydrothermal phases at Tsumeb, and similar to values determined for calcite with native sulphur present in the T7 zone (Hughes, 1987; Fig. 6.1).

6.3.2 Khusib Springs

Dolomite Ia, representing texturally least altered dolomite host found furthest away from the ore body (drill core KH91), shows distinctly higher $\delta^{18}O$ values compared to the other dolomite generations (Fig. 6.1). Dolomite Ib, on the other hand, plots in the same region as Dolomite II, exhibiting a range in $\delta^{13}C$ of -0.3 to -0.4 ‰ and in $\delta^{18}O$ of 18.9 to 19.3 ‰. The position of Dolomite Ib close to and within the deposit is likely to have influenced its $\delta^{18}O$ depletion relative to Dolomite Ia. Limestone immediately adjacent to the deposit is depleted in $\delta^{18}O$ relative to the unaltered host dolomite further away from the deposit, ranging in $\delta^{18}O$ from 19.7 to 22.5 ‰.

Dolomite Ib, IIa, IIb, IIc and III all plot within a rather restricted range of $\delta^{18}O$ values (18.8 to 20.1 ‰; Fig. 6.1), allowing no distinction on this basis. A wider range in $\delta^{13}C$ is apparent, however (-6.4 to -0.8 ‰; Fig. 6.1). This is predominantly due to one anomalous sample of the Dolomite II generation which occurs further away from the ore body.

Calcite I shows average $\delta^{13}C$ and $\delta^{18}O$ values of 3 ‰ and 20.2 ‰ respectively. These values are similar to the mineralised dolomite, although $\delta^{13}C$ values lie at the lower end of the range exhibited by Dolomite II (Fig. 6.1).

6.3.3 Kombat

Dolomite I does not have a distinct composition compared to the other carbonate generations, (Fig. 6.1). The slight degree of calcitisation associated with this generation, along with its close proximity to Calcite II and sulphide mineralisation, may account for this.

Calcite I exhibits $\delta^{18}O$ and $\delta^{13}C$ values of 16.5 ‰ and -7.1 ‰ respectively. These values are significantly low relative to the other carbonate generations (Fig. 6.1). As this generation is associated with the Fe-Mn oxide assemblage, its distinct composition provides a means for differentiating between calcite alteration associated with oxide as opposed to hypogene sulphide mineralisation at Kombat.

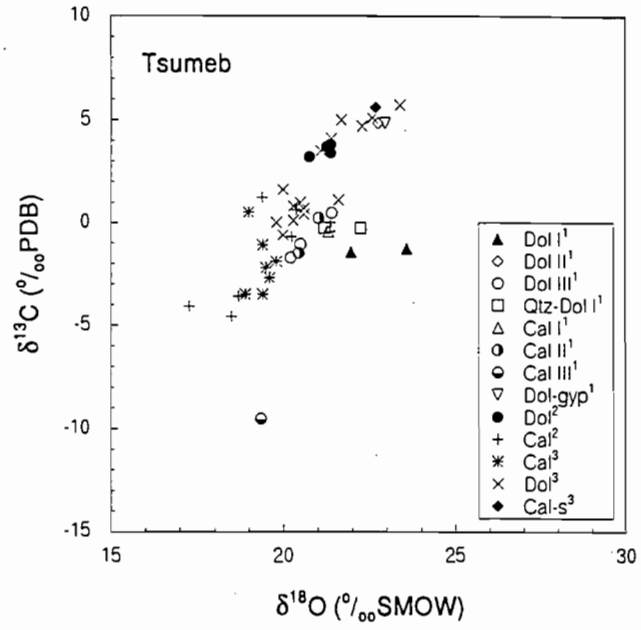

Data sources:
[1] This study; [2] Theron and Beukes (1993);
[3] Hughes (1987)

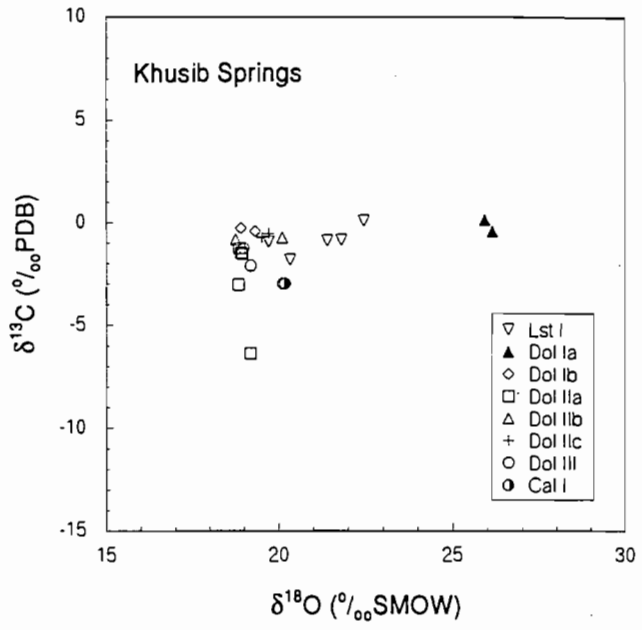

Data source:
Verran (1996)

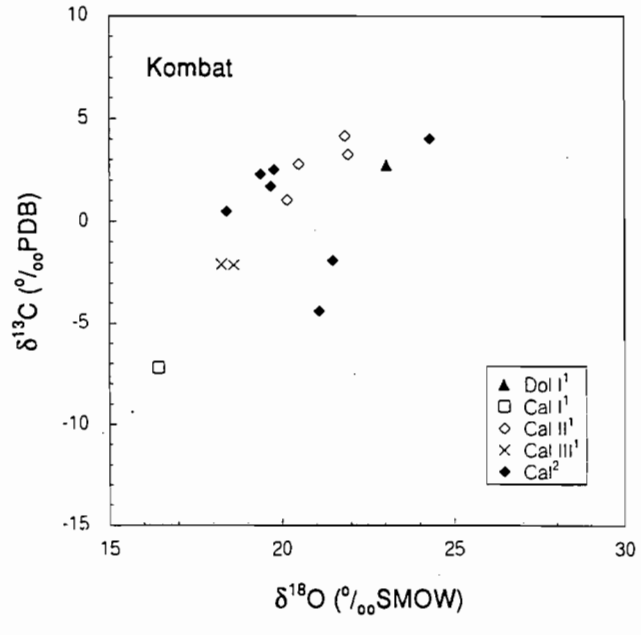

Data sources:
[1] This study; [2] Frimmel *et al.* (1997)

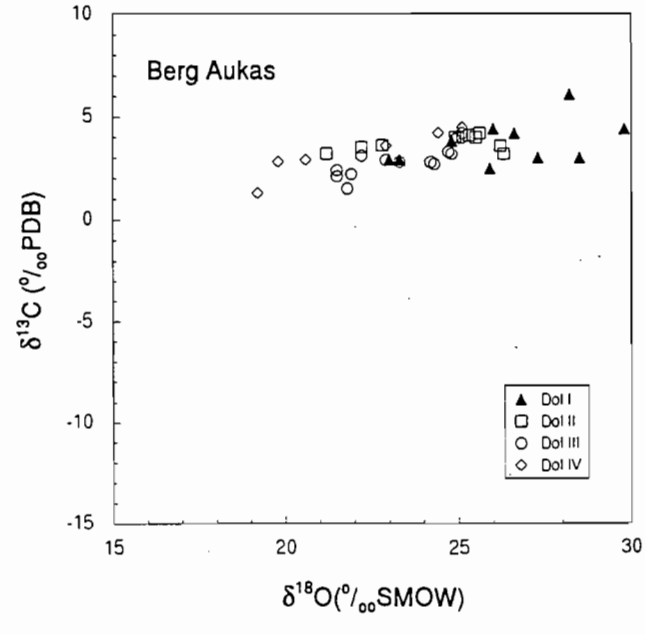

Data source:
Frimmel *et al.* (1997)

Figure 6.1 $\delta^{13}C$ vs $\delta^{18}O$ plots for carbonate generations from the four major deposits in the OML. Cal-s= calcite with native sulphur; for other mineral abbreviations, see Figure 5.5.

Calcite II exhibits a range in $\delta^{18}O$ of 20.2 to 21.9 ‰, and in $\delta^{13}C$ of 1.0 to 4.1 ‰. The lowest value in each range belongs to Calcite IIc, the dark siliceous calcite. A rather wide range in $\delta^{13}C$ and $\delta^{18}O$ values is observed for hydrothermal mineralised calcite at Kombat (Fig. 6.1), as determined by Frimmel *et al.* (1997). The values for Calcite II, as determined in this study, plot within this range. Calcite III is depleted in both ^{13}C and ^{18}O relative to Calcite II and Dolomite I, although this generation plots within the broad range of hydrothermal calcite compositions (Fig. 6.1).

6.3.4 Berg Aukas

Dolomite I exhibits a wide range in $\delta^{18}O$ values (23.0 to 29.8 ‰), and a relatively restricted range in $\delta^{13}C$ values (2.5 to 6.1 ‰; Fig. 6.1). Dolomite II, III and IV overlap in their $\delta^{13}C$ and $\delta^{18}O$ values (Fig. 6.1). Distinction between these generations is therefore difficult in this respect.

6.4 COMPARISON BETWEEN DEPOSITS

Host dolomite compositions are similar in terms of their $\delta^{18}O$ values for Tsumeb and Kombat (21-24 ‰), whereas Khusib Springs and Berg Aukas show somewhat enriched compositions (23-30 ‰; Fig. 6.1). Variations in the $\delta^{13}C$ values occur between these four deposits. Host dolomite from Berg Aukas tends to exhibit the highest $\delta^{13}C$ values; the other three deposits show host compositions ranging from ~-2 to 2.5 ‰ (Fig. 6.1).The hydrothermal dolomites with which mineralisation is associated are very similar in isotopic composition for all four deposits (Fig. 6.2). Fields for these overlap to a great extent. Only mineralised dolomites from Berg Aukas and Khusib Springs appear to plot as distinct fields. This is largely because of the differences exhibited in $\delta^{13}C$ values for these dolomites (Fig. 6.2).

Hydrothermal carbonates from Tsumeb are distributed over a wider range of $\delta^{13}C$ values than those from Berg Aukas. Nevertheless, the overlap in compositions is significant enough to preclude complete differentiation between the isotopic characteristics of these deposits (Fig. 6.2).

The same holds for Kombat, where hydrothermal dolomite shows almost complete overlap in isotope composition with that at Tsumeb. Isotope compositions of hydrothermal carbonates at Khusib Springs plot at the lower end of the range of $\delta^{13}C$ values exhibited by hydrothermal carbonates at Tsumeb and Kombat, and show a similar range in $\delta^{18}O$ values (Fig. 6.2).

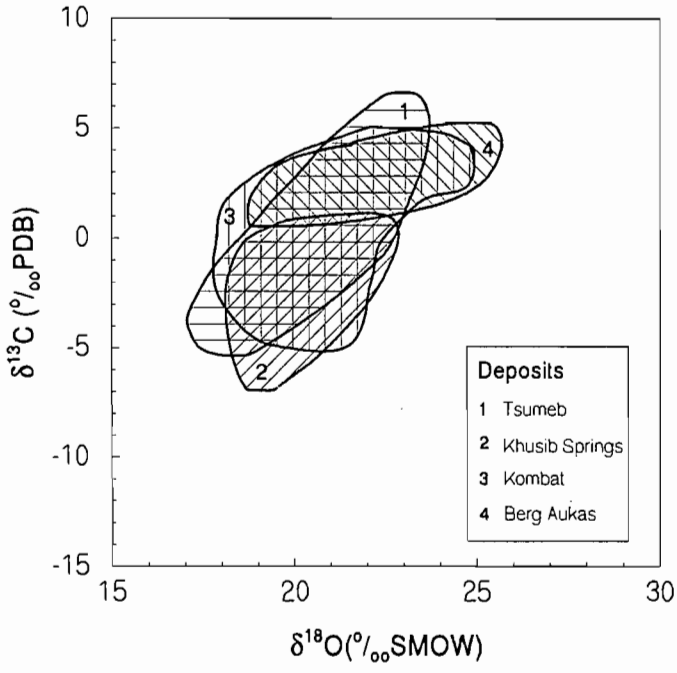

Figure 6.2 Plot of fields of hydrothermal carbonates with which base metal sulphide mineralisation is associated at the major deposits of interest in the OML.

CHAPTER SEVEN: FLUID INCLUSION STUDIES

7.1 INTRODUCTION

The fluid phase plays an important role in the formation of most ore deposits, being often the principal carrier, and hence transporting agent, of the ore constituents to the locus of deposition. Fluid inclusions in minerals provide the most direct source of information on fluids involved in the precipitation of ores. Thus, a study of fluid inclusions in ore and gangue minerals yields information on salinity and chemistry of the fluids related to mineralisation, and conditions of entrapment.

7.2 AIMS

This part of the present study comprises two aspects, firstly, fluid inclusion microthermometry, for the determination of salinity and homogenisation temperatures of fluids related to mineralisation at the deposits under consideration, and secondly, bulk fluid inclusion chemistry, for (i) comparison of major ions in solution with estimates from microthermometry, and (ii) investigation of salinity origin, employing crush-leach methods. In addition, the suitability of two methods of determining bulk fluid inclusion chemistry is discussed.

7.3 MICROTHERMOMETRY

7.3.1 Petrography

Twenty eight samples comprising doubly polished plates and thin section chips of quartz, dolomite, calcite and sphalerite were selected for fluid inclusion microthermometry, as these minerals, in particular, quartz, are the best minerals for hosting optically resolvable inclusions. However, only 11 samples yielded measurable inclusions.

7.3.1.1 Tsumeb

Four samples of quartz associated with Dolomite III and two samples of quartz associated with Calcite II yielded measurable inclusions. In addition, inclusions of suitable size were found in the Dolomite III generation.

Quartz occurs as anhedral grains within vein dolomite and calcite, and textural relations indicate that the quartz and carbonate phases were coeval. Calcite or dolomite are found as solid inclusions in the quartz grains and in places, the abundance of these solid inclusions increases gradually until more homogenous portions of dolomite or calcite are present. Therefore textures vary from murky portions (due to increased carbonate abundance) to clearer portions (more quartz-enriched). In many cases, the quartz is fine-grained (<1 mm). Associated ores in these samples include pyrite, tennantite and chalcocite for Dolomite III and tennantite and pyrite for Calcite II.

Inclusions in the quartz are predominantly secondary, although a number are found either randomly distributed, in small clusters or as large, isolated inclusions (Fig. 7.1b).Three fluid inclusion types are recognised on the basis of phases present at room temperature (Fig. 7.1a):

- Type I : 2-phase liquid + vapour inclusions
- Type II : 3-phase liquid + vapour + solid inclusions
- Type III : 1-phase liquid or vapour inclusions

Types I and II are the predominant fluid inclusion types, accounting for almost all microscopically visible inclusions. Apart from the presence of solid inclusions in Type II, both types of fluid inclusions are aqueous, have similar sizes, shapes and V/L (vapour:liquid) ratios (Appendix A2.6). Typically, optically resolvable fluid inclusions range in size from ~2-16 μm, but the majority are between 3-6 μm. Inclusion shapes are mostly rounded or rectangular, rarely elongate. V/L ratios range from 5-25 %, but narrower ranges are present within samples. Solid phases within the inclusions comprise small (<0.5 μm typically, but up to 1 μm in some inclusions) crystals, recognised by refractive index differences and extreme birefringence. In most cases, these are present as specks, and their contribution to the volume of the fluid inclusion

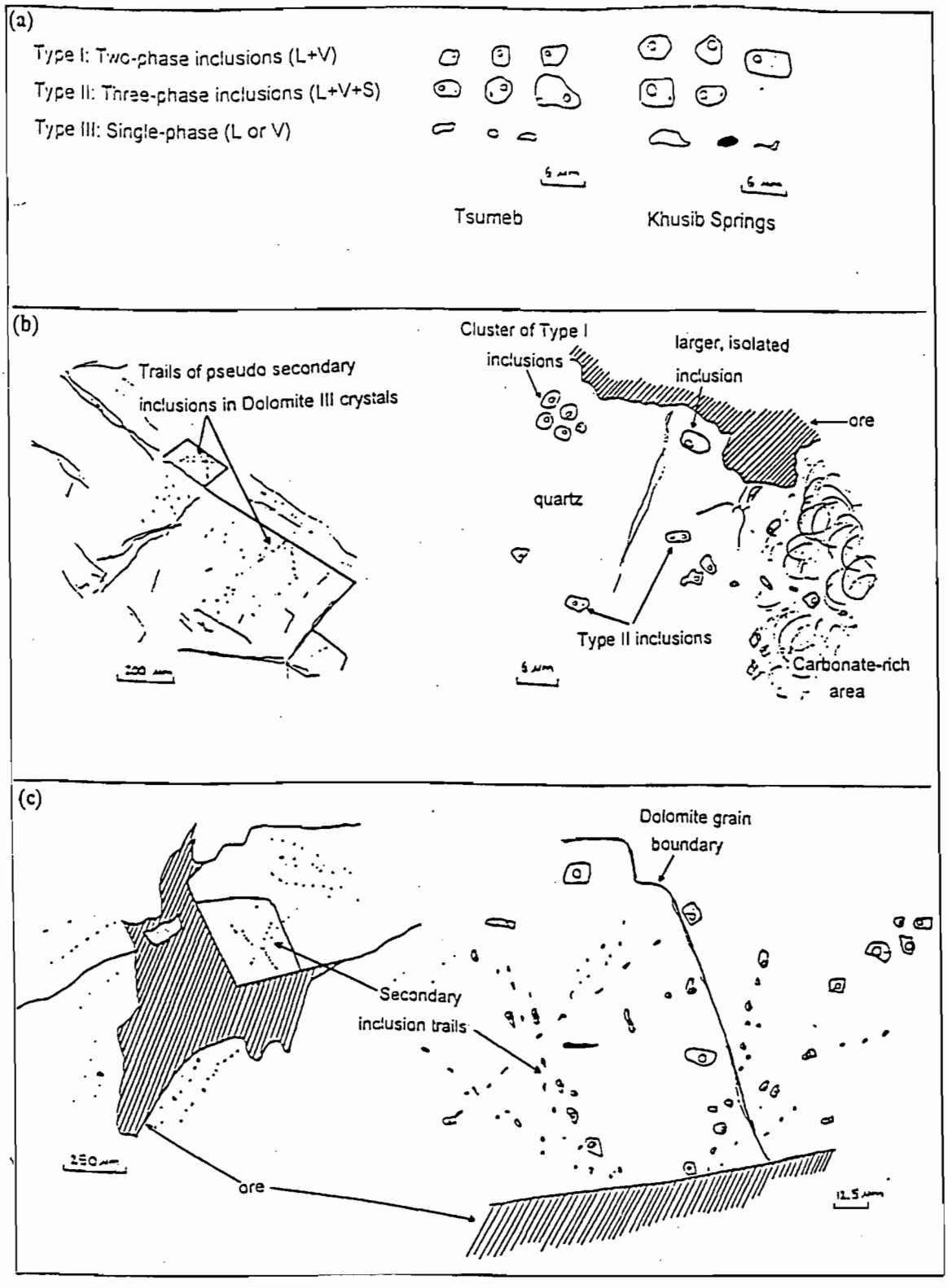

Figure 7.1 **(a)** Fluid inclusion types; **(b)** occurrence in dolomite and quartz at Tsumeb; **(c)** occurrence in dolomite at Khusib Springs.

is minimal, if not insignificant. The lack of a distinct euhedral shape or isotropism precludes halite daughter phases. In addition, the volume taken up by these crystals does not seem to be in constant proportion to the volume of the inclusions in which they occur, suggesting perhaps accidental trapping. Possible phases for these solids include calcite, dolomite or anhydrite. More rarely, minute specks of opaques, possibly sulphides, are also present.

In Dolomite III, types I and II inclusions are rectangular or rhombic, occurring in trails. These trails follow cleavage patterns of the dolomite, but do not cross grain boundaries, thus being confined to single grains. These may be pseudo secondary in origin (Fig. 7.1b). Inclusion sizes and V/L ratios are as described for the quartz-hosted inclusions.

Type III inclusions are most probably the result of necking, and represent the least abundant inclusion type, estimated at <1 % by area of all inclusions present. No measurements were made on these inclusions.

No CO_2-rich inclusions were observed in the quartz hosts. Dolomite and calcite hosts contain many of these inclusions, identified by their large V/L ratios, but they are always too small to be analysed. No double bubbles characteristic of such inclusions were observed, either at room temperature, or on cooling. This may be, in part, a function of the small size of these inclusions (<2 μm).

7.3.1.2 Khusib Springs:

Although a number of samples were chosen for fluid inclusion content, only one dolomite sample belonging to the Dolomite IIa generation, two quartz samples associated with Dolomite IIa and a sample of sphalerite associated with Dolomite IIb yielded suitable inclusion material. With the exception of one sample (KH62/75.3), which occurs further away from the ore deposit, the quartz and dolomite hosts are present in veins containing tennantite ore.

Inclusions in the quartz and dolomite hosts occur as loosely grouped clusters, as large, isolated inclusions, or as trails of secondary inclusions (Fig. 7.1c). The fluid inclusion types are I, II and

III, as described for Tsumeb samples (Fig. 7.1a). Of the three types, Type I is the most dominant, whereas Types II and III are rarely present. The solid inclusions within Type II fluid inclusions are of variable size, and also lack isotropism and a cubic shape. Type III is a product of necking, giving rise to dark vapour inclusions, or liquid inclusions. This type does not contribute significantly to the overall fluid inclusion population.

Sizes of inclusions are variable, ranging from 3-20 μm, and averaging 7±3 μm. V/L ratios are variable, ranging from 10 % to as high as 50 % in a few inclusions. Generally, however, most V/L ratios are between 20-25 %. Shapes range from euhedral, negative quartz crystal outlines to rounded, rectangular, square and anhedral.

CO_2 inclusions are very small, and identified only on the basis of high V/L ratios, which may also result from necking of the aqueous inclusions, as already mentioned. The aqueous inclusions may contain CO_2 in the vapour phase, however, no double bubble could be identified at 25°C, or on cooling.

Sphalerite contains linear arrays of euhedral to subhedral inclusions. The trails in which they occur are either present within individual sphalerite grains, or cross sphalerite grain boundaries. In addition, larger isolated inclusions and inclusion clusters occur. All inclusions are aqueous, containing a dark liquid, and sometimes a dark bubble is visible. The dark colouration of the liquid and bubble may result from reflections of the dark walls of the inclusions, or may be compositionally controlled. The visibility of the bubble is dependent on the walls of the inclusions, which do not appear to be parallel to each other. It is therefore possible that bubbles are hidden in re-entrants. This characteristic posed problems for T_h determination (section 7.3.2.2).

7.3.1.3 Kombat

As with samples from the other deposits, a number of samples from Kombat were chosen for possible measurable inclusions. Quartz is not abundant in samples from Kombat. Where quartz was present, inclusions usable for measurement were lacking. The carbonates were also not good

hosts for measurable inclusions. Only two inclusions, found in an array of predominantly submicroscopic inclusions of secondary origin in the Calcite I generation, could be measured. These may not necessarily be representative of the entire fluid inclusion population in this generation. These inclusions are slightly <2 μm in diameter, with V/L ratio averaging 20 %.

7.3.2 Results

Microthermometry was carried out on a United States Geological Survey (U.S.G.S.) heating-freezing stage. Experimental procedures are described in detail in Appendix A2.6. The data are discussed for each deposit in turn. Phase change measurements include T_e (first ice melting temperature), T_m (final ice melting temperature) and T_h (homogenisation temperature, for vapour to liquid change). Duplicate measurements were carried out for each of these temperatures, and in some cases, up to five measurements were made to check for reproducibility. Salinities of the fluids were calculated from the freezing point depression, as determined from T_m values, using the revised equation of Bodnar (1993) for the H_2O-NaCl system:

$$\text{Salinity (wt\%)} = 0.00 + 1.78\,\theta - 0.0442\,\theta^2 + 0.000557\,\theta^3 \quad (7.1)$$

where θ is the freezing point depression ($-T_m$) in degrees Celsius, and the salinity is expressed in terms of weight percent NaCl equivalent (wt% $NaCl_{eq}$).

7.3.2.1 *Tsumeb:*

Of the fluid inclusion types present, phase changes in Types I and II were measured. Observed values of T_e for inclusions in quartz associated with Calcite II range from -36 to -49.4°C, with most values in the range -40 to -45°C. T_e values for inclusions in quartz and dolomite associated with Dolomite III are similar in range, with most values between -38 and -42°C. The stable eutectic temperature for the system NaCl-H_2O is -21.2°C (Bodnar and Vityk, 1995). The depression of the eutectic temperature implies the presence of salts other than NaCl in solution, notably $CaCl_2$ and $MgCl_2$ (Shepherd *et al.*, 1985), bearing in mind the calcitic and dolomitic fluid

environment. This is supported in part by chemical analysis of inclusion leachates (section 7.4.3).

Inclusions in quartz associated with Calcite II comprise what appears to be two populations, based on T_m values. T_m for the first group ranges from -15.2 to -22°C, whereas the second group shows T_m ranging from -1.6 to -14.2°C, averaging -7.7°C. Calculated salinities yield a range of 20-23 wt% $NaCl_{eq}$ for most inclusions of the first population, and an average of 11 wt% $NaCl_{eq}$ for the second population (Fig. 7.2a). There does not appear to be any correlation between salinity and fluid inclusion type (i.e. I or II), implying that the solid phases do not affect the salinities determined from T_m values. To determine total salinity if these were daughter phases, Type II inclusions were heated to high temperatures to determine the temperature of dissolution of the solid phases. Homogenisation of the vapour bubble to the liquid phase occurred first. With continued heating, up to temperatures in excess of 350°C, no dissolution of the daughter phases was evident. Similar observations, along with optical properties, led Ypma (1984) to conclude that these phases were calcite inclusions trapped along with the fluid. Thus these solid inclusions do not appear to be true daughter phases. The range of T_h values is the same for both salinity groups, being 70 to 138°C (Fig. 7.2a). This range may in part be owed to necking of inclusions, but is also sample dependent, as one sample (3153/36) yields T_h values in the lower part of the range, 70-101°C, whereas inclusions in the other sample (3153/18) yield T_h values in the range of 95-138°C (Fig. 7.3a). As with salinity, there is no correlation between fluid inclusion type and homogenisation temperatures (Fig. 7.2a). In addition, low salinity fluid inclusions in both samples plot within similar T_h ranges as the higher salinity population (Fig. 7.3a).

For the Dolomite III generation, fluid inclusions were studied in one sample of dolomite and four samples containing associated quartz. As with quartz from the Calcite II generation, T_m values plot within similar ranges, indicating a high and low salinity population of inclusions, averaging 22 wt% $NaCl_{eq}$ and 8 wt% $NaCl_{eq}$ respectively (Fig. 7.2b). Homogenisation temperatures range from 80-215°C (Fig. 7.2b). Type II inclusions are not as abundant in the quartz and dolomite as in the Calcite II generation. They do exhibit the same range of salinities, but plot towards the lower end of the range of T_h values. This is a sample dependent relationship, as samples plotting at higher T_h values (DCT5, 2965/106; Fig. 7.3b) lack Type II inclusions. In general, lower salinity fluid inclusion compositions exhibit lower T_h values.

7.3.2.2 Khusib Springs

Phase changes in the aqueous Types I and II inclusions were measured. Similar behaviour was observed for both larger, isolated, possibly primary, inclusions and smaller inclusions present in cross-cutting trails, both in dolomite and associated quartz of the Dolomite II generation. No melting was observed in the vapour-rich inclusions, even when cooled to temperatures <-180°C to test for the presence of CH_4. These vapour-rich inclusions may be the result of necking of aqueous inclusions. The majority of inclusions however, were aqueous-rich, with dark vapour bubbles. The lack of any appearance of a double bubble on cooling the inclusion precludes significant CO_2 being present. Thus Type II inclusions were treated as aqueous inclusions. However, the bubble remained stationary throughout much of the heating cycle, especially as homogenisation was reached. This behaviour suggests the possible presence of hydrocarbons in the system, as pointed out by King (1990) for similar behaviour in quartz-hosted fluid inclusions from the nearby Olifantsfontein locality in the eastern Otavi Mountain Land.

T_e values average -31.6°C, slightly lower than those observed for the Tsumeb samples. T_m was recorded when the last ice raft disappeared, such that a refractive index difference between the melting phase and liquid was no longer visible. The bubble remained stationary during the melting process. Most inclusions range in T_m from -13.2 to -22.3°C, corresponding to salinities of 17 to 23 wt% $NaCl_{eq}$ (Fig. 7.2c). Only a few inclusions plot at lower salinities. T_h values range from 188 to 291°C, with the majority of values between 225 and 245°C. Fluid inclusions in dolomite and quartz samples yielded similar values for T_h and salinity (Fig. 7.3c).

Inclusions in sphalerite exhibit very low T_e values (-41 to -46°C) indicating the presence of various salt species in addition to NaCl, notably $CaCl_2$ and $MgCl_2$. T_m values appear to be very low, averaging -24.4°C. The T_m values were recorded when a large dark vapour bubble floated across the inclusion, free of any obstacles. Prior to this temperature being reached, the bubble would be growing along one of the walls of the inclusion as ice rafts were melting. The free floating behaviour was taken as indicating complete ice-melting. The T_m values measured were below the NaCl eutectic, indicating that the dominant salt species could not be NaCl, but some other salt species. T_m values therefore cannot be interpreted in terms of the NaCl-H_2O system.

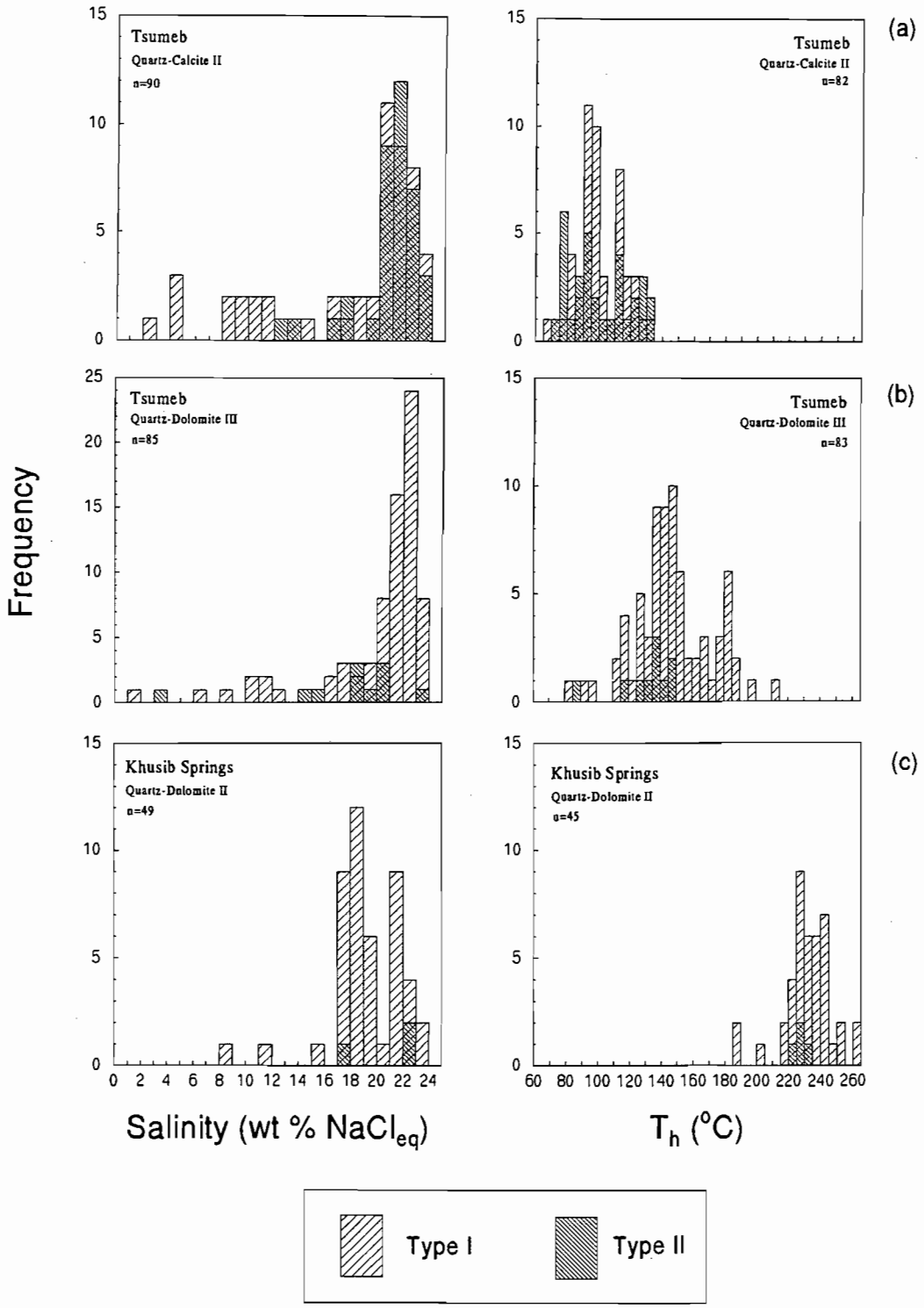

Figure 7.2 Histograms of salinity and T_h for aqueous inclusions in **(a)** quartz associated with Calcite II, Tsumeb, **(b)** Dolomite III and associated quartz, Tsumeb and **(c)** Dolomite II and associated quartz, Khusib Springs.

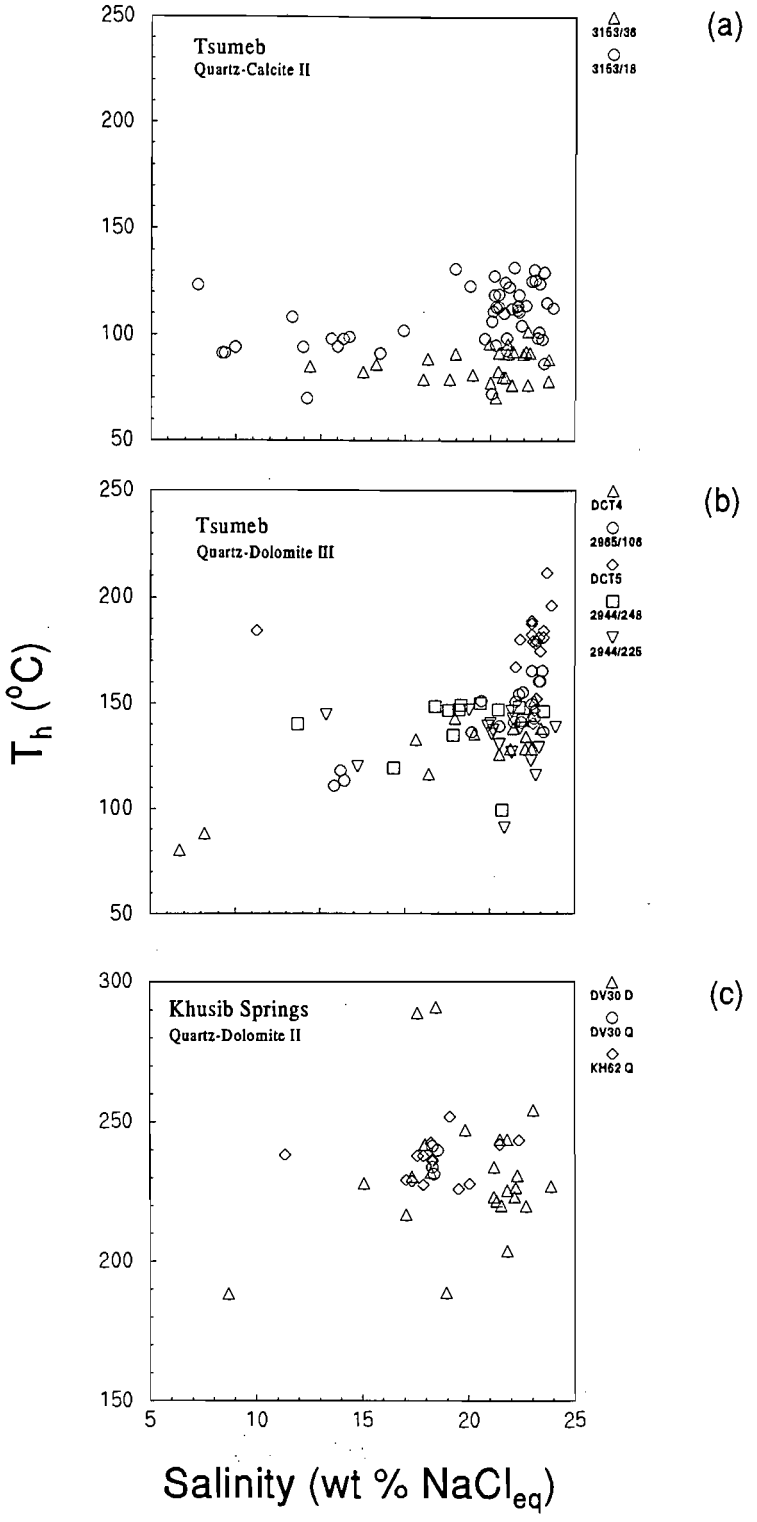

Figure 7.3 T_h vs Salinity plots for aqueous inclusions hosted in **(a)** quartz (samples 3153/18 and 3153/36) associated with Calcite II, Tsumeb, **(b)** Dolomite III (sample 2965/106) and associated quartz (samples 2944/248, 2944/225, DCT4, DCT5), Tsumeb and **(c)** Dolomite II (sample DV30 D) and associated quartz (samples DV30 Q and KH62/75.3 Q).

Should this system be applied, a theoretical salinity of 25 wt% $NaCl_{eq}$ would be obtained. Homogenisation temperatures were not easily obtained via the cycling method owing to "hiding" of the bubble behind re-entrants in the inclusions. Temperatures were increased very slowly in order to minimise sudden movements of the bubble, but this was not successful in preventing the bubble getting "lost" in a re-entrant. Homogenisation could therefore not be measured with any certainty. Only a single inclusion proved successful in the determination of homogenisation temperature via the cycling technique. The bubble moved around vigorously, disappeared (not into a re-entrant) and then burst back into the inclusion at lower temperatures, indicating homogenisation temperature had been exceeded. The T_h thus obtained was 102°C.

7.3.2.3 Kombat

No inclusions of suitable size were present in the quartz examined. One sample of Calcite I yielded mostly submicroscopic inclusions, and an attempt was made at observing phase changes in these, however, results were only obtained on two of the largest inclusions, both of which were ~3 μm in diameter, occurring in an array of submicroscopic inclusions. T_m seems to be quite high, at -1.5°C and -1.1°C for each inclusion. Average salinity is therefore 2.3 wt % $NaCl_{eq}$. The corresponding T_h values are 176°C and 172°C respectively. No T_e measurements could be made on these inclusions.

7.4 FLUID CHEMISTRY

7.4.1 Feasibility of bulk chemical analysis

From microthermometry, both Tsumeb and Khusib Springs samples show a consistent trend of a single dominant population of fluid inclusions of high salinity, with a minor component of inclusions of low salinity. T_h values are variable, and may represent necking effects or entrapment during different stages of cooling of the fluid. First melting temperatures indicate a mixed salt NaCl-$CaCl_2$-$MgCl_2$ -H_2O system for the fluids.

Bulk fluid chemistry was determined on the basis of ions in solution. Thus non-polar compounds such as CO_2 and hydrocarbons which may be present in the system were not accounted for in the chemical analysis as employed here. Because ions in solution will partition strongly into the polar aqueous phase as opposed to the non-polar gaseous (excluding water vapour) phase, the presence of the non-polar component in the fluid inclusions of the samples (particularly the carbonates) is not expected to alter the ionic chemistry of the aqueous phase, except in the case of ions derived from CO_2 dissolution. Furthermore, as the fluid inclusions from microthermometry are dominated by a high salinity fluid, mass balance calculations predict that contamination from the low salinity component should not affect the total salinity to a significant extent. This, coupled with the similar compositions for both salinity components as determined from T_e values, renders bulk chemical analysis feasible in this respect. It should be noted, however, that a complete chemical analysis was not attempted in this study, thus major charge imbalances should be expected. These and other related aspects are discussed in the following sections. Also, although microthermometry was conducted mostly on inclusions hosted in quartz, the bulk fluid chemistry was conducted mostly on the carbonate generations with which the quartz is associated, as textural relationships indicate these minerals were coeval, and microthermometry shows similarities in T_e and T_m values for inclusions in dolomite and coexisting quartz from Tsumeb and Khusib Springs.

7.4.2 Methods

Various techniques have been employed for the chemical analysis of fluid inclusions. These can be either of individual inclusions, or bulk inclusion analysis. Chemical analysis in both cases is usually destructive. Techniques commonly used include the crush-leach method, ICP-linked decrepitation, the identification of solid phases by X-ray methods (e.g. X-ray diffraction, scanning electron microscopy), microanalysis of individual inclusions using laser excited Raman spectroscopy, laser beam ablation, neutron activation, and isotopic analysis (Roedder, 1984; Shepherd *et al.*, 1985). Advances have also been made in the use of cryo-scanning electron microscopy for the determination of ionic species in frozen fluid inclusions (e.g. Tritlla and Cardellach, 1997).

Two methods were employed for the detection of pertinent ions in fluid inclusions in carbonates, sphalerite and quartz: (i) The crush-leach method, employing HPIC for analysis of anions and cations; and (ii) Proton Induced X-Ray Emission (PIXE), for Br and Cl concentrations in groups of fluid inclusions. These methods and their advantages/shortcomings are outlined below.

7.4.2.1 Crush-leach analysis, using High Performance Ion Chromatography (HPIC)

The crush-leach method is based on the extraction of fluids from fluid inclusions into a leaching solution, usually water free of the analytes (doubly distilled, deionised water, DDW), and subsequent analysis of this solution, which is called the leachate. 500-680 mg samples of cleaned mineral grains of dolomite, calcite, quartz and sphalerite were crushed under DDW, and the resultant leachate analysed via HPIC for Na^+, K^+, Ca^{2+}, Mg^{2+}, Cl^-, Br^- and SO_4^{2-}. Details of sample and leachate preparation, and instrumental conditions during analysis, are given in Appendix A2.7. Initial problems with Br^- detection, however, turned attention to the use of PIXE as a means of detecting Br, along with Na and Cl, the two other elements useful in the interpretation of salinity origin.

7.4.2.2 Proton Induced X-ray emission (PIXE) analysis of fluid inclusions

Polished thin sections were carbon-coated and analysed using a proton probe facility at the National Accelerator Centre, Faure, South Africa. As with ion chromatography, the aim was to determine Na, Cl and Br in fluid inclusions in carbonates. A proton beam was directed onto a thin section of the sample, and from the resulting characteristic x-rays, element concentrations were calculated, taking into account matrix corrections for the mineral in which the inclusions were hosted.

7.4.2.3 Comparison of PIXE and HPIC as tools for the detection of Na, Br and Cl in carbonate-hosted fluid inclusions

It should be noted that, although the same ions/elements were being analysed for using each technique, the scales at which the analyses were carried out are very different. However, both can

be considered bulk analyses of fluid inclusions (typical fluid inclusion sizes do not exceed 1μm, which is below the resolution of the proton probe, therefore a number of inclusions were analysed over the scanned area). Nevertheless, PIXE involves the analysis of fluid inclusions over an area of 500 μm x 500 μm, whereas HPIC involves the analysis of ~500-600 mg of sample from which fluid inclusions have been leached into DDW. Converting the area analysed by PIXE to mass gives values of ~1.15 μg and ~3.4 μg for Cl and Br respectively, using a mean depth of X-ray production of ~2μm (W. Pryzybylowicz, pers. comm., 1997). Therefore absolute concentrations obtained via both methods cannot be compared. However, it should be theoretically possible to compare *ratios* obtained via both techniques, as these should remain constant, provided one fluid generation is present in the sample. Microthermometry shows this not to be the case, therefore, comparison of the two different techniques is made somewhat more difficult. Considering the minimal contamination from the lower salinity fluid inclusions as determined from mass balance calculations, a large number of PIXE determinations from representative sections should yield halogen ratios similar to those obtained from HPIC.

PIXE posed a significant problem in that Na could not be analysed, as this would require movement of the sample, thus resulting in Na determinations being carried out in a different area compared to the other elements. The lack of a co-ordination grid system on the instrument makes it extremely difficult to find the same area again. Na analysis can also result in crystal damage, owing to the lack of external shielding of the detector against backscattered protons (W. Pryzybylowicz, pers. comm., 1997).

The problem faced at that stage was therefore Na detection via PIXE, and Br^- detection via HPIC. Assuming that ratios obtained via both techniques were constant, Cl/Br from PIXE and Na/Cl from HPIC could be used to calculate Na/Br. With this in mind, analyses were performed for Cl and Br using PIXE. However, further experimentation with HPIC using larger sample loop volumes finally yielded detectable Br^- in leachate solutions. The detection limit was decreased as sample volume was increased. Using a 200 μl sample volume as opposed to the conventional 50 μl volume thus enabled detection of Br^- (see Appendix A2.7).

In order to compare the errors in the Cl/Br ratios, the same sample was analysed using both

techniques. A comparison of the ratios showed that these differed significantly. In addition, there was a lack of internal consistency with ratios obtained from PIXE analyses (Fig. 7.4). Typical errors in the Cl/Br ratio are ~36 % (1σ) for PIXE determinations. Errors in Cl^- and Br^- determinations using HPIC are in the order of 1 % (1σ) for Cl^- at concentration levels of 9 mg/l, and ~2 % (1σ) for Br^- at concentration levels of 2.5 mg/l. Extrapolating the error for Br^- to typical concentrations of 0.3 mg/l (as found in sample DV10, for example), yields an error of ~3.5 %. Five subsamples of dolomite sample DV10 were crushed and separate leachate solutions from these analysed by HPIC. Errors associated with the Br^- and Cl^- concentrations as determined from the instrumental conditions translate to an error in the Cl/Br ratio of ~4 %, very much better than the error of 36 % obtained from PIXE analysis (Fig. 7.4). The larger error associated with PIXE determinations is, in part, accounted for by fluid inclusion inhomogeneity, considering the very small scale at which the analysis is carried out. However, purely in terms of the analytical conditions, this error is largely controlled by the low concentrations of Br in the sample, which are always very close to the ~2 ppm detection limit of the instrument. Thus the closer the Br concentration is to the detection limit of the proton probe, the larger is the error (Fig. 7.4). Calculated detection limits for HPIC, on the other hand, are in the order of 0.2 ppb. Br^- concentrations are much higher than this, and errors are correspondingly lower.

In view of the above, bulk analysis, using the crush-leach method and HPIC, was the preferred method for obtaining ion ratios of Na^+, Cl^- and Br^- in leachate solutions, especially considering that Na could not be analysed together with Cl and Br using PIXE. In addition, numerous publications considering Na-Cl-Br ratios have involved use of the crush-leach method, and where Br^- concentrations were particularly low, larger sample loop volumes were used for HPIC analysis of leachates (e.g. Kesler *et al.*, 1996; T.J. Huston, pers. comm., 1997).

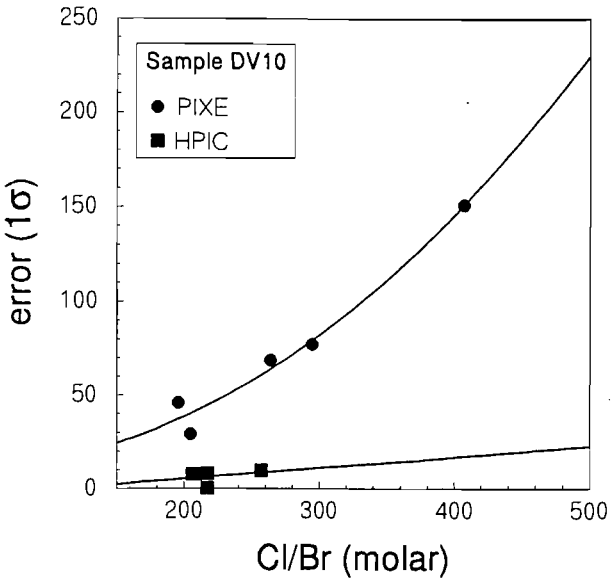

Figure 7.4 Diagram comparing magnitudes of errors (1σ) in the determination of Cl/Br ratios using HPIC as opposed to PIXE as analytical methods for the determination of Br and Cl concentrations in fluid inclusions.

7.4.3 Results of crush-leach experiments

As leachate solutions differ in volume slightly, as well as in dilution, individual concentrations of pertinent ions cannot be compared between different leachate solutions. Ratios or normalised values must instead be used. Concentrations of major ions determined using HPIC are given in Appendix A2.7. Determination of leachate compositions was carried out on those samples for which microthermometric data were available, either from fluid inclusions in coexisting phases or the mineral itself. In addition, a few samples from generations for which microthermometric data were not available, were also crushed and the leachates analysed for Br^-, Na^+ and Cl^- in particular. Where possible, three or more separate crushes were performed from the same sample, and the corresponding leachates analysed to check for reproducibility, which was typically within 7 % for Cl/Br and 5 % for Na/Br.

Normalised plots of the major cation species show that the leachates are significantly depleted in K^+ relative to the other cations Na^+, Ca^{2+} and Mg^{2+}, with no particular trends apparent amongst

the various carbonate generations or the quartz and sphalerite minerals associated with these phases (Fig. 7.5a). Considering Na^+, Ca^{2+} and Mg^{2+}, differences in leachate compositions are found to be mineralogically controlled (Fig. 7.5b). Compositions of fluid inclusions hosted by quartz, however, plot in a similar area to inclusion compositions from coexisting Dolomite III from Tsumeb. Sphalerite compositions show a wider variation, and no correlation with compositions of associated sparry and coarsely recrystallised dolomite (Dolomite II a and b respectively) from Khusib Springs. A plot of Br^--Cl^- -SO_4^{2-} shows a predominance of Cl^- and SO_4^{2-} over Br^- in the leachates (Fig. 7.5c). Cl^- and SO_4^{2-} are variable within individual generations of carbonates.

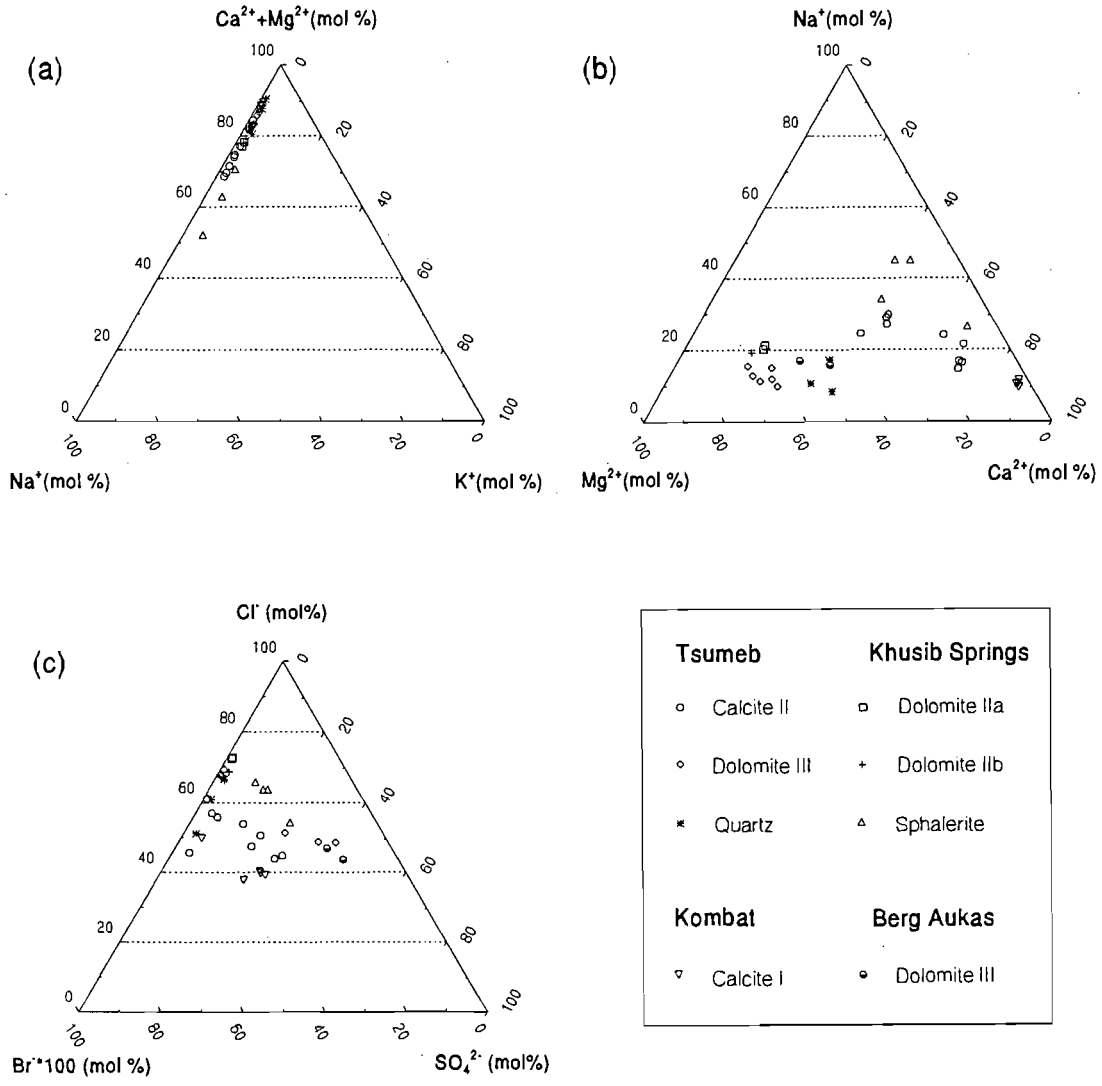

Figure 7.5 Compositional plots of fluid inclusion leachates from different minerals.

7.5 DISCUSSION

7.5.1 Comparison of fluid composition determined by bulk chemistry and microthermometry

In order to compare the data from microthermometry and crush leach analyses, the variables associated with the data from each technique must be considered. From microthermometry, T_e values indicate which dissolved salt species are present in the fluid inclusions. Some workers have attempted quantification of the species present using phase relations (e.g. Crawford, 1981, in Misiewicz, 1988), however, more than one possible phase equilibrium can be correlated with given T_e values, making quantification in this respect difficult. The observed T_e is usually higher than the true T_e, because true T_e is extremely difficult to observe. Nevertheless, based on observed T_e values, an estimation of the type of salt species present can be made. Fluid composition from bulk chemical analysis is somewhat more quantitative. For the crush leach method, charge balance calculations provide a means of assessing data quality. As emphasised by Banks *et al.* (1991), the sum of positive and negative charges should balance when the following criteria are met: (i) the analyses are correct; (ii) the ions which are not analysed are present in very low concentrations such that they will not affect the charge balance to any significant extent; and (iii) no contamination effects arise from foreign material on the minerals being crushed.

Analyses can be affected by the procedure followed. Errors can be attributed to the instrument, and to the manner in which the leaching is carried out. Using the example as discussed under section 7.4.2.3, reproducibility in the Cl/Br ratio for five crushes of dolomite sample DV10 is ~8 %. For the Na/Br ratio, this is ~6.5 %. Considering that errors resulting from the instrument are slightly lower than these values, total errors are therefore associated with the procedure, as well as fluid inclusion inhomogeneity. Errors in the procedure arise from fineness of the crushing, adsorption effects and a number of other parameters. These effects were minimised during the procedure (see Appendix A2.7), so criterion (i) of Banks *et al.* (1991) is considered being satisfied here.

Charge balance calculations on the dolomite, calcite, quartz and sphalerite show that positive charge totals do not equal negative charge totals, with the discrepancy being up to 68 % in some dolomite leachates. A major contribution to this discrepancy must be the carbonate ion, CO_3^{2-}, and associated species, which were not determined in the analysis, as the eluent used in the HPIC procedure was itself a bicarbonate/carbonate mixture. As discussed by Roedder (1984, pp. 133), CO_2 presence can account for large errors in charge balance, owing to the species formed in solution, such as H_2CO_3, HCO_3^- and CO_3^{2-}. These species may have been dissolved in the fluid inlcusions themselves, or may have resulted from CO_2 dissolution during crushing, as this was effected under DDW. Thus criterion (ii) of Banks *et al.* (1991) was not met in this study.

Contamination effects are considered to be minimal, as mineral separation was carefully effected, although the presence of solid inclusions of contaminating phases such as dolomite in sphalerite or quartz, cannot be excluded, and no amount of cleaning will remove inclusions in the mineral being crushed. Homogenous portions of vein quartz and sphalerite grains were separated under the binocular microscope. Although the quartz is intimately intergrown with the Dolomite III at Tsumeb, portions of veins occur in which quartz is the dominant mineral, present in quantities sufficient to separate via hand picking. In this case, the contaminating phase is not considered to contribute significantly to the concentration of certain ions such as Br^-, as similar masses of quartz and dolomite were crushed under similar volumes of water, with the same conditions applying to dolomite and sphalerite from Khusib Springs. Taking sphalerite as an example, a contamination of 12 % by mass of dolomite would need to be present in order to effect the observed Br^- concentrations in the sphalerite, assuming fluid inclusion density is the same throughout the dolomite and that sphalerite inclusions yield non-detectable Br^-. In thin section, dolomite inclusions, although present, account for less than 1 % of the observed sphalerite masses. Thus, the chemistry of the leachate must be derived from the dominant phase being crushed. In addition, Figure 7.5 shows rather different compositions for sphalerite leachates as opposed to leachates of Dolomite II with which it is associated. Thus contamination of sphalerite leachate compositions by dolomite inclusions is considered not being significant in this respect. Even greater amounts of contamination by dolomite in quartz would be required for observed concentrations of Br^- in quartz leachates (up to 50 % by mass). Such a degree of contamination is not encountered here. Compositions for quartz-derived leachates as plotted in Fig. 7.5a do not

overlap with the associated dolomite compositions, indicating that contamination by associated dolomite cannot be a controlling factor in the composition of quartz-derived leachates. Therefore, at worst, the fluid chemistry of the quartz could in part be accounted for by dolomite contamination, such that observed ionic concentrations in leachates are a combination of fluid inclusion compositions from quartz and dolomite phases. At best, the ionic concentrations will be derived from quartz-hosted inclusions only.

The plot of Na^+, Mg^+ and Ca^+ distribution (Fig. 7.5b) shows distinct compositions which can be correlated with different minerals. Partial dissolution of the carbonate phases could account for the observed difference in composition between dolomite- and calcite-derived leachates. However, this does not seem to be the case, even at very small grain size ranges after crushing. Solubility products for dolomite are in the order of 10^{-19}, and for calcite, in the order of 10^{-9} at 25°C (Krauskopf and Bird, 1995). This should translate to a greater concentration of CO_3^{2-} in leachate solutions from calcite as opposed to dolomite-derived leachates, assuming that CO_3^{2-} is the only ion contributing to the negative charge deficit. Correspondingly, the charge imbalance should be higher for calcite-derived leachates as opposed to dolomite-derived leachates. For the carbonate minerals analysed, negative charge deficits in dolomite-derived leachates range from 37-68 %. A similar range of 33-65 % is observed for calcite-derived leachates. Thus partial solubility cannot be a significant factor in controlling the leachate composition. In addition, the large ranges observed in the charge deficits in leachates of each mineral species points to analyses reflecting the fluid inclusion composition rather than mineral dissolution.

Taking the above factors into consideration, a comparison with T_e values can be made, if ratios of $Na^+/(Ca^{2+}+Mg^{2+})$ and Cl^-/CO_3^{2-} are considered, where Na^+, Ca^{2+} and Cl^- are expressed as molar concentrations multiplied by their respective charges (milli-equivalents), and CO_3^{2-} is taken as the deficit in the negative charge. In all cases, ratios of Cl^-/CO_3^{2-} are greater than $Na^+/(Ca^{2+}+Mg^{2+})$ (Fig. 7.6). This points to a predominance of Ca^{2+} and Mg^{2+} in the fluids relative to Na^+, with a corresponding increase in Cl^- relative to CO_3^{2-} in the fluids. Considering that a proportion of CO_3^{2-} may be derived from CO_2 in the fluid inclusions, the aqueous phase may be

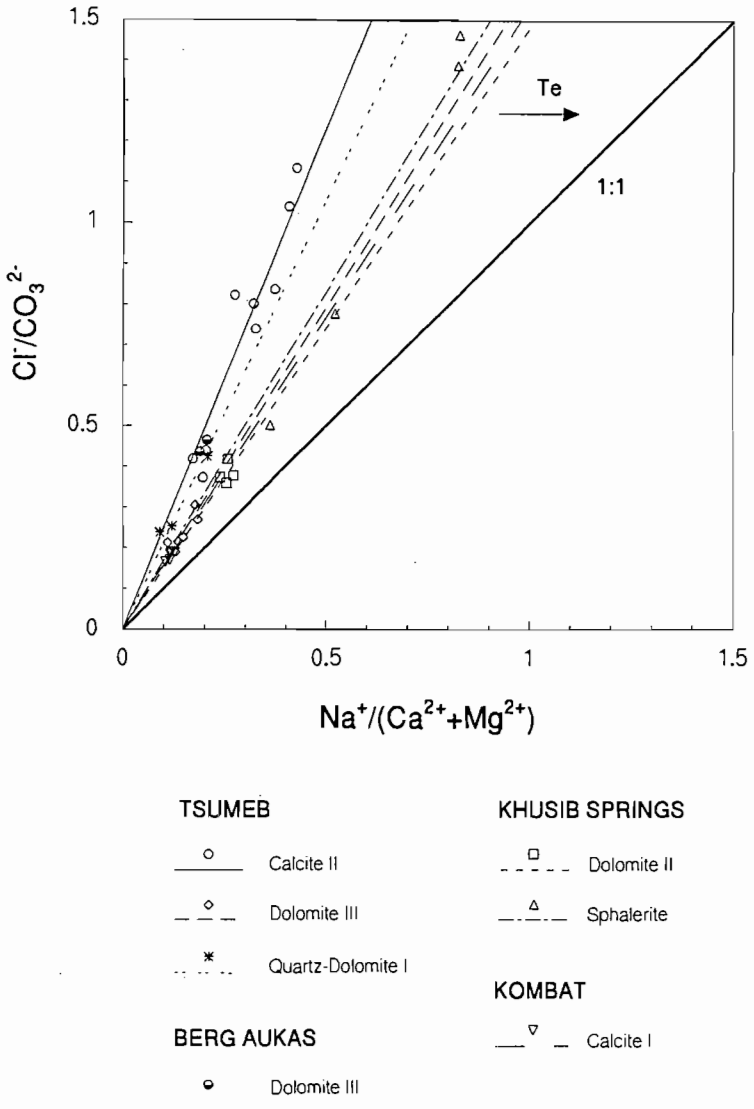

Figure 7.6 Bivariate plot of fluid composition in terms of anion and cation ratios. The charge imbalance is expressed as CO_3^{2-} which, in turn, comprises a number of related species such as HCO_3^-, H_2CO_3 and COO^-. All data plot above the 1:1 curve, indicating a predominance of Cl^- over Na^+ in the fluids. T_e tends to be higher as the slope of the regression lines for each generation approach unity.

even more enriched in Cl^- relative to CO_3^{2-}. Thus Mg^{2+} and Ca^{2+} are most likely present as dissolved salts $CaCl_2$ and $MgCl_2$ in solution, rather than as $CaCO_3$ and $CaMg(CO_3)_2$. Agreement is therefore obtained with T_e values, which predict a saline fluid dominant in $CaCl_2$ and $MgCl_2$ rather than NaCl. A plot of regression lines through data from different generations and minerals

shows that data of Dolomite II from Khusib Springs lie closest to the 1:1 curve (Fig. 7.6). This is in agreement with microthermometric results: observed T_e values for aqueous fluid inclusions hosted by this generation are higher than those observed for fluid inclusions hosted in other carbonate generations from Tsumeb, or in quartz and sphalerite.

In addition to the above species, it is also likely that Ca^{2+} and Mg^{2+} may be present as dissolved sulphates, as SO_4^{2-} was also found to be a significant anion in certain leachates. SO_4^{2-}, as with CO_3^{2-}, may have associated ions in solution, such as HS^- and S^{2-}. For the sphalerite leachates, SO_4^{2-} may actually be derived from the sulphide itself, as sulphide oxidises rapidly in an environment which is not inert during the crushing procedure (e.g. Roedder, 1984, pp.132; Crocetti and Holland, 1989). In this case, the water under which crushing was done was ordinary oxygenated water. Thus the range as observed in anion-normalised SO_4^{2-} is likely due to oxidation effects during crushing. For the carbonate generations, however, the normalised SO_4^{2-} values are derived from the fluid inclusions, as there is no evidence of sulphide mineral presence in the crushed material. In this case, SO_4^{2-} may represent HS^- or S^{2-} ions in the fluids, also oxidised during crushing. However, it is significant to note that Dolomite II from Khusib Springs shows rather low normalised SO_4^{2-} compared to Calcite II and two samples of Dolomite III from Tsumeb (Fig. 7.5c). Should this SO_4^{2-} represent actual SO_4^{2-} in the fluids as opposed to a cushing-derived product, then the implication is that Dolomite II from Khusib Springs represents a more reducing fluid than Calcite II and to a certain extent, Dolomite III, from Tsumeb. For Calcite I from Kombat, SO_4^{2-} concentrations are also relatively high. The association with Fe-Mn oxide ore assemblages supports this observation. Dolomite III from Berg Aukas is also SO_4^{2-} enriched relative to other carbonate generations plotted implying oxidising fluid conditions.

7.5.2 Na-Br-Cl systematics: overview and application to the present study

Saline fluids, or brines, contain significant amounts of Cl^- and Na^+, with Cl^- being an important ligand in metal complexes in solution, particularly with base metals (e.g. Beales and Jackson, 1966, Ruaya and Seward, 1986; Hanor, 1994, 1995). Brine compositions have been extensively studied, with particular reference to the origin of their salinity (e.g., Hanor, 1994, 1997; Land,

1987, 1992; Musgrove and Banner, 1993; Fontes and Matray, 1993a, 1993b).

Halogen fractionation occurs by various mechanisms, one of these being evaporation, and ratios of the halogens may therefore be used to constrain solute source and fluid evolution. In addition, owing to their relative solubility, ratios of the halogens can be used as indicators of fluid sources and mixing processes at depth (Böhlke and Irwin, 1992). During seawater evaporation, Br^- in particular, is incompatible in the precipitation of halite, owing to a distribution coefficient of 0.031 with respect to its substitution for Cl^- in the halite structure (McCaffrey *et al.*, 1987). Thus it has been widely used as a geochemical indicator of evaporation and other processes in brine formation and evolution.

Na-Br-Cl systematics have been extensively applied to the characterisation of basinal brines responsible for MVT mineralisation in the midcontinent United States (e.g. Walter *et al.*, 1990; Kesler *et al.*, 1995, 1996; Viets, 1995). Outside of this area, little work has been conducted on halogen systematics as applied to ore deposits to date (e.g. Tritlla and Cardellach, 1997; Prochaska, 1997). However, such work has found applicability in the study of oilfield brines (e.g. Rittenhouse, 1967; Fontes and Matray, 1993a, 1993b).

Na, Br and Cl are incompatible with respect to carbonate minerals such as dolomite and calcite. Partition coefficients are <1, as both ionic size and charge do not balance in substituting for the major ions. It is therefore most likely that any concentrations of these three ionic species determined in carbonates are derived from salt species present within fluid inclusions in the carbonate. The same applies to other minerals such as sphalerite and quartz (studied here). Ratios of these ions therefore help constrain the origin of the fluids trapped in these phases.

Na-Cl-Br systematics can be explained as follows: during seawater evaporation, halite precipitates when sufficiently high concentrations of Na^+ and Cl^- in the residual seawater compared to that in normal seawater are reached (brine concentration 10.6 times that of seawater, McCaffrey *et al.*, 1987). Owing to the incompatibility of Br^- in the halite structure (D_{Br} = 0.032-0.034, Herrmann, 1980, McCaffrey *et al.*, 1987), the residual fluid becomes progressively enriched in Br^- relative to Na^+ and Cl^-. This leads to a progressive decrease in the Na/Br and

Cl/Br ratios of the residual brine (bittern). On the other hand, as halite incorporates minimal Br, waters made saline by the dissolution of halite become enriched in Na^+ and Cl^- relative to Br^-, thus increasing the Na/Br and Cl/Br ratios (Fig. 7.7). Although closed system recrystallisation of halite may take place to produce second cycle halite (Holser 1979), it has been determined that Na/Br and Cl/Br ratios remain higher than seawater composition (Kesler *et al.*, 1995, 1996). Thus Na/Br and Cl/Br ratios greater than that of seawater can indicate halite dissolution or recrystallisation (Fig. 7.7).

Most brines have formed by one of the above two processes. However, these brines may undergo later modifications such as Na-Ca exchange reactions (where in contact with feldspar-bearing rocks, for example), mixing with other brines or interaction with other evaporite minerals. Most studies have shown that brine compositions plot more or less along the line defined by seawater evaporation or halite dissolution (e.g. Kesler *et al.*, 1995, 1996; Banks *et al.*, 1997; Tritlla and Cardellach, 1997). A seawater evaporation line is constructed from the seawater composition, tending towards the origin, as evaporation to low ratios of Cl/Br and Na/Br results in the precipitation of sylvite and carnallite, such that Na^+ becomes enriched in the residual brine relative to Cl^-, which is continuously removed (Fig. 7.7).

7.5.2.1 Seawater composition

In the published plots of Cl/Br vs Na/Br, mean seawater ratios are used. These are based on compositions derived from fluid inclusions of Permian age in halite hosts as determined by Horita *et al.* (1991). Such compositions are valid for the present study, even though mineralisation and associated alteration are thought to have occurred during the late Proterozoic in the OML. Evidence for a constant seawater composition in terms of halide ratios (as cited by Holser, 1979) is that mantle degassing releasing excess volatiles (including Cl and Br) occurred during early Earth history, so that by at least the mid-Proterozoic, their relative concentrations in seawater would have reached a constant ratio. Secondly, evaporite mineralogy and the order of precipitation of evaporite minerals has remained constant over geological time, suggesting a consistent ratio between evaporite components. Thirdly, analyses of trapped brines in fluid inclusions show that they have ionic ratios similar to present day evaporating seawater. In

addition, Br has a very long residence time in the oceans, and shows no regular variation in primary halites which precipitated during different periods over geological time.

Channer *et al.* (1997) suggested that changes in seawater halide ratios occurred over geological time, based on their fluid inclusion study of Archaean compositions of seawater. However, taking into consideration the argument for mantle degassing early in the Earth's history, Archaean compositions are expected to differ from modern day compositions of seawater.

7.5.2.2 Na-Br-Cl systematics of Otavi Mountain Land leachates

Molar ratios of Cl/Br and Na/Br are presented in Appendix A2.7, along with concentrations of these ions in the leachate solutions. To determine the precision of the crush-leach method, crushes were carried out at least in duplicate. For some samples up to five separate crushes were performed and analysed separately. Precision is dependent on a number of errors. The analytical errors involved with regards to instrumentation have been discussed previously, but errors arising from the crush-leach procedure also need to be taken into account, e.g. size to which samples are crushed and adsorption effects. The same procedure was applied to each sample (see Appendix A2.7), so the precision was determined on the sample which showed the least variation in Cl/Br and Na/Br ratio. Errors on the calculated Cl/Br and Na/Br ratios are ~4 % and 3.5 % respectively, based on five crushes. This is taken as the minimum error of the crush-leach method and subsequent HPIC analysis. Errors greater than this can be ascribed to the samples themselves, i.e. fluid inclusion heterogeneity, combined with occasional errors in the analytical procedure. Maximum errors obtained during this study were in the order of 23 % in the Cl/Br ratio, and 20% in the Na/Br ratio.

A plot of Cl/Br vs Na/Br shows that leachate compositions for dolomite and calcite from the major base metal sulphide deposits in the OML all plot in a linear array along the seawater evaporation line (Fig. 7.7). Sphalerite leachate compositions from Khusib Springs plot in a little cluster slightly to the left of the SW evaporation line. This is consistent with higher Na values relative to Ca and Mg (Fig. 7.5b) compared to the Dolomite II samples. A sample from Berg Aukas also plots near this line. Sphalerite and sparry dolomite from Berg Aukas, as shown by

Misiewicz (1988), contain inclusions of high salinity, on average 23 wt% $NaCl_{eq}$. No significant contamination from other fluid generations has been reported for these dolomites. Calcite I from Kombat shows a very consistent ratio for five separate crushes, plotting at the lower end of the observed array of compositions. Such low ratios appear to be consistent with the low salinity determined from microthermometry.

Although no microthermometric data is available for other generations, leachates were nevertheless obtained for these phases, and the compositions also plot along the seawater evaporation line, indicating a similar origin for the fluids (Fig. 7.7). Owing to the disseminated mineralisation in Dolomite II from Tsumeb, it was not feasible to carry out crush-leach analyses on this generation. Host dolomite and later calcite generations (Calcite III from Tsumeb, Calcite I from Khusib Springs) did not yield measurable Br^-, and show low concentrations of Cl^- and Na^+ in the leachates. Use of the detection limit for Br^- yields ratios very much greater than seawater composition. Prochaska (1997) attributed ratios greater than seawater composition to surface fluids rather than being derived by halite dissolution for inclusions in siderite from the Austrian Alps. Salinities of fluid inclusions are impossible to determine in the host rocks, owing to their extremely fine-grained nature. The calcites do not contain measurable inclusions either. It is suspected that these may be of a lower salinity than the fluids associated with mineralisation, judging by the lower Cl^- concentrations in the leachates, which were derived from similar sample masses and leachate volumes. Thus these carbonate generations are assumed to have been influenced by meteoric components, although it must be stressed that this is based purely on the leachate compositions.

7.5.2.2 (a) Mass balance considerations

Samples from within the same generation of carbonates plot in small separate linear arrays along the evaporation line. This is partly owed to analytical error, but is also a function of the proportion of fluid inclusion populations present in individual samples. As shown from microthermometry, two salinity populations appear evident in the samples studied, although the lack of a proper bimodal distribution shows that the higher salinity fluid was by far the dominant

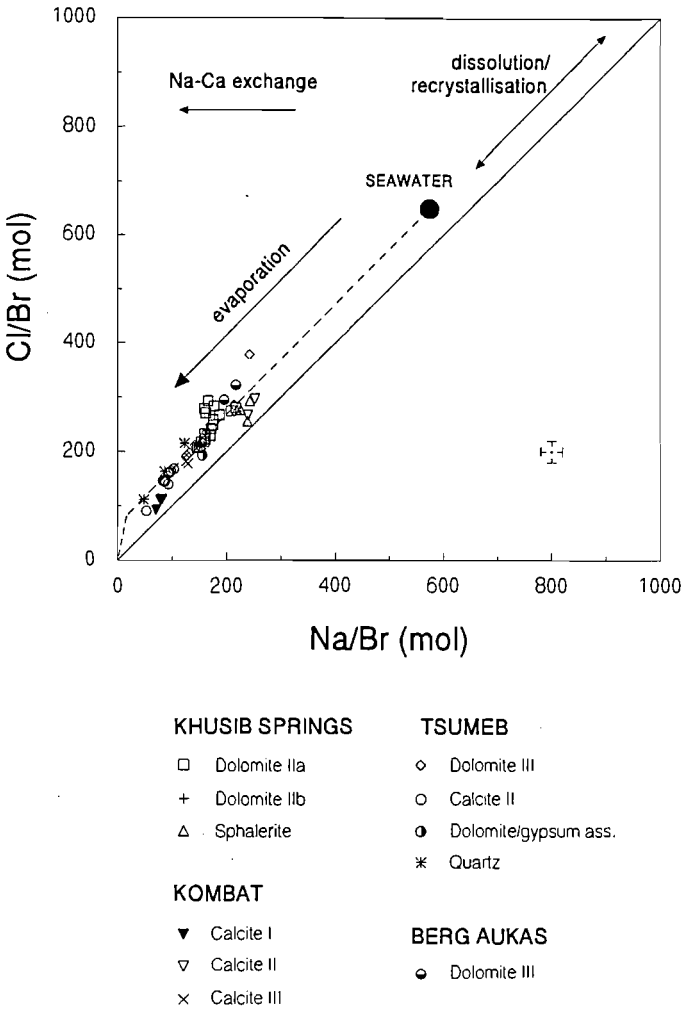

Figure 7.7 Na-Br-Cl systematics of fluid inclusion leachates from various minerals and carbonate generations at the deposits under consideration. Although no microthermometry data were obtainable for certain generations, leachate compositions of these generation were nevertheless included in the plot (after, Kesler *et al.*, 1995; mean seawater composition from Horita *et al.*, 1991). Bars on the right indicate errors in the ratios due to instrument conditions.

fluid. Mass balance considerations based on microthermometric data show that the proportions of lower salinity fluid do not affect total salinity to a great extent. However, if the proportion of the lower salinity fluids were to increase, then changes in the Cl/Br and Na/Br ratios would be effected. For example, a brine of salinity 22 wt% $NaCl_{eq}$ could be contaminated by a brine of salinity 15 wt% $NaCl_{eq}$ using a worst case scenario based on the salinity histograms of Figure

7.2. If this low salinity fluid contributes towards 20 %[4] of the volume of included fluids in the minerals, the bulk salinity is lowered from 22 wt% $NaCl_{eq}$ to 19 wt% $NaCl_{eq}$. Assuming that NaCl accounts for total Cl^-, if a Cl/Br ratio of 300 is taken for the bulk salinity of 22 wt% $NaCl_{eq}$, a bulk salinity of 19 wt% $NaCl_{eq}$ caused by contamination yields a Cl/Br ratio of 259, representing a 14.7 %[5] difference in the ratios. Similar calculations can be used to determine changes in the Na/Br ratio.

The above calculations show that "dilution" by a lower salinity fluid tends to lower the halogen ratios. By how much depends on the salinity of the "diluting" fluid, and its contribution to the total fluid inclusion volume. This differs from sample to sample within a specified generation. Therefore salinity ranges are used, rather than one salinity value, when describing halide systematics, as the range in ratios is normally determined by the range in salinities.

A difference of 34.5 % in the Cl/Br ratio is observed for the Dolomite II generation at Khusib Springs. No evidence was found for any significant presence of the lower salinity fluid in this study. Considering the range in salinity of the mineralising fluid at Khusib Springs (17-23 wt% $NaCl_{eq}$) the difference in the Cl/Br ratio is dependent on the proportion of fluid inclusions with salinities in the lower part of the range as opposed to the higher part of the range. If the higher part of the range is taken, this represents a salinity of 23 wt% $NaCl_{eq}$. If this salinity is correlated with a Cl/Br ratio of 300, a fluid dominated by the lower salinity value of 17 wt% $NaCl_{eq}$ will have a corresponding ratio of 222. The difference in the Cl/Br ratio for fluids represented by the opposing extremes in the salinity range is therefore 30 %. The observed difference is just slightly more than this.

Kesler *et al.* (1996) reported leachate compositions for sphalerite from the Daniel's Harbour mine in Newfoundland, which range in Cl/Br ratio from 200 to 700, representing a difference of

---

[4] Crude estimate based on proportion of low salinity inclusions measured, seeing that fluid inclusion shapes and sizes are similar irrespective of salinity differences.

[5] $$\% \text{ difference} = \frac{\text{highest Cl/Br - lowest Cl/Br}}{\text{(highest Cl/Br + lowest Cl/Br)/2}} * 100$$

111 %. This suggests mixing of brines of significant salinities in similar proportions, although no microthermometric evidence was found for this. Banks *et al.* (1997) obtained even greater ranges in the Cl/Br ratio for fluids of salinity <10 wt% $NaCl_{eq}$ in thrusts in the Pyrenees, representing a maximum difference in the ratio of 700, or 149 %. The largest difference encountered in this study was 65 % for Cl/Br in leachates of Dolomite III at Tsumeb. The observed range in salinity for this generation, based on microthermometry in the dolomite and co-existing quartz, is 20-24 wt% $NaCl_{eq}$. If a Cl/Br ratio of 300 is assigned to a salinity of 24 wt% $NaCl_{eq}$, the corresponding Cl/Br ratios would be 250 for a salinity of 20 wt% $NaCl_{eq}$, a difference of 18 %. Within-sample ranges in the ratio are within 10 % difference, with the exception of sample 2965/106, which shows a range of 163 in the Cl/Br ratio (Appendix A2.7), a difference of 55 %. Omitting this sample, the observed difference in the range of Cl/Br ratios is 19 %, which corresponds more closely with that predicted by microthermometry in coexisting quartz. The wider range in ratios for sample 2965/106 must therefore result from a wider range in the high salinity fluid population, or significant contamination from the lower salinity population, neither of which find support from the microthermometry data. A similar range is observed for quartz leachates, although duplicate crushes on one sample (DCT4) yield a difference of 27 %.

Calcite II at Tsumeb exhibits a maximum difference in Cl/Br ratio of 59 %, but this is due predominantly to one very low ratio, which may be caused by analytical error. Omitting this ratio gives a difference of 18 %, in close agreement with the salinity range and corresponding difference predicted by microthermometry.

7.5.2.2 (b) Salinity relations

All leachate compositions plotted in this study are deemed to have been derived from fluids of high salinity. Those samples whose leachates did not contain detectable Br^- were also depleted in Na^+ and Cl^-. Fluids from these samples are thought to be meteoric in origin. The sympathetic relationship between salinity (as determined from microthermometry) and observable halide systematics (i.e., actual plots on a Cl/Br vs Na/Br variation diagram) is noteworthy, as salinities of ~25 % total dissolved salts are required to generate these leachate systematics. Most MVT

brines are only slightly lower than this in salinity (Kesler *et al.*, 1995), and have produced the observed systematics, thus supporting this "requirement". However, recently, Banks *et al.* (1997) published leachate data for fluids that have been shown to be of rather low salinity (<10 wt% $NaCl_{eq}$). These tend to have a wide range in composition, plotting both in the region of seawater evaporation past halite precipitation, as well as in the region of halite dissolution. Bearing in mind that dilution of saline fluids by meteoric ones should theoretically not change their halide ratios, it is feasible that fluids of low salinity could produce the leachate systematics as outlined thus far. However, this can create problems analytically. Fluids which have been diluted to a large extent with meteoric waters will contain much lower amounts of Cl^-, Na^+, and particularly Br^-. Once the dilution has reached a certain factor, Br^- in particular, is impossible to detect, and it can nor longer be determined where ratios will plot on the variation diagram. For this reason, it has been assumed that the leachates in which Br^- was not detected (also with low Na^+ and Cl^- concentrations), represent fluids of predominantly meteoric origin, as any original evaporitic signature will have been significantly diminished by the high degree of dilution by meteoric fluids.

CHAPTER 8: DISCUSSION

8.1 BERG AUKAS-TYPE MINERALISATION

Berg Aukas-type deposits display attributes typical of MVT deposits. Not only are these reflected in the ore mineral assemblage (sphalerite and galena), stratabound carbonate-hosted occurrence and tectonic setting, but also in the geochemistry of the carbonate gangue in these deposits.

Differences determined between the Berg Aukas and Tsumeb mineralisation types, have led to the conclusion that the formation of such deposits were separated in space and time. In view of the syn-tectonic (D_2) nature of Tsumeb-type mineralisation, the formation of Berg Aukas-type deposits has been attributed to an earlier extensional tectonic regime in the OML (Pirajno and Joubert, 1993; Frimmel *et al.*, 1997). A basin dewatering model, in which basinal brines moved along growth faults related to rift graben formation during extension in the Damara Belt, is envisaged for the formation of deposits of the Berg Aukas-type.

Fluid inclusion results of Misiewicz (1988) showed that entrapment temperatures (T_{form}) for fluid inclusions in sphalerite and dolomite at Berg Aukas ranged from 137-255°C, based on estimated sedimentary overburden of 1500 m, corresponding to a pressure of 0.5 kb. These temperature estimates for Berg Aukas mineralisation overlap with those typical of MVT deposits (80-200°C; Anderson and Macqueen, 1987).

Salinities for fluids related to Berg Aukas-type mineralisation were determined at ~23 wt% $NaCl_{eq}$ (Misiewicz, 1988). In addition, crush-leach analyses of fluid inclusions show that significant amounts of $CaCl_2$ are present, supporting the T_e data of Misiewicz (1988). Highly saline, Na-Ca-Cl rich brines are again, typically found for MVT deposits (Anderson and Macqueen, 1987). The halide ratios determined from crush-leach analyses show further, that the salinity could have been derived from bitterns (residual fluids in the formation of evaporites) in equilibrium with precipitated evaporites. Subsequent fluid interaction should not have changed the halide ratios of the fluids, because the concentrations of these particular ions in most non-

evaporite rocks is much lower than their concentrations in typical brines (Crocetti and Holland, 1989). A possible source for the salinity of Berg Aukas fluids is discussed below.

In the southern part of the Damara Belt, Behr *et al.* (1983) documented a number of minerals within cyclic dolomite-pelite units in the Duruchaus Formation of the Nosib Group (Table 2.1). They interpreted these minerals to be pseudomorphs of evaporitic minerals formed in a continental evaporitic playa lake setting. Of particular significance is the uppermost cyclic unit, which comprises brown laminated dolomite, which, in turn, contains abundant microcline arranged as rosettes, interpreted to be pseudomorphs after primary gypsum. The upper cyclic unit was therefore ascribed to a marine ingression during late Duruchaus times (late-stage continental rifting). A marine sabkha evaporitic environment was thus envisaged for this upper unit, which marks the transition to marine sedimentation during post-Duruchaus times.

It can be expected that regimes similar to those in which the Duruchaus Formation was deposited were also present along the northern margin of the Damara Belt. This has been supported by Weber *et al.* (1983), who documented the presence of discordant breccias of siliceous dolomite and quartz lenses with giant crystals from the northern margin. In the same area, aggregates of "cauliflower quartz" were interpreted by these workers as pseudomorphs after gypsum/anhydrite.

From the above evidence, it is probable that bitterns in the Nosib Group provided the source for salinity of the fluids related to Berg Aukas-type mineralisation. In addition, S isotope ratios from sphalerite (Hughes, 1987) indicate a crustal, probably evaporitic, source for the sulphur. Fluids would thus have been released upward along growth faults during basin dewatering, interacted with evaporitic bitterns and leached metals from other sediments in the Nosib Group— a mechanism similar to the classical MVT models.

O isotope data for Berg Aukas (Frimmel *et al.*, 1997) show trends of decreasing $\delta^{18}O$ ratios with alteration (Fig. 6.1d). Such trends towards sites of mineralisation were also observed in MVT deposits by Sverjensky (1981) and Hannah and Stein (1984). In addition, the $\delta^{13}C$ ratios occur within a restricted range compared to ratios determined from the other deposits studied, due to the confinement of the Berg Aukas deposit to the lower part of the Abenab Subgroup.

With the exception of Mn and the base metals, trace element concentrations in the hydrothermal carbonates at Berg Aukas are similar or depleted relative to those in the host dolomite. Coupled with the Sr isotope evidence of Frimmel *et al.* (1997), which shows a late diagenetic character for the fluids, these trends indicate a local source for the mineralising fluids, i.e. from within the basin in which the Otavi Group was deposited. In addition, the flat REE patterns observed for hydrothermal dolomites at Berg Aukas have also been documented for MVT deposits (Graf, 1984), where mineralising fluids are considered to be derived from within basins. Mn may have been leached from the same source as Pb and Zn, possibly the Askevold Formation volcanics in the Nosib Group.

8.2 TSUMEB-TYPE MINERALISATION

The timing of Tsumeb-type mineralisation is constrained by its syn-tectonic nature with respect to the main deformation in the OML (D_2 of Miller, 1983; Lombaard *et al.*, 1986; Innes and Chaplin, 1986; Hughes, 1987; Pirajno and Joubert, 1993; Frimmel *et al.*, 1997). Karsting at Tsumeb may, in part, be attributed to a hiatus between the deposition of the Tsumeb Subgroup and that of the Mulden Group. Feldspathic sandstones at Tsumeb and Kombat have been correlated with sedimentary rocks of the Mulden Group, deposited as a syn- to post-tectonic molasse. Mineralisation is considered to be at least syn-tectonic, because it is closely associated with the feldspathic sandstone. Furthermore, Pb isotope dating of ores from Tsumeb and Kombat yielded ages of 550-600 Ma (Holmes and Cahen, 1957, in Lombaard *et al.*, 1986; Allsopp *et al.*, 1981; Hughes *et al.*, 1984), during which time continental collision, deformation and metamorphism were considered to be taking place in the Damara Belt (Miller, 1983).

Mineralisation at Khusib Springs is also thought to be synchronous with the D_2 deformation event in the OML (Verran, 1996). There, dolomite veining and associated mineralisation occur along tilted strata on the northern limb of the Harasib syncline (D_2), suggesting a syn-D_2 origin. Mineralisation at Khusib Springs may therefore be consistent with the Tsumeb-type as regards the timing thereof. Further work on the structural controls on mineralisation at Khusib Springs is necessary in this respect, however, because dolomite veining with associated mineralisation,

also occurs in ruptured hinge zones of box or kink folds related to D_3 deformation (Verran, 1996).

Unlike alteration at Berg Aukas, hydrothermal carbonate generations at Tsumeb, Kombat and Khusib Springs show, in addition to Mn, enrichments in Sr, Y and REE compared to the host rock compositions. A possible source for the Sr is the upper Tsumeb Subgroup, where a positive $\delta^{13}C$ value obtained for the dolomite with a gypsum association suggests precipitation in an evaporite environment containing hypersaline brines (Sears and Lucia, 1980). Such environments are usually enriched in Sr, present in aragonite or diagenetic celestite. Celestite may alter to strontianite or be replaced by calcite and sulphur (Nesse, 1991), both of which are present in the T7 zone (Hughes, 1987). Thus stratigraphic and depositional equivalents of the T7 zone elsewhere within or outside the OML could have provided the Sr for the mineralising fluids. Mn, Y and REE may have been derived from the base metal source.

The REE are of particular importance with respect to fluid evolution, as their behaviour in fluids is dependent on temperature, Eh (fO_2) and pH, which affect complexing and subsequent incorporation in the precipitating phase. Fractionation trends reflect these controls.

Distribution coefficients for the REE are >1, with respect to their incorporation into dolomite and calcite, as they readily substitute for Ca owing to similar ionic radii (Shannon, 1976). However, there is a general decrease (with the exception of Ce) in distribution coefficients with decreasing ionic radii from the LREE to the HREE (Palmer, 1985), leading to stronger partitioning of the LREE into the carbonate phase. In addition, stronger substitution for Ca as opposed to Mg, results in a higher concentration of REE in calcite compared to dolomite. However, this is a function of the fluid from which the relevant carbonates are precipitating, so not all calcites are necessarily enriched in total REE compared to dolomites.

The HREE form stronger complexes than the LREE (Goldberg *et al.* , 1963; Graf, 1984; Cantrell and Byrne, 1987). Such complexing behaviour, along with lower distribution coefficients, keeps the HREE mobile, i.e. in the fluid phase. This is reflected in the LREE enrichment in the chondrite normalised patterns of the host dolomites, and certain hydrothermal carbonates at the

three deposits. The most likely complexing ligands in this system were CO_3^{2-} and Cl^- ions, which are strong complexing agents (Cantrell and Byrne, 1987; Möller, 1991; Lee and Byrne, 1992, 1993).

All three deposits display trends of LREE in the earlier carbonates associated with the main mineralisation event, changing to flatter chondrite normalised patterns in later precipitates (Fig. 5.5). Such trends can be explained by a remobilisation process (Möller *et al.*, 1979; Graf, 1984). Initially, the formation of REE-carbonate complexes increases the ratios of La/Sm (both as free ions) and Sm/Lu (Sm/Yb in this case, again, both as free ions). Thus, earlier formed phases, such as Dolomite II at Khusib Springs and Tsumeb, and Calcite II at Kombat, have high La/Sm and Sm/Yb ratios. As precipitation continues, the residual fluid phase becomes progressively depleted in La and enriched in Sm and Lu (Yb). Precipitation at a later stage in the fluid evolution results in the carbonate exhibiting low La/Sm and Sm/Yb ratios, i.e. a flatter chondrite normalised pattern. This is true for Dolomite III at Khusib Springs and Tsumeb.

In chondrite-normalised REE plots, the slope of the pattern (and hence complexing behaviour), and the presence of anomalies in Ce and/or Eu (the two REE exhibiting more than one stable oxidation state) can be explained in terms of the fO_2 prevailing during precipitation. With regards to Ce, no anomalies of note are observed in chondrite-normalised plots for the carbonate generations at each of the three deposits. Eu, on the other hand, exhibits a predominantly negative anomaly in the mineralised dolomites, with concentrations below analytical detection in the host dolomite phases at Tsumeb and to an extent, at Khusib Springs. Later phases tend to lack an anomaly or display a positive anomaly (Chapter 5, Fig. 5.5).

Of the two oxidation states of Eu, the Eu^{3+} ion preferentially substitutes for Ca in the carbonate precipitate. Eu^{2+}, owing to its larger size (~17% greater than Eu^{3+}, McLennan, 1989) is retained in the fluid. A negative Eu anomaly suggests that the fluid may have been deficient in total Eu or, more likely, a predominance of Eu^{2+} over Eu^{3+} in the fluid.

For the hydrothermal mineralised dolomites, temperatures higher than 100°C must be invoked, based on microthermometry data. At temperatures greater than 100°C, thermodynamic

calculations predict that Eu^{2+} is the dominant ion in aqueous solutions (Sverjensky, 1984). However, strong complexing of Eu^{3+} with hard bases such as CO_3^{2-} and SO_4^{2-} results in a shift of the Eu^{2+}/Eu^{3+} redox boundary towards lower fO_2 (Bau, 1991; Fig 8.1). At even higher temperatures (>200°C), mass action expressions indicate that complexing is no longer able to stabilise Eu^{3+}, therefore, Eu^{2+} becomes the dominant oxidation state, resulting in the negative Eu anomaly observed for Dolomite II at Tsumeb and Khusib Springs, Calcite I at Tsumeb, and Calcite I and II at Kombat.

The later calcite generations at Kombat, Khusib Springs and Tsumeb either lack or show positive Eu anomalies. These calcites precipitated at lower temperatures, where Eu^{3+} is more stable; higher fO_2 prevailed in these predominantly post-ore stage precipitates, except at Tsumeb, where both Calcite IIa and IIb are associated with mineralisation. Conditions for these calcites are interpreted in terms of the slopes of their REE patterns.

High La_{CN}/Yb_{CN} ratios are typical of a reducing environment, whereas lower ratios indicate oxidising conditions (Chen and Zhao, 1997). The former is true for the main mineralising fluids from which Dolomite II at Tsumeb and Khusib Springs precipitated, as well as the calcitisation associated with the mineralisation at Kombat (Calcite II). The flatter normalised patterns for later dolomite generations indicate a higher fO_2. Although this may seem to conflict with the negative Eu anomaly for Dolomite III at Khusib Springs and Tsumeb, Bau (1991) found that the fO_2 at which Eu^{3+} is reduced to Eu^{2+} increases with increasing temperature; this is also coupled with a pH increase (Fig. 8.2). The latter variable is considered to have been the dominant factor in controlling the fO_2. Thus, higher fO_2 must have prevailed to account for the reduction in oxidation state of the Eu as pH increased. Additional evidence for the presence of oxidising as opposed to reducing conditions, is found in the ore mineral assemblage. Chalcocite, a typical sulphide found in oxidation zones in ore deposits, occurs with the Dolomite III generation at Tsumeb, along with tennantite and pyrite. At Khusib Springs, malachite and azurite occur with Dolomite III.

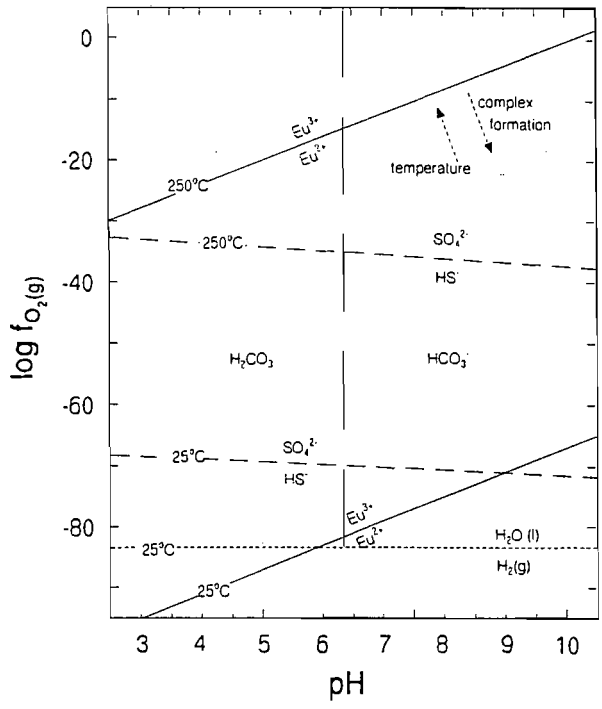

Figure 8.1 fO_2 vs pH diagram for equal activities of Eu^{2+} and Eu^{3+} at 25°C and 250°C. The SO_4^{2-}/ HS^- equilibrium is also shown for the same temperatures (after Sverjensky, 1984; Pourbaix, 1966). The effects of increasing temperature and complex formation on the Eu redox equilibrium are indicated by arrows.

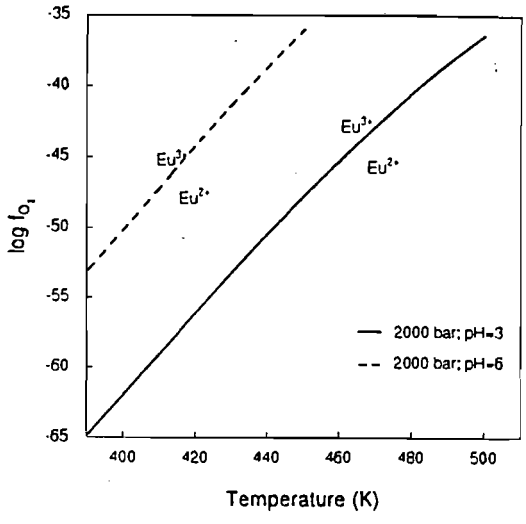

Figure 8.2 Diagram showing the effect of temperature, fO_2 and pH on the Eu redox boundary at constant pressure (after Bau, 1991). Higher temperatures, coupled with a pH increase, result in increased fO_2 for the reduction of Eu^{3+} to Eu^{2+}.

Calcite IIa at Tsumeb can be interpreted in the same way as Dolomite II. The presence of a slight positive Eu anomaly indicates a change to slightly more oxidising conditions, but not oxidising enough to give a flat REE pattern. Thus conditions were still relatively reducing when Calcite IIa precipitated. Calcite IIb, however, shows a flatter pattern, indicating more oxidising conditions, and can be interpreted in the same way as Dolomite III at Tsumeb.

Calcite III from Kombat exhibits HREE enrichment and a pronounced positive Eu anomaly, suggesting rather oxidising conditions. If this pattern is interpreted in terms of the evolution of a single fluid, then the LREE must have been severely depleted, and HREE-complexing became ineffective, such that the HREE were able to substitute into the carbonate lattice.

Although the precise pH and fO_2 cannot be constrained, REE patterns of the various carbonate generations at Tsumeb, Khusib Springs and Kombat suggest that Dolomite II at Tsumeb and Khusib Springs, Calcite I at Tsumeb, and Calcite II at Kombat precipitated at lower pH, lower fO_2 and higher temperature, compared to Dolomite III from Tsumeb and Khusib Springs and Calcite III from Kombat (Fig. 8.1). Calcite II at Tsumeb represents a transition between the conditions under which Dolomite II and Dolomite III precipitated, reflecting both LREE enriched and flat chondrite-normalised patterns (Fig. 5.5). In addition, the simultaneous enrichment in Y and REE reflects their similar chemical behaviour.

$\delta^{13}C$ values may also be used as an indicator of Eh and pH, although the changes required in these physicochemical conditions in order to effect observed changes in $\delta^{13}C$ of the precipitated carbonates, are minimal. Experimental data indicate that increasing fO_2 by 1 log unit or pH by 2 units can cause a decrease in $\delta^{13}C$ of 30 ‰ (Ohmoto, 1972). Most of the carbonate generations experienced minimal changes in conditions of pH and fO_2, especially during the mineralising event. The large range in $\delta^{13}C$ values observed, particularly with respect to hydrothermal carbonates at Tsumeb, is better ascribed to a stratigraphic control, explained below.

Petrographic and trace element characteristics of the Dolomite III generation of Theron and Beukes (1993) correlate very well with the observations for Dolomite III in this study. Sampling

of these similar generations from different stratigraphic levels at Tsumeb gives lower $\delta^{13}C$ in the lower levels (this study) as opposed to higher values in the upper levels (Theron and Beukes, 1993). Such results are further supported by host rock data of Kaufman *et al.* (1991) and Frimmel *et al.* (1997), which reflect secular variations in $\delta^{13}C$ for carbonates of the Otavi Group (Fig. 8.3). Considering the change from negative $\delta^{13}C$ to positive $\delta^{13}C$ values in the host carbonates as one progresses further up the Tsumeb Subgroup, the regional $\delta^{13}C$ isotopic signatures of the mineralising fluids can be interpreted as reflecting, in part, a host rock control. The range in $\delta^{13}C$ for hydrothermal carbonates at Tsumeb is ~9 ‰. The transgression of the pipe from at least the T4 zone in the Elandshoek Formation to the T7 zone, where it is eroded, accounts for this range in $\delta^{13}C$, which includes positive and negative excursions. The range in $\delta^{13}C$ observed for hydrothermal calcites associated with hypogene sulphide at Kombat is also reflected in the range of $\delta^{13}C$ for sedimentary carbonates of lithozone T8 (~0.5 to 10.7 ‰, Deane, 1993).

In addition to large scale stratigraphic control, Kaufman *et al.* (1991) noted ranges in the $\delta^{13}C$ values within individual sedimentary units, which they attributed to local facies controls such as the presence of organic matter. For example, the T7 lithozone contains organic matter thought to be enriched in $\delta^{13}C$. Theron and Beukes (1993) explained this enrichment as resulting from the process of methanogenesis, as described by Land (1983). In this process, biogenic reactions involving the production of isotopically light CH_4 take place. The CH_4 is then driven out of the system, leaving behind isotopically enriched residue. Hydrothermal fluids then interact with this residue, and a corresponding heavy isotope signature is imparted to the resulting precipitate or recrystallised product. The heavy signatures of Dolomite II and the dolomite associated with gypsum could be accounted for using this explanation. Thus, host carbonates with variable enrichment in light organic carbon will have affected the $\delta^{13}C$ composition of the fluids which infiltrated them, and hence controlled the $\delta^{13}C$ ratio of the precipitating/recrystallising phases.

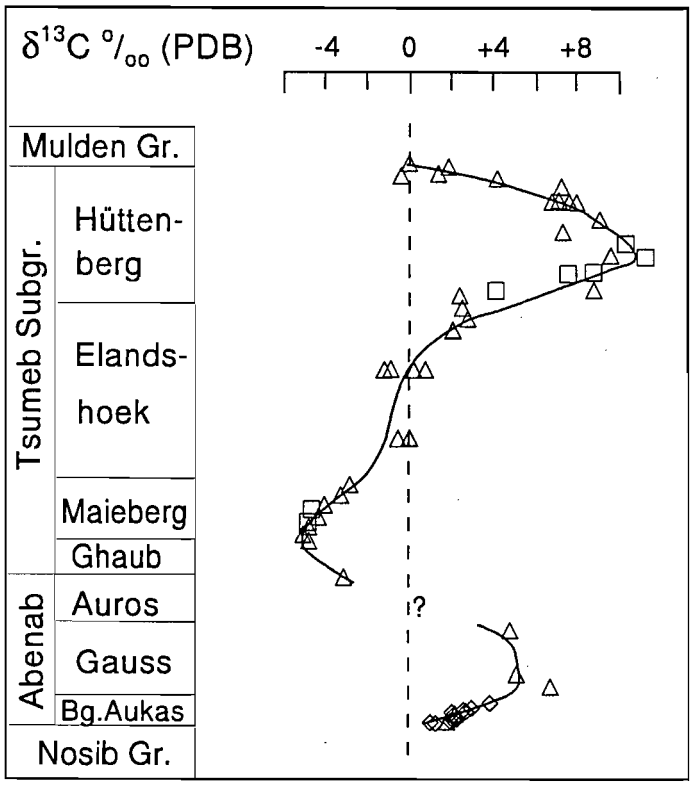

Figure 8.3 Variation in $\delta^{13}C$ values of relatively unaltered carbonates as a function of their stratigraphic position in the OML. Diamonds and squares = data from Frimmel *et al.* (1997); triangles = data from Kaufman *et al.* (1991); after Frimmel *et al.* (1997).

Altered host rocks show decreased $\delta^{18}O$ values compared to unaltered hosts, as seen at Khusib Springs, and to an extent, at Tsumeb and Kombat. The difference in $\delta^{18}O$ ratios in all the deposits reflects either precipitation under conditions of increasing temperature, leading to lower $\delta^{18}O$ values, or alternatively, mixing with isotopically lighter meteoric water. Host rocks exhibit, in general, higher $\delta^{18}O$ values than carbonate alteration products. This may be explained by the higher temperatures at which hydrothermal alteration and ore deposition took place, as well as the different isotopic characteristics of the ore-bearing fluids. The difference in $\delta^{18}O$ ratio is most pronounced between unaltered host dolomite (Dolomite Ia) and hydrothermally altered host dolomite (Dolomite Ib) at Khusib Springs. Although no textural change is evident, an increase in hydrocarbon content suggests a difference in the geochemistry of Dolomite Ib. The significant difference in the $\delta^{18}O$ value between host dolomites within and away from the deposit may

therefore be attributed to a pronounced hydrothermal imprint around the deposit. As discussed for Berg Aukas, trends of decreasing $\delta^{18}O$ ratios in carbonates towards sites of mineralisation are common features in hydrothermal carbonate hosted deposits, and are not only confined to MVT deposits (eg. Frimmel, 1992). Dolomite-calcite fractionation of up to 6 ‰ at surface temperatures (Land, 1983) can result in the difference in $\delta^{18}O$ between the host Dolomite Ia and the limestone host at Khusib Springs. However, this is not a satisfactory explanation, as the $\delta^{18}O$ signatures are not primary, having been modified to some extent during diagenesis. A hydrothermal overprint more likely accounts for the difference in $\delta^{18}O$, as the limestone, owing to its closer proximity to the ore deposit, must have undergone recrystallisation at higher temperatures than the host Dolomite Ia further away from the deposit. Similar arguments of increasing temperature associated with hydrothermal alteration can be used to explain the slightly higher $\delta^{18}O$ value of host dolomite as opposed to mineralised calcite at Kombat. Increased fluid-rock ratios also play a role in determining the $\delta^{18}O$ values of the hosts. Such ratios are again more pronounced closer to hydrothermal activity within the deposit. More massive host dolomite at Tsumeb displays a higher $\delta^{18}O$ value than host dolomite breccia fragments in contact with sparry dolomite matrix (hydrothermal). Thus, differences in temperature and fluid-rock ratios can explain the range in $\delta^{18}O$ observed at these deposits.

Fluid salinities from both Tsumeb and Khusib Springs were found to be high (20-23 wt% $NaCl_{eq}$). In the Khusib Springs area, there is no evidence for a significant low salinity fluid component having been present in the mineralising system, supported by data from King (1990). Previous fluid inclusion studies from Tsumeb indicated that the fluids associated with the main mineralising event were of low to moderate salinity (2-8 wt% $NaCl_{eq}$, Ypma, 1984; 6-12 wt% $NaCl_{eq}$, Haynes, 1984). It is, however, not clear whether the sulphides associated with the gangue phases analysed were primary or in fact later remobilised sulphides. Chalcocite was present in the sulphide assemblage studied by Haynes (1984), suggesting that these sulphides represent remobilised rather than primary ore. If both their interpretations and those of the present study are accepted, the implication would be that initially, lowly to moderately saline fluids precipitated the main phase of sulphide ores, with subsequent infiltration of, and ore remobilisation by, highly saline fluids.

Samples from Tsumeb for which salinity was determined, come from the lower oxidation zone in the pipe. This is confirmed by their REE characteristics, which also indicate that these carbonates, and associated sulphide phases (chalcocite and tennantite) are products of remobilisation. Söhnge (1964) considered the North Break Zone, which occurs stratigraphically higher up, to have been a conduit for oxygenated meteoric water into the pipe, the meteoric water oxidising primary sulphide. Recently, however, Theron (1994) concluded, from detailed petrographic evidence, that the North Break Zone was probably not a conduit for meteoric input after the main phase of mineralisation, as the alteration effected in this zone is very similar to that exhibited in the pipe. He postulated that hydrothermal fluids from within the pipe escaped into the North Break Zone due to fluid overpressuring, thus effecting a similar alteration to that found in the pipe. Again, fluid inclusion data from this zone would yield valuable information as to whether or not it allowed infiltration of meteoric fluids to oxidise the sulphide. Although the REE data indicate that oxidising conditions and remobilisation processes were responsible for precipitating the Dolomite III generation, this is seen as essentially the evolution of a single fluid. Stable isotope data for the Dolomite III and Calcite II generations do not indicate any meteoric input, as may be the case for the later Calcite III generation at Tsumeb. Their isotope signatures are instead similar to other hydrothermal carbonates found at Tsumeb and Khusib Springs. Taking these factors into consideration, it is unlikely that the main phase of sulphide mineralisation was precipitated from fluids of low to moderate salinity, and subsequently remobilised by highly saline fluids. Rather, the remobilising fluids dealt with here are considered to be at least as saline as the main mineralising fluids at Tsumeb. During later remobilisation and oxidation, the primary ore-bearing fluid became progressively diluted by meteoric waters.

No clarity exists with respect to salinities of fluids responsible for the main phase of hypogene sulphide mineralisation at Kombat. Early hydrothermal fluids at Kombat were documented as being of high salinity (~20 wt% $halide_{eq}$, Ypma, 1984), although their relationship to the sulphides was not clearly established. The low salinities (~3 wt% $NaCl_{eq}$) of inclusions in Calcite I, associated with the Fe-Mn oxides in this study, belong to an earlier fluid not related to the hypogene sulphides. This is supported by the low $\delta^{13}C$ of Calcite I compared to carbonates associated with the hypogene sulphides. The high salinities documented by Ypma (1984), on the other hand, may well correspond to fluids from which the sulphides precipitated. Such salinities

are similar to those observed at Khusib Springs and Tsumeb. Furthermore, Innes and Chaplin (1986) documented widespread Cl in the Cu-Pb ores at Kombat, up to 500 ppm. Precipitation from highly saline fluids would adequately account for this observation.

The above evidence shows that highly saline fluids were not only present in areas of cupriferous mineralisation of the Tsumeb-type, but played an active role in the mineralisation process. Such features were also observed in the Duruchaus Formation in the southern Damara Belt, where Cu mineralisation occurs in the vicinity of the metamorphosed evaporite deposits, for which fluid inclusion results show the presence of Na-Ca-K-Cl rich residual brines (Behr *et al.*, 1983). In addition, high salinity fluids, by virtue of their Cl^- content, have been shown to carry larger amounts of base metals compared to lower salinity fluids (e.g. Crerar *et al.*, 1985; Ruaya and Seward, 1986). The metalliferous content of deposits, such as Tsumeb and Kombat in particular, are thus better explained by metal transport via high salinity (Cl- rich) fluids.

As with Berg Aukas fluids, the salinity in Tsumeb-type deposits can be explained by interaction with evaporitic bitterns, which is also supported by S isotope data (Hughes, 1987). Besides evidence in the Nosib Group, progressively more evidence has emerged with respect to the former presence of evaporite deposits in the Otavi Group, such as the gypsum and anhydrite present in the T7 zone at Tsumeb. The confinement of sulphates to this particular zone supports a sedimentary, evaporitic origin. The Augen Marker is a thin (<1 m) nodular limestone bed (Fig. 3.2), also in the T7 zone, and occurs along both limbs of the Tsumeb syncline in the Tsumeb mine environs. Theron (1994) described chevron cleavages within radiating calcite laths of the nodules, and interpreted these as being derived from anhydrite, as described by Lowenstein (1987). Halite is also known to show this type of cleavage, and hence may have also once been present in this bed. Other occurrences in the Otavi Group thought to represent former evaporites are found in the Auros Formation ("quartz cluster dolomite"; Hughes, 1987), and possibly the base of the Gauss Formation (Hedberg, 1979). The examples in the OML may have been prime sources for the sulphate, later reduced to sulphide, in the mineralising fluids during infiltration onto the carbonate platform. Similar occurrences in stratigraphic equivalents outside the OML (Swakop Group further south), along with occurrences in the Nosib Group south of the OML, may have been sources of Cl^-, for leaching of the base metals en route to the carbonates.

Bearing in mind the syn-tectonic nature of the mineralisation at Tsumeb, Khusib Springs and Kombat, formation temperatures for the mineralisation can be calculated using the appropriate pressure corrections. The D_2 deformation event in the Damara Belt was accompanied by peak metamorphism (Miller, 1983). The pelitic metamorphic assemblage in the northern part of the Northern Rift comprises chlorite+muscovite+quartz. The biotite-in isograd is found immediately south of the OML (Miller, 1983), representing the boundary of lower greenschist facies metamorphism, in the temperature range 300-400°C (Yardley, 1989). Frimmel *et al.* (1997), assuming an average geotherm, and using peak metamorphic temperatures, deduced a pressure of 2-3 kb for the peak of metamorphism in the OML. These pressures are somewhat higher than previous pressure estimates of 500-700 bar at Tsumeb, based on inferred hydrostatic/lithostatic loads (Ypma, 1984), but reflect more accurately, prevailing conditions.

Pressures consistent with regional metamorphism in the OML were therefore used in calculating the temperatures of fluid entrapment in the gangue phases on which microthermometry could be performed. Although the inclusions studied were predominantly secondary, T_{form} of these inclusions are considered to be close to the temperatures at which the host minerals precipitated, as the secondary character of some of the inclusions was not established. These inclusions were rather considered possibly primary, and their similar T_h values and salinities to other inclusions deemed secondary, suggest that the secondary inclusions were almost contemporaneously trapped. Average homogenisation temperatures determined for the three generations studied are 100, 150 and 230°C for Calcite II and Dolomite III from Tsumeb and Dolomite II from Khusib Springs, respectively. Isochores for the determination of T_{form} were calculated using the equations of Brown and Lamb (1989) for the NaCl-H_2O system (Fig. 8.4). T_e values and crush-leach data showed, however, that the fluids contained significant $CaCl_2$. The derived T_{form} for a particular T_h results in an overestimation of T_{form} by ~20°C for the pure NaCl-H_2O system compared to the pure $CaCl_2$-H_2O system, for the temperature range dealt with here (Zang and Frantz, 1987). Considering the ratios of NaCl:$CaCl_2$ in fluid inclusion leachates (1:2 for Dolomite III and Calcite II at Tsumeb, and 1:1 for Dolomite II at Khusib Springs), an overestimation of ~10°C in the calculated T_{form} is expected using the NaCl-H_2O system. Thus, using isochores in the NaCl-H_2O system, and accounting for the presence of $CaCl_2$, the calculated T_{form} for Dolomite II at Khusib Springs is 370°C, for Dolomite III at Tsumeb, 275°C and Calcite II at Tsumeb, 210°C.

The lower temperature exhibited by Calcite II as opposed to Dolomite III at Tsumeb, possibly indicates cooling of the fluid under isobaric conditions. The minimum temperature decrease in this case would have been 55°C. Should cooling not have been isobaric, the temperature difference would have been only slightly greater, as a large pressure decrease is not envisaged. Formation temperatures derived for mineralising fluids at Khusib Springs are much higher for the same pressure of formation. REE evidence presented indicates that fluids represented by Dolomite III and Calcite II at Tsumeb were related to remobilisation. No data for the main mineralising fluid at Tsumeb could be obtained, as no suitable inclusion material could be found in Dolomite II. If, however, the average T_h value of 230°C of Haynes (1984) is used for the main mineralising fluid at Tsumeb, recalculation of the T_{form} yields a value of ~395°C, for a mean salinity of 8 wt%, based on his range of 6-12 wt% $NaCl_{eq}$. The mean T_h value derived by Haynes (1984) and that derived for the mineralising fluid at Khusib Springs in this study are identical. Thus, assuming the prevailing pressure at both deposits was the same (considering a similar metamorphic grade at both), temperatures of the mineralising fluids are envisaged to have been very similar during ore precipitation. Other than the 20 wt% $halide_{eq}$ obtained by Ypma (1984) for secondary fluid inclusions hosted by the feldspathic sandstone at Kombat, no salinity data for the mineralising fluids at Kombat exist to date. Using this salinity value and the average T_h of ~250°C (Ypma, 1984), a temperature of formation of ~405°C is calculated for the NaCl-H_2O system. This temperature is higher than those calculated for Tsumeb and Khusib springs, but is consistent with the trend towards increasing metamorphic intensity southwards in the OML.

From the above calculations, peak T_{form} for Tsumeb, Khusib Springs and Kombat are constrained between 370-405°C. These are higher than T_{form} for Berg Aukas mineralisation. Using T_{form} values, along with $\delta^{18}O$ ratios of the corresponding carbonate phases, the $\delta^{18}O$ value of the fluids associated with mineralisation at the deposits ($\delta^{18}O_{fluid}$) can be calculated. These values are summarised in Table 8.1.

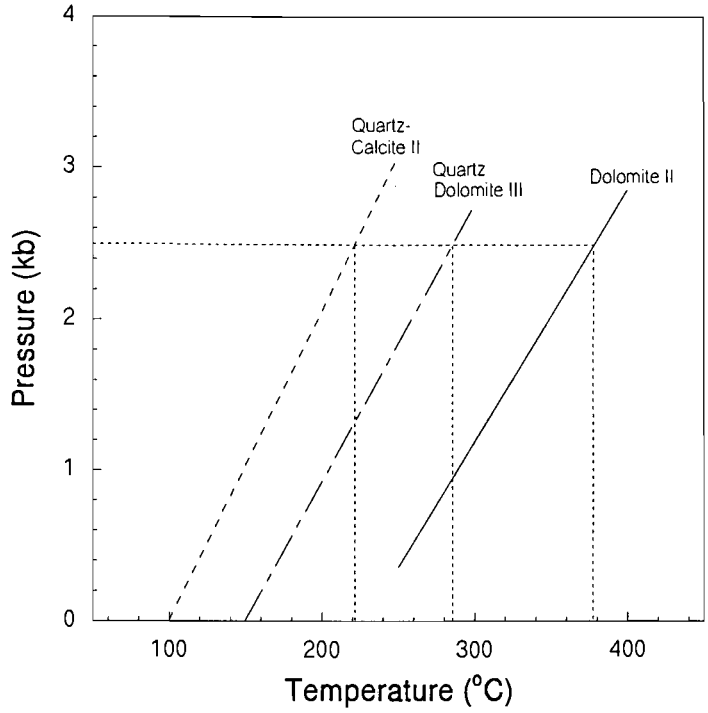

Figure 8.4 Plot of isochores for the dominant fluid populations characterising the Calcite II, Dolomite III (Tsumeb) and Dolomite II (Khusib Springs) generations.

Table 8.1 $\delta^{18}O$ isotope-temperature relations and the calculation of $\delta^{18}O$ of fluids associated with mineralisation

Deposit	**Tsumeb**				**Khusib Springs**	**Kombat**
Carbonate	Dol III	Cal II	Vein Dol*	Vein Cal*	Dol II	hydr. cal+
$\delta^{18}O_{carb}$(‰)	20.7±0.6	11.4	21.5±1.2	19.4±0.3	19.2±0.4	20.6±1.7
T_{form} (°C)	275	210	395	395	370	405
$\delta^{18}O_{fluid}$(‰)	11.5±0.6	12.0	15.8±0.2	16.1±0.3	13.0±0.4	17.4±1.7

* Isotope data and classification from Hughes (1987), recalculation of peak T_{form} after Haynes (1984).

+ Isotope data from Frimmel *et al.* (1997); recalculation of peak T_{form} after Ypma (1984) using 20 wt% $NaCl_{eq}$.

$\delta^{18}O_{fluid}$ calculated using modified equation of Northrop and Clayton (1966, in Friedman and O'Neil (1977) for dolomite-water fractionation, and Friedman and O'Neil (1977) for calcite-water fractionation.

Using values corresponding to the highest temperatures, the mean $\delta^{18}O_{fluid}$ is 15.5 ‰ for Tsumeb, 13± 0.4 ‰ for Khusib Springs and 17.4 ±1.7 ‰ for Kombat. Of the ranges in $\delta^{18}O$ defined for different fluid types (Ohmoto, 1986), all of the above values occur within the range of 3-20 ‰, for metamorphic fluids. The lower value for Khusib Springs also plots within the range for magmatic fluids. There is, however, no geological evidence for contemporaneous magmatism in the OML, and such a theoretical magmatic origin is therefore excluded. The syn-tectonic nature of the mineralisation there supports instead a metamorphic origin of the fluids. Metamorphic fluids, as used in this context, refer to fluids which were active during regional metamorphism. As discussed by Ohmoto (1986), these are recycled fluids, and may themselves originate from a number of different reference waters, hence accounting for the wide range in $\delta^{18}O$ ratios.

Metamorphic fluids derived from devolatilisation reactions during prograde metamorphism are generally of low salinity, which is not sufficient for carrying large amounts of base metals (Phillips *et al.*, 1994). Although isotope data provide a means of differentiating between fluid origins, Phillips *et al.* (1994) caution against using these data as the sole means of differentiation. It is therefore suggested that during deformation (D_2), fluids present within the sediments of the Damara Supergroup in the Damara Belt were mobilised, migrating northwards along thrusts, reactivated faults, shear zones and basement highs. These fluids may have also originated, in part, from metamorphic devolatilisation reactions in the Damara Belt, as suggested by Pirajno and Joubert (1993). En route, the fluids acquired salinities in the order of 20-23 wt% $NaCl_{eq}$ from interaction with evaporitic formation waters within the sediments, as well as within the Otavi Group. These fluids were capable of leaching and carrying significant quantities of base metals (and Mn, Sr, Y and REE). The significant geochemical differences between the host rocks and hydrothermal alteration products at Tsumeb-type deposits further support an external source, i.e. outside the basin, for the fluids, which would also explain the cupriferous nature of these deposits as opposed to the Berg Aukas-type.

Salient differences between Khusib Springs, Tsumeb and Kombat include a simpler ore mineralogy and the absence of feldspathic sandstone at Khusib Springs. The reasons for the simpler mineralogy at Khusib Springs remain unclear, however, the absence of the feldspathic

sandstone may be explained by the lower stratigraphic position of the Khusib Springs deposit. Whereas both the sandstone and brecciation (karst and tectonic) provided an important porosity source for sulphide mineralisation at Tsumeb and Kombat, only syn-tectonic brecciation may have provided the porosity necessary for sulphide deposition at Khusib Springs.

CHAPTER NINE: CONCLUSIONS

Carbonate alteration occurs as dolomite alteration at Berg Aukas, Khusib Springs and Tsumeb; calcitisation at Kombat and carbonate silicification at Tsumeb. Within each of the deposits, a number of carbonate generations exist, some related to mineralisation, others not. Geochemical differences between mineralised and barren carbonates are best seen in REE distribution, although stable isotopes also show differences. Of the generations related to mineralisation, trace element abundances and stable isotope distributions are similar, but differences in chondrite-normalised REE patterns and ore associations allows distinction between these generations.

Geochemical characteristics of the hydrothermal carbonates at each deposit indicate that the main mineralising fluids at Tsumeb and Khusib Springs precipitated carbonates (Dolomite II) under reducing, acidic conditions at temperatures of ~280-295°C. At Tsumeb, remobilisation, postulated to be part of the same event as the main mineralisation, resulted in precipitation of carbonates (Dolomite III) under more oxidising, alkaline, host rock-buffered conditions. A similar process occurred at Khusib Springs, although much later in the paragenesis (Dolomite III), under somewhat more alkaline conditions. Calcitisation at Kombat took place under similar conditions to the main mineralisation event at Tsumeb and Khusib Springs. In terms of their isotope composition, a strong stratigraphic control was imparted on the fluids by the host carbonates through which they migrated. In addition, redox conditions and local facies variations played a role in controlling the isotope composition of fluids associated with mineralisation. Fluids of all three deposits, Tsumeb, Khusib Springs and Kombat, were enriched in REE, Mn, Y and Sr relative to host rock compositions.

From geochemical characteristics, structural relations and ore associations, Khusib Springs appears to be a member of the Tsumeb-type of base metal sulphide mineralisation, rather than having any affinity to the Berg Aukas-type.

Carbonate alteration at Berg Aukas appears to be geochemically distinct from the alteration present at the other three deposits, further distinguishing between Berg Aukas- and Tsumeb-type

mineralisation. Differences are best developed with respect to the trace elements, which are depleted in Berg Aukas alteration phases compared to alteration phases in the other three deposits. In particular, the low REE abundances in the mineralising fluids support an MVT affinity for the Berg Aukas-type. Stable isotope values for the alteration phases at Berg Aukas overlap somewhat with those for alteration phases from Tsumeb and Kombat, but are distinct from values for alteration phases at Khusib Springs. However, fluid inclusion evidence suggests that both Berg Aukas- and Tsumeb-type fluids were of a high salinity, ~ 20-23 wt% $NaCl_{eq}$, and derived from evaporitic formation waters. Both mineralising fluid types were enriched in Mn with respect to pore fluids within the host dolomites. T_{form} was lower at Berg Aukas compared to the other deposits.

Evaporites were apparently important components in providing salinity to the ore-bearing fluids, as indicated by halide ratios of fluids, and may have been a source of some of the trace elements in the hydrothermal carbonates, as well as sulphur for mineralisation.

IMPLICATIONS FOR EXPLORATION

Geochemical exploration has much potential in the OML. Of the geochemical parameters examined in this study, trace element, particularly REE, distribution in the gangue carbonates proved informative with regards to genesis, but also provided a means of differentiating between Berg Aukas- and Tsumeb-type deposits. Within deposits too, these parameters proved useful in distinguishing between barren and mineralised gangue phases. Stable isotopes do not always provide a clear-cut distinction between the different deposit types. Within each deposit, the various generations are difficult to separate on the basis of stable isotope signatures, although barren, later generations tend to exhibit lower O and C isotope values. Nevertheless, this is not diagnostic, as certain mineralised generations show the same characteristics. Fluid salinities, as determined by microthermometry, do not provide a means of differentiating between Berg Aukas- and Tsumeb-type mineralisation, as salinities are similar. A more thorough fluid inclusion study is required, in which salinities between generations within the same deposit can be assessed, to determine whether more than one fluid was present during mineralisation, and how effective a role the fluids may have played during the mineralisation process. Fluid

chemistry, as determined by crush-leach techniques and microthermometry, shows that fluids associated with mineralisation were enriched in $CaCl_2$, and contained other ions such as Mg^{2+}, Na^+ and SO_4^{2-} in generally significant proportions. Halide ratios indicate fluid interaction with evaporite bitterns.

Using the above information, in conjunction with geological features, the following recommendations can be taken into consideration for future exploration in the OML:

- Geological controls on mineralisation should be looked for. Tsumeb-type mineralisation tends to occur in the Upper Tsumeb Subgroup, although Khusib Springs is situated lower in the stratigraphy. Nevertheless, such deposits are associated with areas of high porosity (i.e., provided by dolomite brecciation, karsting or feldspathic sandstone in the upper Tsumeb Subgroup) which are, in turn, in contact with areas of lower porosity (e.g. dolomite/limestone contact, Khusib Springs; dolomite phyllite contact, Kombat). In addition, Tsumeb type deposits occur within large scale D_2 synclinal structures (e.g. Tsumeb Syncline, Otavi Valley Syncline, Olifantsfontein-Harasib Syncline).
- Trace element (Mn; Sr; Y; REE) mapping should be carried out on carbonates on a large (district) scale, using "least altered" host rock concentrations as a background. Once anomalies are delineated, these should be investigated further.
- Mineralisation seems to occur in areas where there is evidence for the former presence of evaporites. Fluid inclusion studies in such areas can help delineate the possible paths that high salinity fluids may have taken should they have interacted with these former evaporites.
- Once a specific area has been targeted, small scale exploration could involve documenting carbonate alteration present, and carrying out stable isotope studies on alteration phases and hosts, to delineate a possible isotope halo, as seen at Khusib Springs. REE data should provide information on which alteration may possibly be associated with mineralisation.

Thus, geochemical parameters investigated in this study, along with other types of information, may help in identifying ore occurrences, and delineating between Berg Aukas and the more economic Tsumeb type deposits in the OML.

ACKNOWLEDGEMENTS

I would like to express sincere thanks to my supervisor, Prof. Hartwig Frimmel, for initiating this project, and for his guidance, constructive criticism, patience and encouragement throughout the course of this study. Thanks are also extended to my co-supervisor, Prof. Anton le Roex, for his expert help and useful discussions in all things analytical.

The Council for Mineral Technology is gratefully acknowledged for funding the analytical work. In particular, I would like to thank Dr. J.P.R. de Villiers, who willingly allowed me to study further. Goldfields Namibia Ltd. are thanked for providing logistical support and samples from their mines. In particular, thanks are extended to Arno Günzel, Malcolm Jolly and Jon Deane, for their help with sample collection at Tsumeb and Kombat. Thanks also to Alex MacKay for obtaining information pertaining to samples for me.

Wojtek Pryzybylowicz is thanked for help with running the proton probe and data reduction at NAC. Ted Huston helped with advice on the Dionex® system and crush-leach analysis.

The following people from UCT are sincerely acknowledged:

- ☞ Prof. James Willis, for advice on XRF and HPIC;
- ☞ Shireen Govender and Fran Pocock for help with XRF;
- ☞ Shaamielah Davids, for help with XRF and REE sample preparation;
- ☞ Dr. Chris Harris and Peter Föelling, for advice on stable isotope analysis;
- ☞ Fayrooza Rawoot, for help with sample preparation for stable isotope analysis;
- ☞ Patrick Sieas, for his enthusiasm and most stimulating discussions during the crush-leach work;
- ☞ Dr. Martin Fey, for his interest and useful discussion concerning crush-leach analyses;
- ☞ Dane Gerneke, for help with CL imaging;
- ☞ David Wilson, for polished section and fluid inclusion chip preparation;
- ☞ Ernest Stout, for help with sample preparation for various techniques;
- ☞ My post-graduate fellows, for their help and advice on various aspects of this project;

☞ Judy Green, for proof-reading parts of this dissertation;

☞ Neville Buchanan, for help with all printing and photocopying;

☞ The various staff members who gave their time willingly when I required help.

Nellie Mutemeri is gratefully acknowledged for taking me into her home when I needed accommodation. Thanks also for her advice and enduring friendship. Heartfelt thanks are also extended to Shireen Govender, for accommodating me on a number of occasions, especially towards the end of my time in Cape Town. Shaamielah Davids, Fayrooza Rawoot and Raneshin Chetty are also thanked for their friendship. Friends like you are hard to find.

Deepest apologies and a warm thank you are due to anyone I may have omitted.

Finally, I extend my greatest appreciation to my parents, for their love and encouragement. Thank you.

REFERENCES

Al-Aasm, I., Taylor, B.E. and South, B. (1990). Stable isotope analysis of multiple carbonate samples using selective acid extraction. *Chem. Geol.*, **80**, 119-125.

Allsopp, H.L. and Ferguson, J. (1970). Measurements relating to the genesis of the Tsumeb pipe, South West Africa. *Earth Planet. Sci. Lett.*, **9**, 448-453.

Allsopp, H.L., Welke, H.J. and Hughes, M.J. (1981). Op jag met isotope. *Kernaktief*, **24**, 8-12.

Anderson, G.M. and Macqueen, R.W. (1982). Ore deposit models- 6: Mississippi Valley-type lead-zinc deposits. *Geoscience Canada*, **9**, 108-117.

Banks, D.A., Davies, G.R., Yardley, B.W.D., McCaig, A.M. and Grant, N.T. (1991). The chemistry of brines from an Alpine thrust system in the Central Pyrenees: An application of fluid inclusion analysis to the study of fluid behaviour in orogenesis. *Geochim. Cosmochim. Acta*, **55**, 1021-1030.

Banks, D.A., Tritlla, J., McCaig, A.M. and Henderson, I. (1997). The use of halogen systematics in deducing fluid sources and processes in the Pyrenees. *ECROFI XIV Conference proceedings,* Nancy, 31-32.

Banner, J.L., Hanson, G.N. and Meyers, W.J. (1988). Rare earth element and Nd isotopic variations in regionally extensive dolomites from the Burlington-Keokuk formation (Mississippian): Implications for REE mobility during carbonate diagenesis. *J. Sed. Petrol.*, **58**, 415-432.

Bau, M. (1991). Rare-earth element mobility during hydrothermal and metamorphic fluid-rock interaction and the significance of the oxidation state of europium. *Chem. Geol.*, **93**, 219-230.

Beales, F.W. and Jackson, S.A. (1966). Precipitation of Pb-Zn ores in carbonate reservoirs as illustrated by the Pine Point ore field, Canada. *Trans. Instn. Min. Metall.*, **75**, B278-285.

Behr, H.J., Ahrendt, H., Porada, H., Röhrs, J. and Weber, K. (1983). Upper Proterozoic Playa and Sabkha Deposits in the Damara Orogen, SWA/Namibia. *In:* Miller, R. McG. (Ed.), *Evolution of the Damara Orogen of South West Africa/Namibia.* Spec. Publ. No. **11**, Geol. Soc. S. Afr., 1-20.

Bodnar, R.J. (1993). Revised equation and table for determining the freezing point of H_2O-NaCl solutions. *Geochim. Cosmochim. Acta*, **57**, 683-684.

Bodnar, R.J. and Vityk, M.O. (1995). Interpretation of microthermometric data for H_2O-NaCl fluid inclusions. *In:* De Vivo, B and Frezzotti, M.L. (Eds.), *Fluid inclusions in minerals: Methods and applications*. Short Course of the working group (IMA) "Inclusions in

minerals", Pontignano-Siena, 1-4 Sept 1994, Virginia Polytechnic Institute and State University. 117-130.

Böhlke, J.K. and Irwin, J.J. (1992). Laser microprobe analyses of Cl, Br, I, and K in fluid inclusions: Implications for sources of salinity in some ancient hydrothermal fluids. *Geochim. Cosmochim. Acta*, **56**, 203-225.

Botha, B.J.V. (1960). *The arenaceous rocks and the pseudo-aplite of the Otavi Mountain Land, South West Africa*. Unpubl. D.Sc. thesis, University of Pretoria, Pretoria, 133 pp.

Brand, U. and Veizer, J. (1980). Chemical diagenesis of a multicomponent carbonate system-1: Trace elements. *J. Sed. Petrol.*, **50**, 1219-1236.

Brown, T.E. (1989). FLINCOR: a microcomputer program for the reduction and investigation of fluid inclusion data. *Amer. Mineral.*, **74**, 1390-1393.

Brown, T.H. and Lamb, W.M. (1989). P-V-T properties of fluids in the system H_2O-CO_2-NaCl: New geological presentation and implications for fluid inclusion studies. *Geochim. Cosmochim. Acta*, **53**, 1209-1221.

Buelter, D.P. and Guillemette, R.N. (1988). Geochemistry of epigenetic dolomite associated with lead-zinc mineralisation of the Viburnum Trend, Southeast Missouri: a reconnaissance study. *In*: Shukla, V. and Baker, P.A. (Eds.), *Sedimentology and Geochemistry of Dolostones*. SEPM, Spec. Publ. No. **43**, 85-93.

Bustillo, M., Fort, R. and Ordoñez, S. (1992). Genetic implications of trace elements in carbonate and non-carbonate phases of limestones and dolostones from western Cantabria, Spain. *Chem. Geol.*, **97**, 273-283.

Cantrell, K.J. and Byrne, R.H. (1987). Rare earth element complexation by carbonate and oxalate ions. *Geochim. Cosmochim. Acta*, **51**, 597-606.

Chadwick, P.J. (1993). *A study of the Berg Aukas-type Pb-Zn-V- deposits in the Otavi Mountain Land, Namibia*. Unpubl. MSc dissertation, University of Cape Town, Cape Town, 138 pp.

Channer, D.M.DeR., de Ronde, C.E.J. and Spooner, E.T.C. (1997). The Cl^--Br^--I^- composition of ~3.23 Ga modified seawater: implications for the geological evolution of ocean halide chemistry. *Earth Plan. Sci. Lett.*, **150**, 325-335.

Chen, Y. and Zhao, Y. (1997). Geochemical characteristics and evolution of REE in the Early Precambrian sediments: evidence from the southern margin of the North China Craton. *Episodes*, **20**, 109-115.

Chetty, D., Verran, D., Frimmel, H.E. and le Roex, A.P. (1997). The Khusib Springs Cu-Pb-Zn-Ag deposit, Otavi Mountain Land, Namibia— Mineralisation of the 'Tsumeb-type'? *In*:

Papunen, H. (Ed.), *Mineral Deposits: Research and Exploration— Where do they meet?* Proceedings of the Fourth Biennial SGA Meeting, Turku, Finland, Balkema, Rotterdam, 531-534.

Chilingar, G.V., Zenger, D.H., Bissel, H.J. and Wolf, K.H. (1979). Dolomites and dolomitisation. *In*: Larsen, G. and Chilingar, G.V. (Eds.), *Diagenesis in sediments and sedimentary rocks. Developments in Sedimentology, 25A*. Elsevier, Amsterdam. 423-536.

Clauer, N. and Kröner, A. (1979). Strontium and argon isotopic homogenisation of pelitic sediments during low-grade regional metamorphism: the Pan-African Upper Damara Sequence of northern Namibia (South West Africa). *Earth Planet. Sci. Lett.*, **43**, 117-131.

Crawford, M.L. (1981). Phase equilibria in aqueous fluid inclusions, 75-100. *In*: Hollister, L.S.and Crawford, M.L. (Eds.), *Short Course in Fluid Inclusions.* Mineral. Assoc. Canada, 303 pp.

Crerar, D., Wood, S., Brantley, S. and Bocarsly, A. (1985). Chemical controls on solubility of ore-forming minerals in hydrothermal solutions. *Can. Mineral.*, **23**, 333-352.

Crocetti, C.A. and Holland, H.D. (1989). Sulfur-lead isotope systematics and the composition of fluid inclusions in galena from the Viburnum Trend, Missouri. *Econ. Geol.*, **84**, 2196-2216.

Cullers, R.L. and Graf, J.L. (1989). Rare earth elements in igneous rocks of the continental crust: Intermediate and silicic rocks-ore petrogenesis. *In*: Henderson, P. (Ed.), *Rare Earth Element Geochemistry*. Developments in Geochemistry, **2**, Elsevier, Amsterdam. 275-316.

Deane, J.G. (1993). *The controls on "Contact type" Cu-Pb(Ag) mineralisation within the Tsumeb Subgroup of the Otavi Valley Syncline, Northern Namibia*. Unpubl. MSc dissertation, University of Cape Town, Cape Town, 240 pp.

Deane, J.G. (1995). The structural evolution of the Kombat deposits, Otavi Mountainland, Namibia. *Communs. geol. Surv. Namibia*, **10**, 99-107.

de Baar, H.J. W., Bacon, M.P., Brewer, P.G. and Bruland, K.W. (1985). Rare earth elements in the Pacific and Atlantic Oceans. *Geochim. Cosmochim. Acta*, **49**, 1943-1959.

Dickson, J.A.D. and Coleman, M.L. (1980). Changes in carbon and oxygen isotope composition during limestone diagenesis. *Sedimentology*, **27**, 107-118.

Dionex® (1988). *Determination of trace anions and keto- organic acids in high purity, ammoniated, and borate waters found in steam cycle power plants.* Dionex Corp., Sunnyvale, California. Application note **56**, 4 pp.

Dromgoole, E.L. and Walter, L.M. (1990). Iron and manganese incorporation into calcite: Effects

of growth kinetics, temperature and solution chemistry. *Chem. Geol.*, **81**, 311-336.

Duncan, A.R., Erlank, A.J. and Betton, P.J. (1984). Analytical techniques and database descriptions. *Spec. Publ. Geol. Soc. S. Afr.*, **13**, 389-395.

Eglington, B. (1992). Results of Pb isotope analysis of three samples from Gold Fields Namibia-Khusib Prospect. *Earth, Marine and Atmospheric Science and Technology*. CSIR, 6 pp.

Emslie, D.P. and Beukes, G.J. (1981). Minor- and trace-element distribution in sphalerite and galena from the Otavi Mountain Land, South West Africa. *Ann. geol. Surv. S. Afr.*, **15**, 11-28.

Fernandes, J.A.D., Tommasi, A. and Porcher, C.C. (1992). Deformation patterns in the southern Brazilian branch of the Dom Feliciano Belt, a reappraisal. *J. S. Amer. Earth Sci.*, **5**, 77-96.

Fontboté, L. and Gorzawski, H. (1990). Genesis of the Mississippi Valley-Type Zn-Pb deposit of San Vicente, Central Peru: Geologic and Isotopic (Sr, O, C, S, Pb) evidence. *Econ. Geol.*, **85**, 1402-1437.

Fontes, J. Ch. and Matray, J.M. (1993a). Geochemistry and origin of formation brines from the Paris Basin, France. 1. Brines associated with Triassic salts. *Chem. Geol.*, **109**, 149-175.

Fontes, J. Ch. and Matray, J.M. (1993b). Geochemistry and origin of formation brines from the Paris Basin, France. 2. Saline solutions associated with oil fields. *Chem. Geol.*, **109**, 177-200.

Friedman, I. and O'Neil, J.R. (1977). Compilation of stable isotope fractionation factors of geochemical interest. *In*: Fleischer, M. (Ed.), *Data of Geochemistry. Geological Survey Professional Paper* 440-KK, KK1-KK12.

Frimmel, H.E. (1992). Isotopic fronts in hydrothermally mineralised carbonate rocks. *Mineralium Deposita*, **27**, 257-267

Frimmel, H.E., Klötzli, U.S. and Siegfried, P.R. (1996). New Pb-Pb single zircon age constraints on the timing of Neoproterozoic glaciation and continental break-up in Namibia. *J. Geol.*, **104**, 459-469.

Frimmel, H.E., Deane, J.G. and Chadwick, P.J. (1997). Pan African Tectonism and the Genesis of Base Metal Sulphide Deposits in the Northern Foreland of the Damara Orogen, Namibia. *In*: Sangster, D.F. (Ed.), *Carbonate Hosted Lead-Zinc Deposits*. SEG Spec. Publ. No. **4**, 204-217.

Frimmel, H.E. and Frank, W. (1998). Neoproterozoic tectono-thermal evolution of the Gariep Belt and its basement, Namibia and South Africa. *Precamb. Res.*, in press.

Fritz, P. (1969). The oxygen and carbon isotopic composition of carbonates from the Pine Point

lead-zinc ore deposits. *Econ Geol.*, **64**, 733-742.

Goldberg, E.D., Koide, M., Schmitt, R.A. and Smith, R.H. (1963). Rare-earth distributions in the marine environment . *J. Geophys. Res.*, **68**, 4209-4217.

Graf, J.L. (1984). Effects of Mississippi Valley-Type mineralisation on REE patterns of carbonate rocks and minerals, Viburnum Trend, Southeast Missouri. *J. Geol.*, **92**, 307-324.

Grant, D.A. (1995). The shape of the Tsumeb ore body, Namibia, in relation to its structural setting and local strain markers. *In*: Barton, J.M. Jr. and Copperthwaite, Y.E. (Eds.), *Centennial Geocongress 1995. Extended Abstracts,* Vol 1 Rand Afrikaans University, Johannesburg, p. 68.

Grobler, N.J. (1961). *The geology of the Western Otavi Mountain Land, S.W.A.* Unpubl. MSc thesis, University of the Orange Free State, Bloemfontein, 119 pp.

Hannah, J.L. and Stein, H. (1984). Evidence for changing ore fluid composition: stable isotope analysis of secondary carbonates, Bonneterre Formation, Missouri. *Econ. Geol.*, **79**, 1930-1935.

Hanor, J.S. (1994). Origin of saline fluids in sedimentary basins. *In*: Parnell, J. (Ed.), *Geofluids: Origin, migration and evolution of fluids in sedimentary basins*. Geological Society Spec. Publ. No. **78**, 151-174.

Hanor, J.S. (1995). Controls on the solubility of lead and zinc in basinal brines: field evidence. *In*: Leach, D.L. and Goldhaber, M.B. (Eds.), *Extended Abstracts, International Field Conference on Carbonate-hosted Lead-Zinc Deposits*. Soc. Econ. Geol., St. Louis, 121-123.

Hanor, J.S. (1997). Sedimentary conditions for generating ore-forming fluids. *In*: Hendry, J., Carey, P., Parnell, J., Ruffell, A. and Warden, R. (Eds.), *Geofluids II '97: Extended abstracts*. Queens University of Belfast, Ireland, 154-157.

Hardie, L.A. (1987). Dolomitization: A critical view of some current views. *J. Sed. Petrol.*, **57**, 166-183.

Hartnady, C., Joubert, P. and Stowe, C. (1985). Proterozoic crustal evolution in southwestern Africa. *Episodes*, **8**, 236-244.

Haynes, F.M. (1984). A geochemical model for sulfide paragenesis and zoning in the Cu-Fe-As-S system (Tsumeb, South West Africa/Namibia). *Chem. Geol.*, **47**, 183-90.

Hedberg, R.M. (1979). Stratigraphy of the Owamboland Basin, South West Africa. *Bull. Precamb. Res. Unit,* **24**, University of Cape Town, 325 pp.

Hemming, N.G., Meyers, W.J. and Grams, J.C. (1989). Cathodoluminescence in diagenetic calcites: The role of Fe and Mn as deduced from electron probe and spectrophotometric measurements. *J. Sed. Petrol.*, **59**, 404-411.

Henry, G., Stanistreet, I.G. and Maiden, K.J. (1986). Preliminary results of a sedimentological study of the Chuos Formation in the Central Zone of the Damara Orogen: Evidence for mass flow processes and glacial activity. *Communs. geol. Surv. S.W. Africa/Namibia*, **2**, 75-92.

Herrmann, A.G. (1980). Bromide distribution between halite and NaCl-saturated seawater. *Chem. Geol.*, **28**, 171-177.

Hoffman, P.F., Hawkins, D.P., Isachsen, C.E. and Bowring, S.A. (1996). Precise U-Pb zircon ages for early Damaran magmatism in the Summas Mountains and Welwitschia Inlier, northern Damara Belt, Namibia. *Communs geol. Surv. Namibia*, **11**, 47-52.

Hoffmann, K.H. (1989). New aspects of lithostratigraphic subdivision and correlation of late Proterozoic to early Cambrian rocks of the southern Damara Belt and their correlation with the central and northern Damara Belt and the Gariep Belt. *Communs. geol. Surv. Namibia*, **5**, 58-67.

Hoffmann, K.H. (1990). Sedimentary depositional history of the Damara Belt related to continental breakup, passive margin to active margin transition and foreland basin development. *Ext. Abstrs. Gecongress 90*. Geol. Soc. S. Afr. Cape Town, 250-253.

Hoffmann, K.H. and Prave, A.R. (1996). A preliminary note on a revised subdivision and regional correlation of the Otavi Group based on glaciogenic diamictites and associated cap dolostones. *Communs. geol. Surv. Namibia*, **11**, 77-82.

Holmes, A. and Cahen, L. (1957). Géochronologie Africaine 1956. *Mèm. Acad. R. Belg. Cl. Sci.*, **5**, 169 pp.

Holser, W.T. (1979). Mineralogy of evaporites. *In*: Burns, R.G. (Ed.), Marine Minerals, *Reviews in Mineralogy*, Vol. **6**, Mineralogical Society of America, Michigan, 211-294.

Horita, J., Friedman, T.J., Lazar, B. and Holland, H.D. (1991). The composition of Permian seawater. *Geochim. Cosmochim. Acta*, **55**, 417-432.

Hudson, J.D. (1977). Stable isotopes and limestone lithification. *J. Geol. Soc. Lond.*, **133**, 637-660.

Hughes, M.J. (1987). *The Tsumeb ore body, Namibia, and related dolostone-hosted base metal ore deposits of Central Africa*. Unpubl. DSc thesis, University of the Witwatersrand, Johannesburg, 448 pp.

Hughes, M.J., Welke H.J. and Allsopp, H.L. (1984). Lead isotopic studies of some Late

Proterozoic stratabound ores of central Africa. *Precamb. Res.*, **25**, 137-139.

Ichikuni (1973). Partitioning of Sr between calcite and solution. Effect of Mn substitution. *Chem. Geol.*, **11**, 315-319.

Innes, J. and Chaplin, R.C. (1986). Ore bodies of the Kombat Mine, South West Africa/Namibia, *In*: Anhaeusser, C.R. and Maske, S. (Eds.), *Mineral Deposits of Southern Africa, vol II.* Geol. Soc. S. Afr., Johannesburg, 1789-1806.

ISODAT operating manual, Issue: (4/93 REV.A) 8-5—8-12. Finnigan MAT.

Jacobson, R.L. and Udowski, H.E. (1976). Sr partitioning between calcite, dolomite and liquid. *Contrib. Mineral. Petrol.*, **59**, 171-185.

Kaufman, A.J., Hayes, J.M., Knoll, A.H. and Germs, G.B. (1991). Isotopic compositions of carbonates and organic carbon from upper Proterozoic successions in Namibia: stratigraphic variation and effects of diagenesis and metamorphism. *Precamb. Res.*, **49**, 301-327.

Kesler, S.E., Appold, M.S., Martini, A.M., Walter, L.M., Huston, T.J. and Kyle, J.R. (1995). Na-Cl-Br systematics of mineralising brines in Mississippi Valley-type deposits. *Geology*, **23**, 641-644.

Kesler, S.E., Martini, A.M., Appold, M.S., Walter, L.M., Huston, T.J. and Furman, F.C. (1996). Sodium-chlorine-bromine systematics of fluid inclusions from Mississippi Valley-type deposits, Appalachian Basin: Constraints on solute origin and migration paths, *Geochim. Cosmochim. Acta*, **60**, 225-233.

King, C.H.M. (1990). *The geology of the Tsumeb carbonate sequence and associated lead-zinc occurrences on the farm Olifantsfontein, Otavi Mountain Land, Namibia.* Unpubl. MSc thesis, Rand Afrikaans University, Johannesburg, 219 pp.

King, C.H.M. (1994*). Progress report on the Khusib Springs Cu-Pb-Zn-Ag prospect on the farm Khusib 8, Olifantsfontein Grant M46/3/1415, Otavi Mountainland, Namibia*. Unpubl. report, Goldfields Namibia. 22 pp.

King, C.H.M. (1995). *Motivation for diamond drilling to test mineral extensions and potential target zones at the Khusib Springs Cu-Pb-Zn-Ag deposit, Olifantsfontein Grant, Otavi Mountainland, Namibia*. Unpubl. report, Goldfields Namibia. 22 pp.

Krauskopf, K.B. and Bird, D.K. (1995). *Introduction to Geochemistry.* 3rd Edition. McGraw-Hill, Inc. New York, 647 pp.

Kröner, A. and Rankama, K. (1972). Late Precambrian glaciogenic sedimentary rocks in southern Africa: A compilation with definitions and correlations. *Bull. Precamb. Res. Unit*, **11**, University of Cape Town, 37 pp.

Land, L.S. (1983). The application of stable isotopes to studies of the origin of dolomite and to problems of diagenesis of clastic sediments. *In*: Arthur, M.A., Anderson, T.F., Kaplan, I.R., Veizer, J. and Land, L.S. (Eds.), *Stable isotopes in Sedimentology.* SEPM Short course no. **10**, Dallas, 4-1– 4-22.

Land, L.S. (1987). The major ion chemistry of saline brines in sedimentary basins. *In*: Banavar, J.R., Koplik, J. and Winkler, K.W. (Eds.), *AIP Conference proceedings, 154, Physics and chemistry of porous media II.* American Institute of Physics, Ridgefield, CT 160-179.

Land, L.S. (1992). Saline formation waters in sedimentary basins: Connate or diagenetic? *In*: Kharaka, Y.K. and Maest, A.S. (Eds.), *Water-Rock Interaction.* Balkema, Rotterdam. 865-868.

Lee, J.H. and Byrne, R.H. (1992). Examination of comparative REE complexation behaviour using free energy relationships. *Geochim. Cosmochim. Acta*, **56**, 1127-1137.

Lee, J.H. and Byrne, R.H. (1993). Complexation of trivalent REE by carbonate ions. *Geochim. Cosmochim. Acta*, **57**, 295-302.

le Roex, A.P. and Watkins, R.T. (1990). Analysis of rare-earth elements in geological samples by gradient ion chromatography: An alternative to ICP and INAA. *Chem. Geol.*, **88**, 151-162.

Lombaard, A.F., Gunzel, A., Innes, J. and Kruger, T.L. (1986). The Tsumeb Lead-Copper-Zinc-Silver Deposit, South West Africa/Namibia, *In*: Anhaeusser, C.R. and Maske, S. (Eds.), *Mineral Deposits of Southern Africa, vol II*, Geol. Soc. S. Afr., Johannesburg, 1761-1788.

Lorens, R.B.(1981). Sr, Cd, Mn and Co distribution coefficients in calcite as a function of calcite precipitation rate. *Geochim. Cosmochim. Acta*, **45**, 53-561.

Lottermoser, B.G. (1992). Rare earth elements and hydrothermal ore formation processes. *Ore Geol. Rev.* **7**, 25-41.

Lowenstein, T.M. (1987). Evaporite depositional fabrics in the deeply buried Jurassic Buckner Formation, Alabama. *J. Sedim. Petrol.*, **5**, 108-116.

Martin, H. (1965). *The Precambrian geology of South West Africa and Namaqualand.* Precamb. Res. Unit, University of Cape Town, Cape Town, 159 pp.

Martin, H., Porada, H. and Wallister, O.H. (1985). Mixtite deposits of the Damara Sequence, Namibia, problems of interpretation. *Palaeogr., Palaeclimatol., Palaeo-ecol.*, **51**, 159-196.

McCaffrey, M.A., Lazar, B. and Holland, H.D. (1987). The evaporation path of seawater and the coprecipitation of Br^- and K^+ with halite. *J. Sed. Petrol.*, **57**, 928-937.

McCrea, J.M. (1950). On the isotopic chemistry of carbonates and a paleotemperature scale. *J. Chem. Phys.*, **18**, 849-857.

McLennan, S.M., (1989). Rare earth elements in sedimentary rocks: influence of provenance and sedimentary processes. *In:* Reeder, R.J. (Ed.), Carbonates: Mineralogy and Chemistry, *Reviews in Mineralogy*, Vol. **11**, Mineralogical Society of America, Michigan, 169-200.

Meert, J.G. and van de Voo, R. (1994). The Neoproterozoic (1000-540 Ma) glacial intervals: no more snowball earth? *Earth Planet. Sci. Lett.*, **123**, 1-13.

Miller, R. McG. (1983). The Pan-African Damara Orogen of South West Africa/Namibia *In:* Miller, R. McG. (Ed.), *Evolution of the Damara Orogen of South West Africa/Namibia.* Spec. Publ. No. **11**, Geol. Soc. S. Afr., Johannesburg, 431-515.

Misiewicz, J.E. (1988). *The geology and metallogeny of the Otavi Mountain Land, Damara Orogen, SWA/Namibia, with particular reference to the Berg Aukas Zn-Pb-V deposit- a model of ore genesis*. Unpubl. MSc thesis, Rhodes University, Grahamstown, 143 pp.

Möller, P. (1991). REE fractionation in hydrothermal fluorite and calcite. *In:* Pagel, M. and Leroy, J.L. (Eds.), *Source, transport and deposition of metals.* Balkema, Rotterdam, 91-94.

Möller, P., Morteani, G., Hoefs, J. and Parekh, P.O. (1979). The origin of the ore-bearing solution in the Pb-Zn veins of the western Harz, Germany, as deduced from rare-earth element and isotope distributions in calcites. *Chem. Geol.*, **26**, 197-215.

Möller, P. and Morteani, G. (1983). On the geochemical fractionation of rare earth elements during the formation of Ca-minerals and its application to problems of the genesis of ore deposits. *In:* Augustithis, S.S. (Ed.), *The significance of trace elements in solving petrogenetic problems and controversies.* Thephrastus, Athens, 747-791.

Morgan, P.J. (1994). *Khusib Springs Prospect, Preliminary Metallurgical Test work From Drill Core.* Unpubl. TCL report, 21 pp.

Morse, J.W. (1983). The kinetics of calcium carbonate dissolution and precipitation. *In:* Reeder, R.J. (Ed.), Carbonates: Mineralogy and chemistry, *Reviews in Mineralogy*, Vol. **11**, Mineralogical Society of America, Michigan, 227-264.

Musgrove, M., and Banner, J.L. (1993). Regional ground-water mixing and the origin of saline fluids: Midcontinent , United States. *Science*, **259**, 1877-1882.

Nesse, W.D. (1991). *Introduction to Optical Mineralogy.* 2nd Edn. Oxford University Press, New York, 335 pp.

Northrop, D.A. and Clayton, R.N. (1966). Oxygen-isotope fractionations in systems containing dolomite. *J. Geol.*, **54**, 174-196.

Ohmoto, H. (1972). Systematics of Sulfur and Carbon isotopes in Hydrothermal Ore Deposits. *Econ. Geol.*, **67**, 551-578.

Ohmoto, H. (1986). Stable isotope geochemistry of ore deposits. *In:* Valley, J.W., Taylor, H.P.J. and O'Neil, J.R. (Eds.), Stable isotopes in high temperature geological processes. *Reviews in Mineralogy*, Vol. **16**, 491-560.

Ohmoto, H. and Rye, R.O. (1979). Isotopes of Sulfur and Carbon. *In:* Barnes, H.L. (Ed.), *Geochemistry of hydrothermal ore deposits.* 2nd Edition, Wiley, New York, 509-567.

Palmer, M.R. (1985) Rare earth elements in foraminifera tests. *Earth Planet. Sci. Lett.*, **73**, 285-298.

Phillips, G.N., Williams, P.J. and de Jong, G. (1994). The nature of metamorphic fluids and significance for metal exploration. *In:* Parnell, J. (Ed) *Geofluids: Origin, Migration and Evolution of Fluids in Sedimentary Basins.* Geological Society Spec. Publ. No. **78**, 55-68.

Pierson, B.J. (1981). The control of cathodoluminescence in dolomite by iron and manganese. *Sedimentology*, **28**, 601-610.

Pirajno, F. (1992). *Hydrothermal Mineral deposits: Principles and Fundamental Concepts for the Exploration Geologist*, Springer Verlag, Berlin, 709 pp.

Pirajno, F. and Joubert, B.D. (1993). An overview of carbonate-hosted mineral deposits in the Otavi Mountain Land, Namibia: implications for ore genesis. *J. Afr. Earth Sci.*, **16**, 265-272.

Porada, H. (1989). Pan-African rifting and orogenesis in southern to equatorial Africa and eastern Brazil. *Precamb. Res.*, **44**, 103-136.

Pourbaix, M. (1966). *Atlas of electrochemical equilibria in aqueous solutions (Atlas d'equilibres electrochemiques).* Translated by J.A. Franklin. Oxford, Pergamon Press. New York, 644 pp.

Prave, A.R. (1996). Tale of three cratons: Tectonostratigraphic anatomy of the Damara orogen in northwestern Namibia and the assembly of Gondwana. *Geology*, **24**, 1115-1118.

Prinsloo, M. (1995). *Report on Percussion drilling done at Khusib Springs Prospect, Olifantsfontein Grant (M46/3/1415), Otavi Mountain Land, Namibia.* Unpubl. GFNL report, 7 pp.

Prochaska, W. (1997). Formation of different siderite provinces during the Alpine tectno-metamorphic event in the Eastern Alps of Austria. *In:* Papunen, H. (Ed.), *Mineral Deposits: Research and Exploration— Where do they meet?* Proceedings of the Fourth Biennial SGA Meeting, Turku, Finland, Balkema, Rotterdam, 845-848.

Ridley, M.K. (1992). *Gradient ion chromatographic determination of rare earth elements in coal and fly ash.* Unpubl. MSc thesis, University of Cape Town, Cape Town, 115 pp.

Rittenhouse, G. (1967). Bromine in oil-field waters and its use in determining possibilities of origin of these waters. *Amer. Assoc. Petrol. Geol. Bull.*, **51**, 2430-2440.

Roedder, E. (1984) Fluid Inclusions. *Reviews in Mineralogy*, Vol. **12**, Mineralogical Society of America. Michigan, 644 pp.

Roesener, H. (1991). *The Geology and Recommendations of the Khusib Springs Prospect, Khusib 8, Olifantsfontein Grant M46/3/1415.* Unpubl. GFNL report, 12 pp.

Rosenbaum, J. and Sheppard, S.M. (1986). An isotopic study of siderites, dolomites and ankerites at high temperatures. *Geochim. Cosmochim. Acta*, **50**, 1147-1150.

Ruaya, and Seward, (1986). The stability of chlorozinc (II) complexes in hydrothermal solutions up to 350°C: *Geochim. Cosmochim. Acta*, **50**, 651-662.

Schermerhorn, L.J.G. (1975) Tectonic framework of Late-Precambrian supposed glacials. *In:* Wright, A.E. and Mosely, F. (Eds.), *Ice ages, ancient and modern. Spec. Issue Geol. J.*, **6**. 241-274.

Schoell, M. (1984). Stable isotopes in petroleum research. *In:* Brooks, I.J. and Welte, D. (Eds.), *Advances in petroleum geochemistry.* Vol. **1**. Academic Press, London. 215-243.

Sears, S.O. and Lucia, F.J. (1980). Dolomitisation of northern Michigan Niagara reefs by brine refluxion and freshwater/seawater mixing. *In:* Zenger, D.H., Dunham, J.B. and Ethington, R.L. (Eds) *Concepts and models of dolomitisation.* SEPM Spec. Publ. **28**, Tulsa, 215-235.

Shannon, R.D. (1976). Revised effective ionic radii and systematic studies of interatomic distance in halides and chalcogenides. *Acta. Cryst.*, **A32**, 751-767.

Shepherd, T., Rankin, A.H. and Alderton, D.H.M. (1985). *A Practical Guide to Fluid Inclusion Studies.* Blackie, Chapman and Hall, New York. 239 pp.

Simpson, W. (1957). Unpubl. report. Tsumeb Corporation Ltd.

Söhnge, P.G. (1957). Revision of geology of the Otavi Mountain Land, South West Africa Unpubl. report., Tsumeb Corporation Ltd., Tsumeb, 116 pp.

Söhnge, P.G. (1964). The geology of the Tsumeb Mine. *In:* Haughton, S.H. (Ed.), *The Geology of Some Ore Deposits in Southern Africa.* Vol **II**, Geol. Soc. S. Afr., 367-382.

Sommers, S.E. (1972). Cathodoluminescence of carbonates. 1. Characterisation of cathodoluminescence from carbonate solid solutions. *Chem. Geol.*, **9**, 257-273.

South African Committee for Stratigraphy (SACS) (1980). Stratigraphy of South Africa, Part 1 (Comp. L.E. Kent) Lithostratigraphy of the Republic of South Africa, South West Africa/Namibia and the Republics of Bophuthatswana, Transkei and Venda. *Handbk. Geol. Surv. S. Afr.*, 8, 690 pp.

Spangenberg, J.E. (1995). *Geochemical (elemental and isotopic) constraints on the genesis of the Mississippi Valley-type zinc-lead deposits of San Vicente, central Peru*, Unpubl. PhD thesis, Université de Genève, Geneva, 123 pp.

Spangenberg, J.E., Fontboté, L. Sharp, Z.D. and Hunziker, J. (1996). Carbon and oxygen isotope study of hydrothermal carboantes in the zinc-lead deposits of the San Vicente district, central Peru: a quantitative modeling on mixing processes and CO_2 degassing. *Chem. Geol.*, **133**, 289-315.

Stanistreet, I.G., Kukla, P.A. and Henry, G. (1991). Sedimentary basinal response to a Late Precambrian Wilson Cycle: the Damara orogen and Nama Foreland, Namibia. *J. Afr. Earth Sci.*, **13**, 141-156.

Sun, S.-S and McDonough, W.F. (1989). Chemical and isotopic systematics of oceanic basalts: implications for mantle composition and processes. *In:* Saunders, A.D. and Norry, M.J. (Eds.), *Magmatism in the ocean basins.* Geol. Soc. Spec. Publ. No. **42**, 313-345.

Sverjensky, D.A. (1981). Isotopic alteration of carbonate host rocks as a function of water to rock ratio-an example from the Upper Mississippi Valley Zinc-Lead District. *Econ. Geol.*, **76**, 154-172.

Sverjensky, D.A. (1984). Europium redox equilibrium in aqueous solutions. *Earth Planet. Sci. Lett.* **67**, 70-78.

Taylor, H.P. (1974). The application of oxygen and hydrogen isotope studies to problems of hydrothermal alteration and ore deposition. *Econ. Geol.*, **69**, 843-883.

Ten Have, T. and Heijnen, W. (1985). Cathodoluminescence activation and zonation in carbonate rocks: An experimental approach. *Geologie en Mijnbouw*, **64**, 297-310.

Theron, S. J. (1994). *The North Break Zone of the late Precambrian Otavi carbonate platform sequence in Namibia: stratigraphic setting, petrography and relationship with Tsumeb Cu-Pb-Zn deposit.* Unpubl. MSc thesis, Rand Afrikaans University, Johannesburg, 165 pp.

Theron, S. and Beukes, N. (1992). *Progress report on the petrography of the North Break Zone and its relationship to the Tsumeb ore body and other mineralized occurrences in the Otavi carbonates, Namibia.* Unpubl. report, Department of Geology, Rand Afrikaans University, Auckland Park, Johannesburg, 36 pp.

Theron, S. and Beukes, N. (1993). *Progress report on trace elements, carbon and oxygen*

isotopic composition of the different carbonate phases in the Tsumeb area, Otavi Mountain Land, Namibia. Unpubl. GFNL report, Rand Afrikaans University, Johannesburg, 32 pp.

Theron, S.J. and Beukes, N.J. (1995). Carbonate petrography and the origin of Neoproterozoic Tsumeb-type Cu-Pb-Zn mineralisation in the Otavi Mountain Land, Namibia. *In:* Barton, J.M. Jr. and Copperthwaite, Y.E. (Eds.), *Centennial Geocongress, Extended Abstracts.* Rand Afrikaans University, Johannesburg, 115-117.

Tritlla, J. and Cardellach, E. (1997). Fluid inclusions in pre-ore minerals from the carbonate-hosted mercury deposits in the Espadán Ranges (eastern Spain). *Chem. Geol.*, **137**, 91-106.

Vahrenkamp, V.C. and Swart, P.K. (1990). New distribution coefficient for the incorporation of strontium into dolomite and its implications for the formation of ancient dolomites. *Geology*, **18**, 387-391.

Veizer, J. (1983a) Trace elements and isotopes in sedimentary carbonates. *In:* Reeder, R.J. (Ed.), Carbonates: Mineralogy and Chemistry, *Reviews in Mineralogy*, Vol. **11**, Mineralogical Society of America, Michigan, 265-299.

Veizer, J. (1983b). Chemical diagenesis of carbonates: Theory and application of trace element technique. *In:* Arthur, M.A., Anderson, T.F., Kaplan, I.R., Veizer, J. and Land, L.S. (Eds.), *Stable Isotopes in Sedimentary Geology.* SEPM Short Course No. **10**, Dallas, 3-1–3-100.

Verran, D. (1996). *Genesis of the Khusib Springs Cu-Pb-Zn-(Ag) Deposit, Otavi Mountain land, Namibia.* Unpubl. Hons. thesis, Department of Geological Sciences, University of Cape Town, Cape Town, 36 pp.

Viets, J.G. (1995). A comparative study of the composition of MVT ore fluids: Solute compositions of inclusions fluids in North American and European MVT deposits, *In:* Leach, D.L. and Goldhaber, M.B. (Eds.), *Extended Abstracts: International Field Conference on Carbonate Hosted Lead-Zinc Deposits.* Soc. Econ. Geol., St. Louis, 328-330.

Walter, L. M., Stueber, A.M. and Huston, T.J. (1990). Br-Cl-Na systematics in Illinois basin fluids: Constraints on fluid origin and evolution. *Geology*, **18**, 315-318.

Weber, K., Arendt, H. and Hunziker, J.C. (1983). Geodynamic aspects of structural and radiometric investigations on the northern and southern margins of the Damara Orogen. *In:* Miller, R. McG. (Ed) *Evolution of the Damara Orogen of South West Africa/Namibia.* Spec. Publ. No. **11**, Geol. Soc. S. Afr., 307-320.

Yardley, B.W.D. (1989). *An Introduction to Metamorphic Petrology.* Longman Earth Science Series, Longman, New York. 248 pp.

Young, G.M. (1995). Are Neoproterozoic glacial deposits preserved on the margins of Laurentia related to the fragmentation of two supercontinents? *Geology*, **23**, 153-156.

Ypma, P.J.M. (1978). Fluid inclusions and ore genesis in the Otavi Mountains, South West Africa. Part 1: Geothermometry and barometry. Unpubl. report, TCL, Tsumeb, Namibia.

Ypma, P.J.M. (1984). Fluid inclusions and ore genesis in the Otavi Mountains, South West Africa. Part 1: Geothermometry and barometry. Unpubl. report, Department of Economic Geology, University of Adelaide, Australia, 84 pp.

Zenger, D.H. (1972). Dolomitisation and uniformitarianism. *J. Geol. Education*, **20**, 107-124.

Zenger, D.H., Dunham, J.B. and Ethington, R.L. (1980). *Concepts and models of dolomitisation.* SEPM Spec. Publ. **28**, Tulsa, 320 pp.

Zhang, Y. and Frantz, J.D. (1987). Determination of the homogenisation temperatures and densities of supercritical fluids in the system NaCl-KCl-$CaCl_2$-H_2O using synthetic fluid inclusions. *Chem. Geol.*, **64**, 335-350.

APPENDICES

APPENDIX A1: SAMPLE DESCRIPTIONS AND LOCALITIES

SAMPLE	DEPOSIT	GENERATION	DESCRIPTION	LOCALITY
2965/300	Tsumeb	Dolomite I	medium grey dolomicrite, homogenous.	borehole core 2965, 44 Level
2965/289	Tsumeb	Dolomite I	medium grey dolomicrite, homogenous. Cross cut by quartz-dolomite vein	borehole core 2965, 44 Level
DCT4H	Tsumeb	Dolomite I	host dolomicrite as fragments in a breccia with sparry dolomite matrix.	48 Level, West Stope
2965/62	Tsumeb	Calcite I	calcitised dolomite, recrystallised. Calcite constitutes ~45 % of rock.	borehole core 2965, 44 Level
DCT10	Tsumeb	Dolomite II	coarsely recrystallised dolomite. Sparry dolomite and minor quartz crystallised into discrete patches defined in part by linings of hydrocarbons. Minor quartz and calcite is also present. Sulphide mineralisation is confined to the hydrocarbon portion.	10 Level
DCT4SV	Tsumeb	Dolomite III	Sparry dolomite, coarse grained, with associated quartz, forming the matrix to host dolomite fragments in breccia.	48 Level, West Stope
DCT5	Tsumeb	Dolomite III	Sparry dolomite, coarse grained, and associated quartz with tennantite and chalcocite mineralisation.	48 Level, West Stope
2965/106	Tsumeb	Dolomite III	Sparry dolomite, coarse grained. Bits of dolomite host present.	borehole core 2965, 44 Level
DCT1	Tsumeb	Quartz-Dolomite I	Very fine grained, silicified dolomicrite.	48 Level, East Stope
DCT2	Tsumeb	Quartz-Dolomite I	Silicified dolomite, with some sparry dolomite in places.	48 Level, East Access

SAMPLE	DEPOSIT	GENERATION	DESCRIPTION	LOCALITY
2944/225	Tsumeb	Quartz-Dolomite I	Milky dolomite with quartz veining. Bits of host dolomite present. Mineralisation oxidised, some chalcocite present.	borehole core 2944, 30 Level
2944/248	Tsumeb	Quartz-Dolomite I	Similar to 2944/225; Cu sulphide mineralisation, brown coloration due to oxidation.	borehole core 2944, 30 Level
3153/18	Tsumeb	Calcite II	Sparry calcite with associated quartz in places, contains tennantite and pyrite. Calcite occurs as a vein in dark grey siliceous dolomite, also mineralised with pyrite and tennantite.	borehole core 3153, 32 Level
3153/19	Tsumeb	Calcite II	Sparry calcite cross-cutting dark grey siliceous dolomite. Although not mineralised, is the same calcite as in 3153/18.	borehole core 3153, 32 Level
3153/28	Tsumeb	Calcite II	Sparry calcite with fine to coarsely crystalline quartz-calcite in places, pyrite and tennantite occur intergrown with the quartz and calcite in places. The calcite-quartz vein occurs in the same host as for 3153/18.	borehole core 3153, 32 Level
3153/35	Tsumeb	Calcite II	Sparry calcite vein.	borehole core 3153, 32 Level
3153/36	Tsumeb	Calcite II	Calcite-quartz vein, similar to 3153/19.	borehole core 3153, 32 Level
2944/210	Tsumeb	Calcite III	Late, cross-cutting calcite vein, Fe-oxide staining. Cross-cuts light grey dolomicrite.	borehole core 2944, 30 Level
2944/240	Tsumeb	Calcite III	Late stage, oxidised calcite vein. Some malachite present.	borehole core 2944, 30 Level
S67B-456.8-457	Tsumeb	Dol-gyp	White sparry dolomite with bits of light grey dolomicrite host; within the sparry dolomite are blebs of pink gypsum.	borehole core S67B, T7 zone

SAMPLE	DEPOSIT	GENERATION	DESCRIPTION	LOCALITY
KH91/181.5	Khusib Springs	Dolomite Ia	Light grey dolomicrite	borehole core KH91
KH91/382.9	Khusib Springs	Dolomite Ia	Light grey dolomicrite	borehole core KH91
KH91/220.2	Khusib Springs	Dolomite Ia	Light grey dolomicrite	borehole core KH91
DV30	Khusib Springs	Dolomite Ib	Dark grey to black dolomicrite; colouration due to carbonaceous content. Grades into coarsely recrystallised dolomite, and sparry dolomite hosting tennantite.	T3 zone; mine, underground
DV23	Khusib Springs	Limestone I	Dark grey limestone; colouration due to carbonaceous content.	T2 zone; mine, underground
DV7	Khusib Springs	Dolomite IIa	Sparry dolomite, greyish- to milky white; hosts sphalerite and galena.	mine, underground
DV10	Khusib Springs	Dolomite IIa	Sparry dolomite, greyish- to milky white; hosts sphalerite. Brecciated dark carbonaceous host dolomicrite fragments in the sparry dolomite matrix. Massive galena and sphalerite in darker portions. In the same area, is massive ore comprising pyrite, tennantite and galena.	mine, underground
DV16	Khusib Springs	Dolomite IIa	Sparry dolomite, greyish- to milky white; hosts sphalerite.	mine, underground
KH62/75.3	Khusib Springs	Dolomite IIa	Sparry dolomite, with intergrown quartz crystals.	borehole core KH62
DV26	Khusib Springs	Dolomite IIa	Sparry dolomite, with sphalerite	mine, underground
DV4	Khusib Springs	Dolomite IIb	Coarsely recrystallised dolomite, grading to sparry dolomite surrounded by carbonaceous material. In places, graphite seems to be present. Galena ore present.	mine, underground
DV 27	Khusib Springs	Dolomite IIb	Coarsely recrystallised dolomite, grading to sparry dolomite.	mine, underground

SAMPLE	DEPOSIT	GENERATION	DESCRIPTION	LOCALITY
KH91/382.9	Khusib Springs	Dolomite IIc	Sparry dolomite vein, with Fe oxide staining in places, along bedding plane in light grey dolomicrite.	borehole core KH91
KH91/293.1	Khusib Springs	Dolomite IIc	Sparry dolomite vein, with crystals of Fe-bearing dolomite, with Fe-oxide staining.	borehole core KH91
DV19	Khusib Springs	Dolomite III	Sparry dolomite, with azurite and malachite stains.	mine, surface
DV21	Khusib Springs	Dolomite III	As for DV19.	mine, surface
DV24	Khusib Springs	Calcite I	Late calcite veins cross-cutting dolomite veins. Associated with the calcite is quartz.	mine, underground
DCK1	Kombat	Dolomite I	Light coloured dolomite, fine-grained	E900 adit
AU 13/88 115.3	Kombat	Calcite I	Sparry pink calcite intergrown with Fe and Mn oxides.	borehole core AU 13/88; Asis West
AU 13/88 120.8	Kombat	Calcite I	As for AU 13/88 115.3	borehole core AU 13/88; Asis West
KSW-1A 1023.3	Kombat	Calcite IIa	Light blue-grey calcitised dolostone. Some disseminated chalcopyrite and bornite present.	borehole core KSW-1A, Asis West
KSW-1A 1037.4	Kombat	Calcite IIa	As for KSW-1A 1023.3.	borehole core KSW-1A, Asis West
KSW-1A 1037.95	Kombat	Calcite IIa	As for KSW-1A 1023.3, but lighter in colour. Hosts bornite, chalcopyrite, minor chalcocite and covellite.	borehole core KSW-1A, Asis West
AU15/13 38.2	Kombat	Calcite IIa	Calcitised dolostone, with patches of bornite and chalcopyrite.	borehole core AU15/13, Asis West

SAMPLE	DEPOSIT	GENERATION	DESCRIPTION	LOCALITY
DCK4	Kombat	Calcite IIb	Light coloured, coarsely crystallised calcitised dolostone.	E900 adit
DCK3	Kombat	Calcite IIc	Dark calcitised dolostone, with very finely disseminated bornite, chalcopyrite and galena. Intergrown with lighter coloured calcitisation.	E900 adit
AU17/83 247.4	Kombat	Calcite III	Blocky white calcite vein in dark algal dolomite	borehole core AU17/83, Asis West
AU17/83 255.5	Kombat	Calcite III	Blocky white calcite vein in dark algal dolomite	borehole core AU17/83, Asis West
Q1-4 (i)	Berg Aukas	Dolomite I	Light grey dolomicrite.	Berg Aukas
BAD14/12	Berg Aukas	Dolomite I	Light grey dolomicrite	borehole core BAD 14
Q1-4 (ii)	Berg Aukas	Dolomite II	Dolomite rhythmite.	Berg Aukas
Q1-4 (iii)	Berg Aukas	Dolomite III	Sparry dolomite replacing in part, the rhythmite.	Berg Aukas
BAD 7/4B	Berg Aukas	Dolomite III	Sparry dolomite.	borehole core BAD 7
HB-2	Berg Aukas	Dolomite III	dolomite breccia hosting sphalerite.	Berg Aukas
HFO-1	Berg Aukas	Dolomite III	Sparry dolomite hosting sphalerite.	Berg Aukas
CH1-b	Berg Aukas	Dolomite IV	Sparry dolomite as void filling.	Berg Aukas

Tsumeb, Kombat and Berg Aukas borehole core information

Core no.	Mine	Level	easting	northing	length (m)	Section	Dip (degrees)	Azimuth (degrees)	Elevation (m)
2965	Tsumeb	44	1796.7	1888.3	340	W90	flat	024	-190.6
3153	Tsumeb	32	1900.7	1899.3	38	-			265.7
2944	Tsumeb	30	1923.7	1876.0	263	W90	-5	204	344.8
S67B	Tsumeb environs	surface	-76.058	-305 113	631.3	~700 m E of pipe	-90		1317
AU 12/23	Asis West	12	-73 3 30.8	-253 575.5	128	W120	-26	180	1187.1
AU 13/88	Asis West	13	-73 316.2	-253 612.2	145.6	W135	-10	180	1141.3
AU 15/13	Asis West	15/1 sublevel	-73 345.7	-253 492.6	166	W105	-4	180	1081.0
AU 17/83	Asis West	17/1 sublevel	-73 150.52	-253 569.9	272	W300	-7	180	997.7
KSW-1A	Asis West		69 877.69	254 639.79	1079	W3645			608.37
BAD 7	Berg Aukas		77 868.2	274 031.9					
BAD 14	Berg Aukas		78 490.8	274 527.1					

Khusib Springs

Boreholes KH62 and KH91 are shown in cross section C-D, Appendix A1.1.
The underground layout is shown in Appendix A1.2.

APPENDIX A1.1 Cross section C-D from Figure 3.5a (after King, 1995; Verran, 1996).

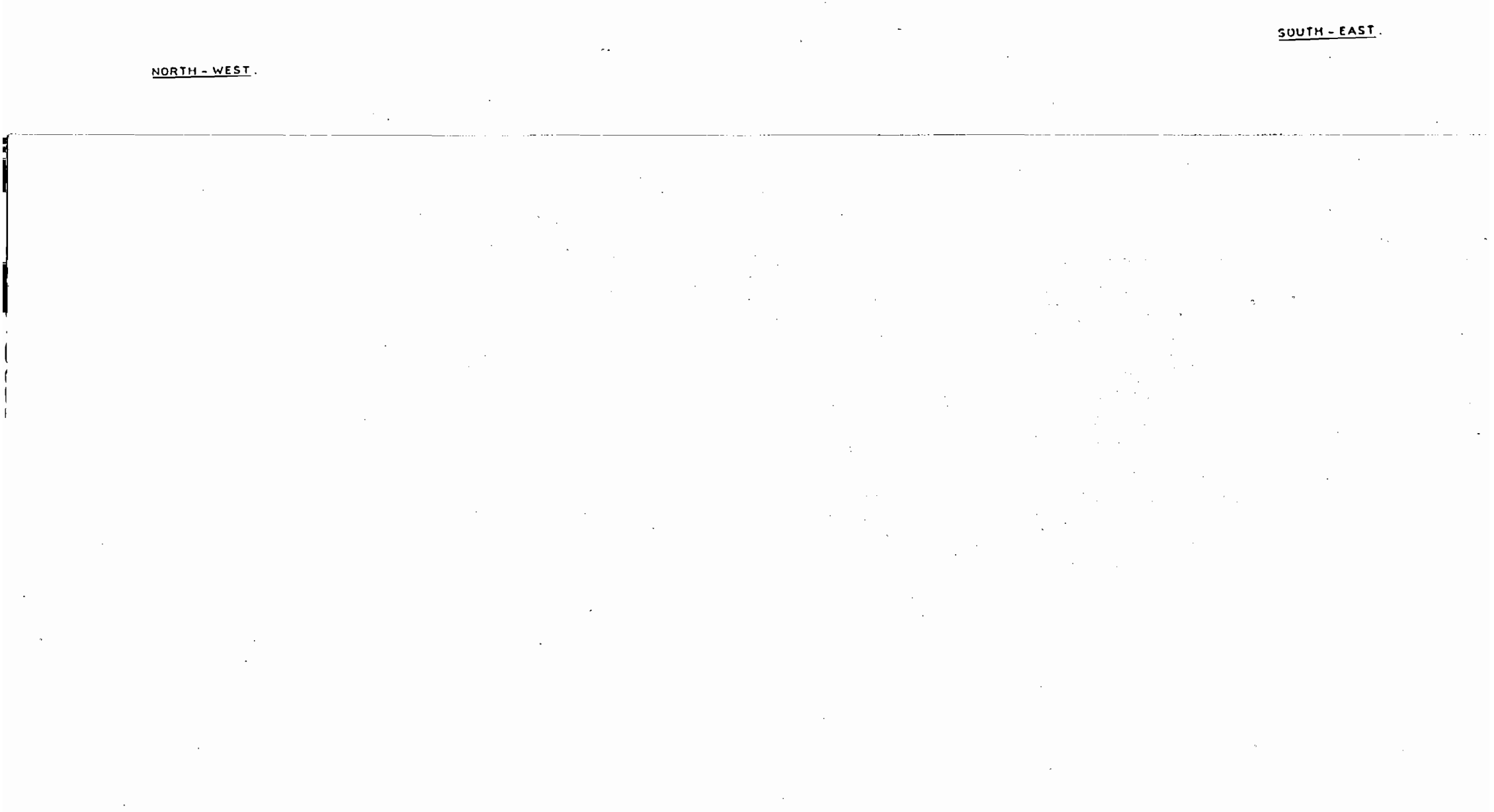

APPENDIX A1.2 Underground sampling map, Khusib Springs

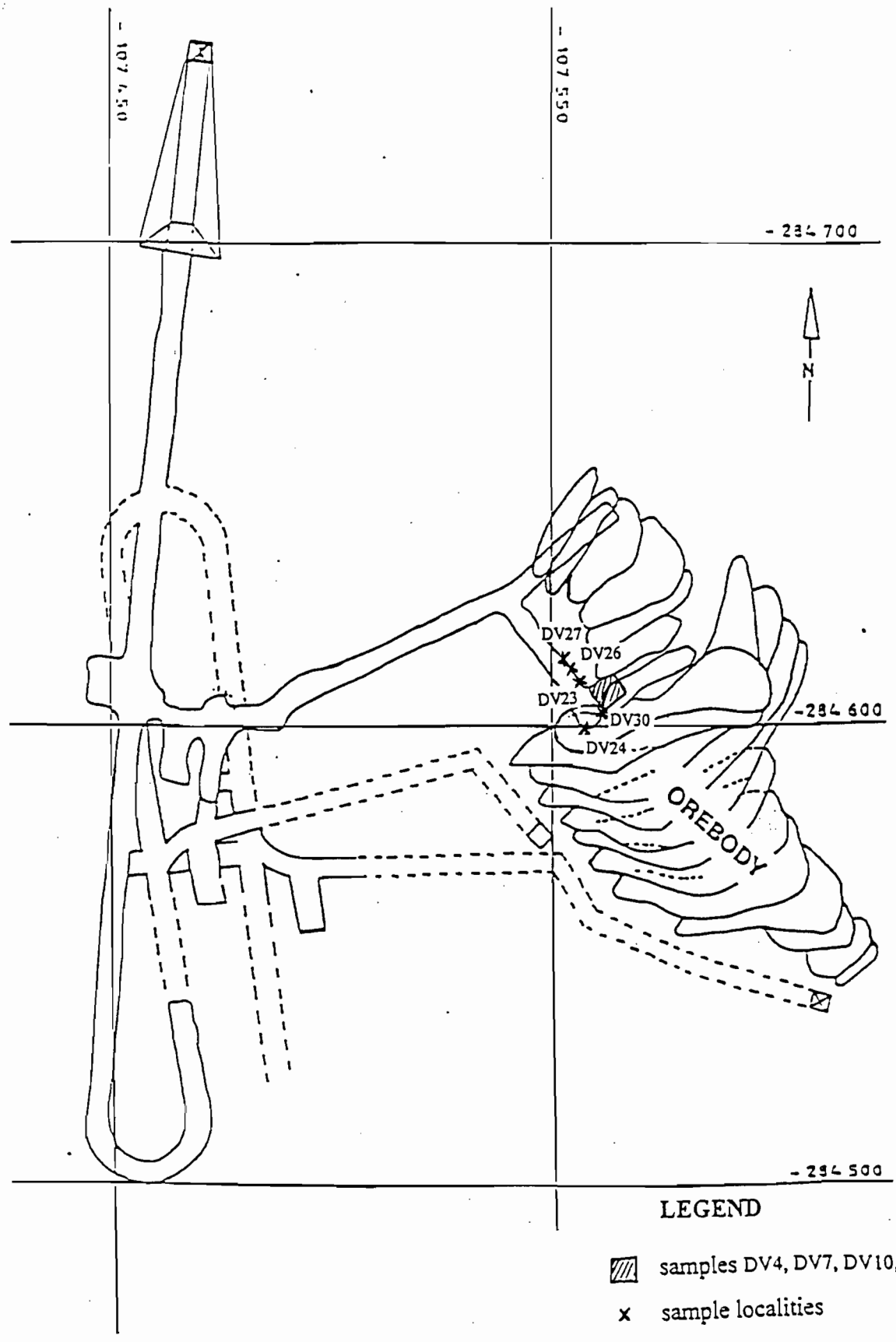

APPENDIX A2: ANALYTICAL TECHNIQUES AND DATA

A2.1 OPTICAL CATHODOLUMINESCENCE IMAGING

Cathodoluminescence imaging was carried out using a Technosyn cold cathodoluminescence model 8200 MkII, with a Wild Photomakroskop M400 photographic attachment at the Electron Microscope Unit, University of Cape Town. Images were obtained at voltages of 10-15 kV and currents of 100-250 μA at a prevailing vacuum of approximately 50 mtorr.

A2.2 ELECTRON PROBE MICRO ANALYSIS

Mineral compositions were determined at the Department of Geological Sciences, University of Cape Town. Polished thin sections were carbon-coated, ensuring a proper thickness was achieved, to minimise charging effects. The carbonate minerals were analysed using a Cameca Camebax Microprobe. Instrument settings were as follows:

Acceleration voltage:15 kV
Beam current: 12 nA (for carbonates)
Defocussed beam diameter of 15 μm
Counting time: 20 s (peak + background) for Ca, Mg, Fe, Si and Mn, 30 s for Sr
Analysing crystals: PET for Ca, LiF for Fe, Mn, TAP for Sr, Si and Mg
Standards used for calibration of the instrument for the elements under consideration were:

- Synthetic diopside (DIOP) for Ca, Si, Mg;
- Synthetic rhodonite (RHOD) for Mn;
- Synthetic Sr-Si glass (SRSI) for Sr;
- Natural Kakanui pyrope (K-P) for Fe

The LLD values for each element are given in Table A2.2.1

Table A 2.2.1 Standards, lower limits of detection (LLD) and counting statistics for analysed samples.

Element	Standard	LLD (wt %)	Conc. (wt %)	2σ error
Ca	DIOP	0.05	21.54	0.52
Mg	DIOP	0.06	12.64	0.38
Fe	K-P	0.12	0.20	0.08
Mn	RHOD	0.11	0.67	0.14
Si	DIOP	0.04	0.004	0.008
Sr	SRSI	0.10	0.05	0.04

$LLD\ (wt\%) = 6/m\ (R_b/T_t)^{½}$

where m = net peak count rate (c/s)/element concentration (wt%)

R_b = background count rate (c/s)

T_t = total counting time (s)

Mineral compositions are presented in Table A2.2.2.

Table A2.2.2 Carbonate mineral compositions (wt% carbonate) for various generations from Tsumeb, Khusib Springs and Kombat

Sample	Deposit	Generation	Grain no.	Ca	Mg	Fe	Mn	Total
2965/289	Tsumeb	Dol I	1	55.42	44.97			100.39
"	"	"	2	54.38	43.93	0.50	0.31	99.12
"	"	"	3	54.05	44.36			98.41
"	"	"	4	55.63	44.85	0.25		100.73
"	"	"	5	55.46	46.05			101.51
"	"	"	6	53.71	46.02			99.73
"	"	"	7	54.28	46.28			100.55
"	"	"	8	55.31	45.28			100.59
"	"	"	9	54.91	45.27			100.18
"	"	"	10	54.79	44.90			99.69
"	"	"	11	54.01	44.78			98.79
"	"	"	12	55.20	43.72			98.92
DCT4H	"	"	1	55.85	43.89			99.74
"	"	"	2	56.21	45.46			101.66
"	"	"	3	55.57	45.58		0.31	101.47
DCT10	"	Dol II	1	54.54	44.62			99.16
"	"	"	2	54.59	44.56			99.15
"	"	"	3	54.66	43.30			97.96
"	"	"	4	55.89	45.61			101.50
"	"	"	5	55.75	45.26			101.01
"	"	"	6	56.03	43.98			100.01
"	"	"	7	56.26	44.62			100.89
"	"	"	8	56.13	45.37			101.50
"	"	"	9	55.90	45.01		0.39	101.29
"	"	"	10	54.45	45.69		0.42	100.56
"	"	"	11	55.76	44.76			100.53
"	"	"	12	56.57	44.44			101.01
DCT4SV	"	Dol III	1	55.94	45.05		0.33	101.32
"	"	"	2	56.81	43.92		0.34	101.06
"	"	"	3	55.11	45.59		0.30	101.01
"	"	"	4	55.87	44.63		0.24	100.74
"	"	"	5	55.82	44.25			100.07
"	"	"	6	56.45	44.98			101.43
"	"	"	7	56.40	43.39		0.25	100.04
"	"	"	8	55.00	44.77		0.48	100.25
DCT5	"	"	1	55.19	44.67		0.44	100.29
"	"	"	2	54.46	45.30		0.27	100.04
"	"	"	3	53.94	44.55	0.32	0.47	99.29
"	"	"	4	55.42	44.84		0.29	100.55
"	"	"	5	55.11	45.35		0.34	100.80
"	"	"	6	56.74	43.44		0.38	100.56
"	"	"	7	55.71	45.30		0.30	101.32
"	"	"	8	55.11	45.62		0.25	100.99
"	"	"	9	54.18	44.44		0.53	99.15
"	"	"	10	55.37	45.41		0.29	101.07
"	"	"	11	55.03	45.09		0.38	100.49
"	"	"	12	54.86	44.41		0.27	99.54
"	"	"	13	55.84	45.31			101.16
"	"	"	14	54.68	45.60	0.25	0.33	100.85
2965/106	"	"	1	55.67	44.62	0.29	0.44	101.01
"	"	"	2	56.29	44.55	0.40	0.52	101.75
"	"	"	3	54.84	44.54	0.28	0.49	100.15
"	"	"	4	55.68	44.26	0.41	0.42	100.77
3153/28	"	Cal II	1	99.49	1.26			100.75
"	"	"	2	99.62	1.16			100.78
"	"	"	3	98.89	1.13			100.02
"	"	"	4	100.15	1.02			101.18

Table A2.2.2 cont.

Sample	Deposit	Generation	Grain no.	Ca	Mg	Fe	Mn	Total
3153/28	Tsumeb	Cal II	5	99.69	1.02			100.70
"	"	"	6	99.45	0.89			100.34
"	"	"	7	98.25	0.83			99.08
"	"	"	8	99.86	1.16			101.02
"	"	"	9	99.88	1.03			100.91
"	"	"	10	98.51	1.14			99.65
"	"	"	11	98.92	1.17			100.09
"	"	"	12	99.69	1.08			100.77
"	"	"	13	98.62	1.17			99.79
"	"	"	14	99.37	0.92			100.29
"	"	"	15	99.29	0.91			100.20
KH91/220.2	Khusib Springs	Dol I	1	54.51	44.43	0.36		99.29
"	"	"	2	54.99	44.62			99.61
"	"	"	3	54.49	44.66	0.25		99.40
"	"	"	4	53.73	45.67			99.40
"	"	"	5	54.02	44.50			98.51
DV7	"	Dol IIa	1	54.56	45.18		1.13	100.87
"	"	"	2	55.18	43.22		1.21	99.60
"	"	"	3	55.78	43.63		1.36	100.77
"	"	"	4	55.30	44.53		1.10	100.93
"	"	"	5	53.52	45.18		1.29	99.99
"	"	"	6	54.20	44.51		1.27	99.97
DV10	"	"	1	55.28	44.11		1.11	100.50
"	"	"	2	53.99	45.10		1.14	100.22
"	"	"	3	54.61	44.68		1.18	100.47
"	"	"	4	55.04	44.82		1.05	100.90
"	"	"	5	54.75	43.42		1.17	99.45
"	"	"	6	54.19	44.58		1.03	99.80
"	"	"	7	53.26	45.74		1.00	100.00
DV16	"	"	1	54.00	44.75		1.54	100.29
"	"	"	2	53.26	45.74		1.31	100.32
"	"	"	3	52.99	46.01		0.91	99.91
"	"	"	4	53.04	46.53		0.32	99.90
"	"	"	5	53.90	46.54		0.46	100.91
"	"	"	6	52.95	45.95		1.11	100.01
"	"	"	7	54.83	43.67		1.16	100.02
"	"	"	8	53.72	44.84		0.98	100.33
"	"	"	9	54.82	45.96		1.17	101.95
"	"	"	10	55.38	44.75		1.06	101.18
DV15	"	Dol IIb	1	55.88	44.16		1.13	101.16
"	"	"	2	55.87	44.64		1.04	101.54
"	"	"	3	56.35	43.34		0.78	100.47
"	"	"	4	55.07	44.74		1.31	101.12
"	"	"	5	55.61	44.67		1.41	101.69
"	"	"	6	55.50	45.10		1.13	101.72
"	"	"	7	55.62	44.32		1.54	101.48
"	"	"	8	55.64	44.17		1.19	101.01
KH91/293.1	"	Dol IIc	1	53.96	43.07		1.26	98.47
"	"	"	2	53.75	44.40		0.67	98.81
"	"	"	3	53.56	44.12		0.51	98.33
"	"	"	4	54.64	43.21		0.28	98.32
"	"	"	5	55.38	42.19		0.94	98.51
"	"	Fe rich grain	1 centre	54.31	39.22	5.08	0.44	99.05
"	"	"	1 centre	53.24	39.51	4.69	0.47	97.92
"	"	"	2 centre	53.83	40.73	3.54	0.21	98.30
"	"	"	2 rim	96.35	2.47			98.99
"	"	"	2 rim	95.60	2.81			98.62

Table A2.2.2 cont.

Sample	Deposit	Generation	Grain no.	Ca	Mg	Fe	Mn	Total
KH91/293.1	Khusib Springs	Fe-rich grain	2 rim	97.36	1.24	0.31		98.91
"	"	"	2 rim	83.87	14.92	1.47	0.14	100.40
KSW-1A 1039.9D	Asis West	Dol I	1	55.49	44.25		0.28	100.02
"	"	"	2	55.34	45.03		0.51	100.88
AU15/13 38.2D	"	"	1	55.42	45.62		0.38	101.43
"	"	"	2	54.54	45.20			99.74
"	"	"	3	54.10	44.32			98.42
AU13/88 115.3	"	Cal I	1	93.34	1.37	2.49	4.36	101.57
"	"	"	2	94.04	0.60	1.04	3.74	99.42
"	"	"	3	93.96	0.47	0.53	5.19	100.14
"	"	"	4	93.95	0.26	0.63	4.53	99.37
"	"	"	5	93.08	0.93	1.68	4.07	99.76
"	"	"	6	92.71	1.00	1.83	3.58	99.12
"	"	"	7	89.72	1.97	2.83	4.23	98.74
"	"	"	8	90.76	1.49	2.39	4.23	98.88
"	"	"	9	94.65	0.00	0.32	4.13	99.30
"	"	"	10	93.91	0.00	0.73	3.90	98.58
KSW-1A 1039.9C	"	Cal II	1	99.44	0.86			100.30
"	"	"	2	99.79	1.79		0.26	101.84
"	"	"	3	98.71	1.02		0.45	100.17
"	"	"	4	97.78	2.01		0.60	100.39
"	"	"	5	99.87	0.90		0.75	101.52
"	"	"	6	98.92	1.31		0.40	100.63
"	"	"	7	98.27	1.82		0.36	100.45
"	"	"	8	99.90	1.23		0.24	101.37
"	"	"	9	98.49	2.09			100.58
"	"	"	10	99.26	1.85		0.40	101.50
"	"	"	11	99.96	0.42		0.88	101.27
"	"	"	12	99.86	0.19		0.91	100.96
"	"	"	13	99.62	0.25		0.90	100.76
"	"	"	14	99.01	0.36		0.62	100.00
AU15/13 38.2C	"	"	1	97.74	1.65		1.05	100.44
"	"	"	2	98.04	0.82		1.10	99.95
"	"	"	3	99.85	1.02		1.09	101.95
"	"	"	4	96.44	0.87		1.37	98.68
"	"	"	5	96.20	1.11		1.36	98.93
AU17/83 255.5	"	Cal III	1	96.99	0.85	0.89	1.24	99.98
"	"	"	2	96.56	2.34	0.92	1.10	100.92
"	"	"	3	96.88	0.70	0.37	1.07	99.02
"	"	"	4	95.66	1.15	0.61	0.96	98.37
"	"	"	5	97.76	1.39	0.74	1.23	101.12
"	"	"	6	96.91	1.00	0.65	1.14	99.70
AU17/83 247.4	"	"	1	97.76	0.50	0.74	1.02	100.02
"	"	"	2	96.97	1.11	0.59	1.19	99.86
"	"	"	3	95.93	1.59	0.88	1.32	99.71
"	"	"	4	95.64	1.44	0.60	1.17	98.86
"	"	"	5	98.72	0.71	0.70	1.44	101.56
"	"	"	6	97.69	1.36	0.65	1.05	101.02
"	"	"	7	99.75	0.25		0.49	100.49

Blank = below detection limit

SrO and SiO_2 not reported, as these were below detection limit in all cases

A2.3 X-RAY FLUORESCENCE SPECTROMETRY

Sample preparation:

Vein material was separated from the host by handpicking. This material was then crushed and ground in an agate mortar to <200 mesh size. At least 5 g of material were obtained for making pressed briquettes. The powdered material was then mixed with 5 drops of Mowiol binding agent, where necessary, and hydraulically pressurised into briquettes using sodium borate as a casing. Host material was hydraulically split, crushed in a jaw crusher, and milled in a Ziebtechnik mill using a carbon steel mortar and ring. The powder was treated in the same manner as the vein material in briquette preparation.

The briquettes were analysed for trace elements using a Philips X'Unique II PW1480 X-ray fluorescence spectrometer. Calibration was carried out using international standards, with correction for spectral overlap as routinely applied in the Department of Geological Sciences, University of Cape Town. Data reduction was effected as outlined by Duncan *et al.* (1984).

Instrument conditions: Philips PIW 1480 WDXRF spectrometer:

Tube targets: Rh, for Mo; Nb; Zr; Y; Sr; U; Rb; Th and Pb analysis;
Au, for Zn; Cu; Ni; Co; Cr; V and Mn;
Cr, for Ba and Sc.

Voltage and current settings: 80 kV and 35 mA for Mo; Nb; Zr; Y; Sr; U; Rb; Th; Pb;
60 kV and 45 mA for Zn; Cu; Ni;
50 kV and 55 mA for Sc; Co; Cr; V; Mn.

Analysing crystal: LiF (220)

Lower limits of detection and counting statistics for trace element analysis using XRF are given in Table A2.3.1

Table A2.3.1 Lower limits of detection (LLD) and counting statistics for trace element analysis by XRF.

Element	Concentration	LLD	2σ error
Mo	2.9	0.97	0.66
Zr	2.4	0.98	0.66
Y	7.1	0.77	0.54
Sr	156	0.82	0.98
Rb	2.3	0.86	0.58
Ba	12.0	2.8	2.0
Sc	0.9	1.9	1.3
Cr	3.1	2.3	1.6
V	10.9	1.6	1.2
Mn	1832	1.8	6.2
Pb	777	2.5	3.9
Zn	489	0.66	1.5
Cu	6122	1.4	6.6
U		1.7	
Nb		0.79	
Co		1.5	
Th		0.69	
Ni		1.0	
S	1889	4.4	8.9

Blank = not detected

A2.4 REE ANALYSIS

Sample Preparation:

REE were analysed by gradient high performance ion chromatography (HPIC) following the procedure described by le Roex and Watkins (1990).

0.5 g portions of powdered vein and host rock material were weighed into cleaned, dried and static-free teflon beakers. A few drops of distilled water were added to the powder to stop caking, such that all of the powder was contained in a large drop of water. The sample was digested using 8 ml perchloric acid and 15 ml hydrofluoric acid. Once dissolved, the solutions were passed through ion-exchange columns containing Spectra/Gel resin. Matrix elements that would otherwise co-elute with the rare earths were removed via this procedure by elution with 150 ml 1.75 M HCl. The REE held by the resin were then eluted using 150 ml 4.2 M HCl. This was evaporated to 2 ml, and made up to 10 ml. The resulting solution was analysed using a Dionex® *4000*i ion chromatograph with microprocessor-controlled eluent proportion and flow rate.

Solutions of the host dolomicrite and coarsely recrystallised dolomite samples were found to contain insoluble residue. However, this was present in small proportions (<2 wt % of initial sample mass weighed out). It is assumed here that the insoluble residue does not contribute significantly to the total REE content of the sample. The minor presence of insoluble residue makes it difficult to positively identify, although it is thought this could be hydrocarbon material or graphite, which is insoluble in HF. On the other hand, the "insoluble residue"may be compounds formed by the reaction of the various acids used in the dissolution procedure with impurities in the samples. A simple dissolution in HCl was not employed here, as other trace element compositions were determined by XRF techniques, which take into account the entire sample, not just an HCl soluble fraction. It was intended that concentrations be comparable in this respect.

Instrument conditions: Dionex® *4000i* HPIC system

Sample-loop volume: 50 µl

Guard column: Dionex HPIC-CG5

Separator column: Dionex HPIC-CS5

Eluent 1: 100 mM oxalic acid

190 mM LiOH

Eluent 2: 100 mM diglycolic acid

190 mM LiOH

Eluent 3: 18 mΩ deionised water

Eluent 4: 6 mM PDCA (pyridine-2,6-dicarboxylic acid)

50 mM glacial acetic acid

Flow rate: 1.0 ml/min.

Post-column reagent: 0.2 mM PAR (4-(2-Pyridylazo)-resorcinol monosodium salt)

3 M NH_4OH; 1 M CH_3CO_2H

Reagent flow rate: 0.7 ml/min.

Mixing device: membrane reactor

reaction coil

Detector wavelength: 520 nm

Injection: For samples in which the REE were present in sufficiently high concentrations, 50 µl of sample solution were loaded onto the column. For samples with very low concentrations, an on-line sample concentration procedure was employed (Dionex®, 1988; Ridley, 1992) in which several millilitres of sample solution were loaded onto a "concentrator column".

Chromatograms were quantified using artificial multi-element standards and peak height as a measure of concentration. Pr, Ho, Tm and Lu were not determined due to spectral overlap or poor resolution. Reproducibility of the REE concentrations is indicated in Table A2.4.1 for the conventional analytical runs of samples in which the REE are present in normally quantifiable concentrations. Table A2.4.2 indicates accuracy and precision of data using the on-line concentration method. Detection limits, as discussed by Le Roex and Watkins (1990), depend on the various parameters which can be changed in order to detect REE. Normally, an injection

volume containing ~2 ng HREE and 13 ng LREE can be detected on passing through the detector.

Table A2.4.1 Reproducibility of the rare-earth element determination by HPIC (after le Roex and Watkins, 1990).

Element	Conc. (ppm)	1σ error	% RSD
La	25.2	0.15	0.6
Ce	52.5	0.80	1.5
Pr	6.55	0.14	2.1
Nd	27.1	1.0	3.7
Sm	5.98	0.14	2.3
Eu	1.95	0.06	3.1
Gd	6.65	0.12	1.8
Tb	1.08	0.06	5.6
Dy	6.52	0.17	2.6
Er	3.51	0.06	1.7
Yb	3.39	0.14	4.1

* % RSD= (SD/mean) x 100

Table A2.4.2 Accuracy and precision of REE data for synthetic standard Std-S against Std-A, after on-line concentration (n=5) (after Ridley, 1992)

Element	Actual conc. (ppm)	$\bar{x}$ (ppm)	sd (ppm)	% RSD
La	3.20	3.33	0.083	2.49
Ce	7.30	7.35	0.103	1.40
Pr	0.79	0.80	0.019	2.34
Nd	3.30	3.32	0.056	1.69
Sm	0.57	0.58	0.017	2.86
Eu	0.15	0.15	0.004	2.97
Gd	0.52	0.53	0.009	1.69
Tb	0.09	0.09	0.008	9.13
Dy	0.58	0.59	0.004	0.77
Er	0.34	0.34	0.019	5.68
Yb	0.31	0.30	0.015	4.93

A2.5 STABLE (C,O) ISOTOPE ANALYSIS

Bremen Line method for isotope analysis of calcites

The Bremen Line technique has found wide appeal in the analysis of carbonates, particularly where extremely small quantities of material are available. Analyses were carried out in the Department of Archaeology, University of Cape Town. Calcite samples containing <10 % contamination from dolomite or other contaminants such as quartz, as determined from XRD, were analysed using this method. The calcite portions of samples were separated by hand-picking, and crushed to <300 mesh size. 40-50 μg of each powdered samples were carefully weighed into small, acid (HCl) cleaned test tubes arranged on a revolving tray. These were then placed in an oven of set temperature of 71°C. Automated analysis was then carried out, in which 5 drops of 100 % H_3PO_4 were reacted with each of the samples for 12 minutes. The resulting CO_2 released was collected in the mass spectrometer. Standard NM 95, a marble from Namaqualand, South Africa, was used as the laboratory standard, and run periodically (once every four to five samples) between samples to correct for drift effects.

Conventional C and O line setup

Problems encountered with dolomite samples using the Bremen Line method, led to the use of the more conventional method of McCrea (1950) for obtaining CO_2 from dolomite and mixed dolomite-calcite samples with >10 % contamination from either mineral before analysis by mass spectrometry. 10 mg of sample (up to 70 mg for very quartz-rich samples) were weighed into reaction vessels containing H_3PO_4 in a separate arm of each vessel. Samples with <5 % calcite were reacted at 25°C overnight. The CO_2 produced from this reaction was collected for analysis. For two mixed dolomite-calcite samples where each mineral constituted >10 % of the mass, the method of Al-Aasm *et al.* (1990) was used to obtain isotope compositions from the individual dolomite and calcite components. This involved reacting the sample for two hours at 25°C, collecting the CO_2 produced (from the calcite fraction), reacting further at 25°C overnight, then discarding the CO_2 (from any remaining calcite). The samples were then reacted at 50°C overnight, and the CO_2 produced from the dolomite fraction collected for analysis. In addition, two samples containing sulphide mineralisation were frozen into a cold finger containing Ag_3PO_4 to remove the sulphide from the collected CO_2, then allowed to warm up. No S peaks were found

during mass spectrometric analysis, indicating efficient removal. Samples of CO_2 from standard NM 95 were also prepared for each batch of (5) samples.

Mass spectrometry and data reduction

Samples of CO_2 obtained from both techniques were analysed in a Finnigan MAT mass spectrometer at the Department of Archaeology, University of Cape Town. Raw $\delta^{18}O$ and $\delta^{13}C$ values were corrected using values of the laboratory standard NM 95 ($\delta^{18}O$ = 25.10 ‰ and $\delta^{13}C$ = 1.57 ‰), which has been calibrated to SMOW and PDB scales using carbonate standard NBS 19 ($\delta^{18}O$ = 28.64 ‰ and $\delta^{13}C$ = 1.95 ‰). In addition, the standard $\delta^{18}O$ and $\delta^{13}C$ values were used to correct sample delta values for shifts in the reference gas values. Fractionation factors used were:

α = 1.009 for calcite at 50°C (Al-Aasm *et al.*, 1990)

α = 1.01065 for dolomite reacted at 50°C (Rosenbaum and Sheppard, 1986)

α = 1.0081069 for calcite reacted at 71°C (ISODAT software manual)

The precision in values, as estimated from repeated analyses of standard NM 95, is better than ±0.1 ‰ for $\delta^{13}C$, and ±0.2 ‰ for $\delta^{18}O$.

The C and O isotope data are presented in Table A2.5.1, along with data from previous workers.

Table A2.5.1 Stable (C, O) isotope data (‰) for various carbonate generations from Tsumeb, Khusib Springs, Kombat and Berg Aukas.

Sample	Deposit	Generation	$\delta^{13}C$	$\delta^{18}O$	Reference
2965/300	Tsumeb	Dol I	-1.3	23.6	This study
DCT4H	"	"	-1.5	22.0	"
DCT10	"	Dol II	4.8	22.8	"
DCT4SV	"	Dol III	-1.1	20.5	"
DCT5	"	"	-1.7	20.2	"
2965/106	"	"	0.5	21.4	"
DCT1	"	Qtz-Dol I	-0.3	22.2	"
DCT2	"	"	-0.3	21.2	"
2965/62 d	"	Cal I d	-0.2	21.4	"
2965/62 c	"	Cal I c	-0.5	21.3	"
3153/18	"	Cal II	0.2	21.0	"
3153/19	"	"	-1.5	20.5	"
2944/240	"	Cal III	-9.5	19.4	"
S67B 456.8-457	"	Dol-gyp	4.8	23.0	"
DMIII	"	Dol*	3.7	21.3	Theron and Beukes, 1993
DMIII	"	"	3.8	21.4	"
NBZ-SMB	"	"	3.4	21.4	"
NBZ-0/17A	"	"	3.2	20.8	"
TS-KAL30	"	Cal*	-4.1	17.3	"
TS-KAL39	"	"	-4.6	18.5	"
TS-KAL30	"	"	-3.6	18.7	"
NBZ-W/4	"	"	1.2	19.4	"
NBZ 3279(48)	"	"	0.6	20.4	"
TS-CL40	"	"	0.0	21.4	"
TSW6	"	"	-0.7	20.2	"
678	"	"	0.5	19.0	Hughes, 1987
718	"	"	-1.9	19.8	"
755	"	"	-2.7	19.6	"
84	"	"	-1.1	19.4	"
240A	"	"	-3.5	18.9	"
242	"	"	-3.5	19.4	"
516	"	"	-2.2	19.5	"
860	"	Cal/rec.dol*	0.7	20.6	"
440	"	"	1.6	20.0	"
240B	"	"	0.4	20.6	"
240C	"	"	1.1	21.6	"
490	"	"	1.0	20.5	"
515	"	"	0.0	19.8	"
601	"	Dol vein*	4.7	22.3	"
609	"	"	3.5	21.1	"
651	"	"	5.7	23.4	"
811	"	"	5.1	22.6	"
726	"	"	5.0	21.7	"
253	"	"	0.8	20.3	"
495A	"	"	-0.6	20.0	"
168	"	"	0.1	20.3	"
857	"	"	4.1	21.4	"
590	"	Cal-sulp#	5.6	22.7	"
DV23	Khusib Springs	Lst I	-1.8	20.3	Verran,1996
DV35	"	"	-1.0	19.7	"
DV34	"	"	-0.9	21.8	"
DV33	"	"	0.0	22.5	"
DV32	"	"	-0.9	21.4	"
KH91/191.4	"	Dol Ia	0.1	26.0	"
KH91/81.9	"	"	-0.4	26.2	"
DV9	"	Dol Ib	-0.3	18.9	"
DV18	"	"	-0.4	19.3	"

Table A2.5.1 cont.

Sample	Deposit	Generation	$\delta^{13}C$	$\delta^{18}O$	Reference
DV10	Khusib Springs	Dol IIa	-1.3	18.9	Verran, 1996
DV7	"	"	-3.0	18.9	"
KH62/75.3	"	"	-6.4	19.2	"
DV30 1	"	"	-1.6	19.0	"
DV30 2	"	"	-1.5	18.9	"
DV5	"	Dol IIb	-0.8	20.1	"
DV27	"	"	-0.8	18.8	"
KH91/292.7	"	Dol IIc	-0.8	19.5	"
KH91/293.8	"	"	-0.6	19.7	"
DV19	"	Dol III	-2.1	19.2	"
DV21	"	"	-1.3	19.0	"
DV24 1	"	Cal I	-3.0	20.1	"
DV24 2	"	"	-3.0	20.2	"
DCK 1	E900	Dol I	2.7	23.0	This study
AU 13/88 115.3	Asis West	Cal I	-7.2	16.4	"
KSW-1A 1037.95	"	Cal II	2.8	20.5	"
DCK 4 cal	E900	"	3.2	21.9	"
DCK 4 dol	"	"	4.1	21.8	"
DCK 3	"	"	1.0	20.2	"
AU 17/83 247.4	Asis West	Cal III	-2.1	18.3	"
AU 17/83 255.5	"	"	-2.1	18.6	"
52	Kombat area	calcite*	-4.4	21.1	Frimmel et al., 1997
48	"	"	-1.9	21.5	"
54	"	"	1.7	19.7	"
58	"	"	0.5	18.4	"
44	"	"	2.5	19.8	"
74	"	"	4.0	24.3	"
42	"	"	2.3	19.4	"
BAD2/1a	Berg Aukas	Dol I	4.4	29.8	Frimmel et al., 1997
BAD2/8	"	"	3.0	28.5	"
BAD7/1a	"	"	6.1	28.2	"
BAD15a	"	"	3.8	24.8	"
Q1-4a	"	"	4.4	26.0	"
Q2-4a	"	"	2.5	25.9	"
Q2-1b	"	"	3.0	27.3	"
K1-1a	"	"	2.9	23.0	"
K1-2a	"	"	4.2	26.6	"
K1-3a	"	"	2.9	23.3	"
BAD7/1c	"	Dol II	4.0	24.9	"
BAD/2a	"	"	3.6	26.2	"
BAD7/4a	"	"	4.0	25.5	"
K1-1b	"	"	3.2	21.2	"
K1-1c	"	"	3.2	26.3	"
K1-1d	"	"	4.2	25.6	"
K1-2b	"	"	3.5	22.2	"
K1-3b	"	"	4.1	25.3	"
K1-3c	"	"	3.6	22.8	"
BAD2/3	"	Dol III	3.2	24.8	"
BAD2/2	"	"	2.7	24.3	"
BAD2/7a	"	"	2.4	21.5	"
BAD15/12	"	"	2.8	23.3	"
BAD15b	"	"	2.8	24.2	"
K1-1e	"	"	1.5	21.8	"
BAS-1a	"	"	3.3	24.7	"
BAS-1b	"	"	2.8	24.2	"
BAS-2a	"	"	4.0	25.1	"
BAS-2b	"	"	3.9	24.9	"

Table A2.5.1 cont.

Sample	Deposit	Generation	$\delta^{13}C$	$\delta^{18}O$	Reference
BAS-3a	Berg Aukas	Dol III	2.9	22.9	Frimmel et al., 1997
BAS-3b	"	"	4.2	25.1	"
HB-1a	"	"	2.2	21.9	"
HB-1b	"	"	3.1	22.2	"
HB-2	"	"	2.1	21.5	"
BAD2/1b	"	Dol IV	4.2	24.4	"
BAD2/7B	"	"	1.3	19.2	"
BAD7/3	"	"	4.0	24.9	"
BAD15c	"	"	2.8	19.8	"
Q1-4c	"	"	3.6	22.9	"
Q1-10	"	"	2.9	20.6	"
K1-2c	"	"	4.5	25.1	"

* = hydrothermal phases, including dolomite, calcite and recrystallised dolomite
# = calcite with native sulphur

A2.6 MICROTHERMOMETRY

Samples of quartz, dolomite and calcite were cut and polished to <100 μm thin wafers. These were studied using conventional transmitted light microscopy to characterise the fluid inclusion populations present, and select inclusions appropriate for microthermometric analysis. The polished wafers were then broken into chips < 10 mm diameter, for use on a heating and freezing stage. A FLUID INC. adapted U.S.G.S. nitrogen gas flow heating-freezing stage was used to measure temperatures of phase changes during heating and freezing of the chips containing the fluid inclusions under consideration. Calibration of the system was carried out using SYNFLINC- synthetic fluid inclusions in quartz, at -56.6°C (CO_2 triple point), 0.0°C (triple point of pure water) and 374.3°C (critical point of pure water). Accuracy of the system is estimated to be better than ±0.5°C for measurements below 0°C, and better than ±5°C for measurements above 30°C, providing the thermocouple tip is not more than 2 mm away from the inclusion being measured. As far as was possible, the full set of parameters was measured for each inclusion. T_{form} was calculated from T_h and T_m values using the FLINCOR programme, as outlined by Brown (1989). The fluid inclusion data are presented in Table A2.6.1.

Table A2.6.1 Fluid inclusion data.

Sample	Deposit	Generation	Origin	Size	Type	V/L (%)	Te	Tm	Th	Salinity	Occurrence
DCT4	Tsumeb	Dol III	s	4.9	I	10-15	-46.7	-20.1	144	22.4	random
"	"	"	"	4.9	I	15		-12.5	116	16.4	"
"	"	"	"	8.5	I	5-10		-19.6	128	22.1	"
"	"	"	"	2.4	I	25		-20.4	151	22.6	trail
"	"	"	"	6.1	I	10	-43	-21	138	23.0	"
"	"	"	"	4.9	I	10-15		-17.3		20.4	"
"	"	"	"	4.9	II	10-15	-36.4	-1.9	88	3.2	random
"	"	"	"	4.9	I	5-10	-48.3	-1	80	1.7	"
"	"	"	"	2.4	I	10		-14.2	143	18.0	"
"	"	"	"	3.7	I	10-15	-36.7	-20.2	128	22.5	"
"	"	"	"	4.9	II	15	-32	-17.5	126	20.6	"
"	"	"	"	3.7	I	15	-41	-15.6	136	19.1	"
"	"	"	"	3.7	II	10		-11.7	133	15.7	"
"	"	"	"	6.1	I	10		-19.7	134	22.2	"
"	"	"	"	4.9	I	10		-18.4	128	21.3	"
"	"	"	"	4.9	I	10		-18.6	138	21.4	"
2965/106	"	"	p.s.	10	I	10	-40.6	-20.2	150	22.5	trail
"	"	"	"	9	I	5			159		"
"	"	"	"	9	I	5-10	-42.7	-20.2	166	22.5	"
"	"	"	"	5	I	10		-19.2		21.8	"
"	"	"	"	4	I	15	-40.4	-21.1	166	23.1	"
"	"	"	"	5	I	10-15	-42.1	-20.8	161	22.9	trail
"	"	"	"	3	I	10-15	-42.1	-20.9	161	23.0	"
"	"	"	"	3	I	10		-7.8	114	11.5	random
"	"	"	"	9	I	10	-38.6	-19.4	155	22.0	"
"	"	"	"	6	I	10	-44	-15.4	136	19.0	"
"	"	"	"	3	I	10	-44.8	-18.7	141	21.5	"
"	"	"	"	4	I	15	-41	-19.3	141	21.9	"
"	"	"	"	4	I	10	-40.8	-20.4	143	22.6	trail
"	"	"	"	5	I	10		-17.5	139	20.6	"
"	"	"	"	5	I	10	-40	-19.1	154	21.8	"
"	"	"	"	5	I	10	-39.5	-21.2	136	23.2	trail
"	"	"	"	2	I	10	-38.2	-16.1	151	19.5	"
"	"	"	"	3	I	10-15	-42.2	-18.8	151	21.5	"
"	"	"	"	3	I	10		-7.3	111	10.9	random
"	"	"	"	3	I	10		-7.6	118	11.2	"
DCT5	"	"	s	4	I	20	-38.1	-21.2	181	23.2	random
"	"	"	"	2	I	20		-17.8		20.8	"
"	"	"	"	2	I	25	-48	-20.9	175	23.0	"
"	"	"	"	4	I	20	-33.9	-21.2	184	23.2	"
"	"	"	p?	10	I	10	-38.4	-3.9	184	6.3	isolated
"	"	"	"	5	I	15	-37.8	-20.6	180	22.8	"
"	"	"	"	2	I	25	-42.4	-19.2	180	21.8	"
"	"	"	"	8	I	15	-45	-21.5	212	23.4	"
"	"	"	"	3	I	10	-35.1	-18.8	167	21.5	"
"	"	"	s	4	I	20	38.3	-20.2	189	22.5	trail
"	"	"	"	6	I	15	-34.1	-20.2	188	22.5	"
"	"	"	"	3	I	15		-20.4	147	22.6	"
"	"	"	p?	3	I	10	-42.1	-20.3	140	22.6	cluster
"	"	"	"	5	I	15		-20.3	179	22.6	"
"	"	"	"	4	I	25	-32.5	-20.2	183	22.5	"
"	"	"	s	4	I	25	-41.7	-20.5	179	22.7	random
"	"	"	"	8	I	25	-41.7	-20.6	152	22.8	"
"	"	"	p?	12	I	10	-39.5	-21.9	196	23.6	isolated
"	"	"	p?	12	I	10	-38.5	-20.8	181	22.9	"
2944/248	"	"	p	16		15	-28.6	-14.5	147	18.2	"
"	"	"	s	4	II	5-10	-29.2	-10.4	119	14.4	trail

Table A2.6.1 cont.

Sample	Deposit	Generation	Origin	Size	Type	V/L (%)	Te	Tm	Th	Salinity	Occurrence
2944/248	Tsumeb	Dol III	s	4	I	10	-32.1	-12.9	148	16.8	trail
"	"	"	"	3	I	5-10	-38	-13.8	147	17.6	"
"	"	"	"	6	I	5	-31.5	-17.4	147	20.5	"
"	"	"	"	4	I	10	-44.2	-14.1	135	17.9	"
"	"	"	"	6	I	5	-34.2	-17.7	99	20.7	"
"	"	"	"	6	I	10	-33.3	-5.6	140	8.7	"
"	"	"	p?	6	I	10	-36.8	-19.4	142	22.0	cluster
"	"	"	"	3	I	5-10	-40.2	-14.6	149	18.3	"
"	"	"	"	4	I	5-10	-45.9	-21.2	146	23.2	"
"	"	"	s	9	I	5	-45.9	-16	150	19.4	random
"	"	"	"	6	I	5-10	-32.3	-19.1	148	21.8	"
2944/225	"	"	s	4	I	10	-36	-18.5	127	21.3	trail
"	"	"	"	4	II	20	-31.7	-15.2	147	18.8	"
"	"	"	"	2	I	20	-44.5	-17.5	131	20.6	"
"	"	"	"	6	I	10	-38.8	-6.9	145	10.4	"
"	"	"	"	6	I	10	-42.8	-8.5	120	12.3	"
"	"	"	p?	2	II	15	-39	-22.3	139	23.9	cluster
"	"	"	"	4	I	15		-18.5	146	21.3	"
"	"	"	"	4	II	10		-16.6	139	19.9	"
"	"	"	s	4	II	5-10	-39	-16.9	136	20.1	random
"	"	"	"	6	I	5-10	-35.7	-19.2	138	21.8	"
"	"	"	"	4	I	5-10	-39.3	-18.6	143	21.4	"
"	"	"	"	3	I	5-10	-37.3	-17	137	20.2	"
"	"	"	"	2	II	5-10	-37.2	-16.8	141	20.1	"
"	"	"	"	4	I	5-10	-47.2	-17.9	91	20.9	"
"	"	"	"	4	I	5-10	-39.5	-20.8	129	22.9	trail
"	"	"	"	6	I	5-10	-40.8		154		"
"	"	"	"	4	I	10-15	-40.8	-20.1	123	22.4	"
"	"	"	"	6	I	5-10	-48	-20.5	116	22.7	"
3153/36	"	Calcite II	s	4.9	I	5-10	-46.9	-19.9	91	22.3	random
"	"	"	"	3.7	I	10	-45.2	-17.3	83	20.4	"
"	"	"	"	6.1	II	10-15	-44.5	-18.1	91	21.0	"
"	"	"	"	3.7	II	15	-42.2	-21.6	78	23.4	"
"	"	"	"	6.1	II	10	-48.6	-16.7	77	20.0	"
"	"	"	"	5	I	5-10	-44.5	-16.6	96	19.9	"
"	"	"	"	5	II	5-10	-46.2	-8.7	82	12.5	"
"	"	"	"	4.9	II	5-10	-47.5	-18.1	96	21.0	"
"	"	"	"	11	II	5-10	-43.3	-18.5	92	21.3	"
"	"	"	"	3.7	I	10	-41.5	-17.9	80	20.9	"
"	"	"	"	6.1	II	10	-46	-17.1	71	20.3	"
"	"	"	"	6.1	II	10	-45	-19.7		22.2	"
"	"	"	"	3.7	I	10-15	-41.3	-18.7		21.5	"
"	"	"	"	9.8	II	10	-42.6	-19.9		22.3	"
"	"	"	"	9.8	II	5-10	-44.4	-18.4	76	21.3	"
"	"	"	"	12.2	II	10		-17.4		20.5	"
"	"	"	"	4.9	I	15	-43.1	-19.8	76	22.2	"
"	"	"	"	7.3	II	15	-38.4	-12.1	79	16.1	"
"	"	"	"	7.3	II	15	-42.1	-13.8	79	17.6	"
"	"	"	"	8.5	II	10	-40.8	-17.7	80	20.7	"
"	"	"	p?	8.5	I	5-10	-38.4	-15.4	81	19.0	cluster
"	"	"	"	7.3	II		-40.8		86		"
"	"	"	"	4.9	II	5-10	-40.8	-14.2	91	18.0	"
"	"	"	"	9.8	II	10	-48.8	-19.9		22.3	"
"	"	"	p?	6	I	5	-48.3	-17.4	92	20.5	cluster
"	"	"	"	4	I	10	-45.1	-6.1	85	9.3	"
"	"	"	"	4	I	20		-19.8	102	22.2	"
"	"	"	"	5.5	I	5-10	-43	-19.6	92	22.1	"

Table A2.6.1 cont.

Sample	Deposit	Generation	Origin	Size	Type	V/L (%)	Te	Tm	Th	Salinity	Occurrence
3153/36	Tsumeb	Cal II	s	3	II	5-10	-42.9	-9.4	86	13.3	random
"	"	"	"	6	II	5-10	-45.2		93		"
"	"	"	"	5.5	II	10	-41.7	-19.4	91	22.0	"
"	"	"	"	5	II	10	-40	-21.6	89	23.4	"
"	"	"	"	5	I	5		-12.4	89	16.3	"
"	"	"	"	5	I	5			97		"
"	"	"	"	5	I	5			96		"
"	"	"	"	4	I	5			91		"
3153/18	"	"	s	9.8	II	5-10	-47.6	-19	111	21.7	trail
"	"	"	"	9.8	II	10	-41	-20.1	126	22.4	"
"	"	"	"	4.9	I	10	-44.3	-21.2	130	23.2	"
"	"	"	"	4.9	II	25	-44.7	-17.9	125	20.9	"
"	"	"	"	9.8	II	5-10		-20.7	102	22.8	"
"	"	"	"	6.1	II	10		-17	119	20.2	random
"	"	"	"	7.3	II	10		-22	113	23.7	"
"	"	"	"	9.8	II	10		-19.1		21.8	"
"	"	"	"	4.9	II	10	-43.4	-18	99	21.0	"
"	"	"	"	6.1	I	10-15	-47.5	-21.4	115	23.3	"
"	"	"	"	9.8	I	5-10	-36.2	-17.1	95	20.3	trail
"	"	"	"	6.1	II	5-10		-18.9	112	21.6	"
"	"	"	"	6.1	II	5-10	-45.3	-18.3		21.2	"
"	"	"	"	7.3	I	5-10	-43.3	-19	119	21.7	"
"	"	"	"	6.1	I	5-10	-47.2	-17.8	111	20.8	"
"	"	"	p?	14.6	II	4	-37	-17.2	113	20.4	isolated
"	"	"	"	7.3	I	10	-41.9	-16.9	111	20.1	cluster
"	"	"	"	3.7	I	10-15	-49.4	-18.4	113	21.3	"
"	"	"	"	6.1	II	10	-40	-17	128	20.2	"
"	"	"	"	7.3	II	5-10	-40	-18.2	123	21.1	"
"	"	"	s	9.8	II	5-10	-44.8	-20.4	126	22.6	random
"	"	"	"	6.1	I	10	-40.5	-18.9	114	21.6	"
"	"	"	p?	12.2	II	5-10		-20.3	131	22.6	isolated
"	"	"	s	3.7	II	10	-40	-18.6		21.4	trail
"	"	"	"	3.7	I	10	-43.3	-18.9	114	21.6	"
"	"	"	"	3.7	I	10	-43.1	-18.5		21.3	"
"	"	"	"	3.7	I	10	-43.1	-17.4	114	20.5	"
"	"	"	p?	4.9	I	5-10	-40	-18	93	21.0	cluster
"	"	"	"	7.3	I	10	-45	-20.8	124	22.9	"
"	"	"	"	4.9	I	10	-41.4	-19.2	105	21.8	"
"	"	"	"	7.3	I	10		-17.1	113	20.3	"
"	"	"	s	7.3	II	10		-16.8	107	20.1	random
"	"	"	"	3.7	I	10	-42	-19.2		21.8	"
"	"	"	"	7.3	I	10		-18.1		21.0	"
"	"	"	"	4.9	I	20		-8	99	11.7	"
"	"	"	"	3.7	I	5		-20.6	99	22.8	"
"	"	"	"	4.9	I	5		-12.7		16.6	"
"	"	"	"	4.9	I	10		-16.8	72	20.1	"
"	"	"	"	4.9	I	5-10		-6	70	9.2	"
"	"	"	"	2.4	I	25		-15.2	123	18.8	"
"	"	"	"	2.4	I	15		-16.3	98	19.7	"
"	"	"	"	9.8	II	10		-18.6	132	21.4	"
"	"	"	"	5	I	10-15	-42.3	-17.4	120	20.5	trail
"	"	"	"	3	I	5-10	-40.1	-19.8		22.2	"
"	"	"	"	7	I	15-20		-19.6	114	22.1	"
"	"	"	"	8	I	5		-1.6	124	2.7	"
"	"	"	"	6	I	5-10		-14.2	131	18.0	random
"	"	"	"	3.7	I	15		-9.6	91	13.5	"
"	"	"	"	3.7	I	10		-3	94	5.0	"

Table A2.6.1 cont.

Sample	Deposit	Generation	Origin	Size	Type	V/L (%)	Te	Tm	Th	Salinity	Occurrence
3153/18	Tsumeb	Cal II	s	7.3	I	5		-2.6	91	4.3	random
"	"	"	"	9.8	I	5-10		-7.7	98	11.3	"
"	"	"	"	4.9	I	10	-45.2	-5.3	108	8.3	"
"	"	"	"	6	I	5-10		-10.9	102	14.9	"
"	"	"	"	8	I	5		-7.4	94	11.0	"
"	"	"	"	7	I	5-10	-46.9	-21	98	23.0	"
"	"	"	"	6	I	5-10	-47.6	-21.2	86	23.2	"
"	"	"	"	6	I	5-10		-2.5	91	4.2	"
"	"	"	"	4	I	10		-5.8	94	8.9	"
"	"	"	"	8	I	10		-7.1	98	10.6	"
DV30	Khusib Springs	Dol II	p?	8	I	15	-30.8	-20.5	220	22.7	isolated
"	"	"	"	3	I	20	-21.2	-5.6	188	8.7	"
"	"	"	"	8	I	25			221		"
"	"	"	"	5	I	25			227		"
"	"	"	"	10	I	10	-32.2	-22.3	227	23.9	"
"	"	"	s	6	I	25		-19.2	226	21.8	trail
"	"	"	"	6	I	25		-18.7	244	21.5	"
"	"	"	"	4	I	25		-19.2	244	21.8	"
"	"	"	"	6	I	25		-18.3	234	21.2	"
"	"	"	p?	10	I	30	-28.8	-14.2	242	18.0	isolated
"	"	"	p?	15	I	20	-29.3	-18.3	223	21.2	cluster
"	"	"	"	6	I	25			228		"
"	"	"	"	14	I	20	-27.7	-14.8	291	18.5	"
"	"	"	"	7	I	25	-31.2	-13.8	289	17.6	"
"	"	"	s	3	I	20	-30.4	-18.5	222	21.3	trail
"	"	"	"	10	I	20	-32.8	-16.5	247	19.8	"
"	"	"	"	20	I	50	-30.4	-20.8		22.9	"
"	"	"	"	9	I	25	-37.9	-21	254	23.0	trail
"	"	"	"	12	I	20	-29.7	-19.2	204	21.8	"
"	"	"	"	8	I	20	-28.8	-15.4	189	19.0	trail
"	"	"	"	3	I	25	-30	-18.8	220	21.5	"
"	"	"	"	9	II	25	-29.8	-19.7	223	22.2	"
"	"	"	"	4	I	25	-30.1	-19.9	231	22.3	trail
"	"	"	"	4	I	20	-30.2	-13.5	231	17.3	"
"	"	"	"	4	I	20	-28.5	-13.2	217	17.1	"
"	"	"	p?	4	I	20	-21.5	-11.1	228	15.1	cluster
"	"	"	"	4	I	20	-29.9	-14.5	232	18.2	"
"	"	"	"	5	I	50		-15.6		19.1	"
"	"	"	"	12	I	30	-29.2	-16.2		19.6	isolated
"	"	"	"	8	I	25		-15.1		18.7	"
"	"	"	"	8	II	25	-28.4	-19.8	227	22.2	"
DV30 qtz	"	Dol II	"	10	I	25	-26.2	-14.7	232	18.4	isolated
"	"	"	"	12	I	25	-27.3	-14.6	234	18.3	"
"	"	"	"	10	I	25	-30.9	-14.6	242	18.3	"
"	"	"	"	12	I	25	-25.8	-14.9	240	18.6	"
"	"	"	"	10	I	20	-29.8	-13.2		17.1	"
KH62/75.3 qtz	"	Dol II	"	15	I	15	-30.9	-15.6	252	19.1	isolated
"	"	"	"	8	I	25	-31.6	-14.1	228	17.9	"
"	"	"	"	20	I	20	-33.2	-14.5	243	18.2	"
"	"	"	"	8	I	25	-32.6	-14.6	237	18.3	"
"	"	"	"	7	I	25	-34.3	-20	243	22.4	"
"	"	"	"	6	I	25	-34.2	-18.7	242	21.5	"
"	"	"	"	10	I	25	-32.5	-14.6	236	18.3	"
"	"	"	"	6	I	20	-39.5	-16.1	226	19.5	"
"	"	"	s	10	I	10	-35.5	-16.8	228	20.1	trail
"	"	"	"	20	I	20	-41.7	-7.7	238	11.3	"
"	"	"	"	5	I	15	-36	-14.7		18.4	"

Table A2.6.1 cont.

Sample	Deposit	Generation	Origin	Size	Type	V/L (%)	Te	Tm	Th	Salinity	Occurrence
KH62/75.3 qtz	Khusib Springs	Dol II	s	8	I	15	-35.6	-16.6		19.9	trail
"	"	"	"	8	II	15	-40	-17.9	231		"
"	"	"	"	5	II	25	-39.2	-13.2	229	17.1	trail
"	"	"	"	10	I	25	-38.4	-14.1	238	17.9	"
"	"	"	"	5	I	25	-38.4	-13.5	229	17.3	"
"	"	"	"	6	I	25	-38.4	-13.8	238	17.6	"
DV16	"	sphalerite	s	4	I	20	-41.6	-24.1		25.0	trail
"	"	"	"	6	I	10	-41	-24.2		25.1	"
"	"	"	"	10	I	20					"
"	"	"	"	10	I	10	-45.3	-24.6		25.3	"
"	"	"	"	8	I	10	-41	-24.1		25.0	"
"	"	"	"	20	I	5	-45.7	-24.6		25.3	trail
"	"	"	"	6	I	10		-23.7		24.8	"
"	"	"	"	10	I	10	-44.5	-24.4		25.2	"
"	"	"	"	4	I			-24.8		25.5	"
"	"	"	"	8	I			-24	102	25.0	"
"	"	"	"	8	I	5-10	-44.2	-24.2		25.1	"
"	"	"	p?	20	I	10	-46.2	-24.8		25.5	isolated
"	"	"	"	8	I			-25.3		25.8	"
"	"	"	"	8	I						"
AU13/88 120.8	Kombat	Cal I	s	3	I	15-20		-1.5	176	2.6	trail
"	"	"	"	3	I	25		-1.1	172	1.9	"

p? = primary?
s = secondary
p.s. = pseudo secondary
blank = not determined

A2.7 ION CHROMATOGRAPHY USING THE CRUSH-LEACH METHOD FOR ANALYSIS OF BULK FLUID INCLUSION COMPOSITION

Bulk fluid inclusion analysis of carbonates associated with MVT deposits has been effected using the crush-leach technique (Kesler *et al.*, 1996). A similar technique was employed in the analysis of carbonate samples from the OML. The technique followed is outlined below.

Sample preparation:

Note: In all steps of the procedure, the water used was doubly distilled, deionised water (DDW) which had been tested to be free of the analytes.

Equipment /materials made use of were:

✔ agate mortar and pestle for carbonate grains
✔ clean, disposable 5 ml syringes
✔ 4 μm, Na free filters, for attachment to the syringes
✔ an acid cleaned (HNO_3) glass beaker
✔ Dilute HNO_3 for cleaning purposes
✔ clean Nalgene® plastic bottles (see cleaning procedure below)
✔ a clean 1 ml syringe for IC injection

Homogenous grains of a particular sample were hand-picked, such that 0.5 g of material was obtained for each analytical run. Where possible, five subsamples of a sample of vein material were separated. The samples were then rinsed and ultrasonically cleaned in DDW.

A blank was prepared by grinding the mortar against the pestle under DDW, and analysing this water by injection into the IC. Once the blank showed a sufficiently insignificant (relative to the sample) concentration of the ions under analysis (i.e., Na^+ and K^+ for the cation run, and Cl^- and Br^- for the anion run), a sample solution was prepared. Typically, Cl^-, Ca^{2+} and Mg^{2+} were the only contaminants in blank solutions. Na^+ and K^+ were rarely detected, Br^- and SO_4^{2-} never. The concentrations of contaminants in the blank were always within the analytical error.

0.5 g of ultrasonically cleaned sample (i.e, the hand-picked grains) was weighed out. Up to 0.65g was weighed out for "drier" samples. The grains were then placed in an acid-cleaned (HNO_3) beaker, and washed with DDW. This was repeated until the grains were free of dust. The grains were washed into the mortar using 2.5-3.5 ml of DDW, depending on how concentrated the leachate needed to be. Crushing of these grains was then carried out whilst they remained submerged under the DDW, and continued until a fine powder was obtained. At this stage, the grittiness disappeared. The resulting leachate (i.e., the DDW now containing the ions which had been liberated from the fluid inclusions during crushing) was left to stand covered for 10 minutes (to allow particles to settle, and minimise adsorption effects), then drawn up into the 5 ml syringe and filtered into clean bottles. At most, 0.2 ml of the initial volume of DDW was lost during crushing and filtration. The solutions were then ready for analysis by HPIC.

Injection: The solutions were drawn into a clean 1 ml syringe and injected into the appropriate column. For the anion runs, two sample loop volumes were used: the conventional 50 µl loop for "normal" samples, and a 200 µl loop for samples with low concentrations of Br^-, for which peak resolution could not be obtained using a 50 µl loop. For the cation run, a 25 µl sample loop volume was used. This was sufficient for the detection of all cations in the solutions.

A blank was run prior to each sample crush, and the solution stored for the next run to assess contamination effects. Cleaning out of the mortar and pestle was effected by grinding the two under HNO_3, and then rinsing and grinding under DDW.

Instrument conditions: DIONEX® DX300 HPIC system

Anion analysis

Sample loop volume: 50 µl/200 µl

Guard column: HPIC-AG4A

Separator column: HPIC-AS4A

Eluent: 1.80 mM Na_2CO_3

1.70 mM $NaHCO_3$

Eluent flow rate: 2.0 ml/min.

Suppressor: Anion MicroMembrane (AMMS)

Regenerant: 25 mN H_2SO_4

Regenerant flow rate: 3 ml/min. With AutoRegen Accessory

Expected background Conductivity: 15 to 20 μS

Cation analysis

Sample loop volume: 25 μl

Guard column: HPIC-CG12A (4x50 mm)

Separator column: HPIC-CS12A (4x250 mm)

Eluent: 22 mM MSA (methane sulphonic acid)

Eluent flow rate: 1.0 ml/min.

Suppressor: Cation self-regenerating suppressor CSRS-I (4 mm)

Expected background conductivity: 2-4 μS

Data reduction:

Chromatograms collected were automatically integrated, although some manual integration was sometimes necessary. The machine was calibrated against a set of standards on each day that leachates were prepared or stored leachates run. Leachates were never stored for more then a few days, to minimise reactions within the bottles. The accuracy of the determinations was tested by periodically running standards as unknowns, and comparing these concentrations with the actual values for the standard. Experiments show precision to be better than ±2% for Na^+, ±4% for K^+, ±1% for Cl^-, and ±2% for Br^-, the most important ions under consideration (Tables A2.7.1, A2.7.2). Extrapolating the Br^- error to concentrations of 0.01 mg/l using equivalent Na^+ values, gives a maximum RSD of 5.5% at the lowest Br^- concentrations of 0.04 mg/l. Thus precision of Br^- determinations can be said to be better than ±6% at the lowest concentrations.

Table A2.7.1 Reproducibility determinations of Na^+ and K^+ on standards AK1, AK3 and AK4.

Standard	Na^+ (mg/l)	K^+ (mg/l)	mean	SD	% RSD
AK1	3.10	0.65	3.17	0.05	1.57
	3.22	0.66			
	3.18	0.65			
AK3	12.40	2.45	12.5	0.113	0.9
	12.45	2.50			
	12.45	2.44			
AK4	25.04	5.05	24.9	0.179	0.72
	24.67	5.02			
	25.06	5.10			

Table A2.7.2 Repeat analyses for Cl^- and Br^- in Std AN3.

AN 3	Cl^- (mg/l)	Br^- (mg/l)
Expected conc. (mg/l)	**9.13**	**2.5**
Repeat no.1	8.98	2.54
2	9.03	2.53
3	9.13	2.64
4	8.93	2.56
5	8.97	2.59
mean	9.01	2.57
SD	0.07	0.04
% RSD	0.76	1.54

Anion and cation concentrations for inclusion leachates are given in Table A2.7.3, along with halide molar ratios.

Table A2.7.3 Anion and cation concentrations, and pertinent molar ratios from fluid inclusion leachates.

Sample	Mine	Generation	Cl^- (mg/l)	Br^- (mg/l)	SO_4^{2-} (mg/l)	Na^+ (mg/l)	K^+ (mg/l)	Mg^{2+} (mg/l)	Ca^{2+} (mg/l)	Cl/Br (mol)	Na/Br (mol)
3153/18-1	Tsumeb	Cal II	17.3	0.24	14.2	6.53	0.80	3.65	27.1	161	93
3153/18-2	"	"	28.4	0.39	9.46	11.0	1.11	3.37	24.4	164	98
3153/18-3	"	"	18.0	0.29	9.43	7.77	0.81	3.40	28.9	140	93
3153/18-4	"	"	26.8	0.36	13.7	10.7	1.23	4.70	37.8	168	103
3153/18-5	"	"	21.7	0.34	17.3	8.43	1.04	2.18	23.0	145	87
3153/35-1	"	"	44.4	0.68	4.22	16.5	1.88	7.25	21.8	146	84
3153/35-2	"	"	41.8	0.58	0.80	16.0	1.73	8.27	23.8	161	96
3153/35-3	"	"	35.0	0.87	4.27	13.3	1.52	6.27	18.1	91	53
3153/35-4	"	"	32.7	0.50	4.76	12.7	1.44	9.28	18.5	147	88
2965/106-1	"	Dol III	15.9	0.10	17.1	6.60	1.26	21.9	16.1	378	241
2965/106-2	"	"	23.2	0.24	15.0	10.6	2.26	22.7	14.7	215	152
2965/106-3	"	"	17.3	0.14	16.5	8.40	1.70	23.2	15.7	285	213
DCT4-1	"	"	25.3	0.30		10.8	2.72			193	127
DCT4-2	"	"	21.8	0.25		9.42	2.45			198	131
DCT4-3	"	"	23.8	0.25		10.3	2.51			212	142
DCT4-4	"	"	19.7	0.22		8.92	2.33			207	144
DCT4-5	"	"	26.8	0.29		13.00	3.08			205	153
DCT5-1	"	"	35.8	0.38	0.55	16.9	2.81	38.2	16.8	215	156
DCT5-2	"	"	27.9	0.27	0.51	12.6	2.09	34.3	17.3	234	163
DCT5-3	"	"	22.5	0.23	0.61	10.4	1.65	31.6	18.1	217	156
DCT4 qtz-1	"	Dol III ass.	11.4	0.12	0.54	4.23	1.18	5.93	7.96	215	123
DCT4 qtz-2	"	"	9.81	0.14	0.44	3.37	0.98	8.84	9.78	164	87
DCT5 qtz-1	"	"	5.01	0.10	0.41	1.42	0.36	4.44	6.23	112	49
S67B	"	Dol-gyp	18.0	0.21		9.15	1.01			193	155
DV16 sphal-1	Khusib Springs	Dol II ass.	4.19	0.04	2.56	2.54	0.49	0.35	2.11	255	239
DV26 sphal-1	"	"	5.06	0.04	1.53	2.72	0.64	0.38	5.90	292	242
DV10 sphal-1	"	"	8.69	0.07	1.84	4.47	0.87	0.80	3.39	276	219
DV10 sphal-2	"	"	5.64	0.05	1.57	2.99	0.66	1.11	3.18	276	226
DV30-1	"	Dol IIa	41.9	0.34	1.07	21.0	3.49	30.8	16.4	280	216
DV30-2	"	"	41.5	0.34	0.90	20.4	3.36	32.3	17.0	274	208
DV16-1	"	"	25.2	0.19		9.2	1.85			292	166
DV16-2	"	"	36.6	0.30		13.6	2.72			278	159

Table A2.7.3 cont.

Sample	Mine	Generation	Cl^- (mg/l)	Br^- (mg/l)	SO_4^{2-} (mg/l)	Na^+ (mg/l)	K^+ (mg/l)	Mg^{2+} (mg/l)	Ca^{2+} (mg/l)	Cl/Br (mol)	Na/Br (mol)
DV16-3	Khusib Springs	Dol IIa	35.1	0.29		13.6	2.96			271	161
DV16-4	"	"	44.2	0.35		17.8	3.62			283	176
DV16-5	"	"	44.2	0.37		20.0	3.73			267	186
DV10-1	"	"	57.7	0.51		25.4	4.68			257	175
DV10-2	"	"	48.3	0.53		22.2	3.77			206	146
DV10-3	"	"	49.8	0.52		23.5	4.41			217	158
DV10-4	"	"	42.1	0.46		19.7	3.43			208	150
DV10-5	"	"	53.6	0.56		24.5	4.48			217	153
DV7-1	"	"	54.2	0.49		24.7	5.07			248	174
DV7-2	"	"	48.7	0.48		23.4	4.30			229	169
DV7-3	"	"	49.6	0.48		22.1	4.24			232	159
DV7-4	"	"	51.2	0.48		23.5	4.73			241	171
DV7-5	"	"	50.2	0.51		23.5	4.73			223	161
DV27-1	"	Dol IIb	53.4	0.57	2.87	24.5	4.14	42.8	18.8	212	150
DV27-2	"	"	47.3	0.45	2.34	21.2	3.57	32.6	18.1	238	164
AU13/88-1	Kombat	Cal I	6.92	0.14	5.57	3.23	0.63	0.57	26.0	112	81
AU13/88-2	"	"	8.92	0.18	1.26	4.14	0.72	0.71	30.2	111	79
AU13/88-3	"	"	5.82	0.12	5.20	2.76	0.54	0.37	19.7	112	82
AU13/88-4	"	"	7.49	0.15	6.28	3.53	0.60	0.59	25.6	110	80
AU13/88-5	"	"	7.35	0.18	5.63	3.67	0.71	0.38	24.4	93	71
KSW1039.4-1	"	Cal II	7.09	0.05		3.91	0.34			296	251
KSW1039.4-2	"	"	6.72	0.06		3.92	0.34			266	239
AU255.5-1	"	Cal III	24.2	0.31		11.40	1.54			177	129
AU255.5-2	"	"	13.8	0.15		6.36	1.12			206	146
AU255.5-3	"	"	19.7	0.24		8.84	1.10			182	126
HFO-1-1	Berg Aukas	Dol III	48.8	0.34	65.0	21.3	3.52	32.7	44.1	322	216
HFO-1-2	"	"	50.3	0.39	53.9	21.7	3.44	35.6	33.1	294	195

Dol = dolomite
Cal = calcite
sphal = sphalerite
Dol-gyp = dolomite associated with gypsum
qtz = quartz

blank =not determined